TOWARD GREEN BUILDINGS:

DESIGN, DEVELOPMENT AND PERFORMANCE EVALUATION OF A SOLAR-POWERED ABSORPTION COOLING SYSTEM

Thesis by

Vahid Vakiloroaya

In Partial Fulfilment of the Requirements for the

degree of Doctor of Philosophy

University of Technology, Sydney

Faculty of Engineering and Information Technology

Sydney, Australia

2014

Supervisor:

A/Prof Quang Ha

Co-Supervisor:

Prof Bijan Samali

Certificate of Original Authorship

I hereby declare that this submission is my own work and has not previously been submitted for a degree and to the best of my knowledge it does not contain materials published and written by another person, nor the materials which have been accepted for the award of any other degree except where due acknowledgement is made in this thesis.

I, in addition, certify that this thesis has been written by me except to the extent that assistance from others is fully acknowledged. I also certify that all information sources and literature quoted are indicated in this thesis.

Vahid Vakiloroaya

ABSTRACT

TOWARD GREEN BUILDINGS: DESIGN, DEVELOPMENT AND PERFORMANCE EVALUATION OF A SOLAR-POWERED ABSORPTION COOLING SYSTEM

Conventional HVAC systems rely heavily on energy generated from fossil fuels, which are being rapidly depleted. This together with a growing demand for cost-effective infrastructure and appliances has necessitated new installations and major retrofits in occupied buildings to achieve energy efficiency and environmental sustainability. As well as contributing to negative environmental outcomes, HVAC system usage is having a serious impact on electrical infrastructure. As such, the development of clean energy air conditioning units remains an urgent engineering challenge. Solar HVAC systems, which convert thermal energy into cool air, are known to be an efficient source of heating and cooling. Unlike traditional HVAC systems, solar air conditioning units produce maximum cooling capacity when the sun is fierce; that is, they are most efficient during the hottest part of the day, in stark contrast to traditional air conditioning units, which are less effective as temperatures increase.

This study represents a synergetic framework of system identification, design, development and performance evaluation of a newly-configured air conditioning system to target energy efficiency and environmental sustainability in buildings. In this study, we have originally designed and developed a single-effect lithium bromide (LiBr)-water absorption air-conditioning system in which hot water is fully supplied by vacuum solar collectors without using any other energy sources such as gas or electricity. Water-cooled condenser of the chiller is supported by a cross-flow cooling tower. In this system, by using water as the working fluid (refrigerant), one can avoid the use of ozone-depletion chlorofluorocarbons and hydro chlorofluorocarbons. Thermodynamic and heat transfer models for absorption chiller components are described in detail. Using these models, a computer simulation software named ABSYS is developed to design the absorption chiller and drive its optimum operating conditions.

Thermodynamic design data for single-effect absorption chiller are presented together with the possible combinations of the operating temperatures and the corresponding concentrations in the absorber and generator. The effect of various operating conditions on the performance and output of the absorption refrigeration system are then evaluated.

Another computer code is developed by using TRNSYS to evaluate the transient performance of the entire system. Several field tests are carried out to demonstrate the technical feasibility of the system. The utilisation of the solar energy as the heat input to the generator of the absorption chiller is reported. Since Australia has great solar resources and large air condition demand, this system can be uniquely suited in Australia. However, absorption cooling technology and especially the application of solar energy in this technology is still in its infancy in Australia.

The proposed design can be helpful to accelerate a global clean society to achieve its sustainable targets, especially in Australia, which has untapped high potential to become a World's green country. Work on this thesis, supported partially by The NSW Government through its Environmental Trust, is therefore aimed to design and explore sustainable solar-powered absorption air conditioning system to show the viability of this system in Australia and reduce the energy consumption of an air-conditioned building by using this eco-friendly cooling technology.

ACKNOWLEDGEMENTS

Undertaking this PhD has been truly life-changing, and it would not have been possible without the support and guidance that I received from many people. I am indebted to the friends, family and colleagues who have made the time working on my PhD an unforgettable experience.

My research could not have been completed without the meticulous guidance, endless encouragement and watchful eye of my supervisor, Associate Professor Quang Ha. His approach to compelling research problems, his high scientific standards, and his hard work taught me a lot about being a researcher, and for this I will remain immensely grateful. I would also like to thank my advisor, Professor Bijan Samali. Working with Bijan has been a real pleasure; he has always listened to my ideas and been willing to engage in discussions that frequently led to new and exciting insights into my work. He is someone I consider a mentor and a friend. Special thanks to Professor Miroslaw Skibniewski from University of Maryland for his helpful guidance and technical suggestions. I am also grateful to Professor Jianguo Zhu for his help and support during my research study. I am thankful to Dr Jafar Madadnia for his valuable comments and suggestions. My sincere thanks also goes to Professor Keith Crews for his support and attention to my thesis.

Richard Dibbs was endlessly supportive, providing valuable advice on numerous occasions during the experimental testing phases of my research. It is impossible to meet Richard and not like him immediately; he is someone whose friendship I hold very dear. I would like to express my gratitude for Richard's generosity in donating his time, ideas, and funding to instrument my experimental rig. His technical capabilities and tremendous grasp of experimental issues have had a huge impact on me.

I would like to take this opportunity to thank the organisations that provided financial support for my research. The New South Wales Government, through its Environmental Trust, Grant 2012/RDS/034, as well as the Faculty of Engineering and Information Technology (FEIT) and the Centre for Built Infrastructure Research (CBIR) at UTS, provided valuable funding that helped get my project off the ground.

I would like to thank local industry organisations who expressed interested in my work, including Independent Products Pty Ltd, ODG Haden and A1Best Air Conditioning Pty Ltd. I would also like to make special mention of the technical team at Stallion Air Conditioning Pty Ltd, particularly Mr Neil Thomson, for their efforts in installing and commissioning of the experimental absorption cooling system. A big thank you goes out to Associate Professor David Eager, who gave me very valuable feedback and suggestions throughout the course of my research. I'd also like to thank Claire Thompson for her invaluable advice and feedback, and for always being so supportive of my work. Furthermore, I am very grateful to Martin Lloyd, Manager of Innovation and Commercial Development at the University of Technology, Sydney, for his insightful comments, his support and for the many motivating discussions we have had. Also I sincerely appreciate the consultancy made by Tim Edwards the president of Australian Refrigeration Association.

In addition, I have been very privileged to get to know and to collaborate with Julian Day, Chief Executive Officer of Australian Consensus Group. I learned a lot from him about how to tackle new problems and develop innovative techniques to solve them. I also really enjoyed having the opportunity to work with Richard Hays, Director of Carbon and Energy Reductions Pty Ltd, whose research and development expertise has been extremely inspiring.

I would like to thank my lovely wife, Mina Khatibi, for her love and encouragement. Finally, I would like to thank my mother and father for their never ending support. Thank you with all my heart.

Vahid Vakiloroaya

Sydney, Australia, 2014

TABLE OF CONTENTS

LIST OF ILLUSTRATIONS

Number *Page*

LIST OF TABLES

Number *Page*

NOMENCLATURE

A	area (m^2)
A_{cross}	cross sectional area (m^2)
A_m	mean surface area (m^2)
A_o	outside area (m^2)
A_V	surface area of water droplets per tower cell exchange volume (m^2)
Cap	capacity (kW)
COP	coefficient of performance
C_p	heat capacity (kJ/(kg°C))
CR	circulation ratio
CV	coefficient of variance
C_{cover}	cloudiness factor
C_s	average saturation slope of the air enthalpy versus temperature
D	diameter (m)
D_e	equivalent diameter (m)
e_o	emittance
Fr_{Dl}	inside fouling factor
Fr_{De}	outside fouling factor
f_i	design energy input fraction
f_o	design energy input fraction
g	gravitational acceleration (m^2/s)
h	enthalpy (kJ/kg)
$h_{s,w,e}$	Enthalpy of the saturated air entering the cooling coil (kJ/kg)
I_t	Total solar radiation intensity (W/m^2)
I	Total horizontal radiation (W/m^2)
I_{bT}	beam radiation incident (W/m^2)

I_d	diffuse radiation incident (W/m^2)
k	thermal conductivity (W/m °C)
k_T	ratio of total radiation on the horizontal surface to the extraterrestrial radiation
L	length (m)
L_d	thermal developing length (m)
M	mass (kg)
$\dot{m}$	mass flow rate (kg/s)
n	number of tubes
Nu	Nusselt number
Ntu	overall number of transfer units
P	pressure (mm Hg)
P_w	wetted area (m^2)
P_{atm}	atmospheric pressure
P_h	atmospheric pressure at the height of h
Pr	Prandtl number
Q	heat transfer capacity (kW)
RE	relative error
Re	Reynolds number
R_r	ratio of the reflected radiation on the tilted surface to the total radiation on the horizontal surface
$RMSE$	root mean square error
RH	relative humidity
s_x	standard deviation
T	temperature (°C)
ΔT_m	logarithmic mean temperature difference (°C)
t	time (sec)
t_p	plate thickness (m)
U	overall heat transfer coefficient (kW/(m^2°C))

v	Water velocity (m/s)
V_{cell}	total cooling tower cell exchange volume (m^3)
W_p	input work of pump (kW)
X	LiBr-water concentration
$y_{data,i}$	measured variables
$y_{data,m}$	average value of data
μ	absolute viscosity (kg/m.s)
ν	kinematic viscosity (m^2/s)
α	heat transfer coefficient (kW/m^2 °C)
α_i	heat transfer coefficient inside the tube ($kW/(m^2$ °C))
α_o	heat transfer coefficient outside the tube ($kW/(m^2$ °C))
α_d	average heat transfer coefficient in thermal developing region ($kW/(m^2$ °C))
α_c	convective heat transfer coefficient due to evaporation of the liquid films ($kW/(m^2$ °C))
ρ	density (kg/m^3)
ρ_{gr}	ground reflectance
β	solar collector slop
γ	surface azimuth
γ_s	solar azimuth angle
ω	mean hour angle of time step
δ	solar declination angle
λ	thermal diffusivity (m^2/s)
η	second law efficiency
η_{col}	solar collector efficiency
ε	effectiveness
ψ	solar altitude angle
θ	angle of incidence of beam radiation on the surface
θ_z	solar zenith angle

φ	latitude
τa	transmittance-absorptance product

Subscripts

a	air, absorber
act	actual
adp	dew-point
aux	auxilury
amb	ambient
atm	atmospheric
b	beam
c	condenser
cap	capacity
cc	cooling coil
col	collector
chw	chilled water
cw	cooled water
ct	cooling tower
Cu	cupper
d	diffuse
db	dry-bulb
e	evaporator, entering
equ	equvalent
elec	electricity
f	fluid
g	generator
gl	glass
gr	ground
h	height
hw	hot water
hx	heat exchanger
k	Kelvin

i	inside
l	liquid
m	mean
max	maximum
n	normal
nom	nominal
o	outlet, outside
pl	plate
pred	predicted
ref	refrigerant
sat	saturated
s	solution
sh	superheated
ss	strong solution
sup	supply
t	tank
tr	transition
v	vapour
w	Water, wet
ws	weak solution
x	point on the cooling coil where condensation beings

ABBREVIATION

ABSYS	Absorption System Simulation
AIRAH	Australian Institute of Refrigeration, Air Conditioning and Refrigeration
ARA	Australian Refrigeration Association
ASHP	Air Source Heat Pump
ASHRAE	American Society of Heating, Refrigeration and Air Conditioning Engineers
AUD	Australian Dollar
CLF	Cooling Load Factors
CLTD	Cooling Load Temperature Differences
CO_2	Carbon Dioxide
CO_2-e	Carbon Dioxide Equivalent
CSIRO	Commonwealth Scientific and Industrial Research Organization
CV	Coefficient of Variance
DEC	Direct Evaporative Cooling
DP	Dew-Point
DX	Direct Expansion
ECC	Evaporative-Cooled Condenser
GHG	Greenhouse Gas
GSHP	Ground Source Heat Pump
GWh	Gigawatt hour
GWP	Global Warming Potential
HVAC	Heating, ventilation and air conditioning
kWh	Kilowatt hour
LMTD	Logarithmic Mean Temperature Difference
ODP	Ozone Depletion Potential
Mt	Megatonne, or million tonnes
PJ	Petajoule
PCM	Phase Change Material
PV	Photovoltaic

PLC	Programmable Logic Controller
RE	Relative Error
RMSE	Root Mean Square Error
RT	Refrigeration Tons
SCL	Solar Cooling Load
TFM	Transfer Function Method
TRNSYS	Transient System Simulation
VB	Visual Basic

Chapter 1

INTRODUCTION

1.1 Summary

Rising temperatures caused by global warming have led to a rapid increase in the installation of air conditioning systems across the globe. This growing demand has created a vicious cycle of energy usage; as more and more HVAC systems are installed, the increase in energy required to power them contributes directly to rising temperatures, which in turn increases the public appetite for indoor climate control. Rapid advances in science and technology today have led to the development of a range of techniques that can be applied to HVAC systems to reduce their environmental impact. This chapter briefly introduces relevant aspects such as energy efficiency, greenhouse gas emission reduction potential, ozone depletion and global warming reduction potential of air conditioning systems to target sustainability in HVAC and buildings. The objective of thesis and our contributions to achieve those purposes are described.

1.2 Background

Nowadays, Heating, Ventilating and Air-Conditioning (HVAC) systems are required to be more energy efficient while adhering to an ever-increasing demand for better performance and indoor air quality. Therefore, there is an immediate need to develop and consider the environmentally friendly sustainable HVAC technologies. Conventional HVAC systems rely heavily on the use of energy derived from fossil fuel. At the same time, the resources of these fuels are rapidly becoming depleted. Furthermore, for greenhouse gas emission reduction, new installations and major retrofits in occupied buildings are rapidly becoming an important issue. Therefore, finding novel ways to reduce energy consumption in buildings without compromising comfort and indoor air quality is an ongoing research challenge.

One proven way of achieving energy efficiency in HVAC systems is to design systems that use novel configurations of existing system components. Therefore, finding novel ways to reduce energy consumption in buildings without compromising comfort and indoor air quality is an ongoing research challenge. While the typical value of the coefficient of performance (COP) for vapour compression systems is between 2 and 3, the performance of these systems can be significantly improved by applying effective configurations of existing system components.

In addition, the possibility of providing cooling by means of renewable energy has intrigued the mind of researchers on how to combine air conditioning systems with free energy sources in order to reduce their power consumption. In recent years, different renewable energy sources such as bio mass, nuclear, wind and solar have been used to meet in the design and development of HVAC systems; solar thermal energy is the most commonly used. The fact that peak cooling demand in summer is associated with high solar radiation offers an excellent opportunity to exploit solar thermal technologies in HVAC engineering. The sun emits energy at a rate of 3.8×10^{23} kW, of which approximately 1.8×10^{14} kW is intercepted by the earth. About 60% of this amount, or 1.08×10^{14} kW, reaches the surface of the earth. About 0.1% of this energy, when converted at an efficiency of 10%, would generate four times the world's total capacity of about 3000 GW if we could harness it, presenting a clear argument for the use of solar thermal energy in HVAC systems [1]. Solar-assisted air conditioning systems can also reduce peak energy demands, which currently cost power companies millions of dollars a year in infrastructure investments. The cost of these investments is one of the underlying causes of increasing electricity prices. On the hottest days of the year, electric air conditioners routinely overwhelm the grid capacity, causing major problems for the Australian power network; over the last few years, hotter weather has meant that peak energy demand is growing much faster than base power demand, compounding the problem. However, abundant sunshine and predictable sunrise pattern, coupled with the difficulties of supplying energy to meet peak demand, make an ideal idea for the use of solar-assisted air conditioning systems. As reported in [2] around 40-50% energy consumption can be saved by implementing solar driven air conditioning systems in

Mediterranean countries. Beside the less energy usage, the solar air-conditioning systems represent smaller ozone depletion (ODP), smaller contribution to greenhouse effects and lower CO_2 emissions than electrically operated plants. Energy usage using fossil fuels are responsible for two third of anthropogenic greenhouse gas emissions which are estimated to increase 60% by 2030 with respect to the 2000 levels [3]. On other hand, the CFCs and HCFCs gases which are used by vapour compression refrigeration systems have high ozone depleting and high global warming potential; this problem can be remedied by employing the environmentally-friendly cooling systems. As reported by United State Environmental Protection Agency [4] building energy consumption accounts for around 40% of greenhouse gas and other air pollutant emissions. For example, a single-effect absorption system was compared with a conventional system in Spain by Rodriguez-Hidalgo et al. [5]. Their results showed that the savings in CO_2 emissions amount can be more than 20% when using the absorption cooling system with the COP between 0.35 and 0.7. In another study, Florides et al. [6] showed that using R22 in a 5-ton refrigeration system can produce about 18 g CO_2/kWh of cooling provided.

Cooling systems that can achieve the benefit of solar energy are: vapour compression refrigeration systems, absorption cooling systems, desiccant cooling systems, ejector systems and adsorption refrigeration systems. There has been always the question about the Priority of using vapour compression systems against of sorption systems. To quote this question various factors such as initial, operation and maintenance cost, location of project, climatic conditions, building type, required comfort level and availability of energy sources should be considered. However, it has been found that solar thermal systems would be cost-competitive by 2030 if thermal collector costs come down significantly [7]. Using vapour compression air conditioning systems is more preferred for small residential and commercial buildings due to their lower initial cost compared with sorption air conditioning systems. Same reason has caused most of efforts for developing of solar cooling plants on the large scale applications and thus further development of small capacity cooling systems are still in high interest [8]. However, although the sorption cooling systems are more expensive than

vapour compression ones, but they can wisely be used from long-term financial and environmental viewpoints.

1.2.1 Energy Saving Aspect

Increased standards of living coupled with dwindling supplies of fossil fuels, have forced researchers and engineers to focus on the issue of energy use in buildings. HVAC systems, which play an important role in ensuring occupant comfort, are among the largest energy consumers in buildings. Performance enhancements to traditional HVAC systems therefore offer an exciting opportunity for significant reductions in energy consumption. Almost 50% of the energy demand is used to support indoor thermal comfort conditions in commercial buildings [9]. Furthermore, as most people spend more than 90% of their time inside [10], the development of energy-efficient HVAC systems that do not rely on fossil fuels will play a key role in reducing energy consumption. A closer look at world-wide energy consumption by HVAC equipment shows noticeable values: With consolidation of the demand for human comfort, HVAC systems are accounting for almost 50% energy consumed in building and around 10-20% of total energy consumption in developed countries [11].

As reported by U.S. Department of Energy (DoE), 31.2% of energy use by U.S. residential buildings is by HVAC equipment [12]. In addition, it has been accounted by DoE that energy use in the built environment will grow by 34% in the next 20 years at an average rate of 1.5% [13]. In China, the building energy consumption has been increasing about 10% a year for the past 20 years and has comprised about 20.7% of the total national energy usage by the year 2004 [14]. In Europe, around 40% of energy consumption is represented in commercial and residential buildings [15]. HVAC technology in all its forms is the single largest electricity consuming class of technology in Australia. There are more than 45 million individual pieces of refrigeration and air conditioning equipment operating in Australia that consumed more than an estimated 59,000 GWh of electricity in 2012, equivalent to more than 22 per cent of all electricity used in Australia that year [16]. In India, air conditioning systems accounts around 32% of electricity consumption of a building [17]. In the subtropical

Hong Kong air conditioning and refrigeration systems accounted for 33% in 2006 [18]. About 40% of the end-use energy demand in Germany is due to space heating and domestic hot water [19]. 16% of the overall energy consumption in Spain is associated to the building sector [20]. More than 70% of building energy consumption is to support cooling systems in Middle East [21]. It was estimated that world energy consumption was increased by 58% between 2001 and 2005 [22]. However, approximately 80% of the energy usage still comes from fossil fuels [23, 24]. With considering that the final goal of HVAC systems is to provide comfort conditions inside the buildings and adding the fact that the fossil fuel sources are limited, the need to find different strategies to reduce the energy consumption of HVAC systems while maintaining comfort conditions inside the building is essential. With rapid changes in science and technology today, there are several methods that can be used to achieve energy-efficient HVAC systems.

1.2.2 HVAC Energy Consumption in Australia

Advice received by the Australian Government [25] suggests that rising temperatures caused by climate change are set to have an adverse impact on Australia's environment and economy. According to the Government, Australia remains one of the world's top 20 polluters, with a larger per capita carbon footprint than any other developed nation. These statistics are set to get worse: between the years 2000 and 2024, our carbon emissions are set to increase by a predicted 24 per cent, adding to already overwhelming global totals and contributing to further damage to the planet [26]. The Government has acknowledged a need to remove the correlation between economic growth and growth in pollution in Australia, and for the country to 'do its part' in reducing greenhouse gas emissions and taking a conscious step towards renewable energies to benefit of the Australian public, the Australian economy and the broader international community.

In order to meet these environmental responsibilities, the Government developed a clean energy futures plan and a Clean Energy Finance Corporation that incorporated a carbon pricing scheme aimed at slashing greenhouse gas emissions, billing major commercial

polluters, delivering a renewable energy target and incentivising investments (with an original target of $20 million) in clean and sustainable energy sources with a view to supplying 20 per cent Australia's electricity via sustainable energy sources by 2020, and reducing carbon pollution by 80 per cent on 2000 levels by the year 2050 [25]. The carbon price is applied per tonne of carbon emissions to some 500 major polluters, providing a financial incentive for companies to reduce their emissions and become part of Australia's low-pollution future. Regular citizens facing increased power prices as a result of the trickle-down impacts from the business sector have already started receiving tax cuts and increasing government benefits in order to offset the costs. Reducing the carbon intensity of existing technologies is one step towards a cleaner future for Australia, but increasing the energy efficiency of other technologies is just as crucial.

As mentioned, it has been estimated that HVAC equipment consumed 59,000 GWh of electricity in 2012, more than 22 per cent of the approximately 265,000 GWh of electricity production in Australia that year. The share of electricity consumption of these systems is illustrated in Fig. 1.1 [16]. In addition, total energy consumption in all commercial buildings in Australia have been about 142.7 Petajoules (PJ) in 2012, a figure that is predicted to rise to just under 170 PJ by 2020 [27].

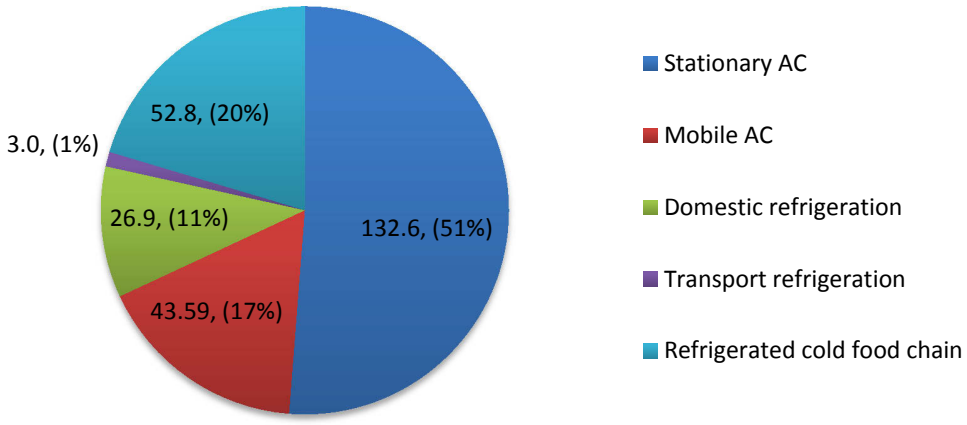

Fig. 1.1 Energy consumption of different HVAC and refrigeration systems in PJ and per cent of total

In terms of overall energy consumption, retail buildings accounted for the largest share of energy consumption in commercial buildings, consuming approximately 47 PJ or 35 per cent of the total as shown in Figs. 1.2. 'Stand alone' office buildings represented the second largest share with nearly 34 PJ or 25 per cent of the total energy consumption. Expected growth in energy consumption by building type over the period from 2009 to 2020 is presented in Fig. 1.3 [27].

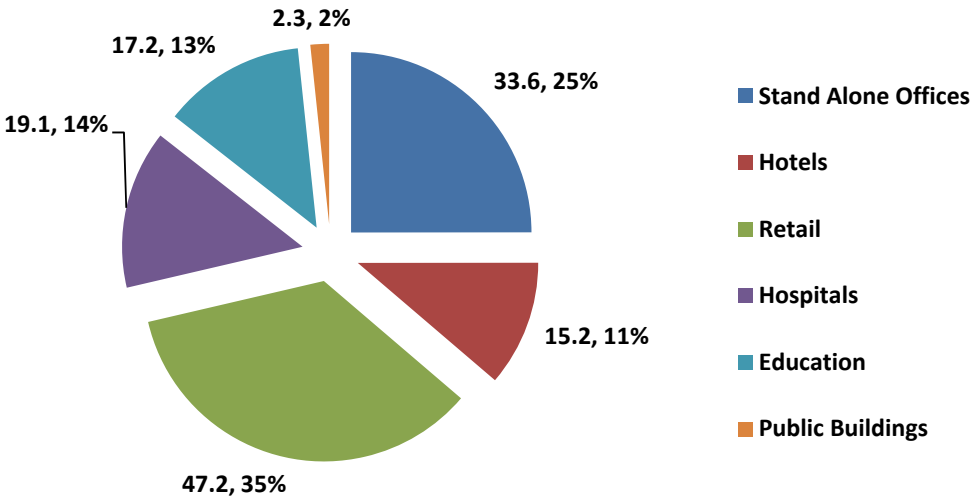

Fig. 1.2 Total Energy Consumption by Building Type, 2009 (PJ, % shares)

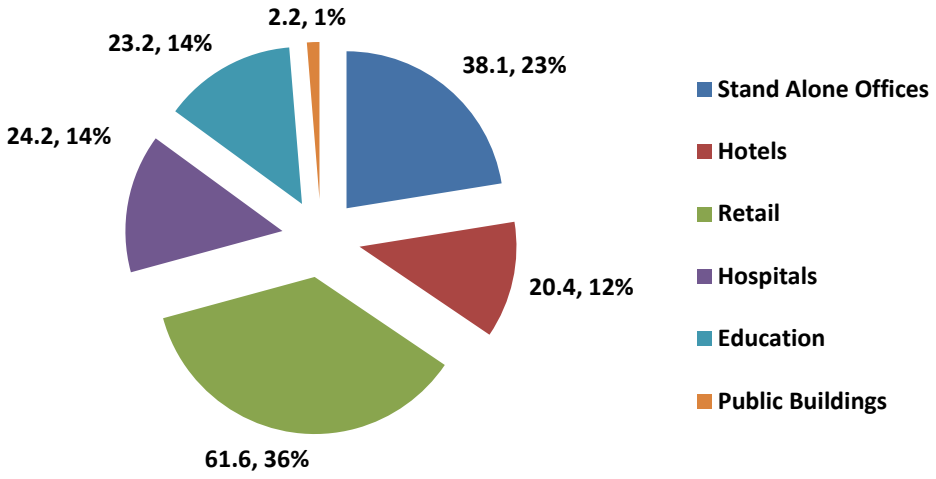

Fig. 1.3 Total Energy Consumption by Building Type, 2020 (PJ, % shares)

According to the statistics and data provided by [27] the energy consumption of HVAC systems in different type of buildings are shown in following figures 1.4 to 1.9.

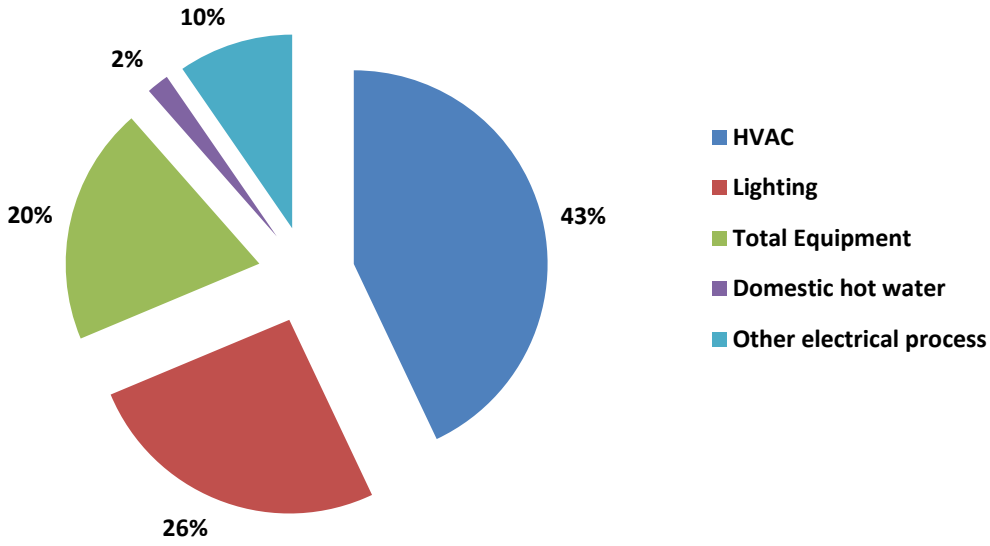

Fig. 1.4 Offices Electricity End Use Shares, 1999 - 2012

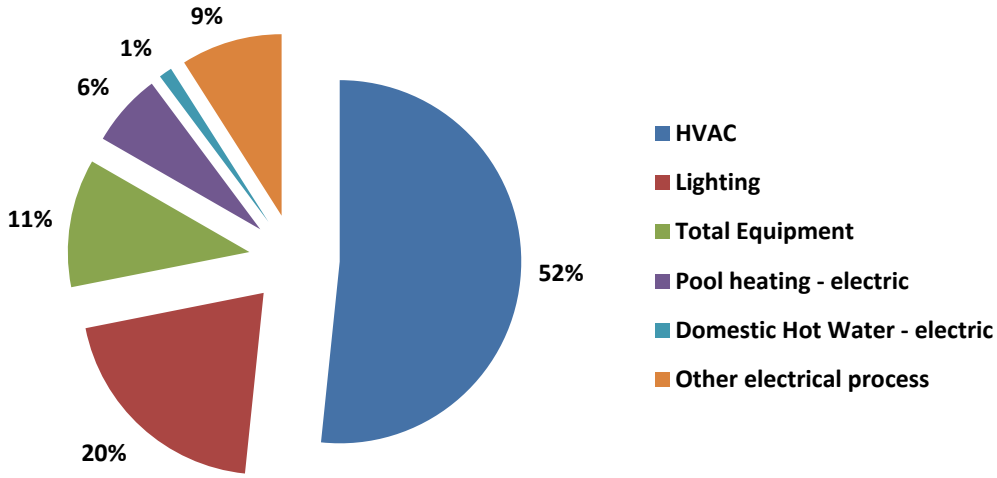

Fig. 1.5 Hotels Electrical End Use Shares, 1999– 2012

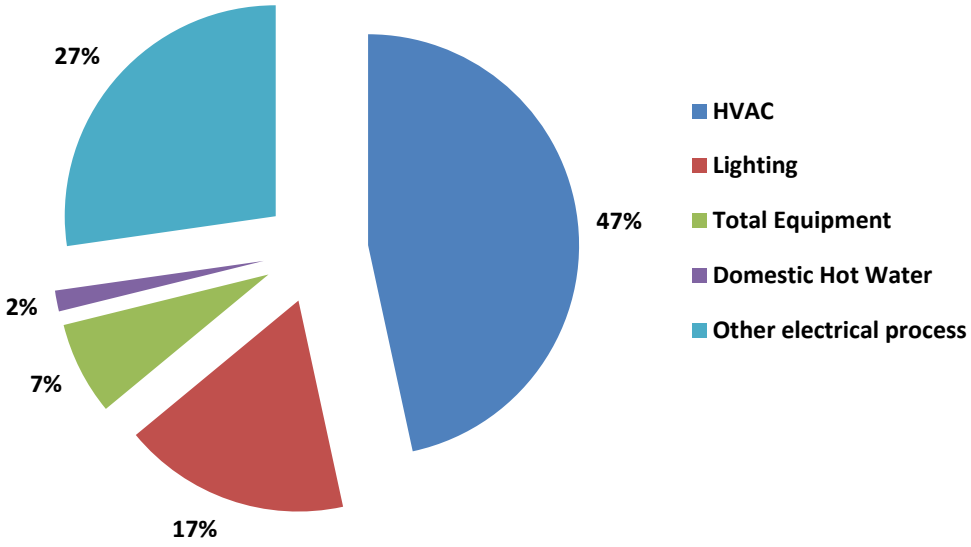

Fig. 1.6 Hospitals- Electrical End Use Shares, 1999 – 2012

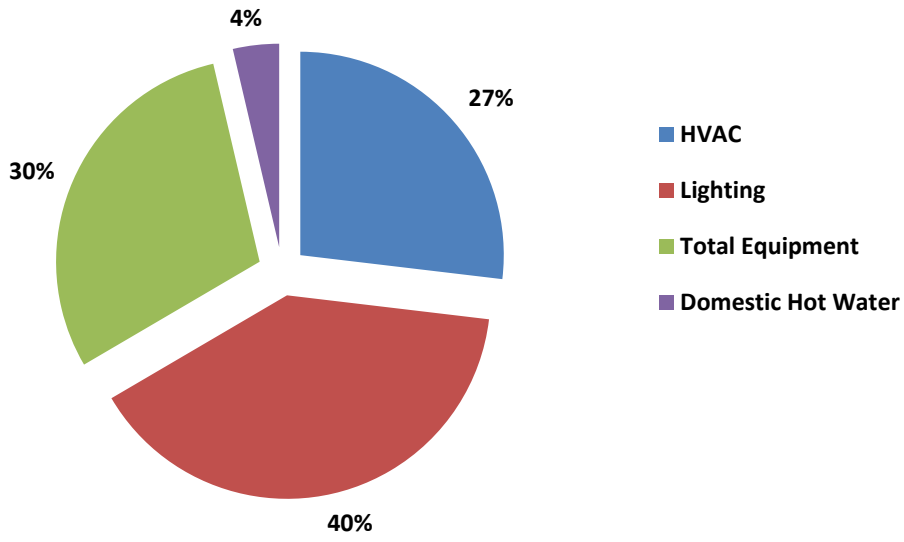

Fig. 1.7 ACT Schools, Electrical End Use Shares, 1999 –2012

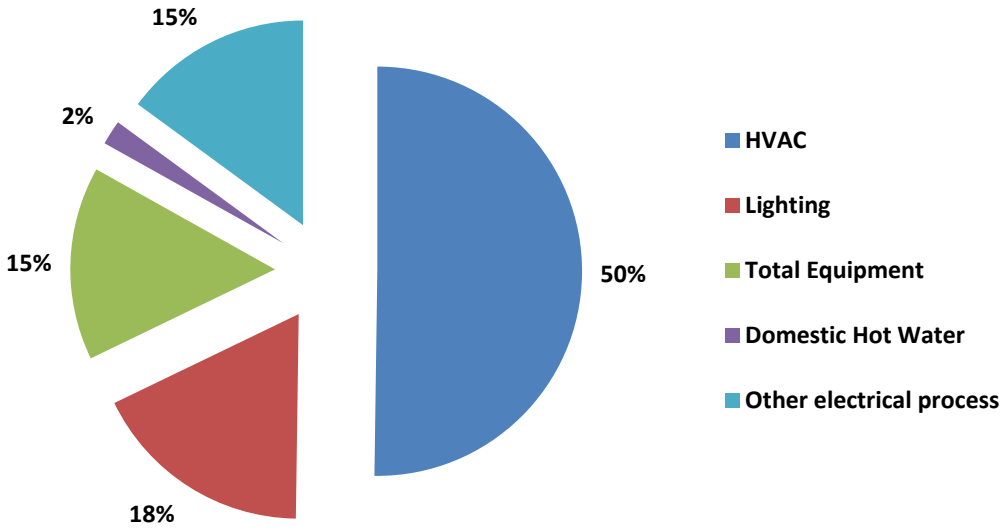

Fig. 1.8 Universities Electrical End Use Shares, Australia, 1999 – 2012

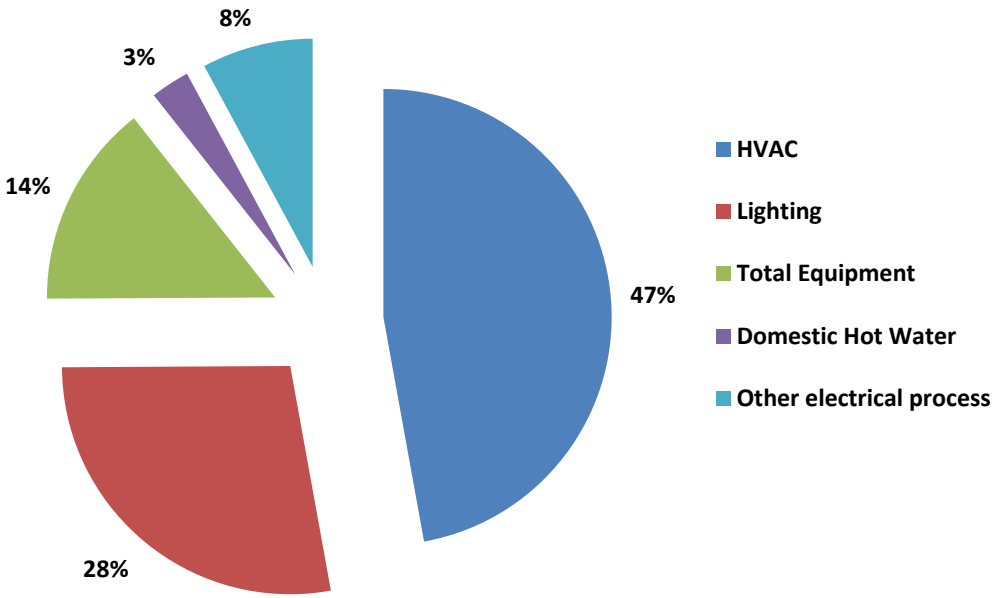

Fig. 1.9 Law Courts- Electrical End Use Shares, Australia, 1999 - 2011

From these statistics, it can clearly be seen that the energy consumption of HVAC systems in different type of buildings is very significant. Therefore high priority should be given to the development of the energy-efficient HVAC systems.

1.2.3 Greenhouse Gas Emissions

Commercial refrigeration includes over one million individual installations, 5.5% of national electricity consumption, over 25% of national HVAC&R CO_2e emissions or about 3-4% of national CO_2e emissions. Residential refrigeration represents over 17 million individual installations consuming 2.5% of national electricity production and responsible for about 1.3 % of national CO_2e emissions[1]. Refrigeration is an important sector of emissions from the built environment, about 8.5% of national electricity use and 4-5% of national CO2e emissions [28]. It is broadly recognised that HVAC is a primary source of emissions in the built environment, typically in excess of 40% of emissions and typically the largest single source of emissions in the built environment. However, HVAC is also understated as a source of emissions. Cold Hard Facts 2 [16] reports that HVAC&R is responsible for 11.7% of national emissions. Direct emissions are the intentional and unintentional release of fluorocarbon refrigerants. It has been considered this source of emissions to be at least 3-4% of national emissions bringing the total from HVAC&R to 13.4 -14.4% of national emissions [28]. This is a central consideration because the reduction in HVAC&R emissions requires both increased energy efficiency and reduced fluorocarbon refrigerant emissions. It is also a central consideration because natural refrigerant-based technologies enable both increased HVAC energy efficiency and the elimination of direct emissions. Natural refrigerants have very low global warming potential (3-20 GWP, as compared to fluorocarbon refrigerants at 1300 to 10,000 GWP) and therefore direct emissions from natural refrigerants are trivial. The energy savings available from Natural Refrigerant based technologies are in the range of 20 to 50% vs. fluorocarbon-based technology [28].

[1] This estimate does not include direct emissions from end of life HVAC& equipment. This is a large number because the vast majority of end of life HVAC&R equipment is shredded without being degassed and about 60% of the synthetic gases in fridges are in the insulation of the equipment, as a blowing agent, rather than the refrigerant.

Almost 80% of homes and the vast majority of commercial premises across the full range of industries have air conditioning / heating facilities. Cold Hard Facts 2 [16] provides two key observations regarding the use of HVAC in the built environment:

Between 1999 and 2012 the number of individual residential size air conditioning systems in Australia grew from an estimated 2.6 million units to just under 11.5 million devices, a number substantially higher than the estimated 8 million private dwellings.

Today, there are few places in the non-residential built environment where refrigerated air conditioning and mechanical ventilation systems are not encountered, from airport terminals and exhibition halls, to offices and shops.

Despite broad recognition that HVAC is a primary source of emissions in the built environment very little progress has been made in addressing HVAC as a source of emissions. There are a number of reasons for this failure, including [29]:

- HVAC is an invisible but highly technical engineering discipline. It is far less obvious as a source of emissions reduction as compared to lighting and hot water. Government initiatives have tended to address other sources of emissions reduction (i.e. lighting, hot water and renewable energy sources).
- The role of HVAC in determining peak demand is a further key issue. It is broadly recognised that it is residential HVAC that drives peak demand. As a result energy efficiency in HVAC would make a major contribution to reduce the peak energy demand and resulting in reduction of impact on peak demand emissions.
- HVAC efficiency requires better life cycle management principles including design, commissioning, maintenance and disposal. The highly decentralised HVAC industry, comprised of over 10,000 firms and 40,000 technicians, does not address the last three considerations effectively. These organisations are far more concerned with new installations rather than energy efficiency, despite the fact that energy efficiency is fundamentally dependant on effective commissioning and maintenance.

1.3 Solution

As discussed, the development of clean energy air conditioning units remains an urgent engineering challenge. Solar HVAC systems, which convert thermal energy into cool air, are known to be an efficient source of heating and cooling. Unlike traditional HVAC systems, solar air conditioning units produce maximum cooling capacity when the sun is fierce; that is, they are most efficient during the hottest part of the day, in stark contrast to traditional air conditioning units, which are less effective as temperatures increase. During periods of lower solar intensity, such as early morning and late afternoon, these solar HVAC systems have the ability to store solar energy for ongoing cooling efficiency. They are also typically designed to rely on non-electrical back-up energy sources during peak periods, reducing pressure on electrical grids without compromising human comfort.

The world overall solar energy resources potential is around 5.6 gigajoules (GJ) in which Australia's portion is approximately 58 million petajoules (PJ) which is about 10,000 times Australia's annual energy consumption [30]. Theoretically, if only 0.1% of the incoming solar radiation could be converted into usable energy at the efficiency of 10%, all of Australia's energy needs could be supplied by solar energy [30].

Solar HVAC systems boast lower energy consumption requirements, lower running costs, and reduced GHG emissions than traditional HVAC systems. They have also been proven to play an important role in managing energy usage targets, slowing energy price growth, maintaining energy security and mitigating the impacts of climate change. Thus, widespread installation of solar HVAC systems would play a critical role in reducing peak electricity demand, as well as assisting home and building owners to manage the costs associated with indoor climate control. Therefore, development of the solar-assisted HVAC system is a sustainable solution which can cut down the energy costs and preserve the environment. This work aims to present the possibility of utilisation of the solar energy as a heat source for absorption cooling technology particularly for Australia. The proposed system can be a suitable solution to the green building emergence in which energy efficiency and environmental sustainability are of important requirements.

1.4 Objectives

As mentioned, supplying ever-increasing peak load requires the installation of more and more energy-efficient HVAC systems. Enough sunlight strikes the Earth in 90 minutes to provide the entire planet's energy needs for one year [31]. Different technologies must then be developed to capture this amount of energy. Although Australian researchers have played an important role in the development of solar energy systems in the past and continue to be at the cutting edge of new technological developments, but still there are lots of opportunities to develop solar-assisted HVAC system in Australia. While the solar cooling sector currently makes a very small contribution to meet world energy demand, estimates show that with concerted action by governments and industry, solar energy could provide more than 17% of total global energy use for cooling by 2050 [32]. In recent years, research on solar cooling techniques has been growing in Australia. The work described in this study aims at contributing to the design, development, manufacturing and testing a single-effect absorption cooling plant which is powered by solar energy.

This project demonstrates the feasibility of providing cooling by using the single-effect absorption chiller where its generator is directly connected to the solar collector without hot water storage tank. The project objectives are:

- To design the absorption chiller heat exchangers such as condenser, generator, evaporator, absorber and solution heat exchanger. For this purpose, heat transfer correlations are used and the influence of different operating variables on the physical dimension of each heat exchanger is investigated.

- To manufacture the single-effect absorption chiller based on original design of its components.

- To develop a user-friendly computer simulation program specially designed for single-effect absorption chiller. For this purpose, a computer code named ABSYS is developed to optimum design of the absorption chiller components and evaluate the

effect of the various operating conditions on the chiller performance. This program can be used by other researchers for design optimisation, development and commercialisation of the absorption chiller.

- To demonstrate thermodynamic feasibility of the desired performance. For this purpose, a thermodynamic model is developed to evaluate the performance of the single-effect absorption chiller in various steady-state conditions.

- To derive the thermodynamic design data for the single-effect absorption chiller for possible combinations of various operating temperatures. These data can be used by other authors to examine the performance of absorption chiller in different design conditions. In addition, the optimum design maps are obtained and presented. These data can serve as a source of reference for designing and developing the single-effect LiBr-water absorption chiller in its optimum operating conditions.

- To experimentally monitor the performance of the entire solar cooling plant and validate its technical capability to support the building cooling demand.

- To demonstrate the ability of solar energy vacuum collectors to achieve the required temperatures necessary to provide the heat input to operate the absorption cooling system.

- Finally, to show the feasibility of this technology in Australia where this technology is still in its infancy.

To the best knowledge of the author, this system is among the first solar-powered absorption chiller installed in Australia in which the solar collector is directly connected to the chiller's generator without using any backup system. This reduces the system cost as well as required space for installation. Since there is no backup system in this design, it runs only when the solar radiation is available.

1.5 Thesis Outline

Description of the research work that has been carried out in this thesis is presented in the following chapters as:

The purpose of chapter two is to survey the various works carried out on the HVAC system energy efficiency. Different approaches which enhance the energy efficiency of HVAC systems are considered and a comparison is given to weigh the respective advantages and disadvantages of these technologies. Particularly, the technical and economic findings for absorption cooling technology is reviewed.

Chapter three describes the building information and represents its cooling demand. The information about HVAC component type in TRNSYS is then presented. The TRNSYS work space and information which were used to calculate the building cooling loads through a dedicated visual interface are presented. Daily and hourly cooling loads are then discussed.

The aim of chapter four is to describe the solar-powered hot water single-effect absorption air conditioning system and explain its working principles. Thermodynamic models for the absorption refrigeration cycle based on the energy and mass balance laws are presented. The thermodynamic properties of the LiBr-water solution are also discussed and presented.

Chapter five presents the parametric study of the designed absorption chiller and predicts its steady-state performance. To achieve this goal, a computer program based on thermodynamic models presented in chapter four is developed. The limitations of the absorption cycle operation and optimum generator temperature to obtain the maximum chiller COP are determined and discussed. The thermodynamic design data for the single-effect absorption chiller are derived which can be used by other studies to achieve the optimum design of the system.

Chapter six presents the heat transfer equations to design the different components of the absorption refrigeration system. The heat transfer correlations for laminar and turbulent flow

for tube-side and shell-side of all heat exchangers used in the absorption chiller are discussed. This models are coded in ABSYS to design the absorption chiller's heat exchangers.

In chapter seven the design details of absorption chiller components are presented. In addition, the design specifications of absorption chiller's heat exchanger are calculated. Required area of heat transfer and number of tubes in the chiller's heat exchangers are also calculated. The influence of the system variables on the heat transfer rate and physical dimension of each heat exchanger is investigated. The design specifications of the cooling coil of the fan-coil unit and the cooling tower are presented. Finally, experimental set-up of the central cooling plant is described.

The objective of chapter eight is to simulate the transient performance of the solar-powered absorption cooling system by using the experimentally monitored data. For this purpose, the developed 7 kW hot water single-effect absorption chiller was manufactured based on obtained designed data in chapter 5 to 7. The absorption chiller combined with the vacuum solar collectors, a cross flow cooling tower and a fan-coil unit is then used for experimentation and data collection. Mathematical model of the system components are developed and implemented in a transient simulation tool, TRNSYS. For the purpose of error analysis, the simulated performance of the system is compared with obtained experimental results. The predictions from the models exhibit a good coincidence with experimental results.

In chapter nine, the major findings in this study are summarised. Moreover, recommendations for future research are proposed.

1.6 Contribution

As mentioned, the intensive usage of fossil fules for HVAC systems has rigorous consequences for earth environment. However, the sun' energy reaching the earth has an ample energy potential. The contribution of this thesis is therefore to design, develop and manufacturing of a solar thermal absorption chiller which relies only on solar radiation to use

high solar irradiation which is mostly unused in hot season of the year. The main contribution is also to demonstrate the technical feasibility of this development. Based on this contribution, optimum design data for single-effect absorption chiller were achieved which can be used by other authors, researchers and manufacturers. In addition, based on developed mathematical models, a software named ABSYS has been developed to design the single-effect absorption chillers in various conditions and select the optimum design for the purpose of manufacturing. Several feid tests have been carried out to show the practical viability of the developed system. The outcomes of this work can be employed for future research and development of solar thermal absorption cooling plants.

Chapter 2

LITERATURE REVIEW

2.1 Summary

In response to the growing demand for energy-efficient infrastructure and appliances, it is rapidly important for engineering practitioners to improve energy efficiency and reduce environmental impact in new installations and major retrofits in occupied buildings. Energy-efficient HVAC system designs depend on new configurations that make better use of existing parts. Another promising potential is to combine air-conditioning systems with renewable energy sources to create an energy-efficient configuration. This literature review investigates and reviews the different technologies and approaches, and demonstrates their ability to improve the performance of HVAC systems to reduce energy consumption. Various solutions in which different configurations, component combinations and mechanical designs are used to improve the energy performance of HVAC systems are discussed in this chapter. In addition, a particular review is carried out for absorption air conditioning system. The application of solar energy to develop the absorption cooling system is investigated. A comparison study between these approaches is carried out.

2.2 Development in HVAC Systems

Air-conditioning units are least efficient at high ambient temperatures, when cooling demand is highest. This leads to increase pollution, excessive investment in standby generation capacity, and poor utilization of peaking assets. Therefore, emerging technologies have for several years highlighted energy-saving strategies for HVAC systems. The aim of this literature review is to explore and compare various sustainable solutions to reduce the energy consumption of air-conditioned buildings as a key consideration.

2.2.1 Evaporative Cooling Systems

Evaporative cooling technology has been widely used since more than a century [33]. Direct evaporative cooling (DEC) systems have low set-up and running costs, and have been proven to significantly improve a building's cooling and ventilation capacity with minimal energy use. Using water as the working fluid, one can avoid the use of ozone-destroying chlorofluorocarbons and hydro-chlorofluorocarbons. Other benefits from this system include easy maintenance, easy installation and operation as well as obviating CO_2 and other emissions. Evaporative cooling systems can provide thermal comfort via the conversion of sensible heat to latent heat; however, the lowest temperature DEC systems can reach is the wet-bulb temperature of the outside air. Therefore, the temperature of the supply air after cooling would be just on the edge of comfort and could rise a few degrees in passing through space, taking the temperature beyond the comfort zone. Therefore, the efforts in this area have been carried out to investigate both the possibility of increasing the utilization potential of the evaporative cooling system by combination of different components with this system and the capability of improving the performance of other HVAC systems when integrating with evaporative cooling system.

Direct evaporative equipment cools air by direct contact with the water, either by a wetted surface material or by spraying water into the supply air. In indirect evaporative cooling, secondary air removes heat from primary air through a heat exchanger. In one indirect method of cooling, water is evaporatively cooled by a cooling tower and circulates through a heat exchanger. For example, the building exhaust air can be used to cool down the ambient air before it passes the evaporative cooler as shown in Fig. 2.1. The idea here stems from the possibility to increase the utilization potential of an evaporative cooling system by the integration of the air-to-air sensible heat exchanger and cooling coil with the DEC process. In such a system, the air is first cooled sensibly, i.e. without any moisture addition, in two stages. In the first stage an air-to-air sensible heat exchanger is used to reduce the dry-bulb temperature of the entering air the cooling coil through energy transfer between the building return airstream and ambient fresh air. In the second stage the air is further cooled sensibly by a cooling coil.

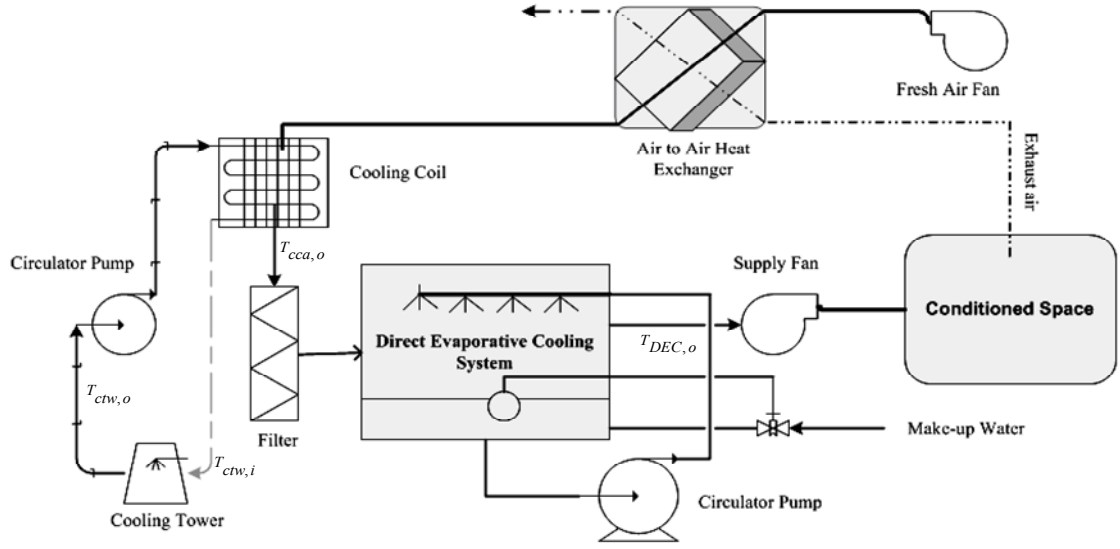

Fig. 2.1 Schematic diagram of the hybrid system of heat exchanger, cooling coil, and direct evaporative cooler

The cooling coil gets its water supply from a cooling tower. Then the air passes through the DEC system to achieve a lower temperature. Consequently, in the proposed hybrid evaporative cooling system the lowest temperature obtained can be lower than the wet-bulb temperature of the outside air.

2.2.2 Evaporative-Cooled Air Conditioning Systems

Recent research reveals that air conditioning systems based on mechanical vapour compression consume significant amounts of electricity. Therefore, increasing the coefficient of performance (COP) of these air conditioning systems with air-cooled condensers is a challenging problem. In fact, as the typical value of COP for the air-cooled vapour compression systems is between 2 to 3, new configuration of these systems can certainly increase their COP [34]. One proven way of achieving energy efficiency in the air-cooled vapour compression air conditioning systems is to reduce the compressor discharge pressure which decreases the compression ratio of the compressor and in turn resulting in less electricity

consumption. The aim of this section is to describe this method which reduces the energy consumption of the air-cooled vapour compression air conditioning system by using the evaporative-cooled condenser technique.

The single-stage air-cooled vapour compression air conditioning system consists of four major components: a compressor, an air-cooled condenser, an expansion device and a direct expansion (DX) evaporator. The schematic diagram of the arrangement is shown in Fig. 2.2 and its p-h diagram is shown in Fig. 2.3. The cycle starts with a mixture of liquid and vapour refrigerant entering the evaporator. The heat from the warm air is absorbed by the evaporator coil. During this process, the state of the refrigerant is changed from a liquid to a gas and becomes superheated at the evaporator exit. Superheat is required to prevent slugs of liquid refrigerant from reaching the compressor and causing any serious damage. The superheat vapour enters the compressor, where the increasing pressure raises the refrigerant temperature. After the compressor, a temperature reduction takes place in the condenser and causes it to de-superheat; thus, the refrigerant liquid is sub-cooled as it enters the expansion device. Sub-cooling prevents flash gas formation before the expansion device and increases the evaporator's refrigeration effect. The high pressure sub-cooled refrigerant flows through the capillary tube, which reduces both its pressure and temperature.

By pre-cooling the air before it reaches the condenser coil, the condenser is able to reject more heat. In the conventional vapour compression refrigeration system, the condensing pressure is designed to allow the refrigerant condensation at high ambient temperature. In this way, the energy is wasted in partial load when the ambient temperature is low and that much condensing temperature is not required. In this method by pre-cooling the air before it reaches the condenser coil, the condenser is able to reject more heat. As a result, cooling capacity increases while energy demand and usage fall.

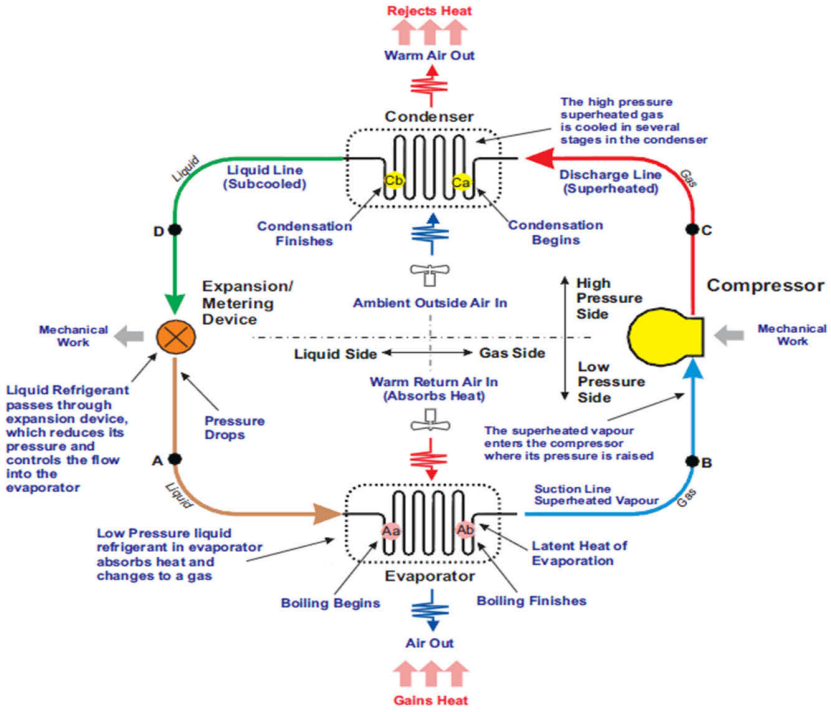

Fig. 2.2 Schematic diagram of the conventional DX air-cooled air conditioning system

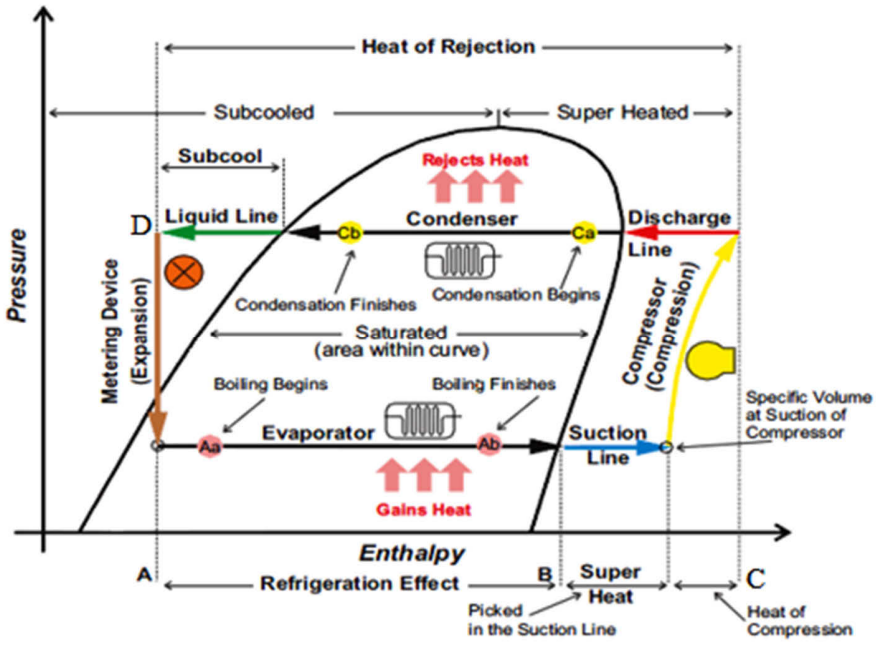

Fig. 2.3 P-h diagram of the conventional DX air-cooled air conditioning system

In the evaporative-cooled air condenser system, the ambient temperature entering the condenser gets cool through passing the wet media installed at the upstream of the condenser coil. A controlled water flow is dripped across the media. Therefore, the condensing temperature is reduced which decreases the compressor discharge pressure, in turn considerably diminishes the electricity usage of the compressor. Therefore, as head pressure is lowered, refrigerant condensing temperatures are reduced. This allows compressor to run less and thus save energy. In this design, normally a frame is built and filled by evaporative media pad and installed in front of the air-cooled condenser. Water circulation system is included of a small pump, a tank and pipes. The water then is injected on the top of the media pad. Hot ambient air passes the wet pad and then the condenser to improve the system performance. On other hand, as hot ambient air is drawn through the media, the water absorbs heat and evaporates. This lowers the temperature of the ambient air, in turn creating a cooler operating environment for the air-cooled condenser which allows condenser to reject additional heat to the atmosphere. Figure 2.4 shows a schematic block diagram of the conventional and developed DX air conditioning system while their pressure-enthalpy diagram is shown in figure 2.5.

As shown in Fig. 2.5, the compressor head pressure is reduced from point (3) (in the conventional cycle) to point (b) at steady state conditions. The superheated refrigerant then enters the air-cooled condenser where a final reduction in the refrigerant temperature takes place and causes it to de-superheat and thus the refrigerant liquid is sub-cooled as it enters the expansion device. As a result, the refrigeration effect of the evaporator is increased enabling the system to deal with higher load demand. As demonstrated in Fig. 2.5, this is occurred by replacing the point (1) to point (a) in the refrigeration cycle. However, due to required minimum pressure difference across the expansion device for proper operation of expansion device, the amount of the discharge pressure that can be reduced is limited. Therefore, the energy saving potential of this method is a function of the minimum acceptable pressure differential across the expansion device as well as ambient temperature.

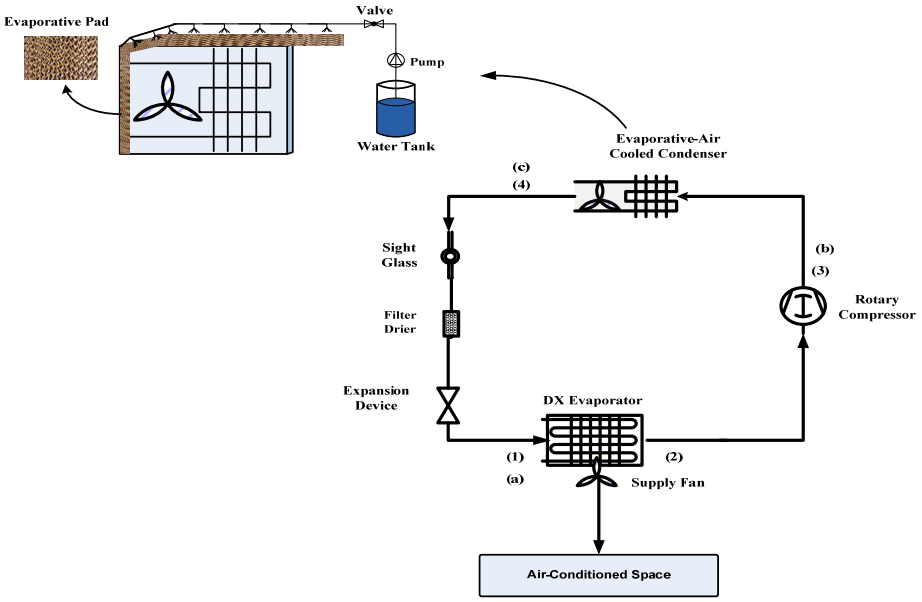

Fig. 2.4 Schematic diagram of the evaporative-cooled DX air conditioning system

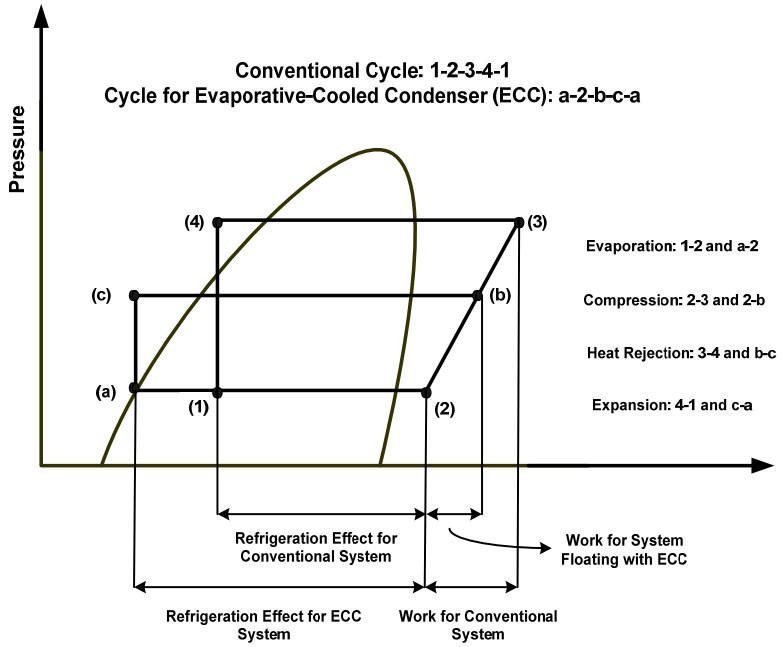

Fig. 2.5 P-h diagram of the conventional and evaporative-cooled DX air conditioning system

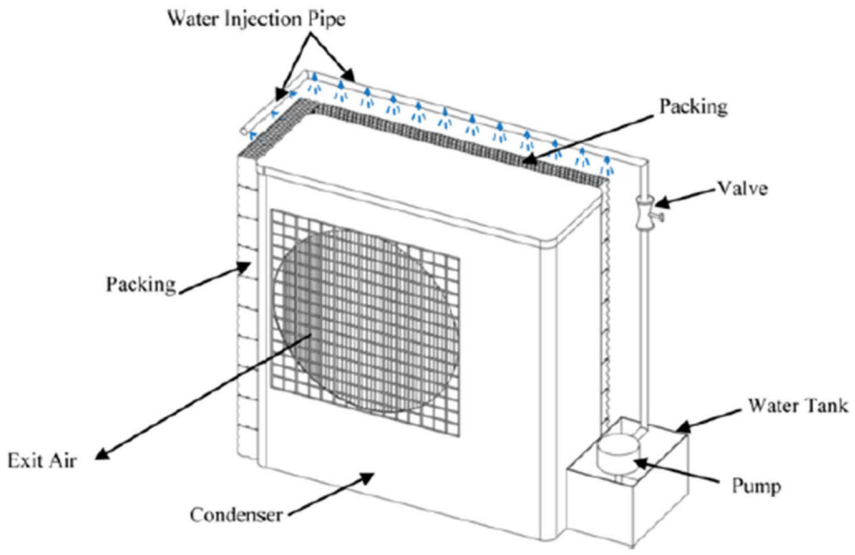

Fig. 2.6 Schematic view of the evaporative-cooled air conditioner

Hajidavallo and Eghtedari [35] built an evaporative cooler and coupled to the existing air-cooled condenser of a split air-conditioner in order to measure its effect on the cycle performance under various ambient air temperatures up to 49°C as shown in Fig. 2.6. Their experimental results showed that the power consumption of the air-conditioner can be reduced up to 20% and the system COP can be improved around 50%. Youbi-Idrissi et al. [36] developed a numerical model for a sprayed air-cooled condenser coupled to the refrigeration system to study the effect of sprayed water flow rate on the energy performance of the system. They found that compared to a dry air-cooled condenser, both the calorific capacity and system COP increase by 13% and 55% respectively.

Yu and Chen [37] investigated how the COP of air-cooled chillers can be improved by using mist pre-cooling as shown in Fig. 2.7 Their results estimated that around 18% decrease in the annual electricity usage could be achieved with mist pre-cooling of air entering the air-cooled condenser of the chiller, serving a hotel in a sub-tropical climate. Similar study was carried out by Vrachopoulos et al. [38]. They used a system of drop cloud via water spraying to an air-cooled condenser. Their results showed the energy saving up to 58% by using this method.

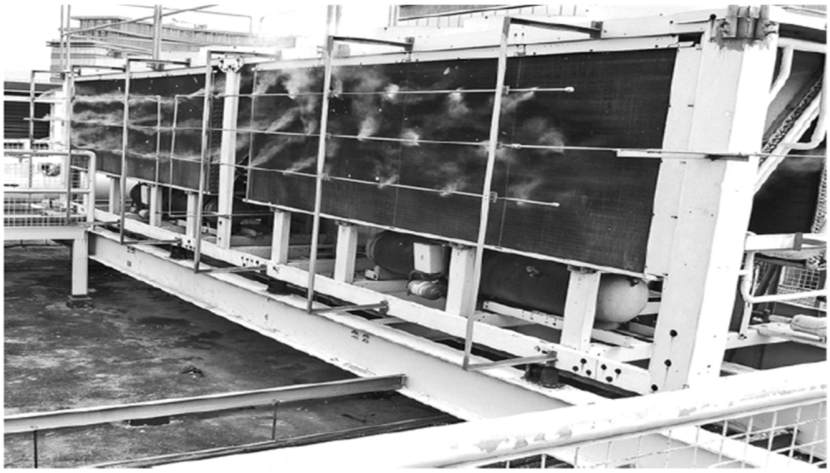

Fig. 2.7 Pipe and nozzle layouts of a mist system for the condenser of an air-cooled chiller

2.2.3 Ground Coupled HVAC Systems

Ground-coupled technology relies on the fact that, at depth, the Earth has a relatively constant temperature that is colder than the air temperature in summer and warmer than the air temperature in winter. In this system, under cooling mode, operation heat is discharged to a ground loop that provides a lower temperature heat sink than ambient outdoor air temperature. During winter heating operations, heat is extracted from a source that is at a higher temperature than ambient outdoor air. This system has been used on a residential and commercial scale since the 1920s [39]. Studies on vertical close-loop ground-coupled heat pumps show a yearly reduction of 30% to 70% in electrical energy consumption for heating and cooling when compared to air-to-air heat pump systems in a southern climate [40]. As reported in one study [41], the COP of a ground source heat pump (GSHP) was higher than that of air source heat pump (ASHP) by 74%, due to lower condensing temperatures in the GSHP system. Another study [42] compared the GSHP and ASHP for an archives building; results showed that while the initial cost for GSHP is more than ASHP, the operating cost of the GSHP can be reduced by 55.8% with a payback time of about two years. However, GSHPs capture only a small percentage of the heating and cooling market due to the high cost of installing the ground heat exchanger, which can increase system costs by 20-30% [43]

and the initial capital cost by 30-50% when compared to air source units [44]. Nevertheless, these systems can reduce operating costs via taking benefit of off-peak electricity tariffs [45, 46]. This system was widely used in Europe and USA between 2004 and 2007 [47], and about 60% of total public HVAC installations in Korea in recent decades [48]. In China, use of this system is rapidly growing [49]; between 1985 and 2007, there has been increased number of patent applications for this system with 278 patents issues and 157 patents under examination [50]. Furthermore, it is estimated that about 1.1 million ground source heat pumps have been installed around the world [47]. Compared with standard technologies such as vapour compression systems, ground-coupled heat pumps create less noise, reasonable environmental safety [51] and can reduce greenhouse gas emissions by 66% or more compared with conventional heating and cooling systems.

Jeon et al. [52] measured and analysed the performance of a hybrid cooling system that combines a screw water chiller with a ground source heat pump (GSHP) as demonstrated in Fig. 2.8. The COP of the combined system was lower than that of a conventional chiller but the configured system helped to stably provide the required cooling demand at high-load conditions. They also simulated the performance of the proposed system by varying operating parameter and found that the chilled water temperature is the effective control parameter. Results showed that by proper control of the chilled water temperature a lower power usage can be achieved while maintaining comfort conditions for the building.

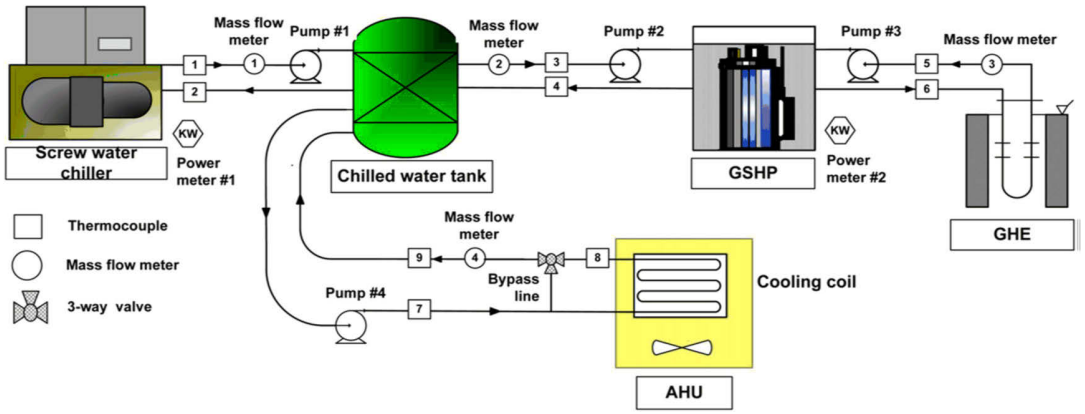

Fig. 2.8 Schematic diagram of the hybrid cooling system that combined an air-cooled screw chiller with a ground source heat pump

2.2.4 Thermal Storage Systems

Thermal storage systems (TSS) shift the energy usage of the HVAC systems from on-peak to off-peak periods to avoid peak demand charges. TSS are also able to rate variance between energy supply and energy demand to conserve energy [34]. In this system, Energy for cooling is stored at low temperatures normally below 20°C for cooling, while energy for heating is stored at temperatures usually above 20°C [53]. Compared to conventional HVAC systems, TSS offers various advantages for heating and cooling systems, such as energy and capital cost savings, system operation improvements, system capacity extending and equipment size reduction, resulting in a technology that is widely used. Yau and Rismanchi reported that in early 1990s, about 1500-2000 units of TSS were employed in the U.S. for office, school and hospital buildings [54]. Cooling thermal storage can be classified according to the thermal medium as presented by Al-Abidi et al. [55] and shown in Fig. 2.9.

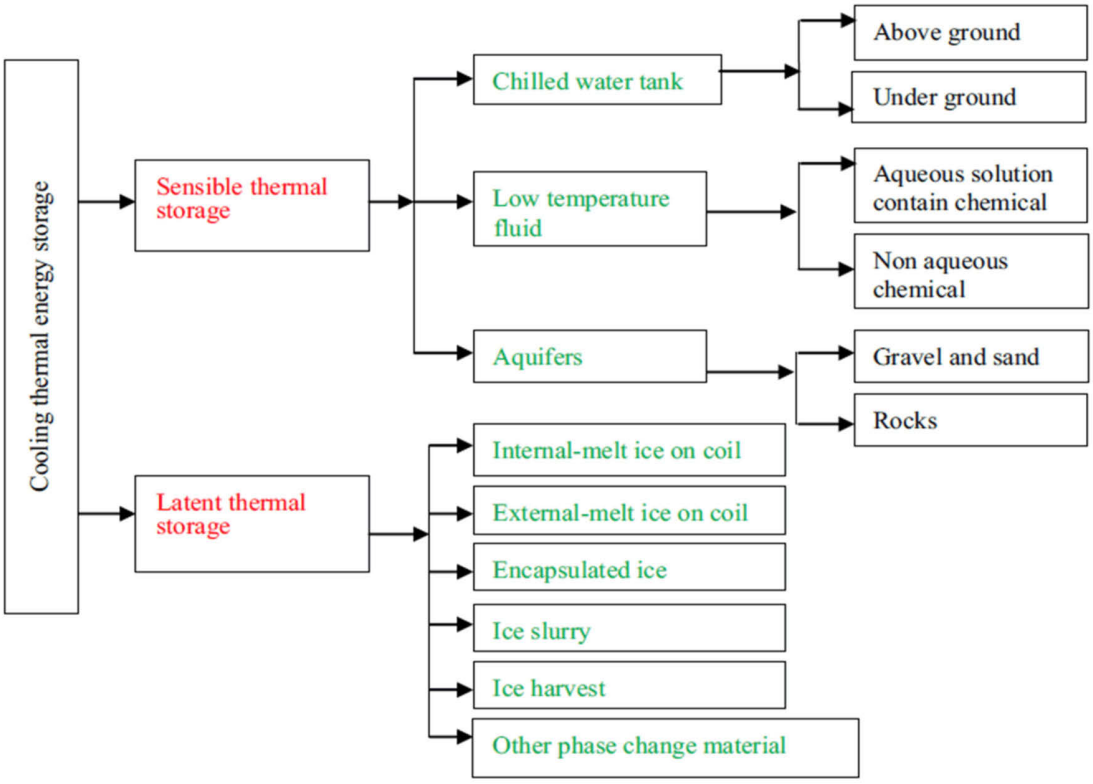

Fig. 2.9. Classification of cooling thermal energy storage

A thermal storage system can meet the building heating and cooling loads when these loads are of short duration, occur infrequently or are cyclical. This system is very beneficial when the building loads are not coextensive with energy source obtainability. Ice and chilled-water storage systems are two most commons TSS. In these systems, ice or chilled water is stored in tanks to cool buildings during peak electricity usage periods. In an ice storage system, ice is usually generated using glycol or brine solutions. There are various types of ice storage systems. An ice harvester system uses an open insulated storage tank and a vertical plate surface which is located above the tank. During the charging period, water flows on the outside surface of the evaporator and forms ice sheets. Ice slurry is another type of the ice storage system in which a glycol-water solution passes through pipes submerged in an evaporating refrigerant to form the ice. The generated ice particles are then dropped into the storage tank.

In an ice-on-coil system, the refrigerant is evaporated by a coil submerged in water. The remaining cold water in the storage tank is then used for cooling in air-handling units. Often, this system is employed for industrial applications as it requires significant amounts of refrigerant. Furthermore, when determining the design parameters of this system, both the energetic and exergetic behaviour of the system should be considered as reported by Ezan et al. [56], whose study concluded that the storage capacity and energy efficiency of this system increases as a result of decreasing the inlet temperature of the heat transfer fluid and increasing the length of the tube, while exergy efficiency increases in response to increasing the inlet temperature of the heat transfer fluid and increasing the length of the tube. However, it is worth noting that ice storage systems may use more natural resources because they have lower COP than conventional air conditioning systems and also because the natural resource usage for generating a kWh electricity during off-peak periods is higher than that in the peak periods. On the other hand, applying the ice thermal storage on air conditioning systems will increase the load of the peak generating unit during the off-peak periods which decreases the natural resource consumption for generating kWh electricity. As a result, it is necessary to calculate the effect of applying ice thermal storage air conditioning system on the natural resource consumption [57].

Chilled water storage tanks are normally charged with water at 4-6°C. Full chilled water storage system can reduced peak cooling electric demand by 80% to 90% compared with conventional cooling systems [58]. It should be noted that thermal storage systems do not necessarily save energy, but can considerably diminish the energy cost: a comparison study between conventional air cooling system and ice thermal storage cooling system carried out by Chaichana et al. [59] showed that the full ice thermal storage can reduce 5% of system energy consumption but can save up to 55% of the electricity cost required for cooling per month.

There are two types of thermal storage systems: full storage and partial storage. In the full TSS, all refrigeration compressors cease to operate in on-peak hours and the building cooling demand during that period is completely offset by the chilled-water supplied from the thermal storage tank. Partial TSS is classified by load levelling mode and demand limited mode. In load levelling mode, compressors are operated at full capacity during on-peak hours, while in demand limited mode only part of the compressors is operated.

Cold storage systems have also been used for the purpose of cold-air distribution, which allows cooled air to be supplied at lower temperatures. This causes a reduction of 30% to 40% in fan electrical demand and energy consumption [60]. For example, Nagano et al. [61] proposed a floor supply air conditioning system in which a granular latent heat storage material was used by impregnating foamed glass beads with paraffin wax. As shown in Fig. 2.10, in this system the temperature of supply air entering the under floor space is reduced by using the granular PMC. Their simulation results for an office building indicated that about 89% of the daily cooling load could be stored each night by this system when using a 30 mm thick packed bed of the granular phase change material.

2.2.5 Heat Recovery Systems

ASHRAE standards recommend the amount of required fresh air for different buildings. Unconditioned air greatly increases the building's cooling needs, which ultimately leads to

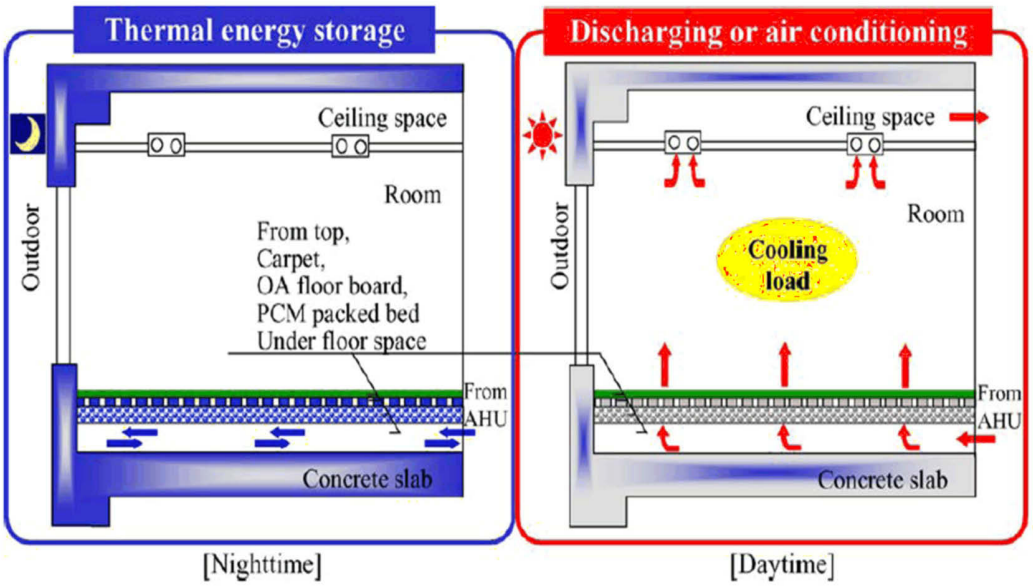

Fig. 2.10 Concept of the floor supply air conditioning system using granular phase change material

an increase in the overall energy consumption of the building's HVAC systems. In the central cooling plant, the amount of fresh air is determined based on the upper limits of the concentrations of indoor air pollutants which normally is between 10% and 30% of the total air flow rate [62]. In modern buildings the ventilation losses can become more than 50% of total thermal losses [63]. However, mechanical ventilation can consume up to 50% of electrical power used in residential buildings [64]. In addition, in hot and humid regions mechanical ventilation systems appropriate about 20% to 40% of the total energy usage of the air conditioning systems [65].

Heat recovery techniques can be used to recover energy that might otherwise be wasted. The objective of heat recovery is to reduce the cost of operating an HVAC system by transferring heat between two fluids such as exhaust air and fresh air. According to ASHRAE handbook of HVAC Systems and Equipment (2008) [60] there are three types of heat recovery systems: comfort-to-comfort, process-to-comfort, and process-to-process. Comfort-to-comfort systems use exhaust air that is captured and reused as the waste heat energy to precondition the fresh

air coming into the HVAC system. This type of heat recovery system can be used as the sensible heat recovery mode and in total heat transfer mode. Usually, rotary wheel heat exchangers are used for comfort-to-comfort heat recovery systems [60]. Process-to-comfort and process-to-process systems perform sensible heat recovery. Different types of heat recovery systems, which are used to recovery energy between supply and exhaust airflows, consist of fixed plate, rotary wheel, heat pipe and run-around coil [60]. However, heat and moisture recovery can save around 70% to 90% of the energy that is used for cooling and dehumidifying the fresh air [66] but it should be noted that the investment and running costs are the major expenses associated with heat recovery systems [67].

To investigate the potential of the heat recovery systems, an experimental analysis was carried out by Fernandez-Seara et al. [68] on an air-to-air heat recovery unit equipped with a sensible polymer plate heat exchanger for ventilation systems in residential buildings. The layout of their system and its heat recovery unit are shown in Fig. 2.11. As a part of their results, the heat transfer rate increased almost linearly as the air flow rate increased. The heat transfer rate increased around 65% by increasing the air flow rate from 50 m^3/h to 175 m^3/h. In their system the fresh and exhaust air were arranged in the counter-flow direction. They also mentioned two key issues for the heat recovery heat exchangers: when using air-to-air heat recovery units it should be considered that water will condense on the heat exchanger surface if the exhaust air is cooled below its saturation temperature. Furthermore, if the incoming air temperature drops below 0°C, the frost formed in the heat exchanger will block the air flow through it.

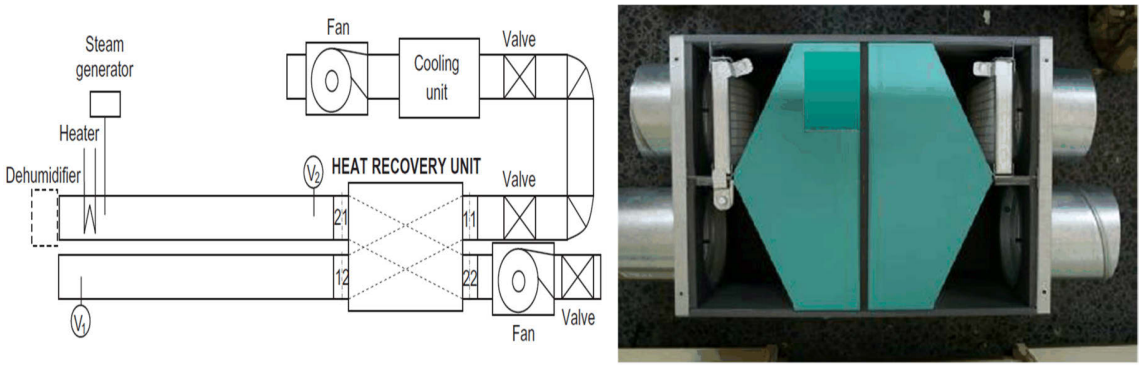

Fig. 2.11 Left: Layout of the experimental facility of the heat recovery unit, Right: Heat recovery unit

2.2.6 Adsorption Systems

The interest in adsorption systems was started to increase in the 1970s [69]; however, the first adsorption cooling system was developed by Michael Faraday in 1848 using ammonia and silver chloride as the working pair. This system can operate at temperature levels where liquid absorption systems cannot work [70]. Adsorption system can be powered by heat sources with temperature as low as 50°C while in absorption systems the source should be at least 70°C. Furthermore, while using heat sources with temperature above 200°C in absorption chillers cause corrosion, the heat sources with temperature close to 500°C does not produce any corrosion problem. In addition although adsorption chillers are more efficient for hot and dry regions, their COP is less than that of absorption chillers under the same conditions which limits them to be widely used. However, when the temperature of heating medium is in the range of 60°C to 95°C, the COP of the adsorption chillers is between 0.6 and 0.7. Comparatively bigger sizes of adsorption cooling systems are preventing successful commercialization of this technology [71]. This system can be classified as solid/gas, liquid/gas, solid/liquid and liquid/liquid [72]. Working pairs used for adsorption chillers are mostly silica gel-water, zeolite-water, activated carbon-methanol, activated carbon fibers-methanol, activated carbon-ethanol and activated carbon-ammonia; the activated carbon-ammonia is preferred for deep freezing application whilst the zeolite-water is the best for air conditioning application. Among different type of these working pairs, silica gel needs less heat of adsorption than zeolite and most carbons. However, when using silica gel-water as working pair, the adsorption bed would be three times as large as one of zeolite to produce the equivalent cooling effect [73].

Results of the solar-assisted adsorption cycle evaluation show that its performance is yet lower than that of the solar-assisted absorption cycle and needs improvement. For example, Lu et al. [74] investigated the performance of a solar thermo-syphon silica gel-water adsorption chiller and a LiBr-H_2O absorption chiller with a compound parabolic concentration solar collector. These systems are shown in Fig. 2.12. Experimental results indicated that the adsorption chiller could provide 15°C chilled water with an average COP of 0.16 while this chilled water

temperature can be produced by absorption chiller with an average COP of 0.19.

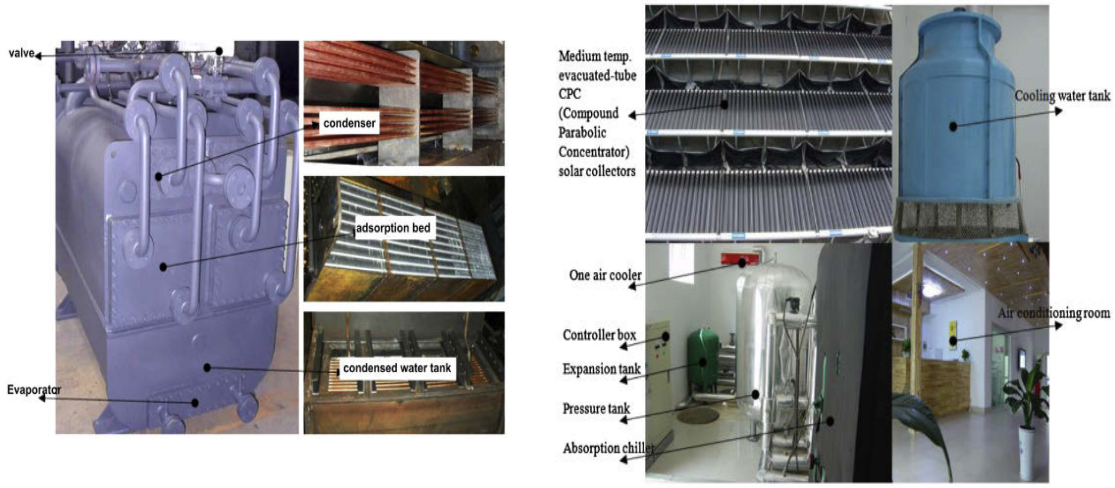

Fig. 2.12 Left: Solar adsorption air conditioning system, Right: Solar absorption air conditioning system

2.2.7 Desiccant Systems

The basic idea of desiccant air conditioning systems is a combination of the dehumidification of the air by desiccant materials and then use of a cooling method which is either an evaporative cooling or a conventional cooling coil to cool the air. A hybrid desiccant/evaporative cooling system is used to improve the cooling potential of the evaporative cooling system while in a combined desiccant/cooling coil, the desiccant unit is used to remove the latent load of supply air and the cooling coil removes the sensible load. However, the performance of this system is significantly dependent on climatic conditions. Desiccant materials such as silica gel, zeolite, activated carbon, activated alumina, molecular sieve, calcium bromide, lithium bromide are commonly used for desiccant air conditioning systems. However, liquid desiccant system has several advantages compared with solid desiccant system including lower required regeneration temperature, lower pressure drop and potential to remove a number of pollutants [75-77]. In the solar desiccant system, solar energy provides the regeneration of the desiccant. The required heat is in the range of 50-100°C depending on desiccant material and degree of dehumidification [78].

Results of experimental work on desiccant systems show that the solar driven desiccant cooling system can handle significant amount of the cooling load when combining with conventional vapour compression system and therefor can reduce their power consumption. For example, Li et al. [79] configured a solar-assisted desiccant cooling system with a conventional vapour compression air conditioning system and studied its energy performance and economic feasibility. The desiccant cooling system could reduce the capacity of vapour compression system in the hybrid configuration to 19 kW while the capacity of stand-alone vapour compression system was 28 kW. The simulation results for the hybrid system showed a reduction of 6760 kWh in annual operation energy usage with a payback period of 7 years. In another project Beccali et al. [80] proposed a hybrid configuration that used two auxiliary cooling coil fed by a conventional compression chiller: one coil for pre-dehumidification and other coil for control the air temperature in the case that desired supply temperature cannot be reached through desiccant evaporative cooling. Fig. 2.12 and 2.13 show system configuration and its main component and the thermodynamic cycle in the psychrometric chart for summer and winter operation. In this design, the heat rejected by the chiller was used to preheat regeneration airflow. This allows a reduction of the solar collector area by about 30%. Results indicated that desiccant evaporative cooling system could cover about half of the total cooling energy delivered by air-handling unit. Also up to 50% primary energy saving was possible in summer when comparing with the conventional central cooling plant.

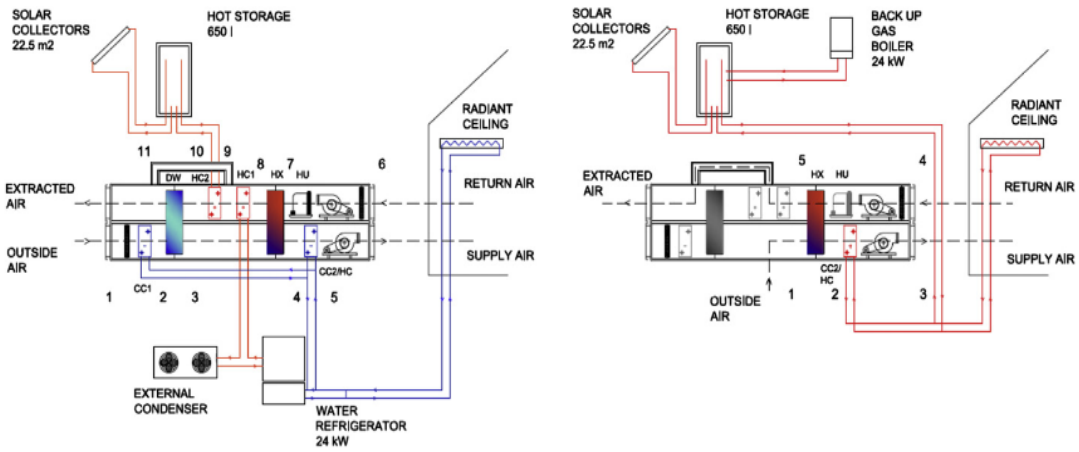

Fig. 2.13 Functional scheme: summer operation (left) and winter operation (right)

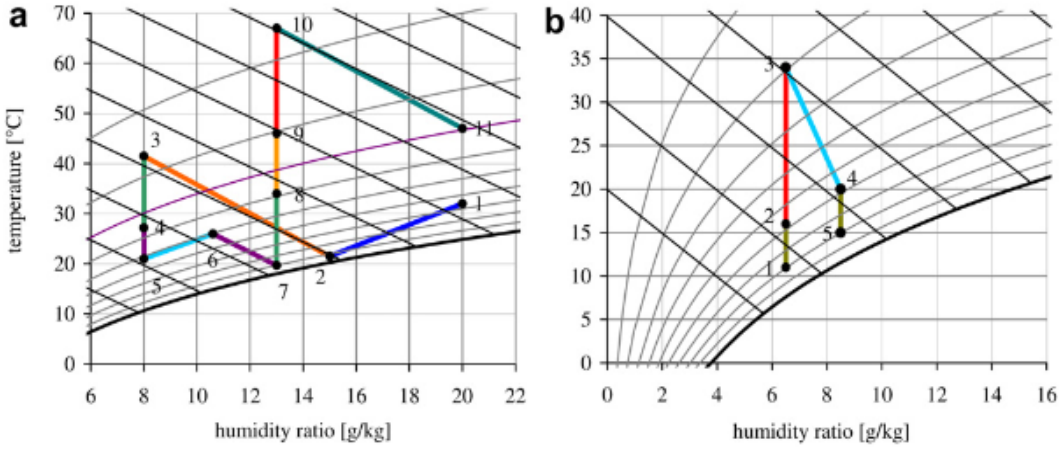

Fig. 2.14 Psychrometric chart: (a) summer operation and (b) winter operation

2.2.8 Photovoltaic and Photovoltaic/Thermal Systems

Basically, the photovoltaic (PV) cells are used to transform the solar radiation into the electricity. They are consists of a surface with two thin layers of doped semiconductor material. Reported price data for more than 150,000 installed PV systems show that, among systems installed in 2011, the median reported price was $6.13/W for residential and small commercial systems 10 kW capacity or less, and $4.87/W for commercial systems larger than 100 kW [81]. Advancements of solar electricity production from photovoltaic have been made since the beginning of 1980s while the first photovoltaic cell was invented at 1950s [82]. The conversion efficiency of PV cells is in the range of 10-20% for commercially available silicon cells and up to 39% for multi-junction cells [83]. However, the electrical efficiency of the PV panel is reduced when its temperature increased [84]. Furthermore, thermal systems can utilize more of the incoming sunlight than photovoltaic systems. The hybrid photovoltaic-thermal (PV/T) collectors are developed to solve this problem by reducing the temperature of PV collectors. At the same time, the heat loss to the environment is reduced due to the lowered surface temperature of the PV/T collectors [85]. The first work on a PV/T system has been reported in 1976 [86]. Using PV/T as a practical technology [87], the electrical and thermal energies can be generated simultaneously which can significantly

improve the energy performance of the HVAC systems. In economic point of view, the costs of solar thermal cooling are not projected to decrease as much as PV cooling over the next 20 years due to the relatively stable cost of collection and storage [88]. However, in the International Energy Agency (IEA) [89] solar PV roadmap vision, PV is projected to provide 5% of global electricity consumption in 2030, rising to 11% in 2050.

Several research have already been reported about the application of the PV and PV/T collectors on HVAC energy efficiency. Hartmann et al. [90] compared the energy performance of a conventional compression chiller when combining to two different solar options: solar thermal and solar electric collector. The grid coupled PV system showed lower costs of primary energy saving than the solar thermal system. Results also indicated that the collector area of the solar thermal system has to be more than six times larger than the corresponding solar electrical collector field to obtain the equal saving energy potential. Sukamongkol et al. [91] investigated the performance of a condenser heat recovery with a PV/T air heating collector to regenerate desiccant for reducing energy use of an air conditioning room as shown in Fig. 2.15. Their experimental test and dynamic simulation indicated that electricity of about 6% of the daily total solar radiation can be gained from the PV/T collector. The proposed system was able to save about 18% of the total energy use by air conditioner.

2.2.9 Ejector Systems

Ejector cooling technology is another energy-efficient strategy with more installation, maintenance and construction simplicity than conventional vapour compression refrigeration systems. In an ejector refrigeration system the compression may be obtained without using mechanical energy [92]. The development trend and history of this technique has been investigated by Elbel and Hrnjak [93]. In a heat pump system, the ejector takes the place of the electrically driven compressor, but uses heat rather than electricity to produce the compression effect. This system usually needs a heat source with the temperature more than 80°C.

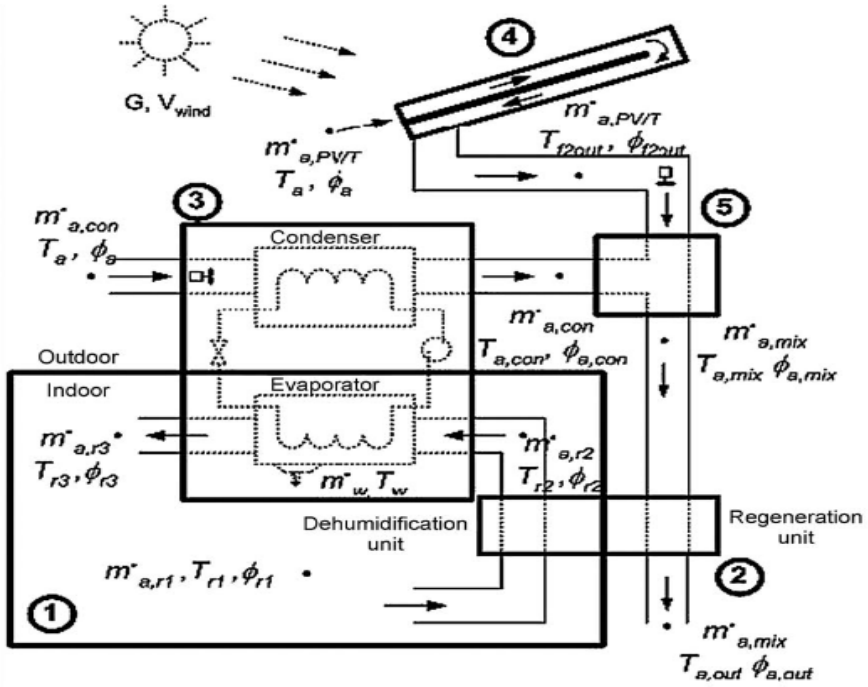

Fig. 2.15 Schematic diagram of a condenser heat recovery with a hybrid PV/T air heater (1): living space, (2): desiccant dehumidification and regeneration unit, (3) air conditioning system, (4) PV/T air heating collector, and (5) air mixing unit

Compared with vapour compression systems, the ejector cooling systems have lower COP normally less than 0.3 [94].Due to ejector advantages such as its simplicity construction, absence of moving parts, operation at low temperature and low operational cost, the ejector cooling system has been attractive for the air conditioning and refrigeration applications. The ejector is composed of a primary nozzle, a mixing chamber, a throat and a diffuser as shown in Figs. 2.16 [95] and 2.17 [96]. The primary flow enters the ejector at high temperature and high pressure, the superheated steam accelerates and expands through the primary nozzle, at the outlet of the nozzle exit, this flow spreads out with a supersonic speed and creates a low pressure region, the secondary flow is then entrained into the mixing chamber. In the beginning the two fluids don't choke until the entrained flow rise to sonic value, once choked, the mixing process begins and causes the primary flow to be delayed whilst secondary flow is accelerated,

at the end of the mixing chamber domain, the two flows are completely mixed, a shock wave takes place at the level of the throat due to the high pressure downstream of the mixing chamber throat [95].

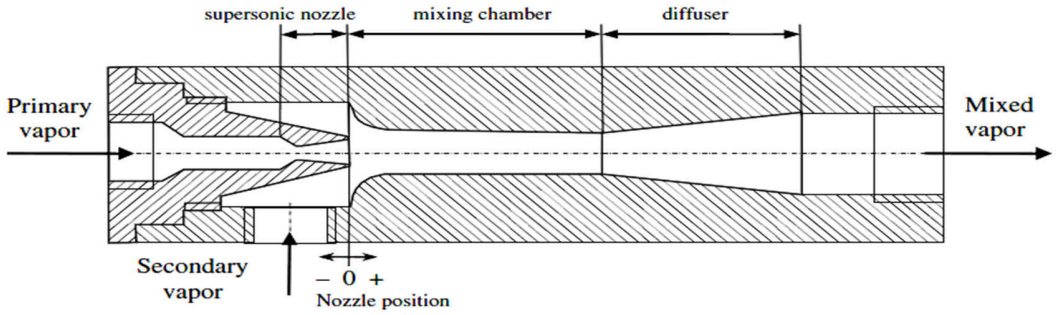

Fig. 2.16 Ejector geometries

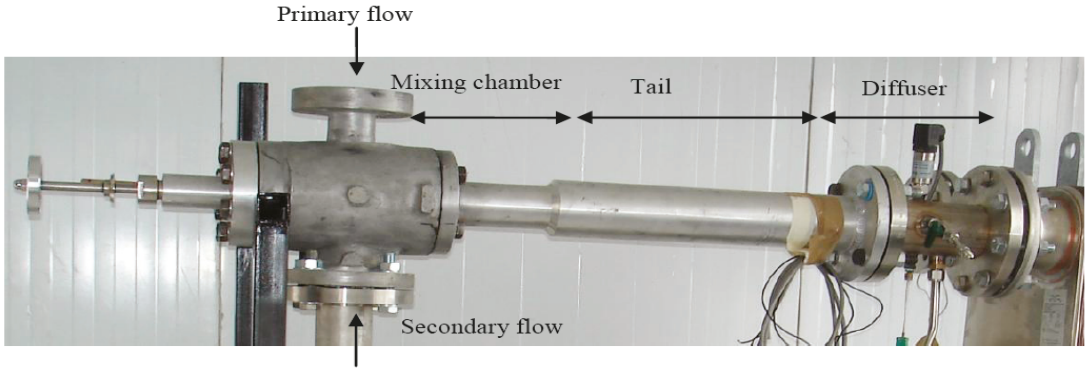

Fig. 2.17 Photo of Ejector

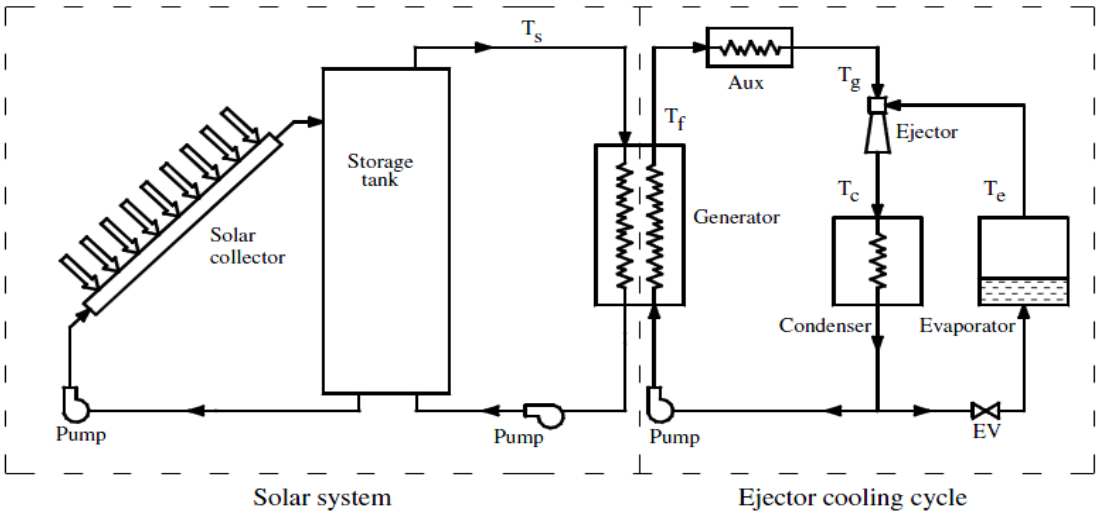

Fig. 2.18 Ejector cooling system assisted by solar energy

The main components in a solar-driven ejector refrigeration system are solar collector, hot water storage tank, auxiliary heater and ejector cycle as shown in Fig. 2.18 [97]. According to this cycle, the water is warmed up and circuited between collector and storage tank using the pump located in the upstream the collector. The hot water from the storage tank is then carried to the generator to vaporise the refrigerant coming from the condenser. If the heat provided by the generator is not sufficient, the auxiliary heater located downstream the generator will perform as an additional source to provide the required conditions for the ejector. This high pressure superheated vapour flow is then mixed with the low pressure vapour flow of the refrigerant coming from the evaporator at the mixing section of the ejector where an aerodynamic shock is induced to create a compression effect [97]. The mixed stream is discharged by using a diffuser to the condenser where heat rejection is occurred. The refrigerant flow leaving the condenser passes the expansion device where its pressure is decreased and then goes to the evaporator to absorb the heat at low temperature from the air or water. The remaining refrigerant is pumped into the generator and vaporised using the heat from the solar collector and hence completing the cooling cycle. Figures 2.19 (a) and (b) demonstrate the schematic diagram of the ejector cooling system and its P-h diagram respectively [97]. It has been shown that the performance of this system is highly dependent on design parameters such as condensing temperature and pressure and evaporative temperature [98].

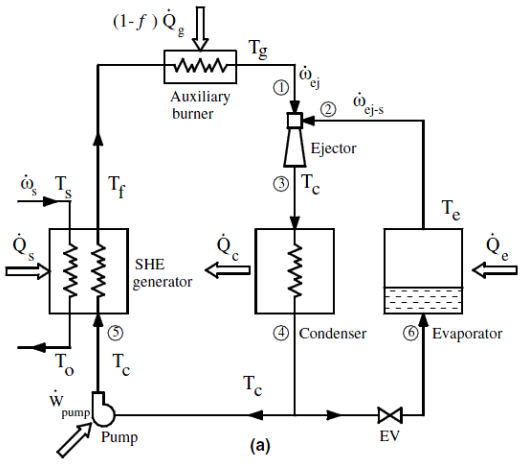

Fig. 2.19 (a) Schematic diagram of ejector cooling cycle with heat exchanger conjugated

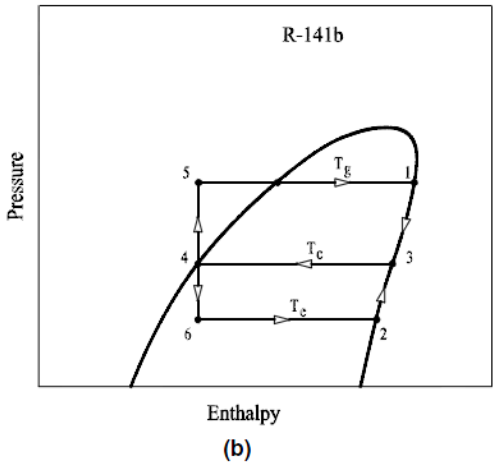

Fig. 2.19 (b) P–h diagram of the ejector cooling cycle

The potential of integrating a conventional vapour compression system with a solar-powered ejector cooling system is evaluated by Chesi et al. [99] as shown in Fig. 2.20. Their simulation results showed that the proposed system included of 100 m^2 solar collector, a 5 m^3 water storage tank and an ejector with 6.5 mm primary throat diameter can increase the average yearly COP of the conventional vapour compression system by 15% for a cooling capacity of 1 kW.

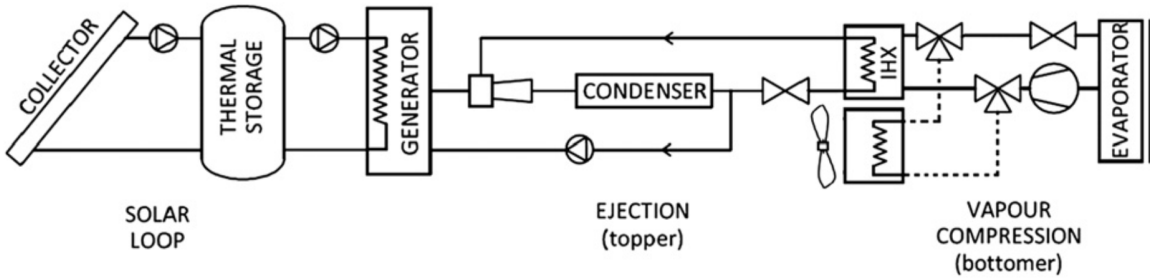

Fig. 2.20 Layout of solar-assisted ejector cooling system

2.3 Other Strategies

Many studies have been carried out on energy savings for HVAC systems that result from the use of materials with enhanced capacity to absorb, store and release the mass or heat. Sometimes, modifying the design criteria enables air conditioning systems to work more efficient without imposing additional costs. One of the criteria that can be modified is adjusting the building's indoor temperature at a hogher set point during the period in which the building is unoccupied. Another option is to re-circulate the outdoor air inside the building during the unoccupied period when its temperature is less than the desired unoccupied indoor temperature. Sometimes although new configuration of HVAC systems leads to reduce their energy consumption, it may change the system operational set-points. This can reduce the potential of the system to maintain the comfort conditions inside the building [100]. The solution here is to employ other techniques to fulfil the problem, although this has the potential to increase the initial system cost [101]. In these cases, an economic

comparison must be made to determine whether the new system will provide payback of the additional costs within a reasonable timeframe.

Some methods are only effective under special conditions. One example is liquid pressure amplification (LPA) approach, which results in significant energy savings for vapour compression refrigeration systems. In this method, a liquid pressure pump is installed in the outlet line of the condenser after the liquid receiver. The pump provides the stable pressure needed for the expansion valve and allows the condensing pressure, and hence the compressor delivery pressure, to float with ambient temperatures [102]. Figure 2.21 shows the concept of this method on p-h diagram. In the conventional vapour compression refrigeration system, the condensing pressure is designed to allow the refrigerant condensation at high ambient temperature. In this way, the energy is wasted in partial load when the ambient temperature is low and that much condensing temperature is not required. In this method, a refrigerant pump is considered after the condenser's receiver in the liquid line to preserve the high pressure differential across the expansion valve. Consequently, condenser pressure can be varied with variation of the ambient temperature resulting in lower discharge pressure during the partial load period and in turn reduction of the compressor power consumption. Therefore, the compressor head pressure is reduced from point (3) to point (b) at steady state conditions as shown in Fig. 2.21. In addition, a small amount of the liquid sub-cooled refrigerant is injected into the compressor discharge line using a secondary pump. Therefore, the temperature of discharge refrigerant gas entering the condenser is decreased which yield to reduce the difference between the ambient and condensing temperature and thus increase the effective efficiency of the condenser. This is shown in Fig. 2.21 by moving the point (b) to point (c). The superheated refrigerant then enters the air-cooled condenser where a final reduction in refrigerant temperature takes place and causes it to de-superheat and thus the refrigerant liquid is sub-cooled as it enters the expansion valve. As a result, refrigeration effect of evaporator is increased enabling the system to deal with higher load demand. As demonstrated in Fig. 2.21, this is occurred by replacing the point (1) to point (a) in the refrigeration cycle. The high pressure sub-cooled refrigerant flows through the expansion valve, at point (d), which serves to reduce its pressure.

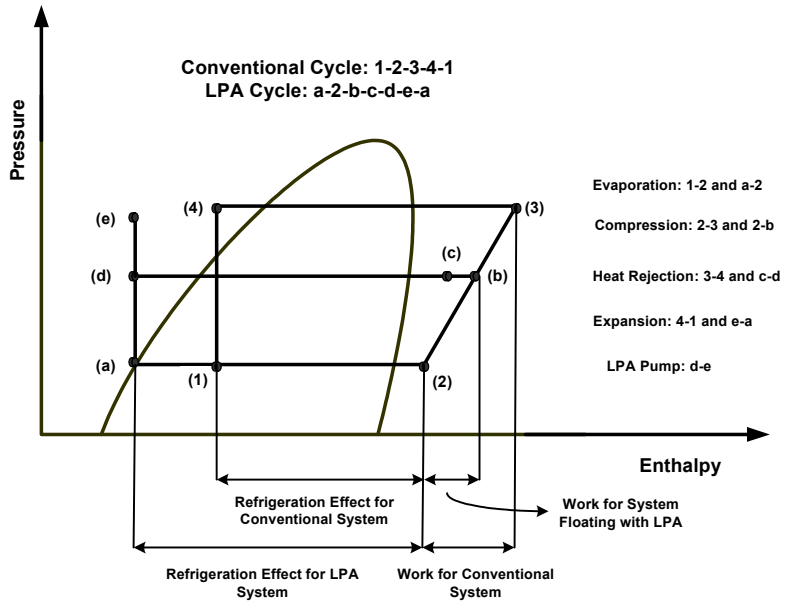

Fig. 2.21 P-h diagram for LPA system

However, due to required minimum pressure difference across the expansion valve for proper operation of thermostatic expansion valve, the amount of the discharge pressure that can be reduced is limited [103]. Therefore, the energy saving potential of this method is a function of the minimum acceptable pressure differential across the expansion valve as well as ambient temperature.

Fasiuddin and Budaiwi [104] investigated the impact of different HVAC system strategies on energy conservation in a commercial building in Dhahran, Saudi Arabia. Their results demonstrated that using variable air volume (VAV) system instead of unitary system could save energy around 22%. Also they found that an increase in indoor temperature by 3°C results in 17% of saving. Modifying the fan operation schedule gave saving about 21.4%. The use of 28°C set point temperature during unoccupied periods resulted in 18% saving. However, they concluded that energy saving of about 25% can be achieved in combination of different HVAC operation strategies.

Using the energy management systems (EMS) can be considered as another efficient method which can lead to HVAC energy usage reduction. It has been reported in several studies that adjusting the system variables to their optimum set-points can significantly reduce the energy consumption. Lee et al. [105] developed and implemented an energy management system for a series of centrifugal chillers. The EMS system was able to reduce the total annual electricity consumption of the chillers by 23.2%. Plessis et al. [106] developed an energy management system for a deep-mine cooling system. The energy management system was consisted of a supervisory controller which optimized the variable set-points of the real-time system component. Their energy management system led to an average electrical energy saving of 33.3%.

2.4 Discussion on Different Strategies

Energy-efficient HVAC system designs depend on new configurations of traditional systems that make better use of existing parts. One effective way of achieving energy efficiency has been the design of HVAC system configurations that combine a range of different traditional HVAC system components. Recent research has demonstrated that a combination of existing air conditioning technologies can offer effective solutions for energy conservation and thermal comfort [107]. Each HVAC discipline has specific design requirements and each presents opportunities for energy savings. It must be understood, however, that different configurations in one area may augment or diminish savings in another. For example, a new configuration might improve system performance and thus raise its energy saving potential, but this raises the upfront cost of the system. Consequently, it is important that the use of a new configured system results in electricity savings that are large enough to pay back initial investments in a suitably short time. In this regard, a newly-developed system that can heat and cool at low cost is very desirable because of the increased financial savings on offer. The literature shows that a blend of air conditioning technologies can offer effective solutions for energy conservation and thermal comfort. The main aim of this comparison study between various types of HVAC systems is to find the optimum configuration for air conditioning systems that provide maximum cooling performance while minimizing electrical power

consumption, with a view to slowing the rampant growth of daily peak demand on the electricity grid in summer. In this regard, the architectural limitations of the building must be taken into account. This would reduce the number of possible HVAC systems that are suitable for installation in a commercial or residential building. Additionally, climatic conditions may influence the final system selection. In vapour compression air conditioning systems, the water-cooled units have a higher COP than air-cooled units due to their lower refrigerant condensing temperature [108]. However, since the performance of cooling tower as the main part of water-cooled systems is highly dependent on ambient relative humidity, then water-cooled air conditioning systems cannot be used in areas with high ambient relative humidity. It has been estimated that the efficiency of evaporative cooling system such as cooling tower and air washers is significantly increased when the ambient relative humidity is lower than approximately 40% [109]. However, in dry regions, evaporative cooling systems can cut the electricity consumption of the vapour compression systems as discussed in this chapter. Furthermore, when lower comfort conditions are required, then using the evaporative cooling system alone is an appropriate selection. However, evaporative cooling systems require 100% outdoor air and exhaust capability and thus the cost of equipment area, filter capacity and air delivery must be weighed against the energy savings of evaporative cooling versus refrigeration cooling.

Another issue that drastically increases the energy usage of HVAC systems is the requirement for fresh air in the buildings they cool. The amount of fresh air for a building is dependent on the type of activities taking place in the building. However, in the case that a building needs more fresh air to produce positive pressure inside the space, using a heat recovery system is the best option. For buildings with lower fresh air level quotas, controlling and adjusting the fresh air flow rates based on design criteria is a more efficient method. Thermal storage systems are appropriate when maximum cooling load is significantly higher than the average load. Therefore, these systems are normally used for commercial and industrial buildings but have fewer benefits in residential buildings. Among the buildings most suited to thermal storage systems are buildings with high cooling, short duration demands. Although capital costs for this sort of systems tend to be higher than a conventional system, but smaller

ducting system for the thermal storage system can compensation that additional cost. While this system has higher upfront costs, its reduced energy usage will result in significant long-term savings as a result of lower energy bills. A ground-source heat pump takes advantage of more benign climates belowground, limiting the efficacy of this sort of system for aboveground installations. Furthermore, other factors such as maintenance and cost of repairs would cost more compared to other HVAC systems. Determining the most appropriate HVAC system option for a given building is a complex exercise that requires detailed analysis of cost and energy savings and offsets, as well as a holistic analysis of various internal and external factors. Perhaps, one strategy is suitable for summer while it is not energy-efficient for winter. In this case, choosing individual systems for summer and winter should be analysed to give the optimum solution. Although due to practical matters, considering all of these factors simultaneously is difficult, but a designer should heed and exploit the best energy reduction strategies by attending all technically, economically and applicability facts. However, some of discussed methods in this chapter can be retrofitted to the existing conventional HVAC system. The cost, advantages, disadvantages, application and projected improvement of all aforementioned technologies are summarised as followings:

- **Direct Evaporative Cooling Systems**

•Capital cost: They are among the very cheap air conditioning systems.

•Advantages: Reduction of pollution emissions/ life cycle cost effectiveness/ reduction of peak demand. In areas where the 0.4% mean coincident wet-bulb design temperature is 19°C or lower, average annual cooling power consumption of indirect/direct systems may be as low as 0.06 kW/kW of refrigeration [60].

•Disadvantages: Cannot effectively work when ambient relative humidity if higher than 40%. This system has the disadvantage that if the ambient wet-bulb temperature is higher than about 21°C, the cooling effect is not satisfactory for indoor comfort cooling; however, cooling is still sufficient for relief cooling applications such as greenhouses and industrial cooling [60].

- Application: When comfort conditions are not target.
- Projected improvement: Their performance can be significantly improved using several approaches.

- **Indirect Evaporative Cooling Systems**

- Capital cost: Their running and capital cost is higher than DEC systems but lower than vapour compression air conditioning systems.
- Advantages: Their air quality is considerably higher than DEC/ more energy efficient compared with vapour compression refrigeration systems.
- Disadvantages: Their installation and operation are more complex than DEC systems.
- Application: All buildings.
- Projected improvement: Still there are several opportunities to improve their performance.

- **Evaporative-Cooled Air Conditioning Systems**

- Capital cost: Water usage cost is increased while electricity usage cost is reduced. In total, this method adds less cost than other discussed methods to the air condition system.
- Advantages: Can significantly reduce the energy consumption of the air conditioning system in peak demand conditions.
- Disadvantages: Their energy saving potential is limited to a period that ambient temperature is high.
- Application: Can be applied on air-cooled vapour compression air conditioning systems.
- Projected improvement: Control methods can reduce the water usage of the evaporative-cooled condenser.

- **Liquid Pressure Amplification Systems**

- Capital cost: More expensive than conventional vapour compression refrigeration systems but cheaper than thermal storage, heat recovery, ground-coupled and desiccant cooling

systems.

- Advantages: This system results in significant energy savings for vapour compression refrigeration systems and therefore provides reasonable timeframe payback of the additional costs.
- Disadvantages: Their energy saving potential is limited to a period that ambient temperature falls to low temperature.
- Application: Can be applied on air-cooled vapour compression air conditioning systems.
- Projected improvement: This method can be applied in more air-cooled vapour compression air conditioning systems in operation today worldwide.

- **Ejector Cooling Systems**

- Capital cost: Reasonable timeframe payback of the additional costs.
- Advantages: More installation, maintenance and construction simplicity than conventional vapour compression refrigeration systems.
- Disadvantages: This system needs a heat source with the temperature more than 80°C/ Compared with conventional vapour compression systems, the ejector cooling systems have lower COP.
- Application: When enough heat source temperature is available.
- Projected improvement: Studies should be carried out to enhance the coefficient of performance of this system.

- **Thermal Storage Systems**

- Capital cost: Expensive in both capital and running cost.
- Advantages: They significantly reduce the electric energy cost/Required smaller ducting system than conventional air systems.
- Disadvantages: Their coefficient of performance is less than conventional vapour compression air conditioners.

- Application: Buildings with high cooling, short duration demands.
- Projected improvement: Robust control method can enhance the efficiency of this system.

- **Variable Refrigerant Flow (VRF) Systems**

- Capital cost: Expensive in both capital and running cost.
- Advantages: Efficient in part load conditions.
- Disadvantages: Required extra control systems/cannot provide full control of humidity.
- Application: Residential and commercial buildings
- Projected improvement: Several efforts are currently carrying out to enhance the performance of this system.

- **Heat Recovery Systems**

- Capital cost: Expensive in both capital and running cost.
- Advantages: Highly energy efficient in temperate climates.
- Disadvantages: Larger than conventional air-handling units.
- Application: Commercial buildings and buildings with high exhaust air flow rate.
- Projected improvement: Their dimension can be reduced by increasing the efficiency of heat recovery devices.

- **Ground-Coupled Systems**

- Capital cost: Expensive in both capital and running cost.
- Advantages: Compared with standard vapour compression systems, this system creates less noise and reduces greenhouse gas emissions.
- Disadvantages: Requirements of deep below the earth's surface/ Very high upfront costs.
- Application: Residential and commercial buildings
- Projected improvement: Investigations should be done to optimize the installation method and cost.

- **Chilled Ceiling Systems**

- Capital cost: Reasonable timeframe payback of the additional costs.
- Advantages: They require cooled water instead of chilled water which leads to less refrigeration.
- Disadvantages: Are unable to moderate indoor humidity/Risk of condensation at cold surface.
- Application: Public buildings
- Projected improvement: More study is required to reduce the risk of condensation using new materials.

- **Desiccant Cooling Systems**

- Capital cost: Expensive in both capital and running cost.
- Advantages: When used in conjunction with conventional air conditioning systems, humidity control is improved.
- Disadvantages: Some desiccants are corrosive/ Response time is relatively large.
- Application: Commercial buildings/Supermarkets
- Projected improvement: This system can gradually attain wider market penetration.

- **Adsorption Systems**

- Capital cost: Expensive in capital cost.
- Advantages: They are environmentally-friendly systems and consume less energy than vapour compression air conditioning system.
- Disadvantages: Their COP is very low.
- Application: Commercial buildings.
- Projected improvement: This system can gradually attain wider market penetration if their initial cost can compete with the conventional HVAC systems.

- **HVAC Systems integrated with PV or PV/T**

•Capital cost: Expensive in capital cost.

•Advantages: They can reduce the electricity consumption of the conventional air conditioning systems.

•Disadvantages: Required extra control systems

•Application: Commercial buildings/Supermarkets

•Projected improvement: New materials should be used to increase the efficiency of the PV panels. However, the cost of these materials are important.

2.5 Absorption HVAC Systems

Absorption cooling systems are the best suited for solar thermal applications [98]. The idea of the absorption cooling system was introduced in the 1700s and first patent about ammonia-water absorption system was registered by Ferdinand Carre in 1859. However, the commercial development of absorption chillers powered by solar energy began in the 1940s. Among solar air conditioning systems, solar absorption systems are most widely used as they include 59% of installed systems in Europe while this amount is respectively 11% and 23% for adsorption and desiccant cooling systems [110]. In China almost all large scale solar cooling systems during the last twenty years have been based on absorption system [111]. Absorption chillers are classified as direct- or indirect-fired and as single, double and triple effect. The COP of the single effect absorption chillers are within the range of 0.6 to 0.8 while the double and triple effect absorption chillers have respectively COP of 1 and 1.4 to 1.6.

To select of the refrigerant and absorbent for the absorption chillers, several properties should be considered. The solubility of the refrigerant in the absorber must be as low as possible at the generator temperature and pressure and as high as possible at the absorber temperature and pressure. Additionally, the absorbent should be non-volatile to avoid moving the absorbent into the condenser and evaporator. The working fluid should be non-flammable,

non-toxic and chemically stable. In terms of working fluids used mostly in commercially available units, this system is divided to LiBr-water and NH_3-water systems. In the LiBr-water system, LiBr is the absorbent and water is the refrigerant while in the NH_3-water system, water is the absorbent and NH_3 is the refrigerant. However, the COP of the LiBr-water system is higher than that of NH_3-water system [112]. Moreover, due to low freezing point of NH_3 around -77°C, the NH_3-water system can be used for low temperature applications. However, most solar absorption HVAC systems use LiBr-water. Among different types of absorption chillers, single-effect LiBr-water absorption chillers can be powered by ordinary flat plate or evacuated solar collectors due to low required operating temperature ranges. For this reason, the single-effect LiBr-water absorption chillers are most popular machine in solar cooling. Double-effect LiBr-water absorption chillers need the heat source temperature about 150°C and thus the flat plate and vacuum solar collectors cannot meet their request; a parabolic trough solar collector is required. Absorption chiller can also be classified based on the method of providing heat as:

- Direct fired chiller in which the absorbent is reconcentrated from the heat input through the combustion of gas.

- Indirect fired chiller in which the absorbent is reconcentrated from heat input from steam or hot water.

The ANSI/ARI Standard 560 [113] has specified the following rang of operating limits for the absorption chiller:

- Cooled-water temperature entering the absorber and condenser should be in the range of 26.7°C to 32.2°C.

- Cooled-water mass flow rate entering the absorber and condenser limits are 0.05 to 0.11 L/s per system refrigeration kW.

- Chilled-water flow rate in the evaporator should be in the range of 0.03 to 0.05 L/s per system refrigeration kW.

In ASHRAE Refrigeration Handbook [114], the heat input rate has been quantified for the indirect fired single-effect LiBr-water absorption chiller as 1.43 to 1.54 kW per kW of refrigeration. The heat input for indirect fired double effect LiBr-water absorption chiller is specified as 0.83 kW per kW of refrigeration.

For lithium bromide absorption chillers, the chilled water temperature leaving the evaporator is normally between 4˚C to 15˚C. The lower limit is because water freezes at 0˚C. In addition, there are limitations for cooling water entering and leaving the LiBr absorption chiller. In the very low cooling water temperature the condenser pressure drops too low and unnecessary vapour velocities convey over solution to the refrigerant in the condenser.

The LiBr-water working fluid appears more promising for solar application, however LiBr crystallise out of solution when the concentration is higher and temperature is lower than at saturation and thus blocking pipes and passages. In addition, LiBr is corrosive to metals. Nowadays, absorption chillers are designed for operation away from crystallisation. LiBr-water absorption chillers operate under vacuum. In contrast, ammonia-water absorption chillers operate at pressure higher than atmospheric pressure. Although, ammonia-water absorption chillers can always operate as air-cooled chillers, LiBr-water absorption chillers are essentially water-cooled due to the crystallisation problem. In solar applications, water-cooled condenser are preferred compared with air-cooled condenser.

There are two ways to connect the cooling tower to the water-cooled condenser in the absorption chillers. Normally, absorber and condenser are connected in series to the cooling tower where the absorber is fed first as low temperature is more critical for absorber. In another way, the absorber and condenser are connected in parallel so that both receive the cooled-water at its lowest temperature. A larger cooling tower will be required when connecting the absorber and condenser in parallel.

Several studies have investigated the technical and economic feasibility of the conventional and solar absorption HVAC systems. Du et al. [115] evaluated the feasibility and performance of an air-cooled two-phase NH_3-H_2O absorption prototype with 2 kW capacity as shown in Fig. 2.22. They achieved the system COP within the range of 0.18-0.25 in summer. Therefore, this plant can be used as a low-cost small scale cooling system for residential buildings. Elsafty and Al-Daini [116] compared the general cost associated with single- and double-effect vapour absorption and vapour compression air conditioning systems. Using the equivalent annual comparison method, they found that the total cost of the vapour compression system and double-effect vapour absorption system are respectively 6% and 45% less than that of single-effect absorption system while the double-effect system costs 37% less than the vapour compression system.

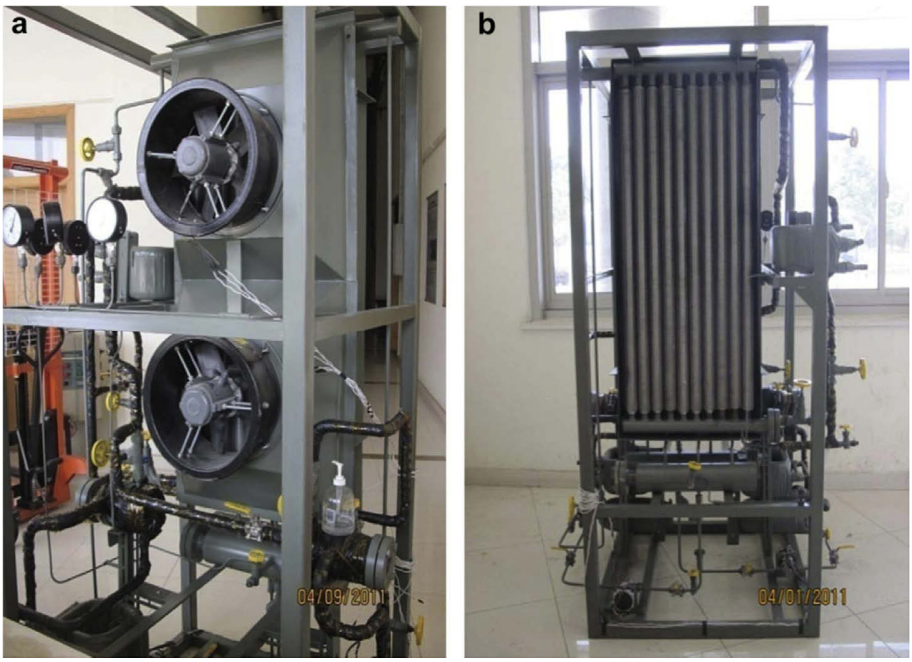

Fig. 2.22 Photos of the experimental prototype (a) front view of the prototype, (b) back view of the prototype.

Romero et al. [117] compared the performance of a solar absorption cooling system operating with water/lithium bromide and an aqueous ternary hydroxide mixture consisting of sodium, potassium and cesium hydroxides. They found that the system with the hydroxide blend can operate very stable at absorber and condenser temperature of 40°C and 50°C. However, the

system operating with hydroxide blend needs to use evacuated tube solar collectors instead of flat plate solar collectors to produce the necessary heat in the generator. Xu et al. [118] presented a solar powered absorption refrigeration system with mass energy transformation and storage technology to balance the inconsistency between the solar radiation and the cooling load. In this system, the collected solar energy was converted into the potential energy of the working fluid and stored in the storage tank. They obtained the system COP equal to 0.7525 for the system with air-cooled condenser and 0.7555 for the system with water-cooled condenser.

Escriva et al. [119] studied the cooling performance of a direct coupled solar collector with a single effect absorption system. In other hand, they did not use the intermediate solar storage tank. They presented the results of how to make a quick pre-sizing of the proposed system for 12 climates of Spain. Li and Sumathy [120] investigated the possibility of increasing the COP of a solar absorption air conditioning system by partitioning its storage tank into two parts. In this design the upper part of storage tank was activated when sunshine was low while the whole tank was connected to the collector when high sunshine was available. Their simulation results showed that the partitioned hot water storage tank can make an earlier cooling effect which in turn increases the system COP.

Different configurations for a solar absorption system was studied by Molero-Villar et al. [121] in which they investigated whether there is considerable benefit for using hot or cold storage for the small solar cooling system of the residential buildings as shown in Fig. 2.23. In the first configuration, a thermal storage was located in the hot side between the solar field and the absorber. In the second configuration, a cold storage was located between the evaporator of the absorption chiller and the cold water distribution network. Results revealed that the advantage of the cool storage was vanished with increasing the collector area. A mini-type solar absorption cooling system with 8 kW capacity was designed, installed and investigated by Yin et al. [122]. Their system contains 96 m^2 solar collector area and 3 m^3 hot water storage tank. Their system was able to provide the comfort conditions inside the air-conditioned space as predicted mean vote (PMV) was measured in the range of -0.29 to

0.32. During continuous operation of 9 hours, they obtained an average COP for chiller about 0.31. The cost, advantages, disadvantages, application and projected improvement of absorption HVAC systems are summarised as followings:

- Capital cost: Expensive in capital cost. Maintenance on absorption chillers are about the same or slightly higher compared to electric chillers.
- Advantages: they are environmentally-friendly systems and consume less energy than vapour compression air conditioning system. Their COP is higher than that of other thermally operated cycles. Another advantage os absorption chiller over the vapour compression chillres is in the absence of moving parts, except for small pumps, which permits for silent operation even in huge sizes of several hundered tons. Absorption chillers have lower utility bill.
- Disadvantages: Their COP is very low compared with vapour compression HVAC systems. They are heavy in weight. Crystallization may be a problem.
- Application: Residential, commercial and industrial buildings.
- Projected improvement: This system can gradually attain wider market penetration if their initial cost can compete with the conventional HVAC systems. If the facility has a low grade heat source which is wasted, a single-effect absorption chiller is an ideal system to use it.

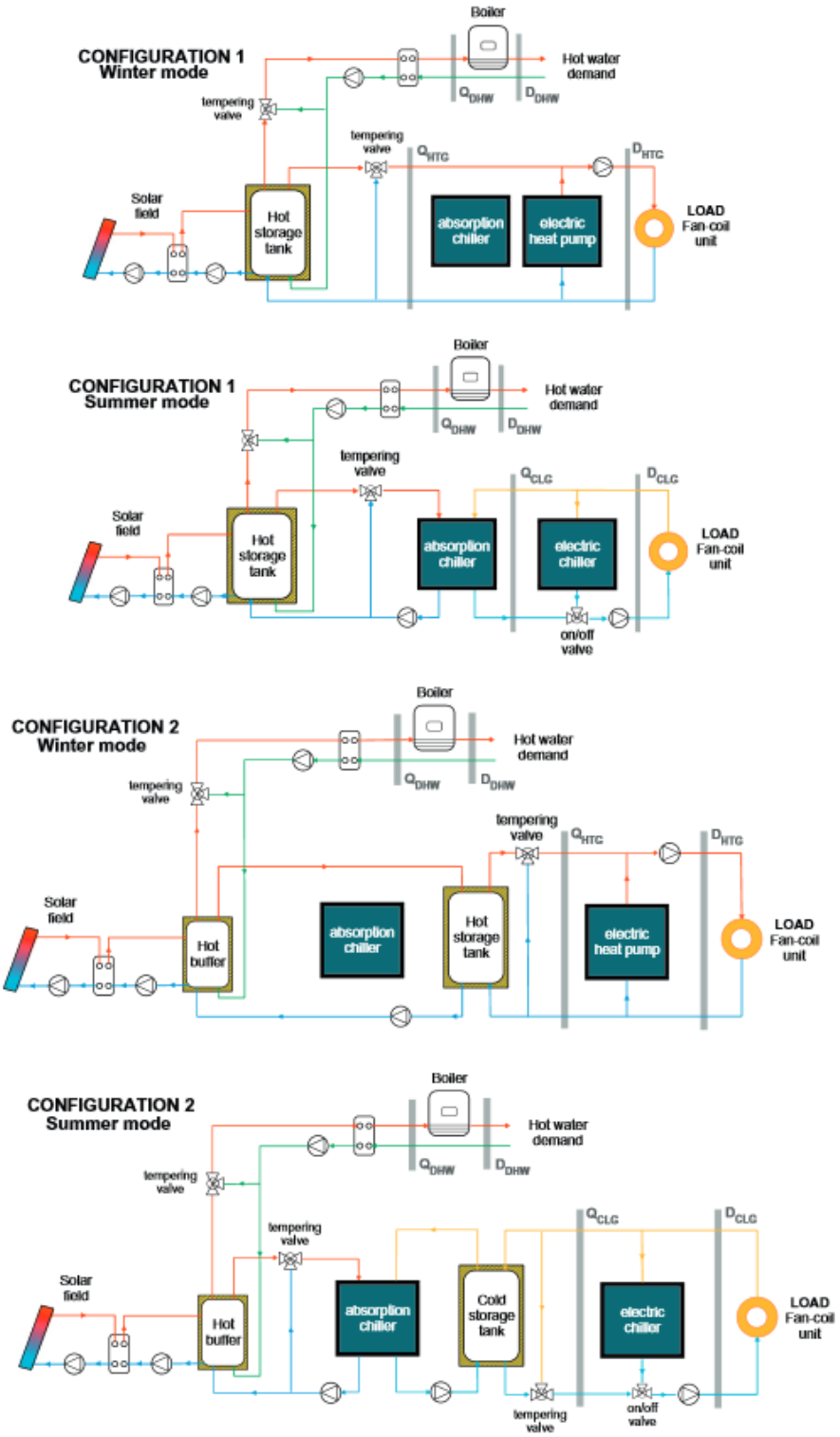

Fig. 2.23. Different configurations for solar absorption cooling system

Chapter 3

BUILDING LOAD CALCULATION

3.1 Summary

This chapter describes the building information and represents its cooling demand. The TRNSYS work space in which the building data were entered through a dedicated visual interface are demonstrated. The building model in TRNSYS is a balance model with one air node per zone which models the thermal capacity of the zone air volume that is connected to the air zone. The simulation-based data which are used to simulate the performance of the central absorption cooling plant are presented. Daily and monthly cooling load of the building is then determined and used to select the nominal cooling capacity of the single-effect absorption chiller.

3.2 Methodology

TRNSYS uses the transfer function method (TFM) to calculate the cooling loads which is the cooling calculation procedure most closely approximating the heat balance concept. This method was first introduced in the 1972 ASHRAE Handbook of Fundamentals [123]. This computer-based procedure takes place in two steps, first establishing the heat gain from all sources and then determining the conversion of such heat gain into cooling load. Developed as an hour-by hour calculation technique oriented to simulate annual energy use, its normalizing characteristics make it mainly suitable for that application. A simplified version of the TFM, which can be used with certain types of buildings for which application data are available, was presented in the 1977 ASHRAE Handbook of Fundamentals [124]. This one-step procedure uses cooling load temperature differences (CLTD), solar cooling load factors (SCL), and internal cooling load factors (CLF), to calculate cooling loads as an approximation of the TFM. In fact, TFM method can be described as the method to tell the thermal behaviour of the building walls. The full description of this method can be found in 1997 ASHRAE Handbook of Fundamentals.

3.3 TRNSYS Development

TRNSYS (TRansieNt SYstem Simulations) [125] is a graphically based software environment used to simulate the performance of transient systems. TRNSYS is a commercial software package developed at the University of Wisconsin, USA. TRNSYS consists of an engine that reads and processes the input file, iteratively solves the system, determines convergence, and plots system variables. It has a library of components that range from various building models to standard HVAC equipment. TRNSYS is based on a modular approach to solve thermal energy systems and requires an input file in which the user specifies the components that constitute the system and the manner in which they are connected. In TRNSYS each component of the solar thermal system is described by an algorithm which is programmed in FORTRAN. The user has access to the code of each component. New algorithms characterizing new system components can be developed and implemented in the simulation environment. These Newly-developed components can be validated against experimental data. TRNSYS can also be used for building transient load calculation before running the simulation of HVAC systems.

3.3.1 Building Information Implementation

The building cooling load must be determined first to properly select the nominal refrigeration capacity of the cooling system. In this study the absorption cooling plant is selected to serve a control room as our case study. This room controls the operation of the elevators and escalators for an eight levels building. The floor area of the air-conditioned room was 32 square meters with a height of 3 meters. The walls, windows, floor and roof are modelled according to ASHRAE transfer function approach [126]. Figures 3.1 and 3.2 show the typical input data for the building's walls. The occupant density in the building is about one person and its associated heat gain is 95W and 90W for sensible and latent loads respectively. The mechanical ventilation rate for acceptable indoor air quality is one air changes per hour (ACH). The infiltration is selected to be 1.5 ACH. Lighting power density is 10 W/m^2, according to the existing lights inside the building. We assume the heat gain from the lights is 40% convective. The equipment load inside the building is taken as 16

W/m^2, corresponding to a medium load type. These internal loads related data are shown in Figs 3.3. The clothing factor for people in the building is specified as 0.5 clo and relative air velocity is fixed at 0.1 m/s. The metabolic rate is 1.2 met and no external work is assumed as shown in Fig. 3.4. These data are used for the purpose of building load calculation. During this process, the indoor temperature and relative humidity set-points were fixed at 23°C and 50% respectively which is demonstrated in Fig 3.5.

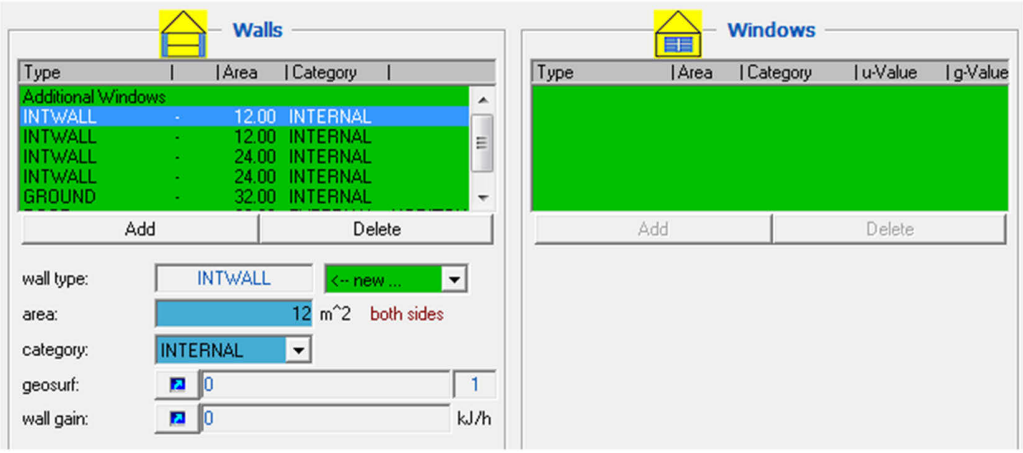

Fig. 3.1 Wall type and area for case study

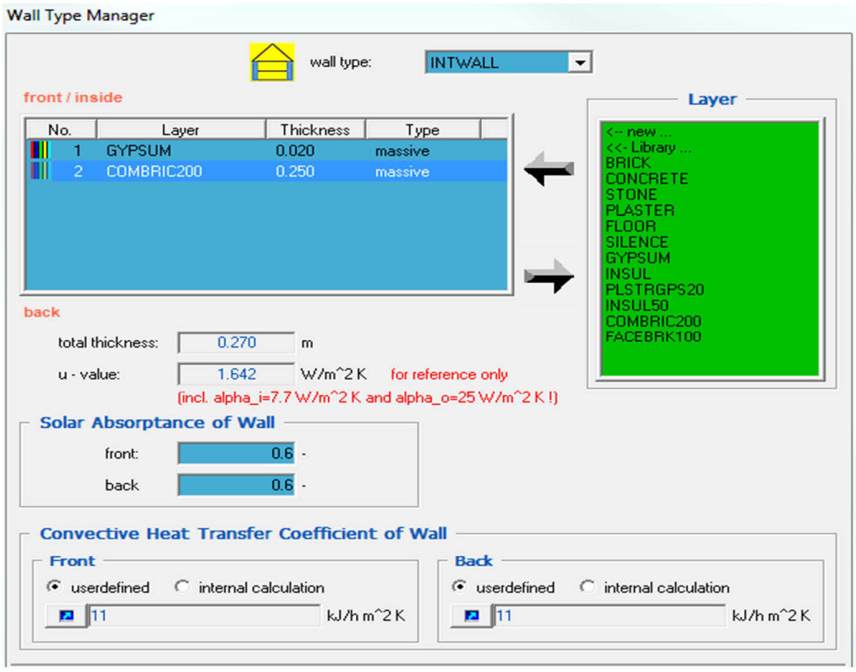

Fig. 3.2 Input data for typical wall of building

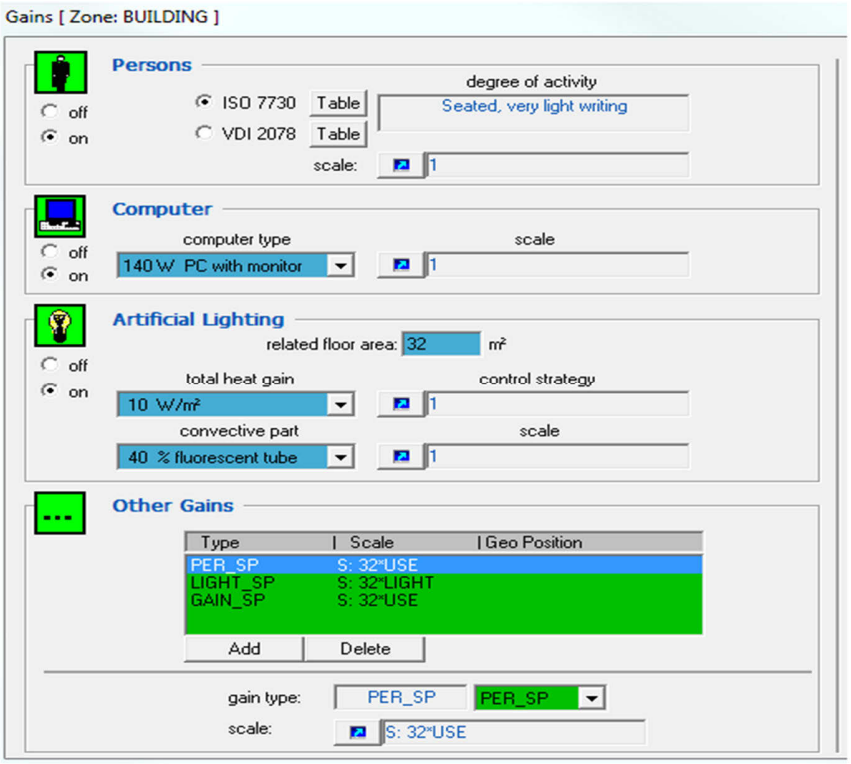

Fig. 3.3 Input data for internal load

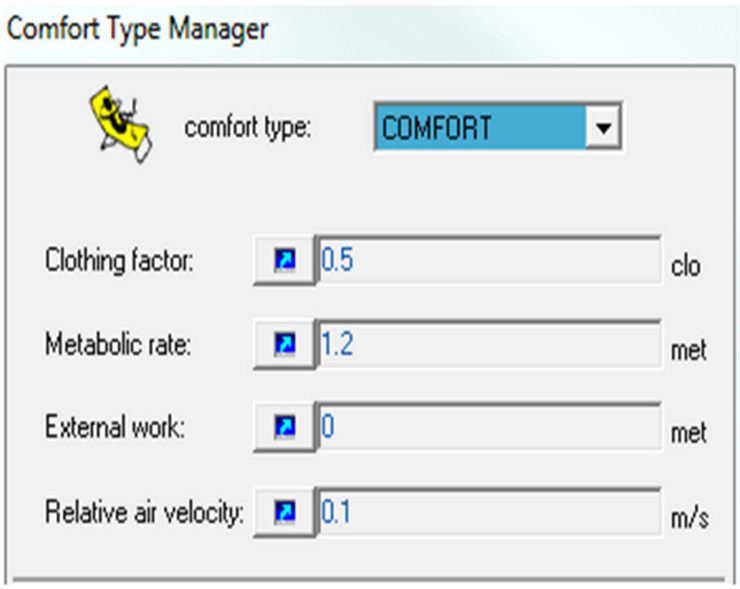

Fig. 3.4 Input data for comfort conditions

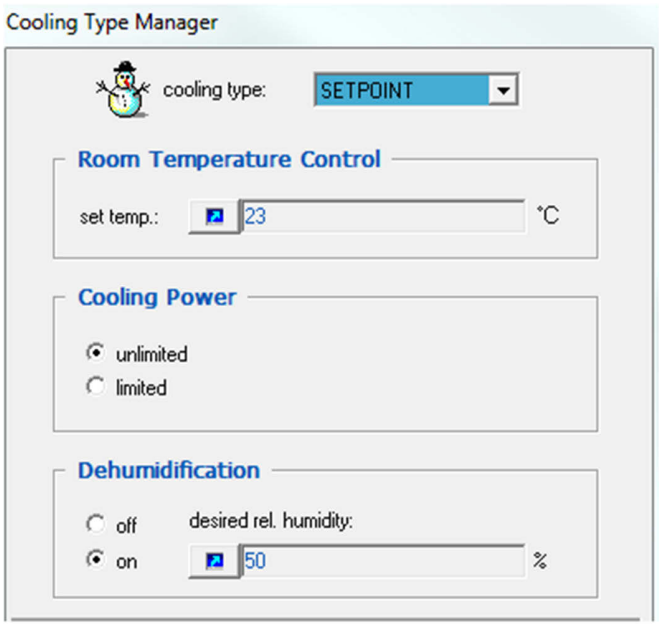

Fig. 3.5 Indoor set-points for temperature and relative humidity

3.3.2 Weather Data

The weather data that drive the project simulations are based on a typical meteorological year (TMY). The data file distributed with TRNSYS 16 is generated using "Meteonorm" including Synthetic hourly weather data. Meteonorm is a meteorological database containing climate data for solar energy application. The hourly meteorological data used in this study include information about the month of the year, hour of the month, direct normal solar radiation, global solar radiation, dry-bulb temperature, humidity ratio and wind speed.

3.4 Simulation-Based Data

To calculate the building cooling load and evaluate the system performance in each summer month, the ambient conditions such as ambient dry-bulb and wet-bulb temperatures and solar radiation intensity must be used. However, the experimentations have been carried out in two typical summer weeks and extended ambient conditions for each summer month are required for the purpose of simulation. These data file distributed with TRNSYS 16 is generated using

"Meteonorm" including Synthetic hourly weather data. The dry-bulb temperature and daily solar radiation statistics are presented in table 3.1 and 3.2 while their time of occurrence for maximum and minimum are demonstrated in table 3.3. The simulation-based ambient dry-bulb and wet-bulb temperatures are shown in figures 3.6 to 3.11. The solar radiation intensity used for simulation is presented in figures 3.12 to 3.17 [126]. These data have been used to simulate and determine the building cooling loads.

City: Sydney
Location: Australia
Latitude: 34.0 Deg
Longitude: 151.2 Deg

Month	Absolute Maximum	Average Maximum	Average	Average Minimum	Absolute Minimum
January	34.5	25.5	22.0	18.6	14.6
February	34.3	26.5	22.9	19.9	15.0
March	30.0	24.5	21.3	17.8	12.6
April	29.0	22.8	18.7	14.4	10.0
May	26.4	19.1	15.9	12.4	6.7
June	19.8	16.9	13.4	9.8	6.0
July	23.5	17.1	12.3	7.7	1.0
August	26.9	18.7	13.6	8.6	5.6
September	28.3	19.5	15.3	11.0	7.6
October	37.0	23.2	18.4	13.6	7.6
November	29.4	22.9	19.7	16.3	9.7
December	43.0	24.8	21.2	18.0	12.8

Table 3.1 Dry-Bulb temperature statistics (°C)

	Daily Total Solar on Horizontal (kJ/m²)		
Month	Maximum	Average	Minimum
January	31807.0	23727.5	7637.5
February	28822.6	20218.1	7571.0
March	24888.3	17477.5	5022.2
April	19548.8	13414.7	5392.9
May	13459.1	9556.3	4249.2
June	10550.0	7823.4	2565.4
July	12474.5	9220.4	2541.6
August	17239.9	12793.4	3915.9
September	22021.4	16546.0	4579.5
October	27559.2	20332.9	7911.0
November	29846.1	21561.8	7106.8
December	31568.3	22964.7	7834.3

Table 3.2 Daily total solar radiation statistics

Month	Highest Dry-Bulb Temperature	Lowest Dry-Bulb Temperature	Maximum Total Solar	Minimum Total Solar
January	Jan 12, 1200	Jan 18, 0900	Jan 2	Jan 16
February	Feb 10, 1500	Feb 27, 0400	Feb 2	Feb 11
March	Mar 28, 1400	Mar 9, 0600	Mar 3	Mar 31
April	Apr 7, 1300	Apr 21, 0700	Apr 1	Apr 16
May	May 6, 1500	May 18, 0600	May 4	May 30
June	Jun 5, 1500	Jun 12, 0600	Jun 1	Jun 7
July	Jul 23, 1500	Jul 27, 0700	Jul 30	Jul 2
August	Aug 17, 1500	Aug 25, 0600	Aug 31	Aug 22
September	Sep 30, 1200	Sep 11, 0600	Sep 28	Sep 9
October	Oct 18, 1300	Oct 8, 0300	Oct 28	Oct 19
November	Nov 3, 1500	Nov 18, 0600	Nov 17	Nov 1
December	Dec 21, 1300	Dec 11, 0600	Dec 21	Dec 9

Table 3.3 Time of occurrence for maximums and minimums

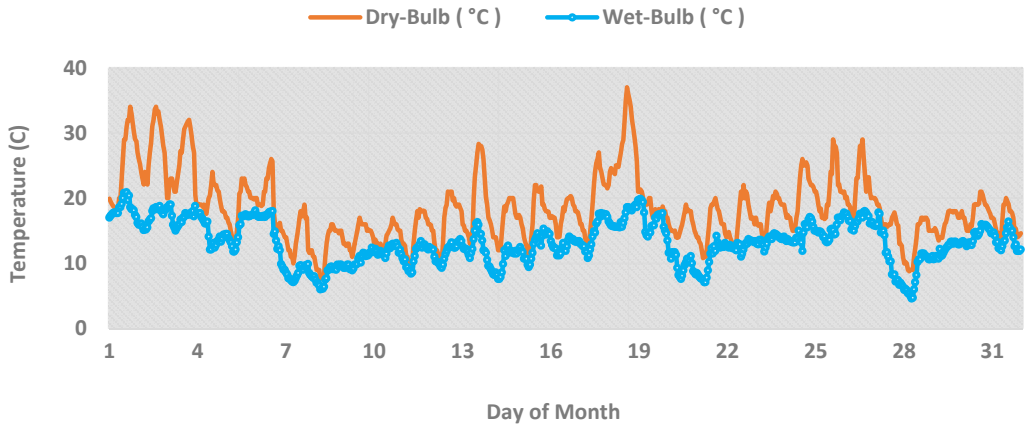

Fig. 3.6 Ambient dry-bulb and wet-bulb temperatures for October

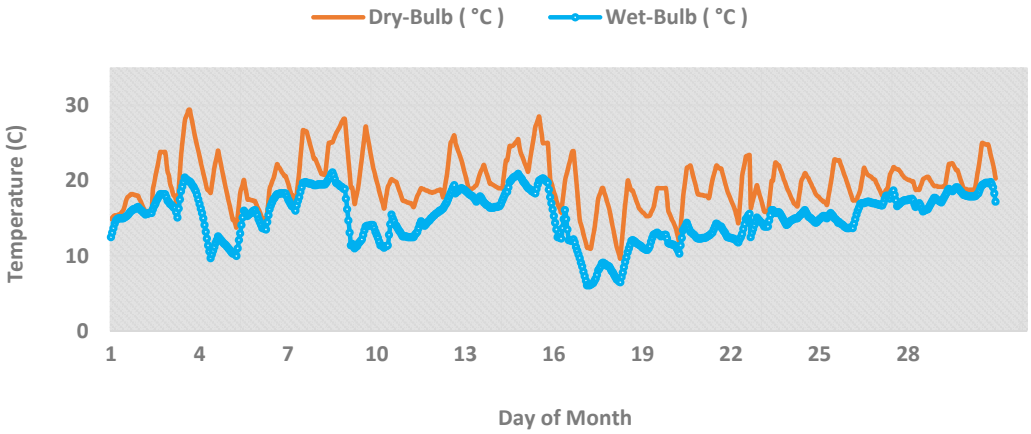

Fig. 3.7 Ambient dry-bulb and wet-bulb temperatures for November

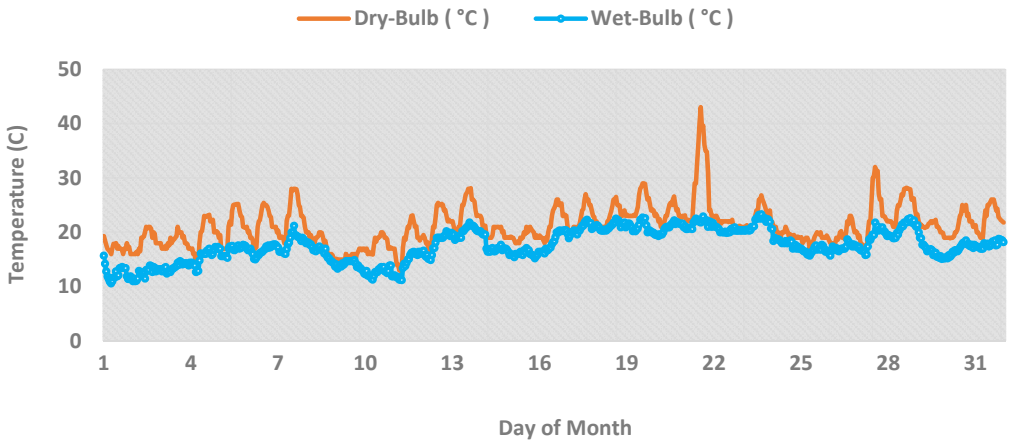

Fig. 3.8 Ambient dry-bulb and wet-bulb temperatures for December

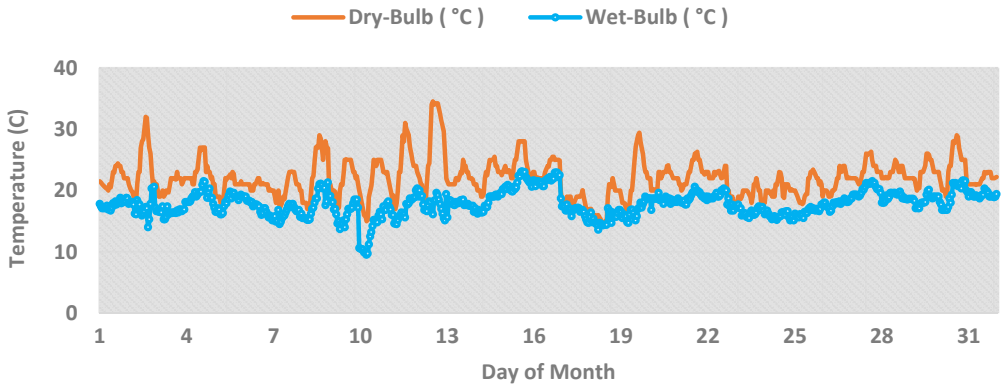

Fig. 3.9 Ambient dry-bulb and wet-bulb temperatures for January

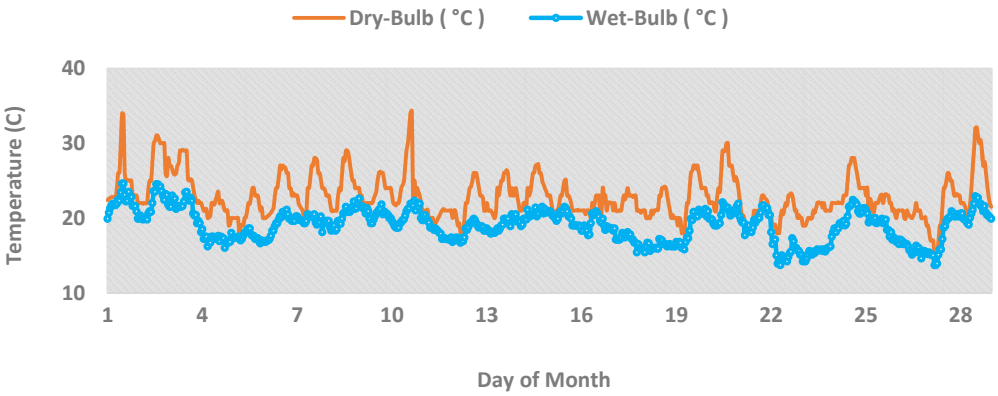

Fig. 3.10 Ambient dry-bulb and wet-bulb temperatures for February

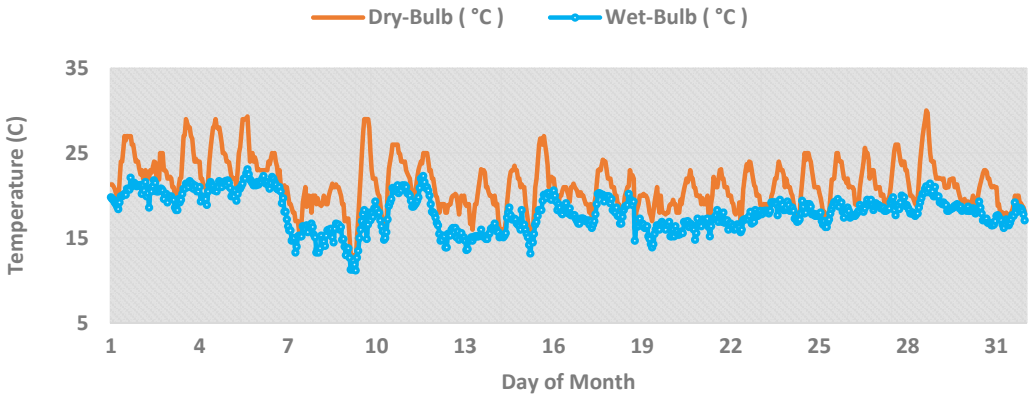

Fig. 3.11 Ambient dry-bulb and wet-bulb temperatures for March

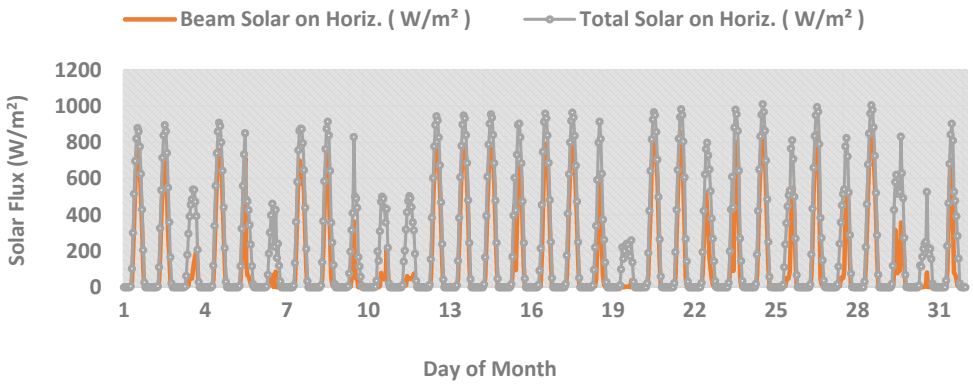

Fig. 3.12 Solar radiation profile for October

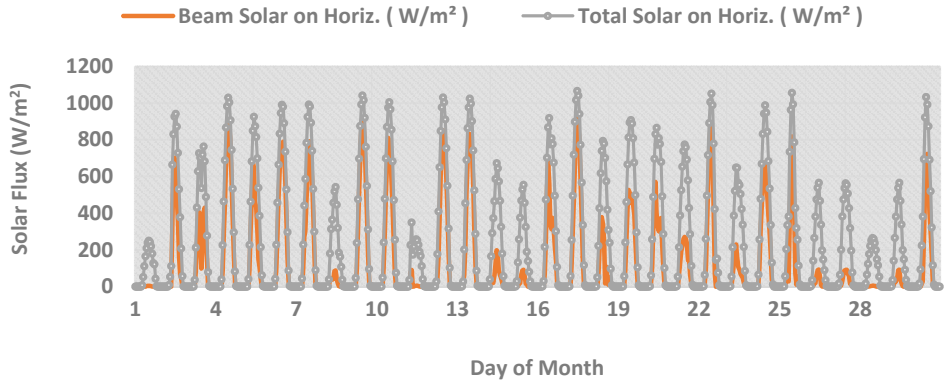

Fig. 3.13 Solar radiation profile for November

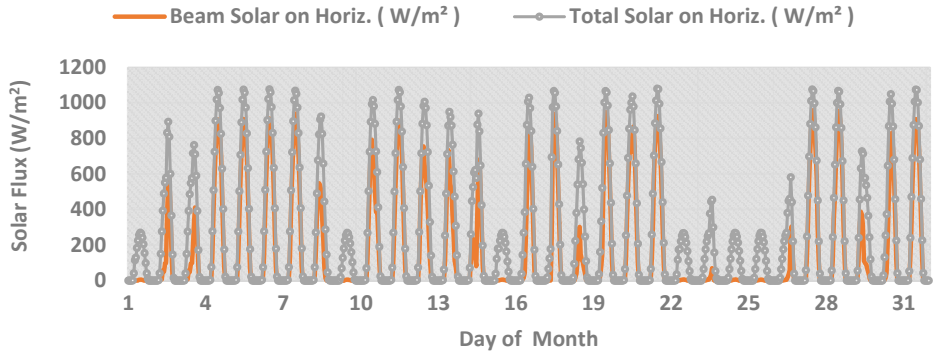

Fig. 3.14 Solar radiation profile for December

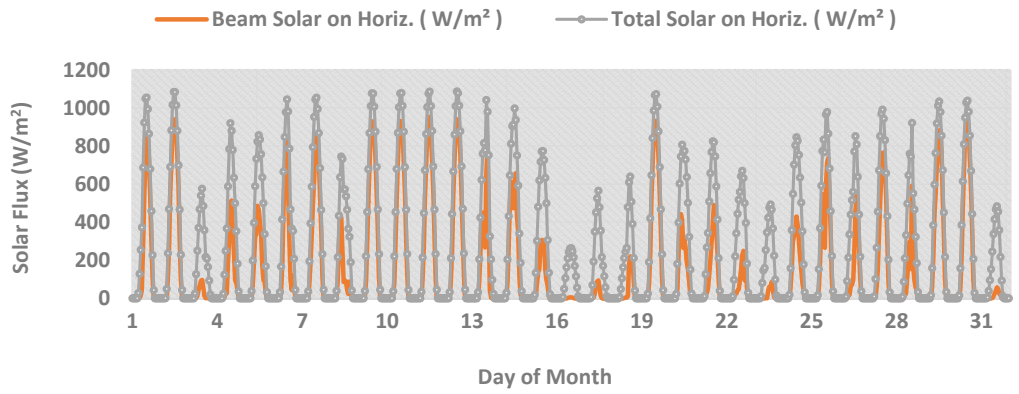

Fig. 3.15 Solar radiation profile for January

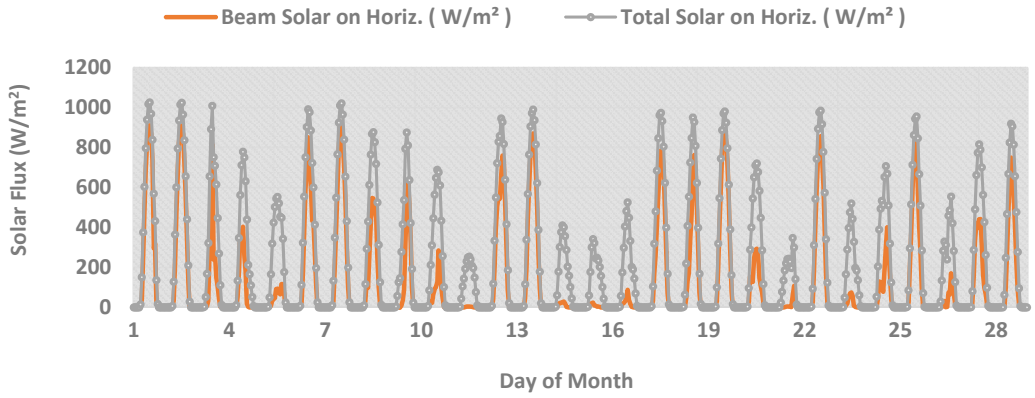

Fig. 3.16 Solar radiation profile for February

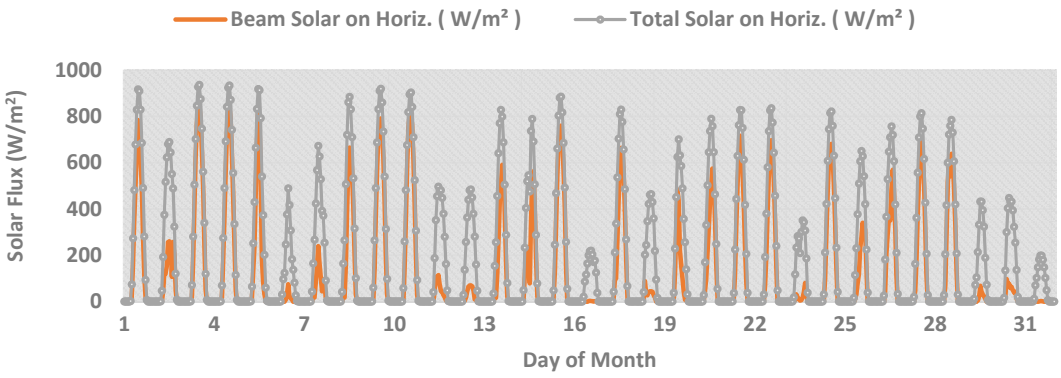

Fig. 3.17 Solar radiation profile for March

3.5 Building Cooling Load Results

To predict the system performance throughout the summer, the cooling load is calculated by using TRNSYS prior to the simulation process. The references for the indoor temperature and relative humidity during the cooling load calculation were set respectively at 23°C and 50%. The peak cooling load is estimated at 6.4 kW in the middle of February. For Sydney, the space cooling is required from October to March.

The proposed systems must match their capacity with the actual building cooling demand. Because building cooling loads vary with the time of the day, an HVAC system should be designed in tandem with an optimum design scheme that will keep the process variables within their required set-point in order to maintain comfort under any load conditions. The sustainability, energy consumption and life-cycle-cost of an HVAC system depend not only on its performance and operational parameters, but also on the characteristics of the heating and cooling demand and the thermodynamic behaviour of the building. Therefore, the most important factors that contribute to HVAC energy usage reduction in a given building is via properly adjusting and tuning of the heating and cooling demand. Therefore, the transient cooling load of the building is determined and used for system performance evaluation. Based on these results, the refrigeration capacity of the single-effect absorption chiller as well as cooling capacity of the fan-coil unit and heat rejection capacity of the cooling tower can be determined. The hourly and daily building cooling loads for each considered month (months in which building needs air conditioning) are presented in the following figures.

The required montly average cooling load for each month can be obtain using the cooling load calculation resuts. The average cooling load of the aforementioned building for December, January and February are 52.58 kWh, 58.1 kWh and 65.28 kWh respectively. The building has an average cooling load of 57.64 kWh, 42.8 kWh and 39.13 kWh respectively for March, November and October.

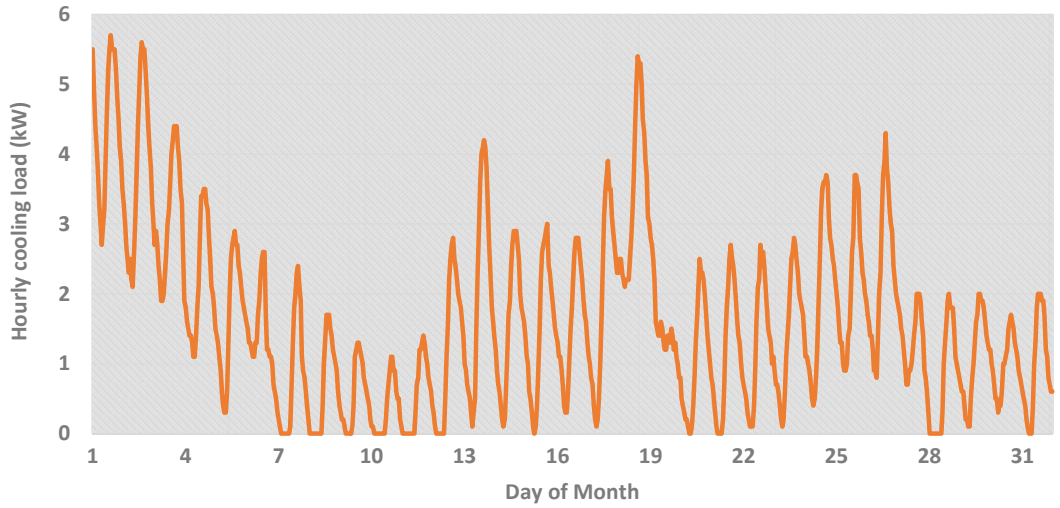

Fig. 3.18 Hourly cooling load of the building for October

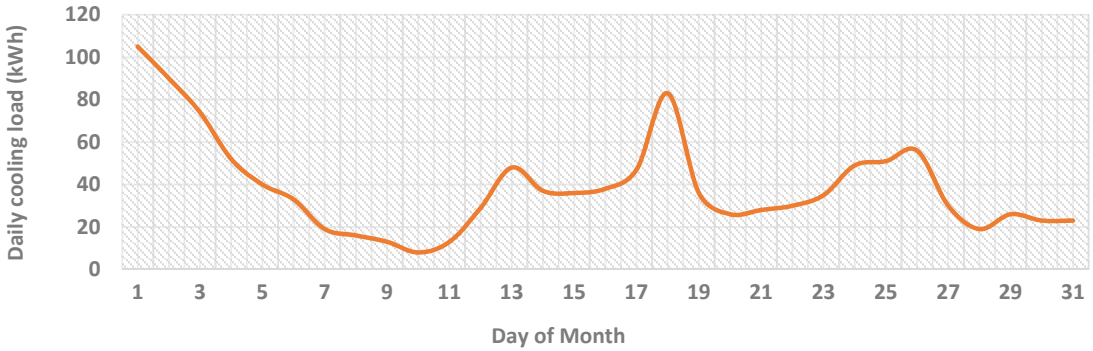

Fig. 3.19 Daily cooling load of the building for October

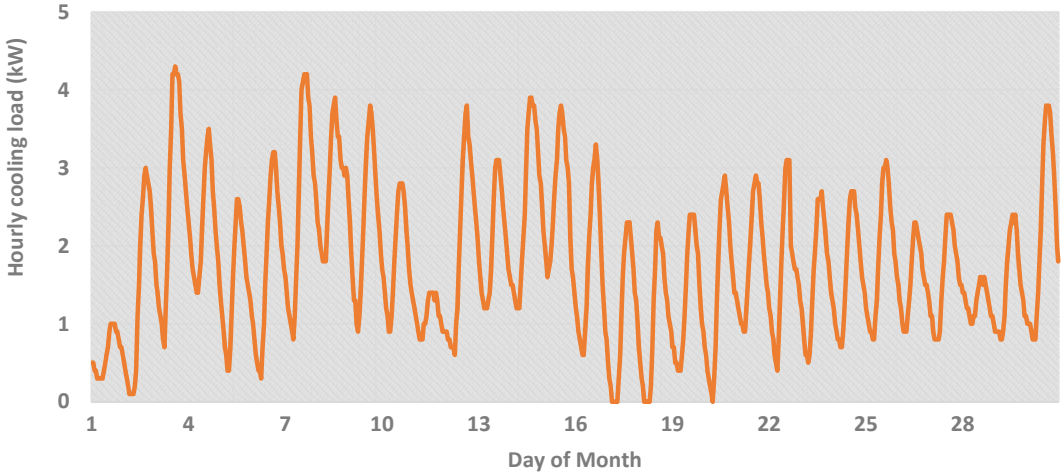

Fig. 3.20 Hourly cooling load of the building for November

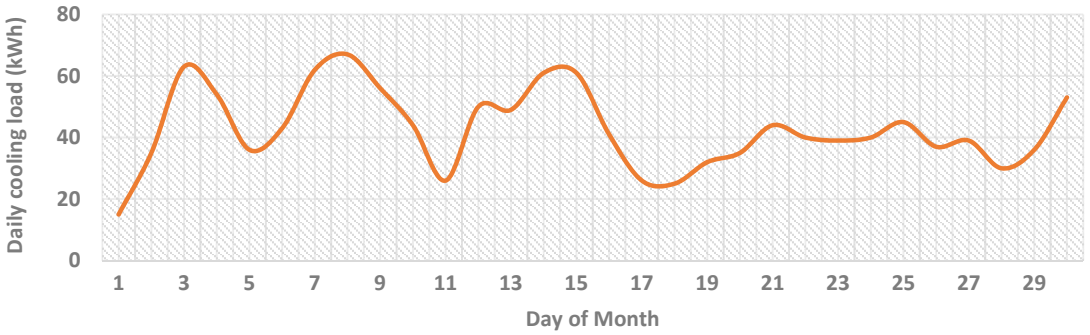

Fig. 3.21 Daily cooling load of the building for November

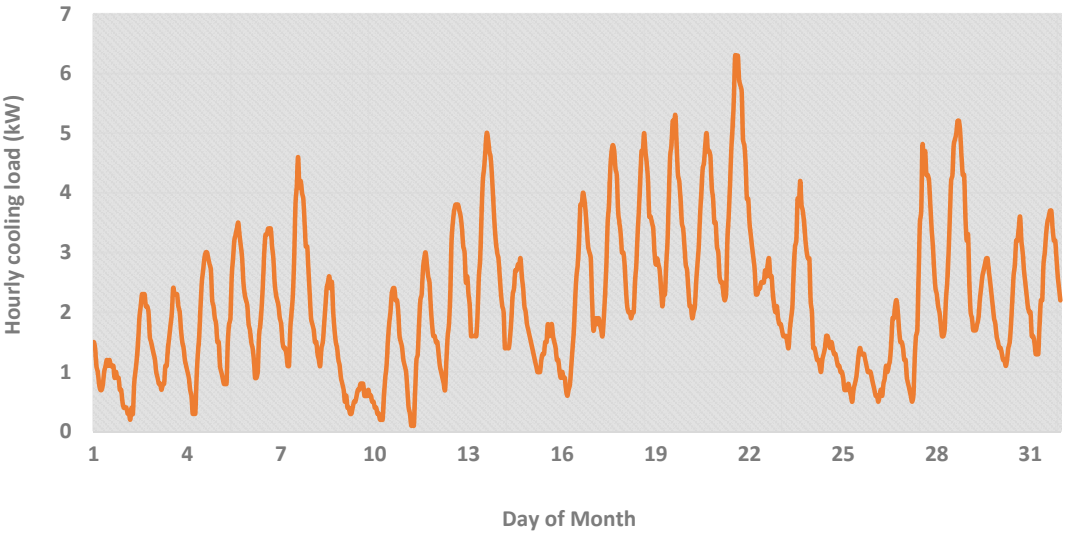

Fig. 3.22 Hourly cooling load of the building for December

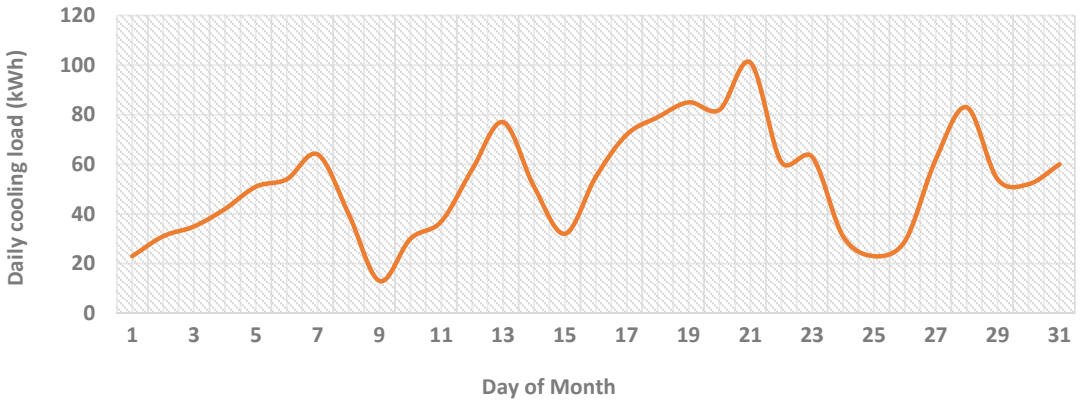

Fig. 3.23 Daily cooling load of the building for December

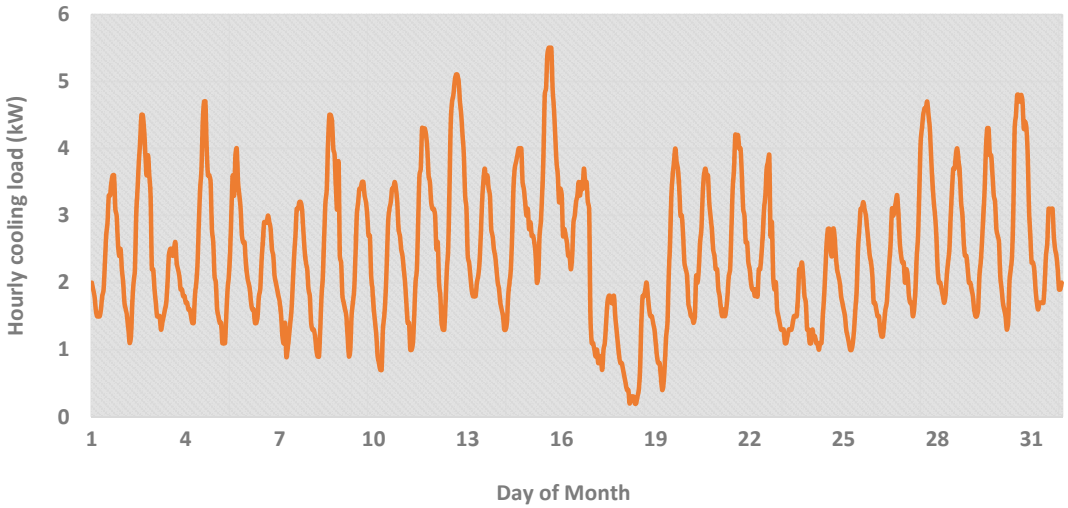

Fig. 3.24 Hourly cooling load of the building for January

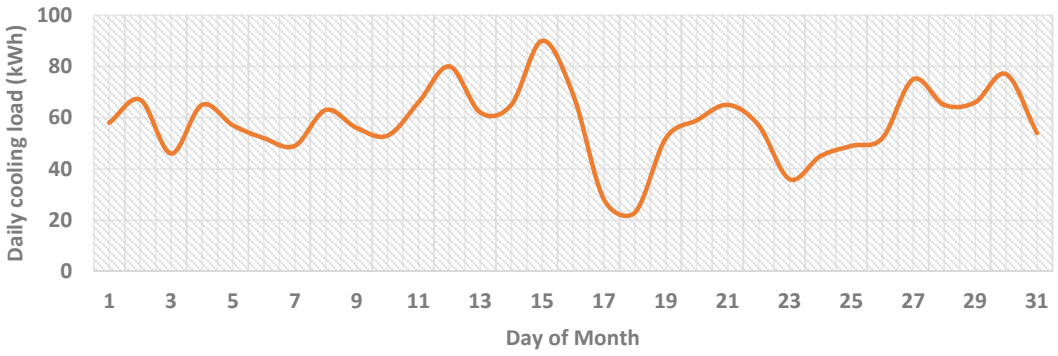

Fig. 3.25 Daily cooling load of the building for January

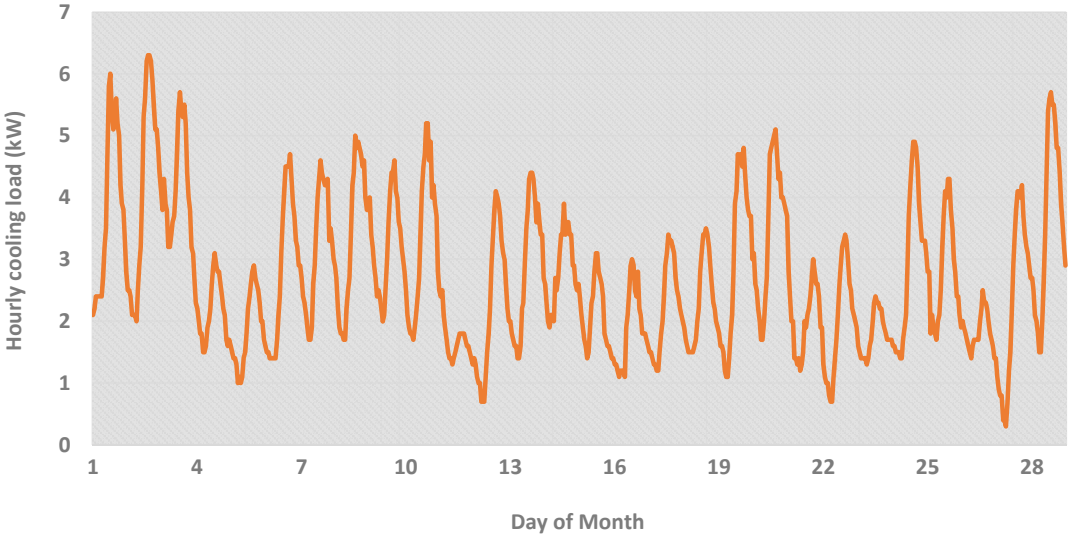

Fig. 3.26 Hourly cooling load of the building for February

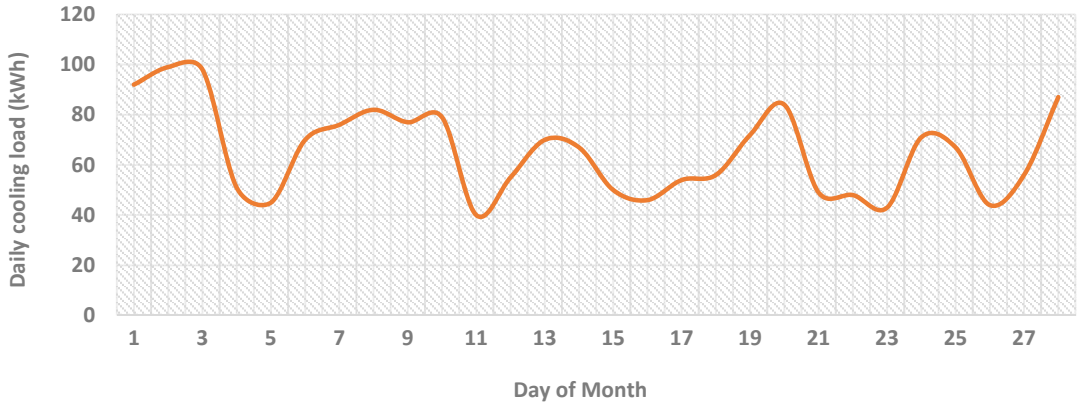

Fig. 3.27 Daily cooling load of the building for February

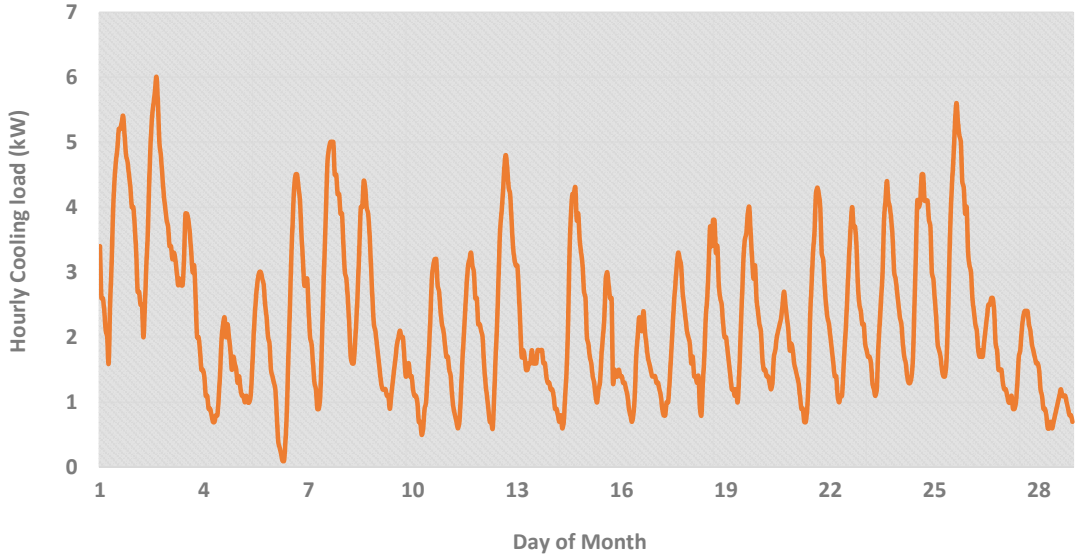

Fig. 3.28 Hourly cooling load of the building for March

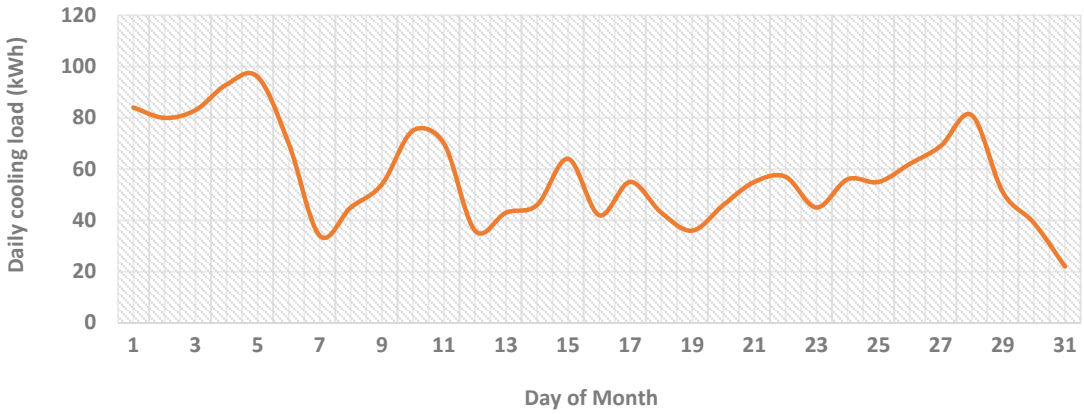

Fig. 3.29 Daily cooling load of the building for March

Chapter 4

SYSTEM DESCRIPTION AND THERMODYNAMIC MODEL OF THE SINGLE-EFFECT ABSORPTION CHILLER

4.1 Summary

The objective of this chapter is to describe a developed solar-powered hot water single-effect absorption air conditioning system and explain its working principles. The Analysis and synthesis of this system require the thermodynamic model of its components. Therefore, this chapter presents the thermodynamic models for the absorption refrigeration cycle based on the energy and mass balance laws. The thermodynamic properties of the LiBr-water solution is also discussed and presented. These models will later be used for parametric study and performance prediction of the single-effect absorption chiller which is the topic of next chapter.

4.2 System Description

The schematic of a single-effect vapour-absorption cooling system is shown in Fig. 4.1. The system comprises major components such as generator, condenser, evaporator, absorber, solution heat exchanger, solution pump as well as expansion valves and connection tubes. In the absorption cooling cycle, when the lithium bromide as the solid salt is dissolved in the water, the solution is produced. Since the lithium bromide is virtually non-volatile, then when the aqueous solution of the LiBr-water is boiled the pure water vapour is produced. In our study, hot water provided from the vacuum solar collector is the heat source in the generator and cooled water supplied by the cooling tower is the cooling fluid in the absorber and condenser. There are two pressure levels in the cycle. The pressure in the generator and condenser is high while the pressure in the absorber and evaporator is low. However, both pressure are below the atmospheric pressure and thus the specific volume of the water vapour is large. Therefore, to avoid the vapour pressure drop, the diameter of the piping tubes should be big. To minimise these losses the generator and condenser are combined in one shell and

the evaporator and absorber are located in one shell. In actual system, the generator pressure is greater than condenser pressure and the evaporator pressure is greater than absorber pressure. As the vapour pressure of the solution in the absorber and at the absorber temperature is lower than that of the refrigerant at the evaporative temperature, the refrigerant is evaporated in the evaporator. It causes the water temperature inside the evaporator tubes to decrease and produces the chilled water.

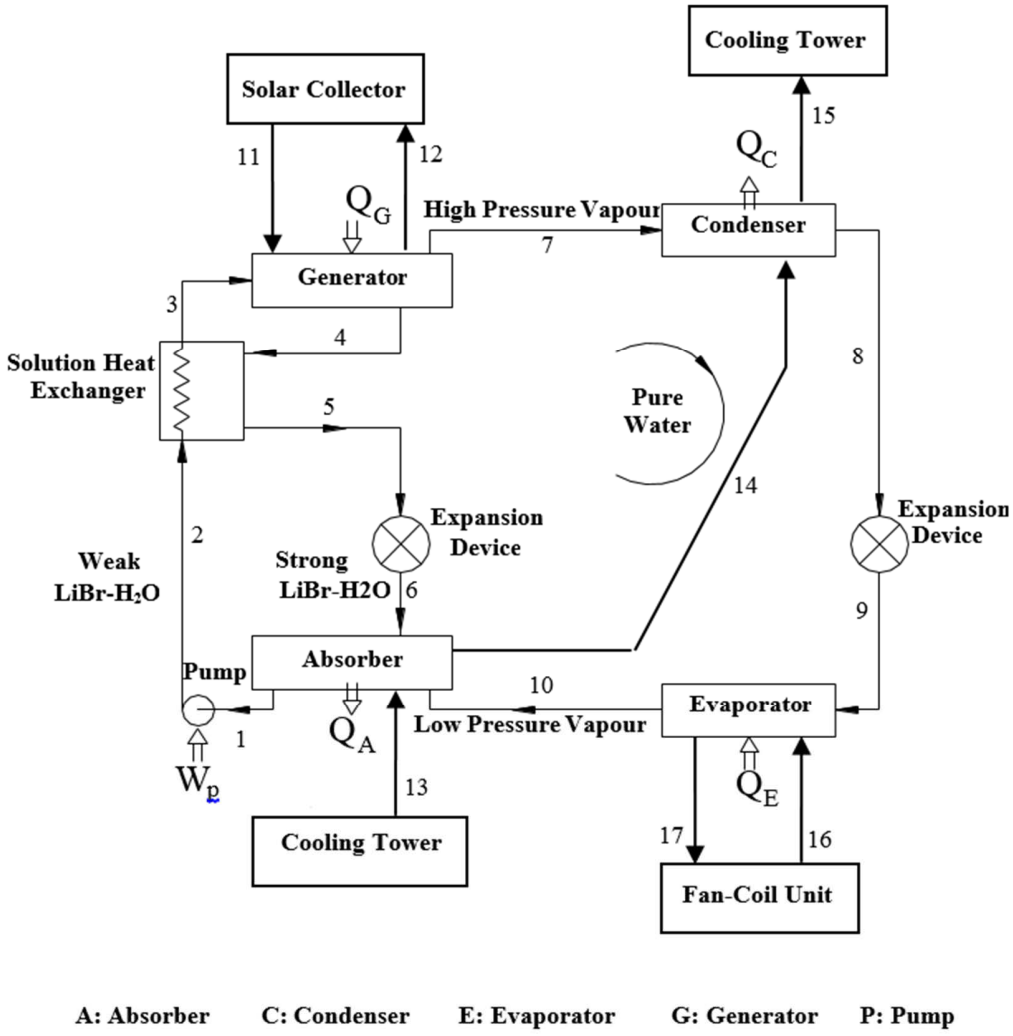

Fig. 4.1 Schematic diagram of the solar-powered single-effect hot water absorption air conditioning system

4.2.1 Operational Cycle

In the LiBr-H_20 system, lithium bromide is the absorbent and water is the refrigerant. The chiller is pumped into deep vacuum by a vacuum pump which creates the necessary condition for boiling of water at a low temperature. The resulting refrigerant vapour is attracted to the absorber by a pressure difference between the lithium bromide solution and the refrigerant water and then absorbed by concentration of the lithium bromide solution, and therefore performing continuous boiling of the refrigerant water. In the hot water-operated single-effect chiller, the diluted solution in the absorber is pumped into the generator via a solution pump and then concentrated within the concentrator when heating by hot water. The refrigerant vapour generated at the same time is condensed into water in the condenser. This causes an amount of latent heat to be carried out of the chiller by the cooling water supplied from a vertical cross-flow cooling tower. The refrigerant water then enters the evaporator and then pumped to the spray through a spraying device with the use of a refrigerant pump. The transfer of heat from the air-handling unit water to the refrigerant causes the refrigerant water to vaporize again, producing the chilled water. Finally, the chilled water is pumped to the air-handling unit to produce cooled air for the building. On the other side, the concentrated solution from the generator directly enters the absorber and the cycle is repeated. The working principle of each component is described in the following.

- **Generator:**

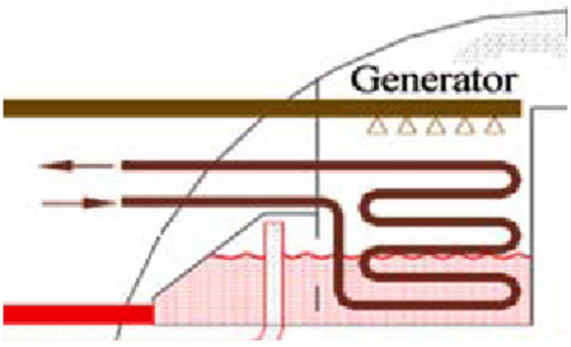

Fig. 4.2 Schematic of generator

As mentioned, the purpose of the generator is to separate the water refrigerant from the LiBr-water solution. In the generator the hot water supplied from vacuum solar collector flows inside the tubes immersed in the dilute solution of the water and LiBr. The solution is surrounded the bundle of tubes. The solution absorbs heat from the hot water and as the results the water refrigerant is boiled and separated from the solution. Therefore, the absorbent solution becomes more concentrated. This concentrated absorbent solution flows to the absorber and the water vapour travels to the condenser. During the manufacturing the absorption chiller, the generator and condenser are located inside the same shell. However, because the temperature of the cooled water flowing through the condenser tubes is less than the hot water temperature flowing the generator tubes, the condenser pressure is less than the generator pressure.

- **Condenser:**

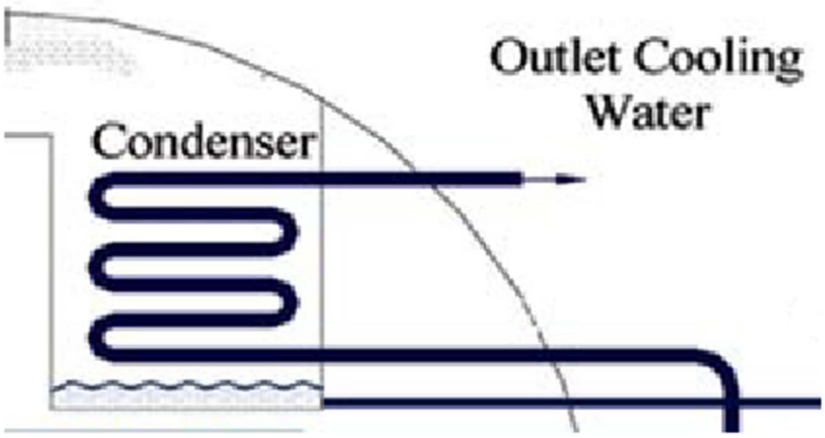

Fig. 4.3 Schematic of condenser

In the condenser, cooled water supplied by cooling tower flows inside the tubes and water vapour migrates through the mist eliminators to the condenser tube bundle. Therefore, due to heat transfer between water vapour and cooled water, the water vapour condenses on the tube surfaces. As the water vapour condenses, it collects in a trough at the bottom of the condenser.

- **Evaporator:**

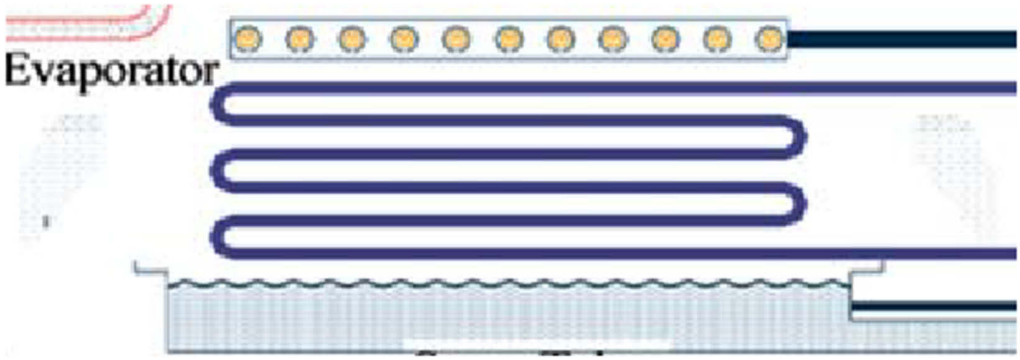

Fig. 4.4 Schematic of evaporator

In the evaporator, the chilled water leaving the fan-coil unit flows inside the tubes and water liquid as the refrigerant moves from the condenser in the evaporator shell side and sprays over the evaporator tube bundle. Due to vacuum in the shell side, the refrigerant liquid boils at low temperature. Normally the evaporative pressure is about 0.8 kPa absolute pressure in which the water liquid is boiled at 3.9°C. Therefore, the created refrigeration effect cools down the water inside the tubes. The chilled water goes to the fan-coil unit to support the building cooling load and the refrigerant vapour is drawn into the absorber. The evaporator and absorber are usually contained inside the same shell.

- **Absorber:**

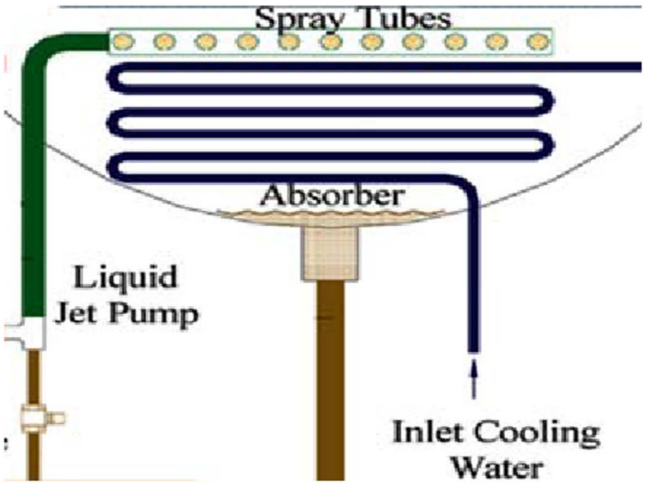

Fig. 4.5 Schematic of absorber

The refrigerant vapour travels from the evaporator to the absorber where the strong solution from the generator is sprayed over the top of the absorber tube bundle. The refrigerant vapour is then absorbed by solution and creates a low pressure area within the absorber. During this process, the refrigerant vapour is condensed to the liquid and releases the heat obtained in the evaporator. The cooling tower cooled water circulated through the absorber tubes. The concentrated absorbent solution returning from evaporator is then mixed with dilute solution from the bottom of the absorber.

- **Solution Heat Exchanger:**

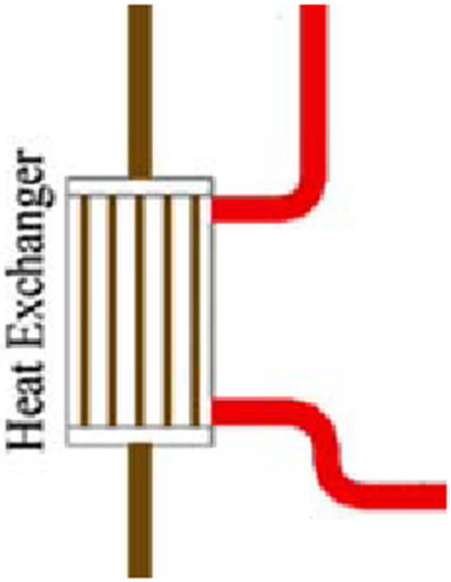

Fig. 4.6 Schematic of solution heat exchanger

In the heat exchanger the heat transfer occurs between cool dilute solution which is pumped from the absorber to the generator and the hot concentrated solution returning from generator. This heat transfer preheats the dilute solution and hence decrease the required heat energy to boil the refrigerant in the generator. In addition, it precools the concentrated solution which in turn reduces the required cooled water flowing from cooling tower to the absorber tubes. The cooled water passes through the condenser after passing through the absorber. In this study a plate type solution heat exchanger is used. The schematic diagram of the single-effect absorption chiller operation cycle with all components is shown in Fig. 4.7.

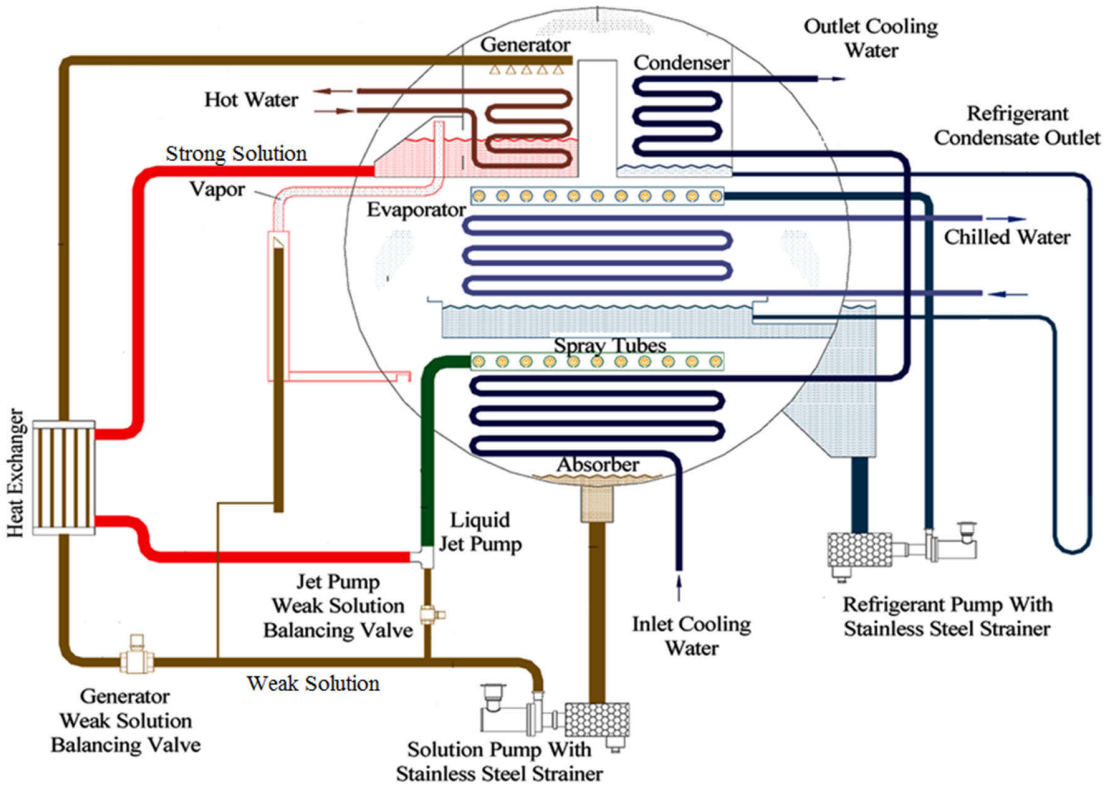

Fig. 4.7 Operation cycle of the single-effect absorption chiller

4.3 System Modelling

In this section, a detailed thermodynamic models of the LiBr-water absorption air conditioning system is presented. Following assumption are considered for this purpose:

- The analysis is carried out considering steady-state conditions
- Refrigerant leaving the condenser is saturated at the condenser temperature.
- Refrigerant leaving the evaporator is saturated at the evaporator temperature.
- The strong solution leaving the generator and the weak solution leaving the absorber are saturated.
- The heat transfer from the components to the surroundings is negligible.
- Pressure drop due to friction is negligible in heat exchangers and the piping system.

The thermodynamic state of each point in the cycle demonstrated in Fig. 4.1, is presented in table 4.1 and are used for system modelling. From this table, there are three saturated liquid (points1, 4 and 8), three sub-cooled liquid (points 2,3 and 5), one superheated vapour (point 7) which is vapour state at the generator outlet, one saturated vapour (point 10) at the evaporator outlet and two points are two phase vapour-liquid states (point 6 and 9). However, in the actual absorption chiller, the thermodynamic conditions at the points 1, 4, 7, 8 and 10 may not be exactly the saturated.

Table 4.1 Thermodynamic state points for Fig. 4.1

Point (Fig. 4.1)	Thermodynamic State
1	Saturated liquid solution
2	Sub-cooled liquid solution
3	Sub-cooled liquid solution
4	Saturated liquid solution
5	Sub-cooled liquid solution
6	Vapour-liquid solution
7	Superheated water vapour
8	Saturated liquid water
9	Vapour-liquid water
10	Saturated water vapour

4.3.1 Mass and Energy Balance for Absorption Chiller

The main components of the absorption chiller include the generator, condenser, evaporator and absorber, can be modelled by using the mass and energy balance laws. Referring to Fig. 4.1, the mass balance equations for each component are as follows:

$$\frac{dM_C}{dt} = \dot{m}_7 - \dot{m}_8, \tag{4.1}$$

$$\frac{dM_E}{dt} = \dot{m}_9 - \dot{m}_{10}, \tag{4.2}$$

$$\frac{dM_A}{dt} = \dot{m}_{10} + \dot{m}_6 - \dot{m}_1, \tag{4.3}$$

$$\frac{dM_G}{dt} = \dot{m}_3 - \dot{m}_4 - \dot{m}_7, \tag{4.4}$$

$$\dot{m}_8 = \dot{m}_9, \tag{4.5}$$

$$\dot{m}_1 = \dot{m}_2 = \dot{m}_3, \tag{4.6}$$

$$\dot{m}_4 = \dot{m}_5 = \dot{m}_6, \tag{4.7}$$

where $\dot{m}$ is the water flow rate, M is the water mass and subscripts 1 to 10 indicate the inlet and outlet of each component, as shown at corresponding points in Fig. 4.1.

The energy balances for the components are given as:

$$\frac{d}{dt}(M_C h_C) = \dot{m}_7 h_7 - \dot{m}_8 h_8 - Q_C, \tag{4.8}$$

$$\frac{d}{dt}(M_E h_E) = \dot{m}_9 h_9 - \dot{m}_{10} h_{10} - Q_E, \tag{4.9}$$

$$\frac{d}{dt}(M_A h_A) = \dot{m}_{10} h_{10} + \dot{m}_6 h_6 - \dot{m}_1 h_1 - Q_A, \tag{4.10}$$

$$\frac{d}{dt}(M_G h_G) = \dot{m}_3 h_3 - \dot{m}_4 h_4 - \dot{m}_7 h_7 - Q_G, \tag{4.11}$$

$$W_p = \dot{m}_2 h_2 - \dot{m}_1 h_1, \tag{4.12}$$

$$h_8 = h_9, \tag{4.13}$$

$$h_5 = h_6, \tag{4.14}$$

where h is the enthalpy, Q is the heat transfer rate, W_p is the input work of pump, and subscripts A, C, E, G, and p represent respectively the absorber, condenser, evaporator, generator and pump.

In the steady state conditions the mass and energy balance for the system components are as:

$$\sum \dot{m}_i = \sum \dot{m}_e, \tag{4.15}$$

$$\sum \dot{Q} - \sum \dot{W} = \sum \dot{m}_o h_o - \sum \dot{m}_e h_e. \tag{4.16}$$

Therefore, equations (4.1) to (4.4) and (4.8) to (4.11) can be re-written for the steady state conditions as:

$$\dot{m}_7 = \dot{m}_8, \tag{4.17}$$

$$\dot{m}_9 = \dot{m}_{10}, \tag{4.18}$$

$$\dot{m}_{10} + \dot{m}_6 = \dot{m}_1, \tag{4.19}$$

$$\dot{m}_4 + \dot{m}_7 = \dot{m}_3, \tag{4.20}$$

$$Q_C = \dot{m}_7 h_7 - \dot{m}_8 h_8, \tag{4.21}$$

$$Q_E = \dot{m}_9 h_9 - \dot{m}_{10} h_{10}, \tag{4.22}$$

$$Q_A = \dot{m}_{10} h_{10} + \dot{m}_6 h_6 - \dot{m}_1 h_1, \tag{4.23}$$

$$Q_G = \dot{m}_3 h_3 - \dot{m}_4 h_4 - \dot{m}_7 h_7. \tag{4.24}$$

The concentration of LiBr is defined as the ratio of the mass fraction of LiBr in the solution to the total mass of LiBr and water contained in the solution as:

$$X = \frac{LiBr\ mass}{LiBr\ mass + H_2O\ mass}. \tag{4.25}$$

Referring to Fig. 4.1, equation (4.20) can be re-written as:

$$\dot{m}_4 + \dot{m}_7 = \dot{m}_3 \Rightarrow \dot{m}_{ss} + \dot{m}_{ref} = \dot{m}_{ws}, \tag{4.26}$$

in which $\dot{m}_{ws}$, $\dot{m}_{ss}$ and $\dot{m}_{ref}$ are mass flow rate of the weak solution, strong solution and water refrigerant respectively.

For LiBr balance, the following equation is given:

$$\dot{m}_{ws} X_{ws} = \dot{m}_{ss} X_{ss}, \tag{4.27}$$

where X_{ws} and X_{ss} are the concentration of the LiBr in weak and strong solution.

Now from equations (4.26) and (4.27) the following equations can be derived:

$$\frac{\dot{m}_{ws}}{\dot{m}_{ref}} = \frac{X_{ss}}{X_{ss} - X_{ws}}, \tag{4.28}$$

$$\frac{\dot{m}_{ss}}{\dot{m}_{ref}} = \frac{X_{ws}}{X_{ss} - X_{ws}}, \tag{4.29}$$

To evaluate the thermal performance of the absorption chiller, the thermodynamic properties of the LiBr-water solution are needed which are discussed in the next section.

4.3.2 Thermodynamic Properties of Water and LiBr-Water Solution

The following expressions are used to calculate the thermodynamic properties of the water and LiBr:

- The enthalpy of pure water liquid h_w (kg/kJ) at temperature T (°C) can be calculated as:

$$h_w = 4.187(T - 25) + 104.8. \tag{4.30}$$

- The enthalpy of the saturated water vapour $h_{w,sat}$ (kg/kJ) at temperature T (°C) is:

$$h_{w,sat} = 4.187(572.8 + 0.417T). \tag{4.31}$$

Florides et al. [127] present the following correlation for saturated water vapour enthalpy:

$$h_{w,sat} = -0.00125397T^2 + 1.88060937T + 2500.559. \quad (4.32)$$

- The enthalpy of the superheated vapour at temperature T (°C) and at the pressure equal to the saturation pressure of vapour at temperature T_{sat} (°C) is:

$$h_{sh} = 4.187(572.8 + 0.46T - 0.043T_{sat}). \quad (4.33)$$

- Other thermodynamic properties of water can be determined by [127-128]:

Density:

$$\rho = 15.451\times10^{-6}T_w^{\,3} - 0.0059003T_w^{\,2} - 0.019075T_w + 1002.3052. \quad (4.34)$$

Specific heat:

$$C_p = (3.216145833\times10^{-6}T_w^{\,4} - 0.000798668982T^3 - 0.0780295139T_w^{\,2} - 3.0481614T_w + 4217.7377)\times0.001. \quad (4.35)$$

Absolute viscosity:

$$\mu = (31.538716146\times10^{-6}T_w^{\,4} - 8.913055428199999\times10^{-3}T_w^{\,3} + 0.9795876934T_w^{\,2} - 55.4567974T_w + 1791.74424)\times10^{-6}. \quad (4.36)$$

Thermal conductivity:

$$k = -6.5104167\times10^{-10}T_w^{\,4} + 1.8923611\times10^{-7}T_w^{\,3} - 2.671875\times10^{-5}T_w^{\,2} + 0.0027103175T_w + 0.5520119. \quad (4.37)$$

- The specific heat of LiBr-water solution of the concentration X (kg LiBr/kg solution) can be determined by [129]:

$$C_{ps} = 4.187(1.01 - 1.23X + 0.48X^2). \quad (4.38)$$

In ASHRAE Fundamental Handbook 1997 [124], the graph for specific heat of the aqueous LiBr solution can be found as shown in Fig. 4.8. Using these data, the following correlation is presented by Florides et al. [127]:

$$C_{ps} = 0.001 \times (3825.4 - 37.512X + 0.0976X^2), \tag{4.39}$$

where X is the solution concentration given in (4.25).

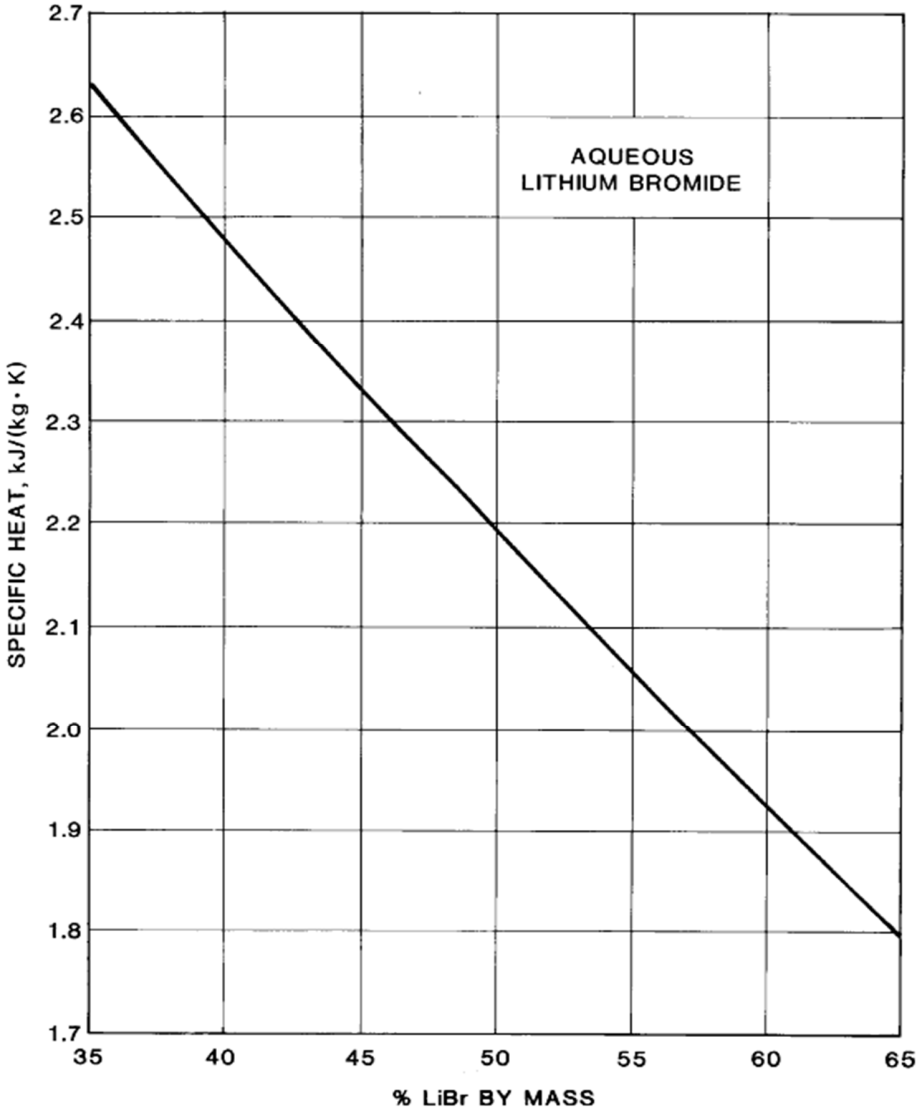

Fig. 4.8 Specific heat of aqueous Lithium Bromide solution

Other correlations for specific heat of the LiBr solution are as:

Correlation by Jeter et al. [130] for $62°C \le T \le 151°C$ *and* $44\% \le X \le 64.8\%$:

$$C_{ps} = \left(3.067819 - 2.15232\times10^{-2} X\right) + \left(6.018\times10^{-3} - 7.31\times10^{-5} X\right)T. \tag{4.40}$$

Correlation by Rockenfeller [131] for $65°C \le T \le 205°C$ *and* $40\% \le X \le 65\%$:

$$C_{ps} = \left(3.462023 - 2.679895\times10^{-2} X\right) + \left(1.3499\times10^{-3} - 6.55\times10^{-6} X\right)T. \tag{4.41}$$

Correlation by McNeely [132] for $16°C \le T \le 166°C$ *and* $40\% \le X \le 60\%$:

$$C_{ps} = 2.326\{1.8B\times T + 3.6C(1.8T + 32)\} \tag{4.42}$$

in which B and C are defined as:

$$B = 4.68108 - 0.3037766X + 0.00844845X^2 - 0.0001047721X^3 + 4.80097\times10^{-7} X^4, \tag{4.43}$$

$$C = -0.0049107 - 0.000383184X - 1.078963\times10^{-5} X^2 + 1.3152\times10^{-7} X^3 - 5.897\times10^{-10} X^4. \tag{4.44}$$

- The enthalpy of LiBr-water solution of the concentration X (kg LiBr/kg solution) at temperature T (°C) is given by [129]:

$$h_s = 4.187\left[\left(1.01 - 1.23X + 0.48X^2\right)T + \left(42.81 - 425.92X + 404.67X^2\right)\right] \tag{4.45}$$

The following correlation is presented by ASHRAE [124] for $15°C \le T \le 165°C$ *and* $40\% \le X \le 70\%$ and illustrated graphically in Fig. 4.9.:

$$h_s = \sum_{n=0}^{4} A_n X^n + T\sum_{n=0}^{4} B_n X^n + T^2 \sum_{n=0}^{4} C_n X^n, \tag{4.46}$$

in which the coefficients A_n, B_n and C_n $(n=0,1,...,4)$, are obtained as:

$A_o = -2024.33$	$B_0 = 18.2829$	$C_0 = -0.03700821$
$A_1 = 163.309$	$B_1 = -1.1691757$	$C_1 = 0.0028877666$
$A_2 = -4.88161$	$B_2 = 0.03248041$	$C_2 = -0.81313015 \times 10^{-4}$
$A_3 = 0.0630294$	$B_3 = -0.00040341$	$C_3 = 0.9116628 \times 10^{-6}$
$A_4 = -0.0002913705$	$B_4 = 0.18520569 \times 10^{-5}$	$C_1 = -0.44441207 \times 10^{-8}$

Based on these data the following diagram is presented by ASHRAE [124]:

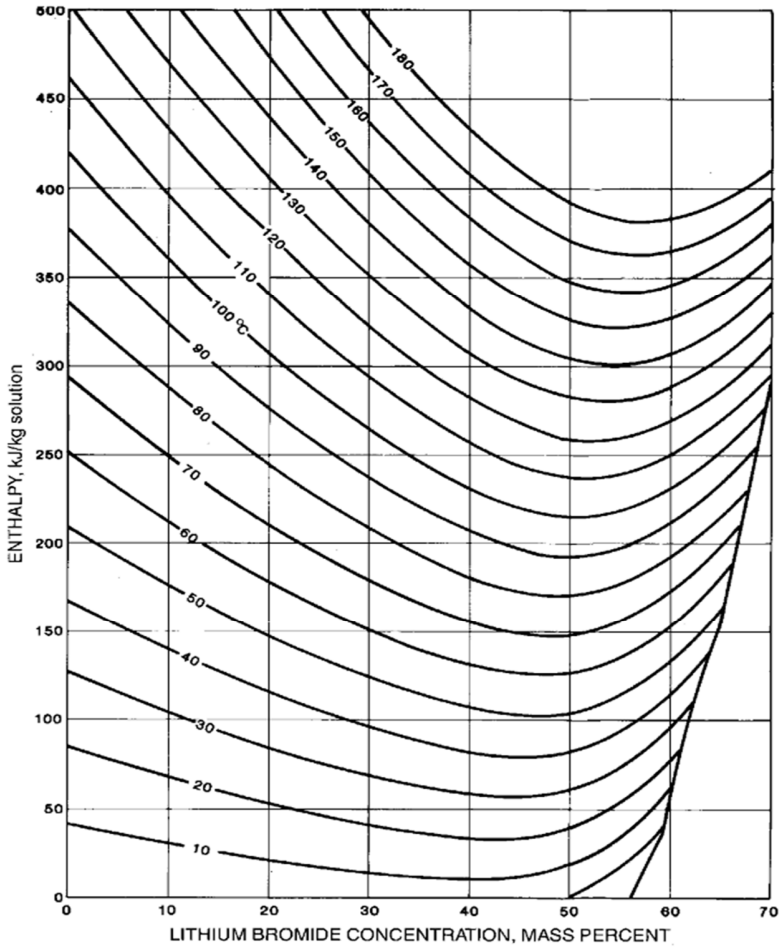

Fig. 4.9 Enthalpy-Concentration diagram for LiBr-water solution

Paul et al. [133] gave the following correlation:

$$h_s = \left(1.74X^2 - 1.91X + 0.285\right)\times 10^6 + \left(2.01X^2 - 5.15X + 4.23\right)\left(T - 25\right)\times 10^3. \quad (4.47)$$

McNeely [132] presented the following correlation:

$$h_s = 2.326\left[A + B(1.8T + 32) + C(1.8T + 32)^2\right], \quad (4.48)$$

in which B and C can be determined using equations (4.43) and (4.44) and A can be calculated as:

$$A = -1015.07 + 79.5387X - 2.358016X^2 + 0.03031583\ X^3 - 0.000140026\ X^4. \quad (4.49)$$

The following correlation is presented by Kaita [134] for $20°C \le T \le 210°C$ *and* $40\% \le X \le 65\%$:

$$h_s = \left(A_0 + A_1X\right)T + 0.5\left(B_0 + B_1X\right)T^2 + \left(D_0 + D_1X + D_2X^2 + D_3X^3\right), \quad (4.50)$$

in which the constant coefficients can be are determined as followings:

$A_0 = 3.462023$	$B_0 = 0.0013499$	$D_0 = 162.81$	$D_2 = 0.0045384$
$A_1 = -0.02679895$	$B_1 = -6.55\times 10^{-6}$	$D_1 = -6.0418$	$D_3 = 0.0012053$

- In the concentration range between 0.5 and 0.65 kg LiBr/kg solution, Lansing [129] found the following fits with the standard deviation of ±0.2%:

$$T_{ref} = (49.04 - 134.65X) + (1.125 - 0.47X)(T_m), \quad (4.51)$$

$$X = \frac{49.04 + 1.125T_m - T_{ref}}{134.65 + 0.47T_m}, \quad (4.52)$$

where T_{ref} and T_m are the refrigerant and saturated solution temperature respectively.

- The saturated vapour pressure P (mm Hg) corresponding to saturated temperature T_k (K) for pure water is [129]:

$$log_{10} P = 7.8553 - \frac{1555}{T_k} - \frac{11.2414 \times 10^4}{T_k^{\,2}}. \tag{4.53}$$

- Density of LiBr-water solution can be determined by using the following correlation [135] for $0°C \le T \le 200°C$ *and* $20\% \le X \le 60\%$:

$$\rho_s = 1145.36 + 470.84\left(\frac{X}{100}\right) + 1374.79\left(\frac{X}{100}\right)^2 - \left(0.333339 + 0.571749\left(\frac{X}{100}\right)\right)(T + 273). \tag{4.54}$$

The following diagram is presented by ASHRAE [124] for density of LiBr-water solution:

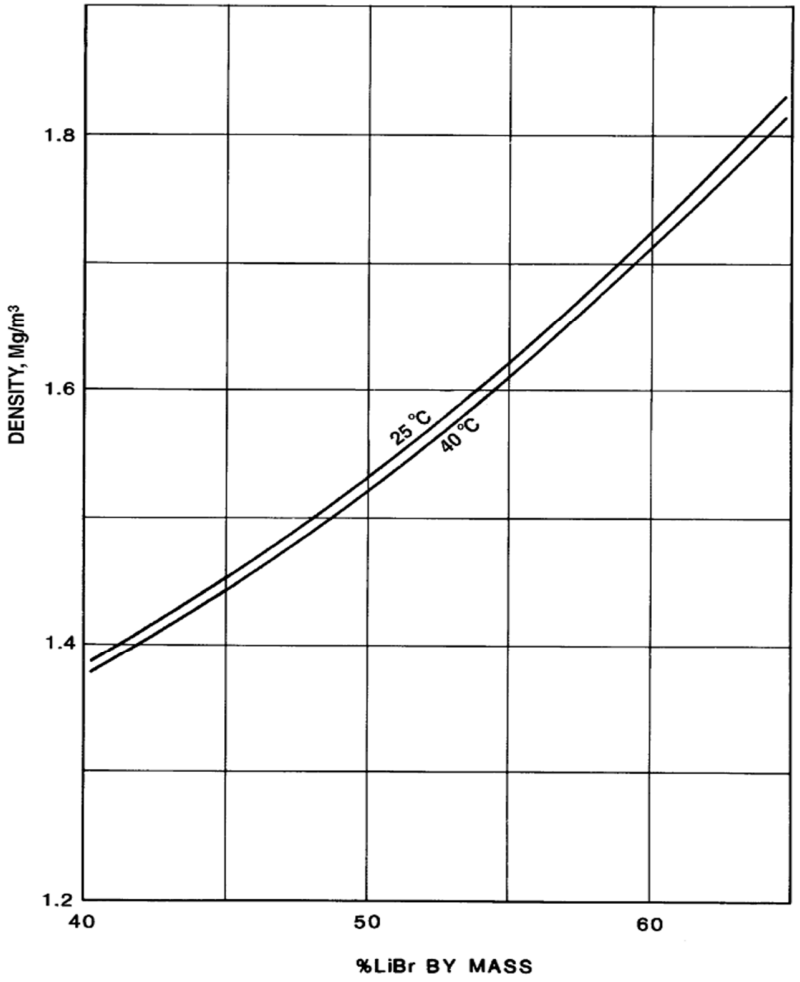

Fig. 4.10 Density of aqueous solution of LiBr

- Absolute viscosity of LiBr-water solution can be determined by using the following correlation [135] for $45\% \le X \le 65\%$:

$$\mu_s = 0.001 e^{A_1 + \left(\frac{A_2}{T_k}\right) + A_3 \ln(T_k)}, \tag{4.55}$$

in which T_k is the solution temperature in Kelvin and A_1, A_2 and A_3 can be calculated as:

$$A_1 = -494.122 + 16.396X - 0.14511X^2, \tag{4.56}$$

$$A_2 = 28606.4 - 934.68X + 8.52755X^2, \tag{4.57}$$

$$A_3 = 70.3848 - 2.35014X + 0.0207809X^2. \tag{4.58}$$

The following diagram is presented by ASHRAE [124] for viscosity of LiBr solution:

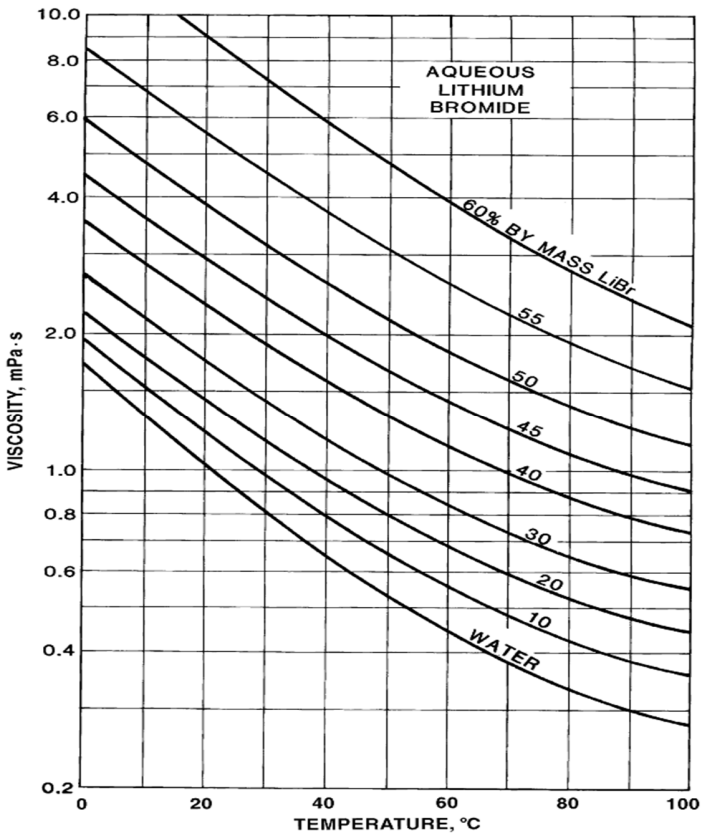

Fig. 4.11 Viscosity of aqueous solution of LiBr

- Thermal conductivity of LiBr-water solution can be determined by using the following correlation [136]:

$$k_s = \begin{Bmatrix} K_1 + S & for\ T_k \geq 313 \\ K_2 + S & for\ T_k < 313 \end{Bmatrix}, \tag{4.59}$$

where *S* can be determined as:

$$S = \left(\frac{K_2 - K_1}{20} \right)(T_k - 313), \tag{4.60}$$

and K_1 and K_2 can be determined by the following correlations:

$for\ T_k \geq 313$:

$$K_1 = -0.3081\left(\frac{X}{100} \right) + 0.62979\ , \tag{4.61}$$

$$K_2 = -0.3191795\ \left(\frac{X}{100} \right) + 0.65388\ , \tag{4.62}$$

$for\ T_k < 313$:

$$K_1 = -0.3081\left(\frac{X}{100} \right) + 0.62979, \tag{4.63}$$

$$K_2 = -0.291897\left(\frac{X}{100} \right) + 0.59821. \tag{4.64}$$

4.4 Performance Evaluation

The equations in section 4.3.2 can be used to evaluate the performance of the single-effect absorption chiller. To determine the heat transfer rate of each component and flow rate at different lines, the following equations can be used:

The weak solution concentration leaving absorber in kg LiBr/kg solution can be calculated as [129]:

$$X_{ws} = X_1 = X_2 = X_3 = \frac{49.04 + 1.125T_a - T_e}{134.65 + 0.47T_a}, \tag{4.65}$$

where T_a and T_e are the absorber and evaporator temperature respectively.

The strong solution concentration leaving generator can be calculated as:

$$X_{ss} = X_4 = X_5 = X_6 = \frac{49.04 + 1.125T_g - T_c}{134.65 + 0.47T_g}, \tag{4.66}$$

in which T_g and T_c are the generator and condenser temperature respectively.

For the rest of the points in Fig. 4.1:

$$X_7 = X_8 = X_9 = X_{10} = 0. \tag{4.67}$$

The enthalpy of saturated liquid water at point (8) can be calculated using the following equations:

$$h_8 = 4.187(T_c - 25) + 104.8. \tag{4.68}$$

For the throttling process from point 8 to point 9 and point 5 to point 6 in Fig.4.1, the enthalpy of the entering and leaving solution are equal, therefore:

$$h_8 = h_9. \tag{4.69}$$

$$h_5 = h_6. \tag{4.70}$$

The enthalpy of saturated water vapour in point (10) can be obtained by:

$$h_{10} = -0.00125397T_e^{\,2} + 1.88060937T_e + 2500.559. \tag{4.71}$$

Using the first law of thermodynamic for evaporator the refrigerant (water) flow rate which is equal to difference between the strong and weak solution rates can be calculated as:

$$\dot{m}_{ref} = \frac{Q_e}{h_{10} - h_8}. \tag{4.72}$$

The mass balance for absorber gives:

$$\dot{m}_{ss}X_6 + \dot{m}_{ref}X_{10} = \dot{m}_{ws}X_1 = (\dot{m}_{ss} + \dot{m}_{ref})X_1. \tag{4.73}$$

Using equations (4.67) and (4.72), equation (4.73) can be rewritten to give:

$$\dot{m}_{ws} = \left(\frac{Q_e}{h_{10} - h_8}\right)\left(\frac{X_4}{X_4 - X_1}\right), \tag{8.74}$$

$$\dot{m}_{ss} = \left(\frac{Q_e}{h_{10} - h_8}\right)\left(\frac{X_1}{X_4 - X_1}\right). \tag{4.75}$$

The water vapour enthalpy leaving the generator and entering the condenser can be determined by using the followings equation:

$$h_7 = 4.187\left(572.8 + 0.46T_g - 0.043T_c\right). \tag{4.76}$$

The heat balance for the condenser gives:

$$Q_c = \dot{m}_{ref}(h_7 - h_8). \tag{4.77}$$

Using equation (8.72), the condenser capacity can be rewritten as:

$$Q_c = \frac{(h_7 - h_8)}{(h_{10} - h_8)} \times Q_e. \tag{4.78}$$

The heat balance for combined control volume of the generator and heat exchanger gives:

$$Q_g = \dot{m}_{ss} h_5 + \dot{m}_{ref} h_7 - \dot{m}_{ws} h_2, \tag{4.79}$$

applying equations (8.72), (8.74) and (8.75), and assuming that pump work is negligible *($h_2=h_1$)* the generator capacity can be calculated as:

$$Q_g = \frac{Q_e}{(h_{10} - h_8)} \left[\frac{X_1 h_5}{(X_4 - X_1)} + h_7 - \frac{X_4 h_1}{(X_4 - X_1)} \right]. \tag{4.80}$$

Using heat balance the absorber capacity can be determined as:

$$Q_a = \dot{m}_{ss} h_6 + \dot{m}_{ref} h_{10} - \dot{m}_{ws} h_1, \tag{4.81}$$

using equations 4.69, 4.70, 4.72, 4.74 and 4.75, the absorber capacity can be calculated as:

$$Q_a = \frac{Q_e}{(h_{10} - h_8)} \left[\frac{X_1 h_5}{(X_4 - X_1)} + h_{10} - \frac{X_4 h_1}{(X_4 - X_1)} \right]. \tag{4.82}$$

The overall heat balance gives the following equation:

$$Q_a + Q_c = Q_e + Q_g. \tag{4.83}$$

The solution heat exchanger should be analysed to determine the weak and strong solution temperature leaving the heat exchanger T_3 and T_5. For this, the effectiveness of the heat exchanger, the weak and strong solution mass flow rate and concentration should be known. The effectiveness of the solution heat exchanger can be determined as [129]:

$$\varepsilon_{hx} = \frac{T_g - T_5}{T_g - T_a} = \frac{(\dot{m}_{ss} C_{X1})(T_3 - T_a)}{(\dot{m}_{ws} C_{X4})(T_g - T_a)}, \tag{4.84}$$

in which C_{X4} and C_{X1} are the specific heat of strong and weak solution with concentration of the X_4 and X_1 respectively and can be determined as [129]:

$$C_{x1} = 4.187\left(1.01 - 1.23X_1 + 0.48X_1^{\,2}\right). \tag{4.85}$$

$$C_{x4} = 4.187\left(1.01 - 1.23X_4 + 0.48X_4^{\,2}\right). \tag{4.86}$$

Now using equations (4.74), (4.75), (4.84), (4.85) and (4.86), the weak and strong solution temperature leaving the heat exchanger T_3 and T_5 can be calculated as:

$$T_5 = T_g - \varepsilon_{hx}\left(T_g - T_a\right), \tag{4.87}$$

$$T_3 = T_a + \left[\varepsilon_{hx}\left(\frac{X_1}{X_4}\right)\left(\frac{C_{X4}}{C_{X1}}\right)\left(T_g - T_a\right)\right]. \tag{4.88}$$

The enthalpies h_1 and h_5 can then be calculated using equation:

$$h_1 = 4.187\left(1.01 - 1.23X_1 + 0.48X_1^{\,2}\right) + \left(42.81 - 425.92X_1 + 404.67X_1^{\,2}\right) \times T_a, \tag{4.89}$$

$$h_5 = 4.187\left(1.01 - 1.23X_5 + 0.48X_5^{\,2}\right) + \left(42.81 - 425.92X_5 + 404.67X_5^{\,2}\right) \times T_5. \tag{4.90}$$

4.4.1 Cycle Pressure

The saturated pressure P in mm Hg for water can be calculated by [129]:

$$log_{10} P = 7.8553 - \frac{1555}{T_k} - \frac{11.2414 \times 10^4}{T_k^{\,2}}, \tag{4.91}$$

where T_k is saturation temperature in Kelvin. Therefore, the pressure in every line can be evaluated as follows:

- Evaporator pressure (P_e)

$$\log_{10} P_e = 7.8553 - \frac{1555}{T_e + 273.15} - \frac{11.2414 \times 10^4}{(T_e + 273.15)^2}, \tag{4.92}$$

and

$$P_e = P_1 = P_6 = P_9 = P_{10}. \tag{4.93}$$

- Condenser pressure (P_c):

$$\log_{10} P_c = 7.8553 - \frac{1555}{T_c + 273.15} - \frac{11.2414 \times 10^4}{(T_c + 273.15)^2}, \tag{4.94}$$

and

$$P_c = P_2 = P_3 = P_4 = P_5 = P_7 = P_8. \tag{4.95}$$

4.4.2 Coefficient of Performance (COP)

Coefficient of performance is actually the measure of energy use efficiency and for the absorption chiller is defined as the ratio of refrigeration effect produced to the energy input for the system. Neglecting the small work input to the solution pump, the COP of the absorption cycle is:

$$COP = \frac{Heat\ load\ in\ the\ evaporator}{External\ heat\ input} = \frac{Q_e}{Q_g}, \tag{4.96}$$

To find the maximum possible COP of the absorption chiller, the second law of thermodynamic should be used. The general statement of the second law is that when the system experiences a change of state, the total change in the system entropy and its surroundings is greater than or equal to zero. It means that the processes can occur in the direction that the net total change of entropy increases. However, the real processes are irreversible and when the working fluid of the system goes through a process, some of the available work is lost.

To determine the maximum possible COP of the absorption cycle its processes are considered as the reversible processes. The absorption cycle can be evaluated as the combination of a heat engine and a mechanical vapour combination system. An ideal absorption cycle operating between a heat source temperature of T_g, a heat sink temperature of T_o for heat rejection and low temperature reservoir at T_e as shown in Fig. 4.12. The ideal cycle operating with thermodynamically reversible processes between two temperatures is the Carnot cycle. Therefore, the ideal absorption cycle demonstrated in Fig.4.12, can be represented by a combined cycle of a Carnot heat pump operating between T_e and T_c driven by a Carnot heat engine operating between T_g and T_a as shown in Fig 4.13. From the overall heat balance the following equation can be written as:

$$Q_g + Q_e = Q_c + Q_a, \tag{4.97}$$

For a thermodynamically reversible process in the evaporator and condenser, the reduction in the entropy in the condenser would equal the gain in entropy in the evaporator [128]. This results in:

$$\frac{Q_e}{T_e} = \frac{Q_c}{T_c}. \tag{4.98}$$

For the ideal absorption cycle, the change in entropy for the whole cycle is zero, therefore;

$$\frac{Q_g}{T_g} + \frac{Q_e}{T_e} = \frac{Q_c}{T_c} + \frac{Q_a}{T_a}, \tag{4.99}$$

Now combining equations (4.98) and (4.99) gives:

$$\frac{Q_g}{T_g} = \frac{Q_a}{T_a}. \tag{4.100}$$

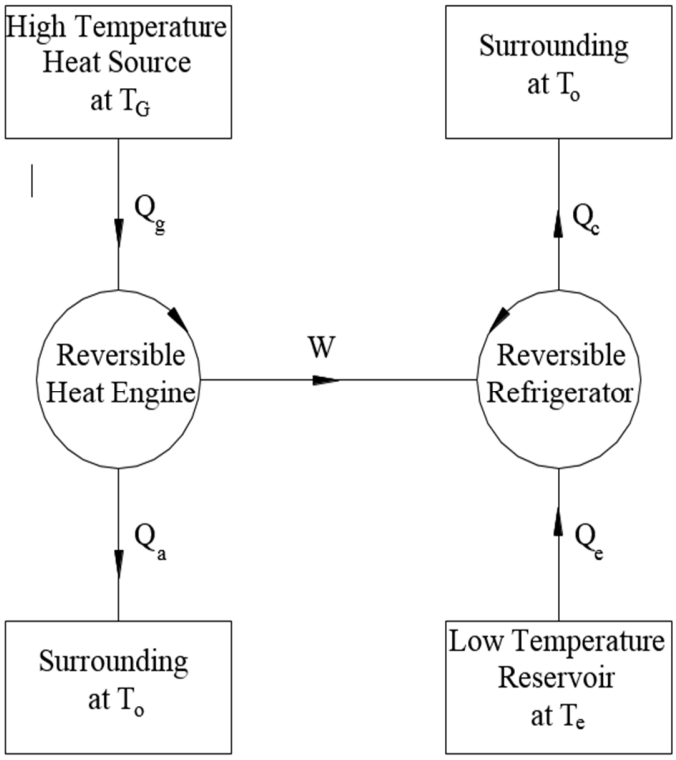

Fig 4.12 Combined Carnot heat pump and Carnot heat engine

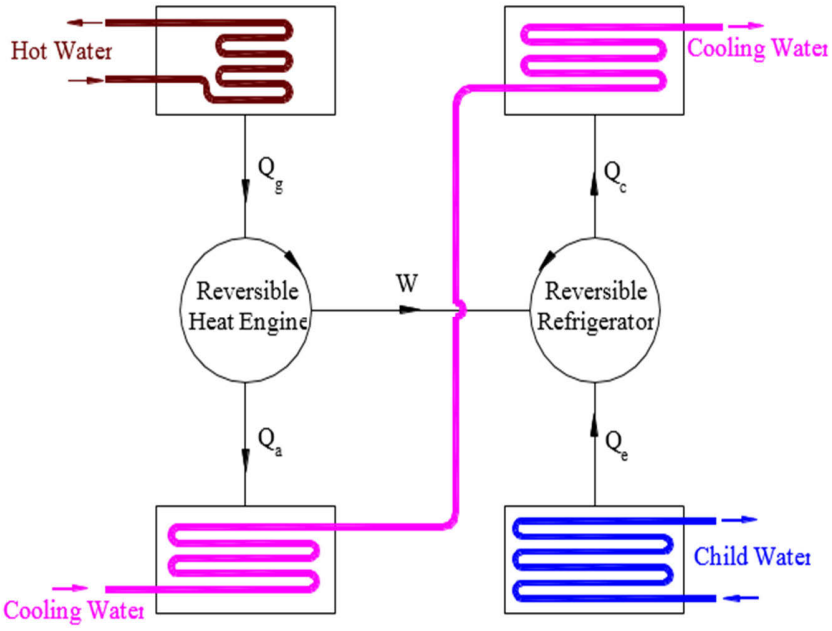

Fig. 4.13 Idea absorption cycle

From equations (4.96), (4.97) and (4.98), the Carnot COP for the single-effect absorption system can be concluded as:

$$COP_{\max} = \frac{Q_e}{Q_g} = \left(\frac{T_g - T_a}{T_g}\right)\left(\frac{T_e}{T_c - T_e}\right) \tag{4.101}$$

The COP_{max} represents the maximum possible obtainable coefficient of performance for the absorption cycle. In fact, the actual COP is always less than COP_{max} due to unavoidable thermodynamic inefficiencies. From equation (4.101) it can be seen that maximum achievable COP for the absorption cycle is only dependent on its cycle operation temperatures. However, as it will be discussed in next chapter, the actual COP is significantly less than ideal COP which suggests a significant potential for cycle design improvement.

Using the actual and ideal COP, it is possible to define the thermodynamic efficiency of the absorption cycle to show the effectiveness of the energy utilization. The second law efficiency is defined as the ratio of the required minimum energy input for an ideal system to the actual energy input of a real system as:

$$\eta = \frac{(Q_g)_{ideal\ cycle}}{(Q_g)_{actual\ cycle}} = \frac{\frac{Q_e}{COP_{\max}}}{\frac{Q_e}{COP}} \Rightarrow \eta = \frac{COP}{COP_{\max}} \tag{4.102}$$

4.5 Absorption Cycle Plot Representation

Plot representation of the absorption cycle assists to understand all cycle solutions. One common way to depict the absorption cycle is Duhring plot which allows designer to view all of the important operating data in one plot as shown in Fig. 4.14. In this plot, the solution temperature is given on the x-axis, the corresponding refrigerant pressure on the left y-axis and the refrigerant temperature on the right y-axis. The grey lines are solution concentration. The water vapour pressure is a function of both the temperature and the solution concentration. Number of drawbacks such as the approach of the operating envelope to the

crystallisation line can be eschewed by scheming the absorption cycle in the Duhring plot. If the operating design conditions violate the design limits, the new operating design data must be considered and the Duhring plot will be re-formed again.

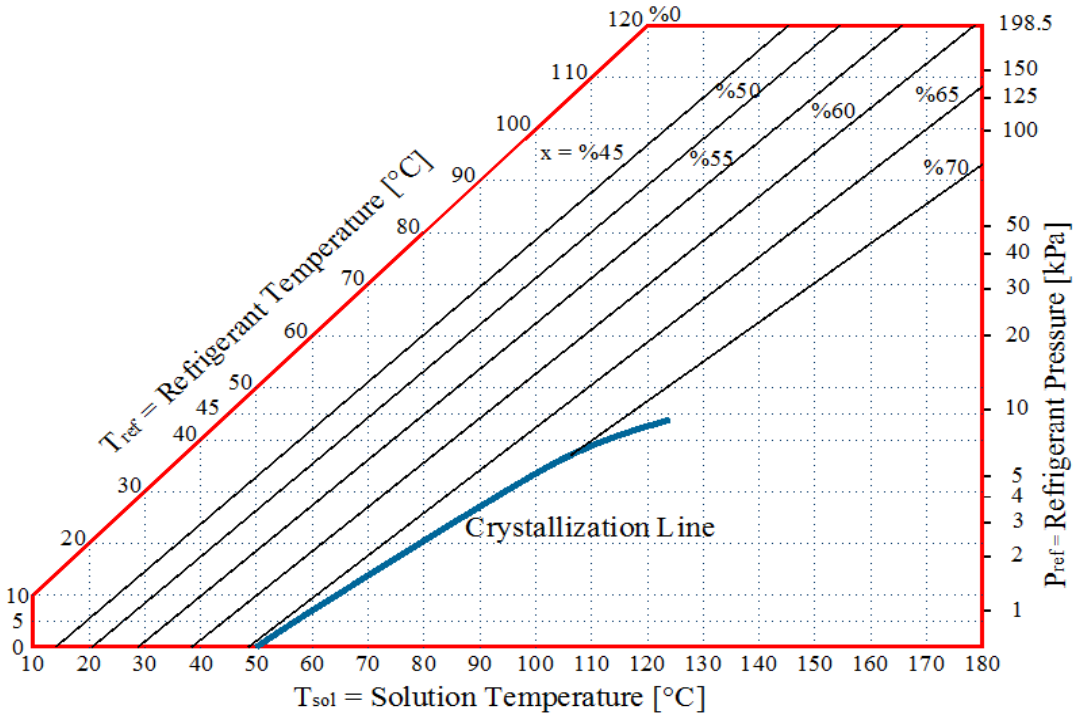

Fig. 4.14 Duhring plot for absorption cycle

Chapter 5

PARAMETRIC STUDY AND PERFORMANCE PREDICTION OF THE SINGLE-EFFECT ABSORPTION CHILLER

5.1 Summary

The objective of this chapter is to evaluate the characteristics and performance of the single-effect LiBr-water absorption chiller. The operating cycle functions with hot water in the generator, chilled water in the evaporator and cooled water in the absorber and condenser. First, the thermodynamic parameters of the absorption chiller operation cycle are determined using a developed computer code, ABSYS. Heat transfer rates in the chiller's heat exchangers are calculated for the selected set of cycle operating parameters. A parametric study is then conducted over the entire admissible ranges of the generator, condenser, evaporator and absorber temperatures. The effect of solution heat exchanger on the system performance is also investigated. It is concluded that the coefficient of performance (COP) of the chiller increases with increasing generator and evaporator temperatures but decreases with increasing the condenser and absorber temperatures. Finally, table of possible combinations of operating temperatures, concentrations, flow ratio, coefficient of performance and maximum possible COP are presented which can be used by other authors to develop the single-effect LiBr-water absorption chiller.

5.2 Solution Procedure

The sequence of the solution procedure is illustrated in Fig. 5.1 and described in this section. For this analysis, the cooling capacity of the absorption chiller is known. The thermodynamic design of LiBr-water absorption chiller by using the first law is based on steady state operating conditions. The generator, evaporator, condenser and absorber temperatures as well as solution heat exchanger effectiveness are assumed. The purpose is to determine the capacity of the generator, condenser and absorber, the mass flow rates in the cycle and the

pressure and enthalpy of each point in the operation cycle. By using these calculated data, the overall heat transfer coefficient, area and tubes arrangement for each heat exchanger is then designed in chapter seven. The lowest generator temperature below which the cycle will not operate is determined. During the design procedure, the absorber and evaporator are assumed at the same pressure while in actual absorption chiller a small pressure difference is essential. In addition, the condenser and generator are assumed to operate at the same pressure.

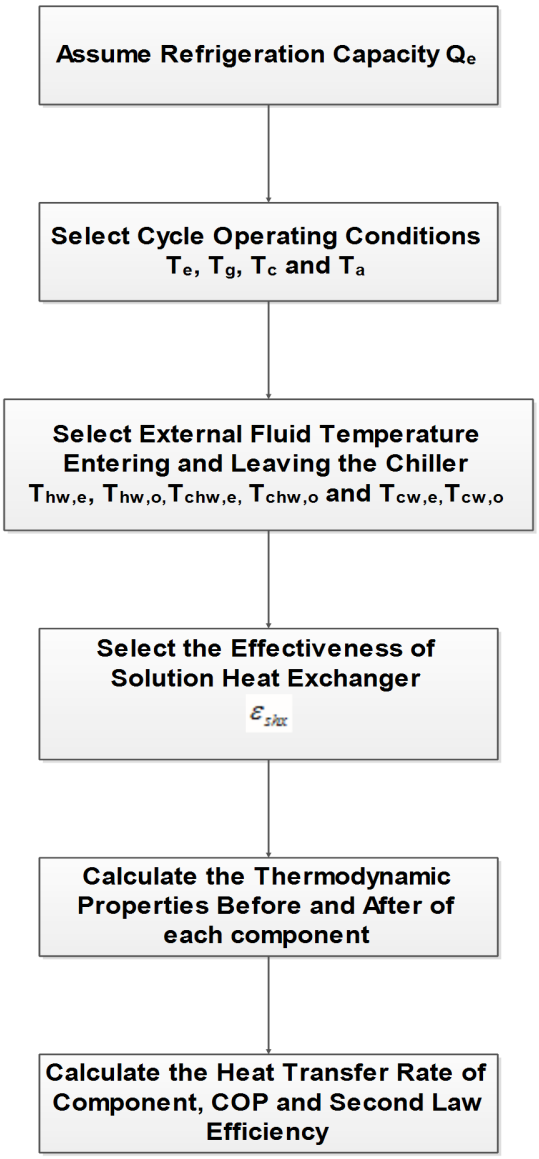

Fig. 5.1 Schematic representation of solution procedure

The thermodynamic cycle of the cooling plant operates with hot water in the generator, chilled water in the evaporator and cooled water in the absorber and condenser. The inlet and outlet temperatures of these external fluids can be varied. These parameters are selected based on various factors such as building cooling load, required supply air temperature, ambient wet-bulb temperature and solar radiation intensity of the region. In this study a LiBr-water single-effect absorption chiller with the nominal refrigeration capacity of 7 kW is designed. The generator temperature, T_g depends on the water temperature leaving the solar collector. In this study a temperature of 78°C is used to provide efficient operation. The hot water temperature entering and leaving the generator at the steady state conditions is considered as 85°C and 81°C. For an efficient air conditioning application, the evaporative temperature, T_e should be low enough to dehumidify the air. In practice the evaporative temperature in usually between 4°C and 12°C dependent on required designed chilled water temperature. For the air conditioning purposes in which the space temperature is normally considered between 22°C and 27°C, an evaporative temperature of 10°C to 12°C is sufficient to cool the air, however, a lower evaporative temperature is required for air dehumidification. In addition, as it will be discussed in this chapter, reducing the evaporator temperature leads to a higher second law efficiency for the absorption refrigeration cycle. In this study, the leaving and entering chilled water temperature are considered as 7°C and 12°C and thus the evaporative temperature is considered as 5°C. For the condenser and absorber, a lower temperature increases the cycle efficiency, however, these temperature should be assumed based on cooling water available. In practice a temperature difference of 5°C is normally used between ambient wet-bulb temperature and cooled water leaving the cooling tower. Since the wet-bulb temperature of the Sydney at steady state designed condition is 22.7°C [137], the cooled water temperature of 27.7°C can be achieved by cooling tower. However, the water temperature leaving and entering the cooling tower is considered as 28°C and 32°C. The cooling water leaving the cooling tower first passes the absorber where its temperature is increased due to heat transfer between cooled water and solution LiBr-water. It is assumed that the cooled water temperature is increased by 2°C in the absorber before goes to the condenser. Another 2°C increment in cooling water temperature is considered in the condenser. Therefore, in designed steady state condition, the cooled water enters the absorber

at 28°C and leaves the absorber and enters the condenser at 30°C and leaves the condenser at 32°C. In this study absorber and condenser temperatures are considered as 36°C and 37°C respectively.

The operational function of the solution heat exchanger is reduction of the strong solution temperature leaving the generator and increasing the weak solution temperature leaving the absorber. The effectiveness of the solution heat exchanger is assumed as 70% in this design. As presented in chapter five, the building heat load is about 6.4 kW and therefore a cooling capacity of 7 kW is selected for the single-effect absorption chiller. Consequently, the assumptions used to design the absorption chiller are as:

- Refrigeration Capacity=7 kW

The refrigeration capacity is the thermal capacity of the evaporator heat exchanger. The thermal capacity of the generator, condenser and absorber can then be calculated based on their operating temperature and required refrigeration capacity.

- Generator temperature=T_g=78°C

Hot water enters the generator at a temperature 7°C higher than assumed operating generator temperature and leaves the generator after a drop of 4°C in its temperature.

- Evaporator temperature=T_e=5°C

Chilled water leaves the evaporator at a temperature 2°C higher than assumed operating evaporator temperature and enters the evaporator after an increase of 5°C in its temperature.

- Absorber temperature=T_a=36°C

Cooled water leaves the cooling tower and enters the absorber at a temperature 8°C less than assumed operating absorber temperature and leaves the absorber after an increase of 2°C in its temperature.

- Condenser temperature=T_c=37°C

Cooled water leaves the absorber and enters the condenser at a temperature 7°C less than assumed operating condenser temperature and leaves the condenser after an increase of 2°C in its temperature.

- Solution heat exchanger effectiveness=0.7

Referring to the design procedure and above assumptions, the thermodynamic parameters and heat transfer capacity of each heat exchanger can be determined as follows:

The weak solution concentration in kg LiBr/kg solution leaving the absorber can be calculated as:

$$X_{ws} = X_1 = X_2 = X_3 = \frac{49.04 + 1.125T_a - T_e}{134.65 + 0.47T_a} = \frac{49.04 + 1.125 \times 36 - 5}{134.65 + 0.47 \times 36} = 0.5577 \frac{kg\ LiBr}{kg\ water}. \quad (5.1)$$

The strong solution concentration leaving the generator can be calculated as:

$$X_{ss} = X_4 = X_5 = X_6 = \frac{49.04 + 1.125T_g - T_c}{134.65 + 0.47T_g} = \frac{49.04 + 1.125 \times 78 - 37}{134.65 + 0.4 \times 78} = 0.5825 \frac{kg\ LiBr}{kg\ water}. \quad (5.2)$$

The enthalpy of the refrigerant leaving the condenser is calculated as:

$$h_8 = 4.187(T_c - 25) + 104.8 = 4.187(37 - 25) + 104.8 = 155.04 \frac{kJ}{kg}. \quad (5.3)$$

For the throttling process from point 8 to point 9:

$$h_8 = h_9 = 155.04 \frac{kJ}{kg}. \quad (5.4)$$

The enthalpy of saturated water vapour in point (10) can be obtained by:

$$h_{10} = -0.00125397T_e^2 + 1.88060937T_e + 2500.559 = 2509.93 \frac{kJ}{kg}. \quad (5.5)$$

The refrigerant, strong solution and weak solution mass flow rate are determined as:

$$\dot{m}_{ref} = \frac{Q_e}{h_{10} - h_8} = \frac{7}{2509.93 - 155.04} = 0.00297 \frac{kg}{s} = 10.692 \frac{kg}{hr}, \tag{5.6}$$

$$\dot{m}_{ss} = \left(\frac{X_4}{X_4 - X_1} \right) \dot{m}_{ref} = \left(\frac{0.5577}{0.5825 - 0.5577} \right) \times 0.00297 = 0.0669 \frac{kg}{s}, \tag{5.7}$$

$$\dot{m}_{ws} = \left(\frac{X_1}{X_4 - X_1} \right) \dot{m}_{ref} = \left(\frac{0.5825}{0.5825 - 0.5577} \right) \times 0.00297 = 0.0699 \frac{kg}{s}. \tag{5.8}$$

The specific heat of strong and weak solution with concentration of the X_4 and X_1 can be determined by:

$$\begin{aligned} &C_{X1} = 4.187\left(1.01 - 1.23X_1 + 0.48X_1^{\,2}\right) = \\ &4.187\left(1.01 - 1.23 \times 0.5577 + .48 \times (0.5577)^2\right) = 1.98 \frac{kJ}{kg\,°C}, \end{aligned} \tag{5.9}$$

$$\begin{aligned} &C_{X4} = 4.187\left(1.01 - 1.23X_4 + 0.48X_4^{\,2}\right) = \\ &4.187\left(1.01 - 1.23 \times 0.5825 + 0.48 \times (0.5825)^2\right) = 1.91 \frac{kJ}{kg\,°C}. \end{aligned} \tag{5.10}$$

The weak solution temperature leaving the heat exchanger, T_3 can be calculated as:

$$\begin{aligned} &T_3 = T_a + \left[\varepsilon_{hx} \left(\frac{X_1}{X_4} \right) \left(\frac{C_{X4}}{C_{X1}} \right) \left(T_g - T_a \right) \right] = \\ &37 + \left[0.7 \times \frac{0.5577}{0.5825} \times \frac{1.91}{1.98} \times (78 - 37) \right] = 63.5°C. \end{aligned} \tag{5.11}$$

The strong solution temperature leaving the heat exchanger, T_5 can be calculated as:

$$T_5 = T_g - \varepsilon_{hx}\left(T_g - T_a\right) = 78 - 0.7(78 - 37) = 49.3°C. \tag{5.12}$$

The enthalpies h_1 and h_5 can then be calculated using following equations:

$$h_1 = 4.187\left(1.01 - 1.23X_1 + 0.48X_1^{\,2}\right)\times T_a + 4.187\left(42.81 - 425.92X_1 + 404.67X_1^{\,2}\right) = 216.97\frac{kJ}{kg}, \tag{5.13}$$

$$h_5 = 4.187\left(1.01 - 1.23X_5 + 0.48X_5^{\,2}\right)\times T_5 + 4.187\left(42.81 - 425.92X_5 + 404.67X_5^{\,2}\right) = 191.76\frac{kJ}{kg}. \tag{5.14}$$

The water vapour enthalpy leaving the generator and entering the condenser can be determined by:

$$h_7 = 4.187\left(527.8 + 0.46T_g - 0.043T_c\right) = 4.187\left(527.8 + 0.46\times 78 - 0.043\times 37\right) = 2541.88\frac{kJ}{kg}, \tag{5.15}$$

The heat balance for the condenser gives:

$$Q_c = \dot{m}_{ref}\left(h_7 - h_8\right) = 0.00297\times\left(2541.88 - 155.04\right) = 7.1\ kW. \tag{5.16}$$

Generator capacity is calculated as:

$$Q_g = \dot{m}_{ws}h_1 + \dot{m}_{ref}h_7 - \dot{m}_{ss}h_5 = 0.0699\times 216.97 + 0.00297\times 2541.88 - 0.0669\times 191.76 = 9.88\ kW. \tag{5.17}$$

Absorber capacity can be determined as:

$$Q_a = \dot{m}_{ws}h_1 + \dot{m}_{ref}h_{10} - \dot{m}_{ss}h_5 = 0.0699\times 216.97 + 0.00297\times 2509.93 - 0.0669\times 191.76 = 9.48\ kW. \tag{5.18}$$

The evaporator and condenser pressure can be determined as:

$$\log_{10} P_e = 7.8553 - \frac{1555}{T_e + 273.15} - \frac{11.2414\times 10^4}{\left(T_e + 273.15\right)^2} = 7.8553 - \frac{1555}{5 + 273.15} - \frac{11.2414\times 10^4}{\left(5 + 273.15\right)^2} = 6.48 mm\,Hg = 0.864 kPa, \tag{5.19}$$

$$\log_{10} P_c = 7.8553 - \frac{1555}{T_c + 273.15} - \frac{11.2414 \times 10^4}{(T_c + 273.15)^2} = \\ 7.8553 - \frac{1555}{37 + 273.15} - \frac{11.2414 \times 10^4}{(37 + 273.15)^2} = 47.09 mm\,Hg = 6.28 kPa. \quad (5.20)$$

The coefficient of performance for absorption chiller can be calculated as:

$$COP = \frac{Q_e}{Q_g} = \frac{7}{9.88} = 0.708, \quad (5.21)$$

The maximum attainable COP for this design is:

$$COP_{max} = \left(\frac{T_g - T_a}{T_g}\right)\left(\frac{T_e}{T_c - T_e}\right) = \left(\frac{78 - 36}{78 + 273.15}\right)\left(\frac{5 + 273.15}{37 - 5}\right) = 1.04, \quad (5.22)$$

Finally, the second law efficiency of this design is determined as:

$$\eta = \frac{COP}{COP_{\max}} = \frac{0.708}{1.04} = 0.68. \quad (5.23)$$

A set of operating conditions and calculated thermodynamic properties for the proposed design of the absorption chiller is listed in Table 5.1. This design is plotted on the single-effect absorption cycle in Fig. 5.2. In addition, Fig.5.3 presents the cycle in the Duhring plot.

Point (i) (based on Fig 4.1)	$h_i\,(kJ/kg)$	$P_i\,(kPa)$	$T_i\,(^\circ C)$	$X_i\,(\%LiBr)$
1	216.9	0.864	36	55.7%
2	216.9	6.279	36	55.7%
3	145.6	6.279	63.1	55.7%
4	184.4	6.279	78	58.2%
5	191.7	6.279	49.3	58.2%
6	191.7	0.864	41.5	58.2%
7	2541.8	6.279	72.6	0
8	155.04	6.279	37	0
9	155.04	0.864	4.9	0
10	2509.93	0.864	4.9	0
$COP = 0.708$		$Q_e = 7\ kW$		$P_e = 0.864\ kPa$
$COP_{max} = 1.039$		$Q_g = 9.88\ kW$		$P_c = 6.279\ kPa$
$\varepsilon_{shx} = 0.7$		$Q_a = 9.48\ kW$		$\dot{m}_{ws} = 0.0699\ \frac{kg}{s}$
$\dot{m}_{ref} = 0.00297\ \frac{kg}{s}$		$Q_c = 7.1\ kW$		$\dot{m}_{ss} = 0.0669\ \frac{kg}{s}$

Table 5.1 Operating conditions and thermodynamic properties of the proposed single-effect absorption chiller

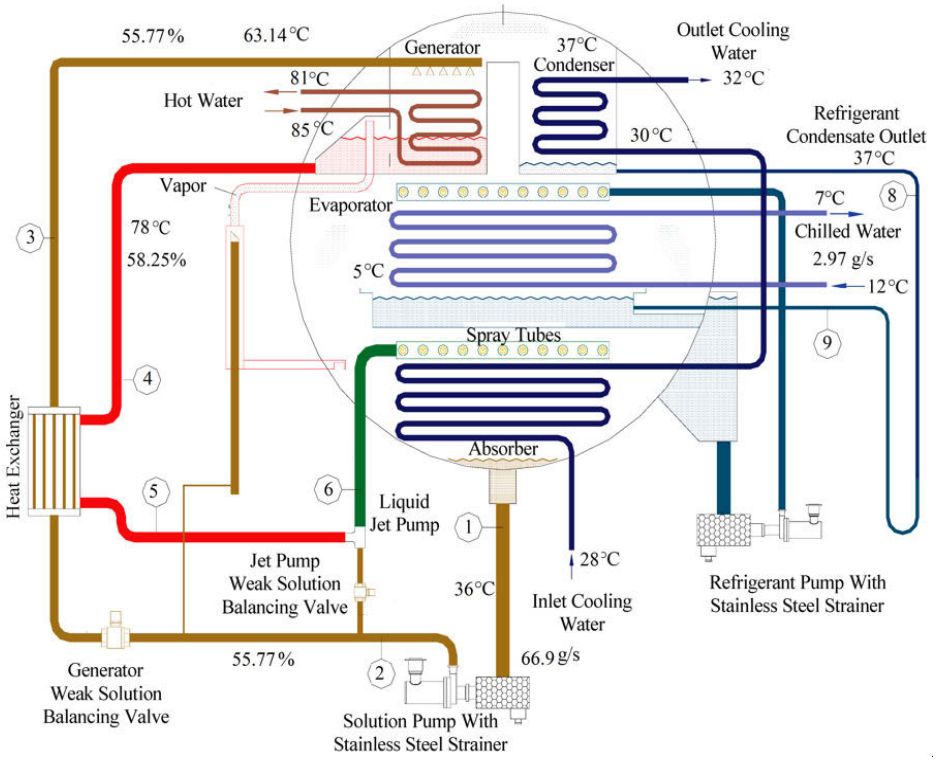

Fig. 5.2 Operating cycle of absorption chiller in designed steady state conditions

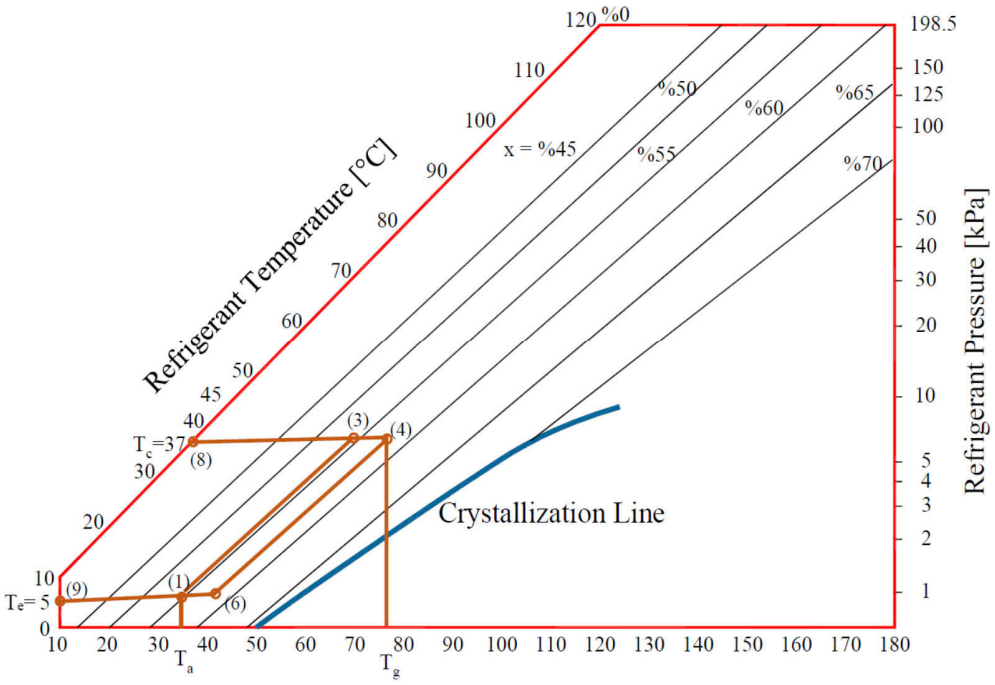

Fig. 5.3 Duhring plot for absorption chiller at designed steady state conditions

5.3 Parametric Study

In this section, the sensitivity of the absorption chiller performance to the variations of the selected input parameters is discussed. The influence of operating temperatures and effectiveness of the solution heat exchanger on the thermal capacity of the components, coefficient of performance and efficiency ratio are investigated and shown in Figs 5.4 to 5.30. This study is a comprehensive and useful source to perceive all parameters affecting system performance and to explore the importance of their efficacy. The consequences obtained from this analysis can be used for design and optimisation of single-effect absorption machine. These results are concluded from a detailed solution algorithm developed in ABSYS.

5.3.1 Effect of Generator Temperature Variations on Chiller Performance

To investigate the generator temperature variations on the performance of the absorption chiller, the following parameters were considered as constant:

Evaporator Capacity, Q_e=7 kW

Effectiveness of Solution Heat Exchanger, ε_{shx}=0.7

Evaporator Temperature, T_e=5°C

Condenser Temperature, T_c=37°C

Absorber Temperature, T_a=36°C

To investigate the effect of generator temperature on the system performance, it varies from 75°C to 95°C. As it can be seen in Fig. 5.4, the COP values increases with increasing the generator temperature. Results show that COP increases from 0.57 to 0.77, representing a 36% improvement. In addition, Fig. 5.4 shows the variation of the maximum possible COP of the absorption chiller with the generator temperature. It can be seen that the maximum COP is increased in a quasi linear style. The maximum possible COP is increased from 0.97 to 1.39.

Fig. 5.5 shows the effect of the generator temperature on the heat rejection of the condenser and absorber as well as thermal capacity of the generator. When the generator temperature increases, the generator and absorber thermal loads decrease. In fact the heat rejection at the absorber slightly reduces and then remains constant. However, over the entire generator temperature variations, the absorber heat rejection is reduced by 26.8%. The heat rejection at the condenser is smaller than that at the absorber and rises as the generator temperature is increased. Results show that increasing the generator temperature from 75°C to 95°C, increases the condenser heat rejection by less than 2%. Also increasing the generator temperature from 75°C to 95°C leads to generator thermal capacity reduction by 25%.

Fig. 5.6 shows the influence of the generator temperature variation on the mass flow rate of the solution leaving the generator and absorber. It can be seen that at low generator temperature, both the weak and strong solution mass flow rate are very close to one another and then sharply decrease as the generator temperature increases. However, the difference between weak and strong solution mass flow rate is increased gradually. It should be noted that the largest flow rate is that of the weak solution circulated through the pump. Another parameter which can be used to investigate the performance of the cooling cycle is circulation ratio and defined as the ratio of the weak solution mass flow rate leaving the absorber and the refrigerant mass flow rate:

$$CR = \frac{\dot{m}_{ws}}{\dot{m}_{ref}} \tag{5.1}$$

As it can be seen in Fig. 5.7, a considerable decrease occurs for circulation ratio as generator temperature increases. This means a large reduction of required pumping energy per produced cooling effect. The variation of solution concentration with increasing generator temperature is shown in Fig. 5.8. The LiBr concentration as the strong solution leaving the generator rises with increasing the generator temperature whilst the weak solution concentration leaving the absorber is almost unaffected by the generator temperature variations. However the concentration of the strong and weak solutions are very close at the generator temperature of 75°C. This means a very low cooling effect can be generated in this

temperature as refrigerant has not been separated from LiBr in the generator. Therefore, to prevent the cooling effect reduction the generator temperature should not be less than 75°C. This will be discussed later in this chapter.

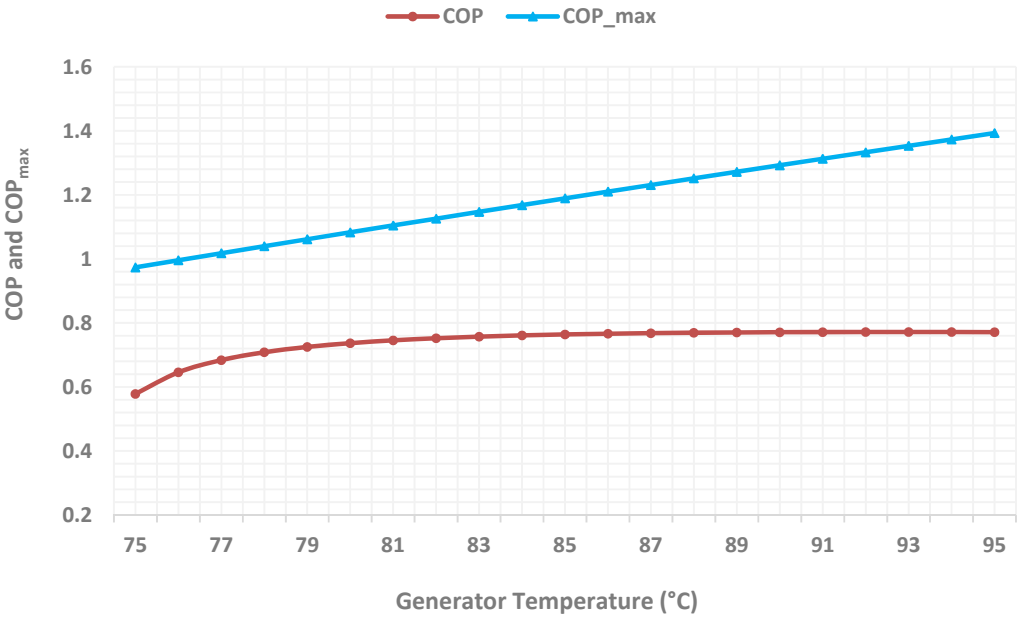

Fig 5.4 Effect of generator temperature on COP and COP_{max}

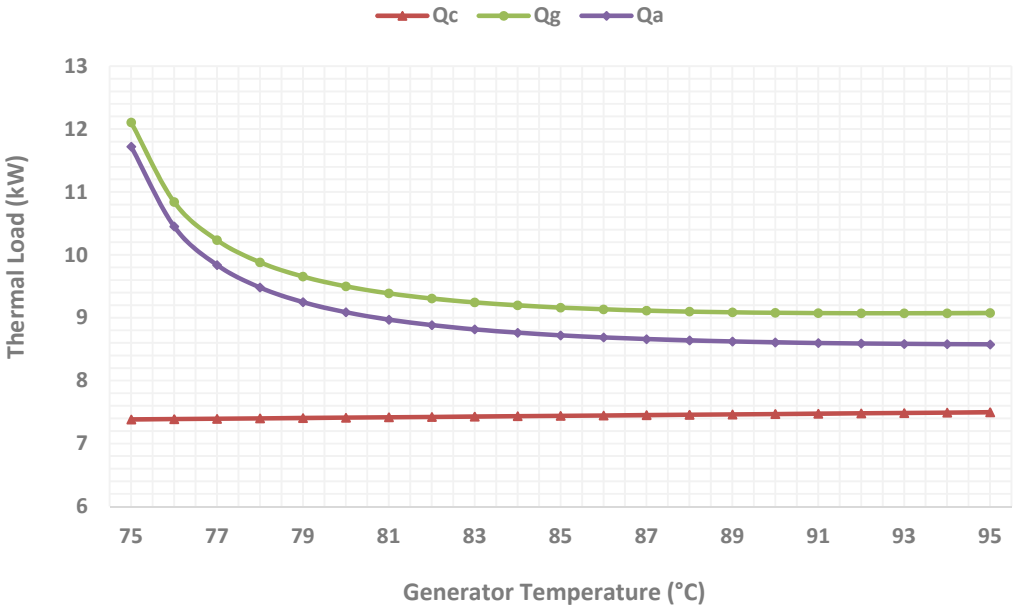

Fig 5.5 Effect of generator temperature on thermal capacity of other components

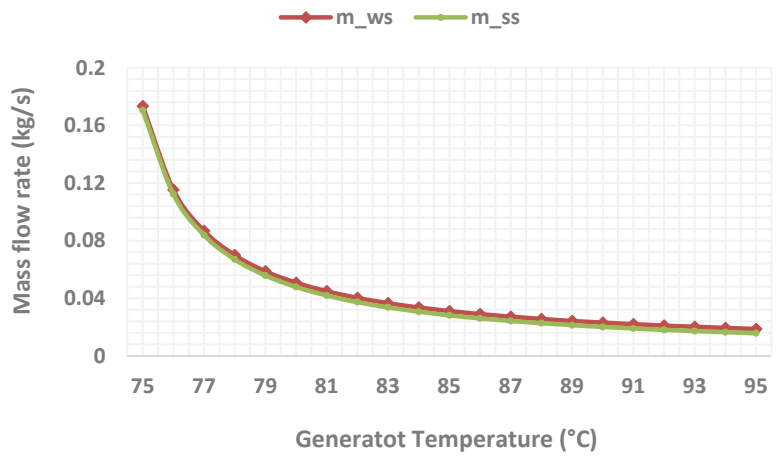

Fig 5.6 Effect of generator temperature on weak an strong mass flow rate

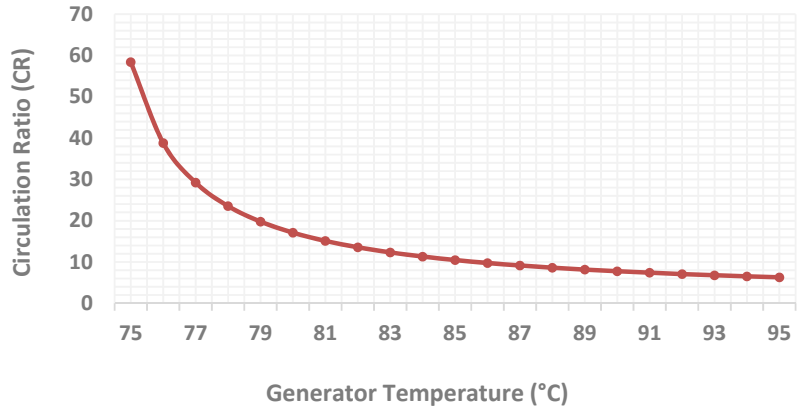

Fig 5.7 Effect of generator temperature on circulation ratio

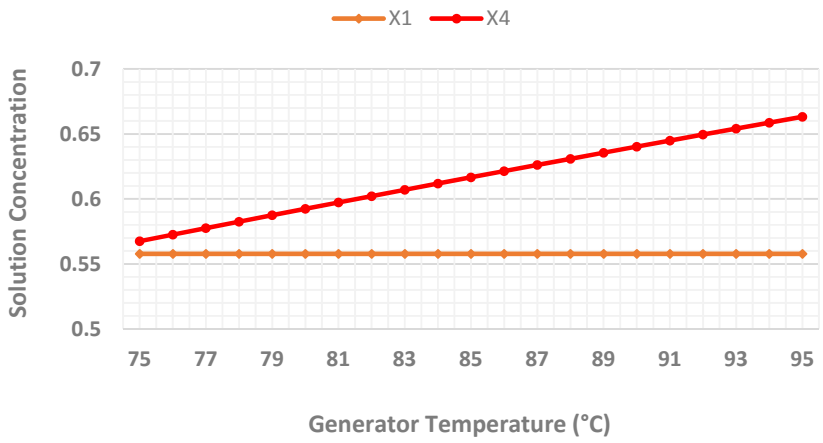

Fig 5.8 Effect of generator temperature on weak and strong solution concentration

5.3.2 Effect of Evaporator Temperature Variations on Chiller Performance

In this section the behaviour of the absorption chiller is investigated with increasing the operating temperature of the evaporator. The practical range for evaporator temperature is normally between 2°C to 15°C. To examine the effect of evaporator temperature on the system performance, the following design conditions were assumed as constant:

Evaporator Capacity, Q_e=7 kW

Effectiveness of Solution Heat Exchanger, ε_{shx}=0.7

Generator Temperature, T_g=78°C

Condenser Temperature, T_c=37°C

Absorber Temperature, T_a=36°C

Fig. 5.9 shows the behaviour of the absorption chiller COP with evaporative temperature variations. When the evaporative temperature increases from 2°C to 15°C, the COP increases gradually from 0.41 to 0.83 which shows the significant improvement. Furthermore, the maximum possible COP increases precipitously from 0.94 to 1.56. However, the evaporator temperature affects the low pressure of the chiller. Results show that increasing the evaporator temperature from 2°C to 15°C, increases the evaporator pressure by 58.9%. If the evaporator temperature rises, the weak solution concentration decreases as shown in Fig. 5.10. This causes a decrease in the absorber thermal load and on the other hand reduces the generator thermal load. As a result, the mass flow rate of the strong solution leaving the generator also decreases as shown in Fig. 5.10. Since the evaporator thermal capacity is maintained as constant, increasing the evaporator temperature leads to increasing the enthalpy of the low pressure vapour leaving the evaporator while the refrigerant enthalpy leaving the condenser and entering the evaporator is almost invariant. Consequently, the refrigerant mass flow rate reduced marginally as demonstrated in Fig. 5.11. Decreasing the refrigerant mass flow rate lessens the condenser thermal capacity. In the case of this study, increasing the evaporator temperature from 2°C to 15°C, reduces the thermal capacity of

absorber, generator and condenser by 50.6%, 49.7% and 0.96% respectively as shown in Fig. 5.12.

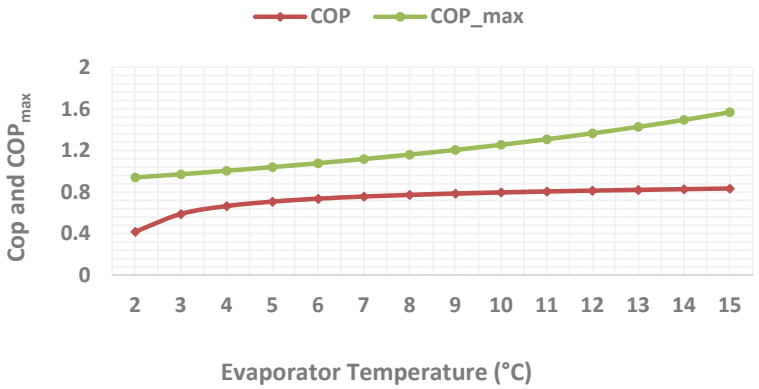

Fig 5.9 Effect of evaporator temperature on COP and COP_{max}

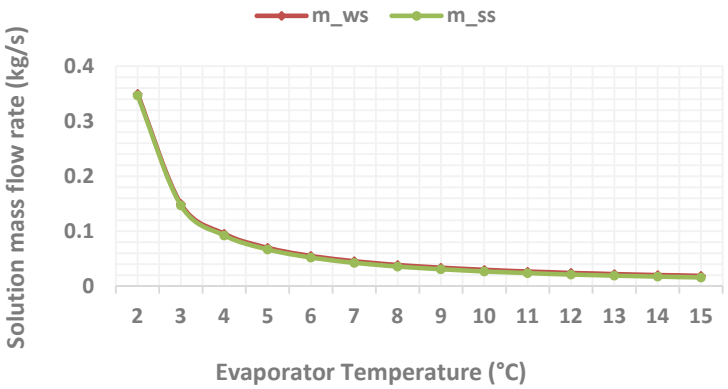

Fig 5.10 Effect of evaporator temperature on weak and strong solution mass flow rate

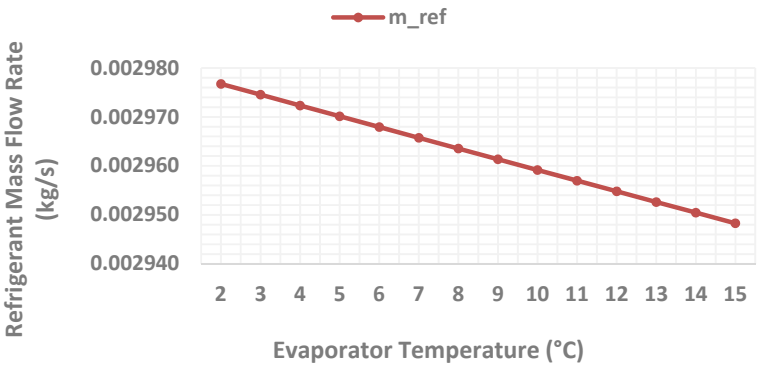

Fig 5.11 Effect of evaporator temperature on refrigerant mass flow rate

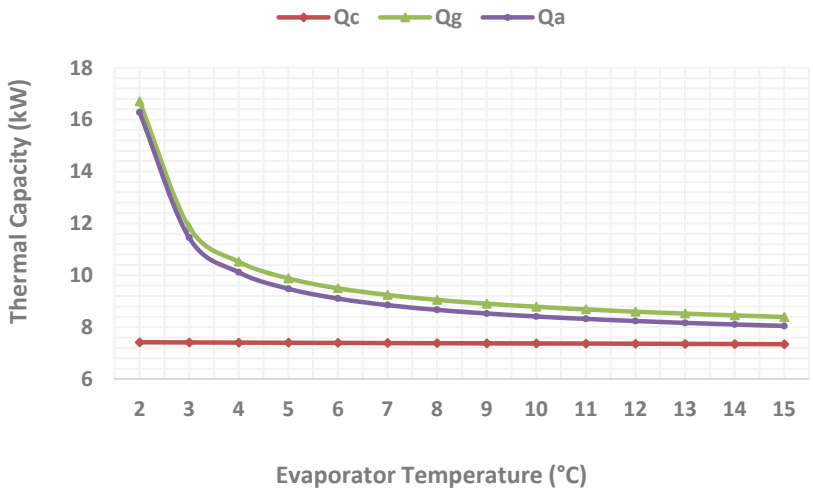

Fig 5.12 Effect of evaporator temperature on thermal capacity of other components

5.3.3 Effect of Condenser Temperature Variations on Chiller Performance

To study the influence of the condenser operating temperature on the performance of the absorption chiller, the following variables were assumed as constant:

Evaporator Capacity, Q_e=7 kW

Effectiveness of Solution Heat Exchanger, ε_{shx}=0.7

Evaporator Temperature, T_e=5°C

Evaporator Temperature, T_g=78°C

Absorber Temperature, T_a=36°C

The condenser temperature is then varied from 16°C to 40°C. Results show that increasing the condenser temperature leads to 38.7% reduction in the COP of the chiller. As shown in Fig. 5.13, the COP decreases significantly, dropping from 0.81 when the condenser temperature is 16°C to 0.51 when the condenser temperature is 40°C. Results also reveal that the maximum obtainable COP of the system is reduced by 68.5% when increasing the condenser temperature from 16°C to 40°C which is shown in Fig. 5.13. Furthermore, by

increasing the condenser operating temperature from 16°C to 40°C, the high pressure of the chiller increases about 407.7%. Therefore, the concentration of the LiBr-water solution leaving the generator is decreased while the weak concentration is unaffected as shown in Fig. 5.14. In addition, increasing the condenser temperature, increases the enthalpy of the refrigerant leaving the condenser and entering the evaporator. Since the evaporator thermal capacity is constant, this results in increasing of the refrigerant mass flow rate. Furthermore, increasing the enthalpy of the refrigerant leaving the condenser slightly dropps the condenser thermal capacity.

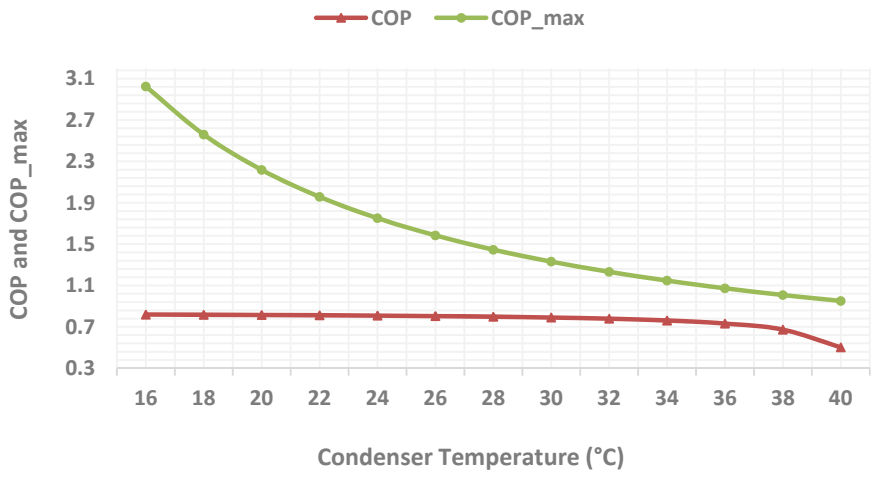

Fig. 5.13 Effect of condenser temperature on COP and COP_{max}

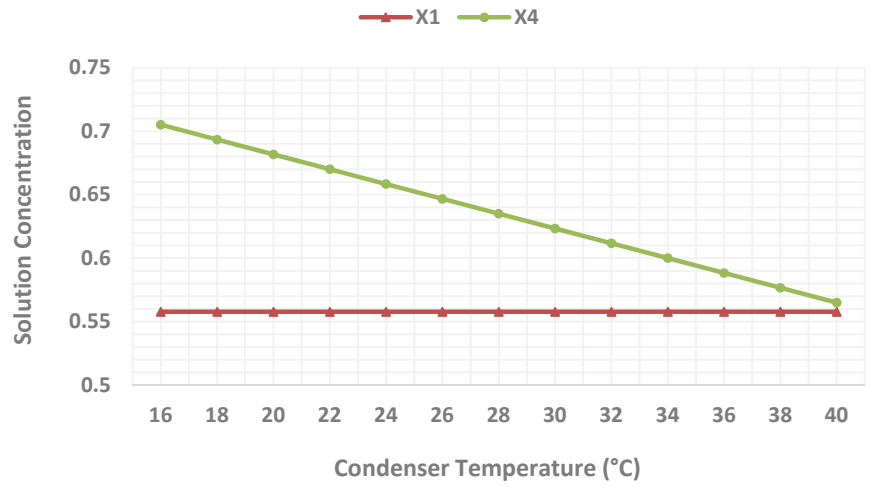

Fig. 5.14 Effect of condenser temperature on weak and strong solution concentration

In addition, since the thermal capacity of the evaporator is considered constant, the refrigerant mass flow rate is almost unchanged and because the strong solution is significantly reduced, the strong and weak mass flow rate increases. The effect of condenser operating temperature on the weak and strong solution mass flow rates is shown in Fig. 5.15. Moreover, increasing the weak and strong mass flow rate, increases the thermal capacity of the absorber and generator as shown in Fig. 5.16. Therefore, increasing the condenser temperature leads to increasing the cooling tower capacity as more heat rejection is required.

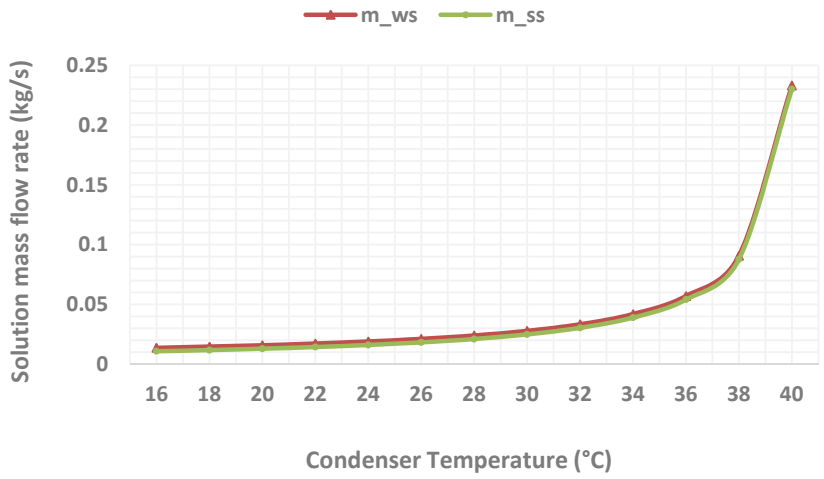

Fig. 5.15 Effect of condenser temperature on weak and strong solution mass flow rate

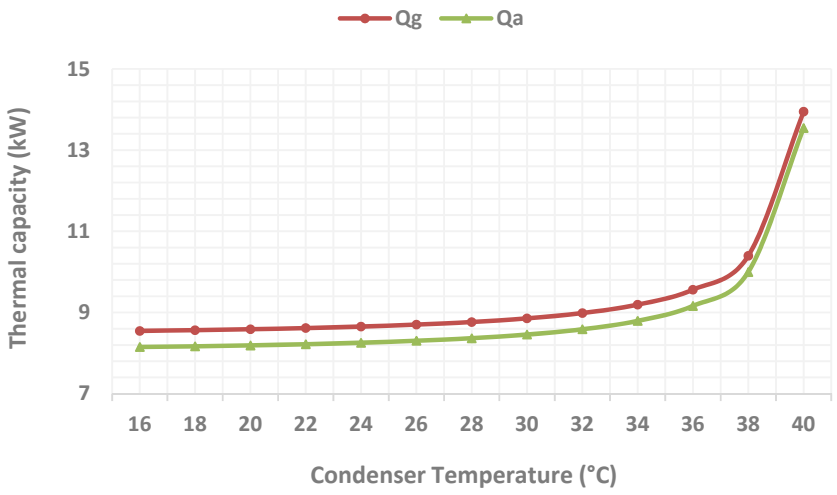

Fig. 5.16 Effect of condenser temperature on thermal capacity of other components

5.3.4 Effect of Absorber Temperature Variations on Chiller Performance

To investigate the influence of absorber operating temperature variations on the performance of the absorption chiller, the following parameters were considered as constant:

Evaporator Capacity, Q_e=7 kW

Effectiveness of Solution Heat Exchanger, ε_{shx}=0.7

Evaporator Temperature, T_e=5°C

Condenser Temperature, T_c=37°C

Generator Temperature, T_g=78°C

The absorber operating temperature varies from 16°C to 40°C. Fig. 5.17 shows the variation of the maximum possible COP of the absorption chiller with the absorber temperature. It can be seen that the maximum COP is reduced from 1.53 to 0.94. In addition, the COP values lessens with increasing the absorber temperature. Results show that COP decreases from 0.82 to 0.62, however, it rapidly reduces from 0.62 when the absorber temperature is 38°C to 0.28 when the absorber temperature increases to 40°C. To explain this behaviour, the weak and strong concentration should be studied as shown in Fig. 5.18.

In fact, increasing the absorber operating temperature increases the absorber solution concentration while the concentration of the strong solution at generator is maintained constant. The concentration of strong solution in the constant condenser temperature of 37°C is 58.25% and concentration of the solution in absorber is increased from 43.63% at absorber temperature of 16°C to 56.9% at absorber temperature of 38°C. Increasing the absorber temperature to 40°C leads to the concentration of the absorber solution about 58%. As a result, the concentration of the strong and weak solutions are very close at the absorber temperature of 40°C. This means a very low cooling effect can be generated in this temperature as refrigerant has not been separated from LiBr in the generator. To prevent this, the absorber and condenser operating temperature in which the difference between the weak

and strong solution concentrations are sufficient must be derived.

To analyse this effect, the evaporator and generator operating temperature maintain constant while the condenser and absorber operating temperature increase from 16°C to 40°C. Result shows that increasing the condenser temperature reduces the concentration of the strong solution leaving the generator. Meanwhile, increasing the absorber temperature at same increment, increases the concentration of the weak solution in the absorber as shown in Fig. 5.19. It can be seen from this figure that for our design, in the case of running the absorption chiller in the same absorber and condenser operating temperature, these temperatures should not be greater than 37°C. However, changing the design conditions will lead to different result. In our design, the absorber temperature is 1°C less than the condenser operating temperature to prevent the chance of low cooling effect problem.

As mentioned, by increasing the absorber temperature the concentration of the weak solution approaches the concentration of the strong solution and therefore the thermal capacity of the absorber and generator increase. However, the thermal capacity of the condenser is unaffected by the absorber temperature as shown in Fig. 5.20.

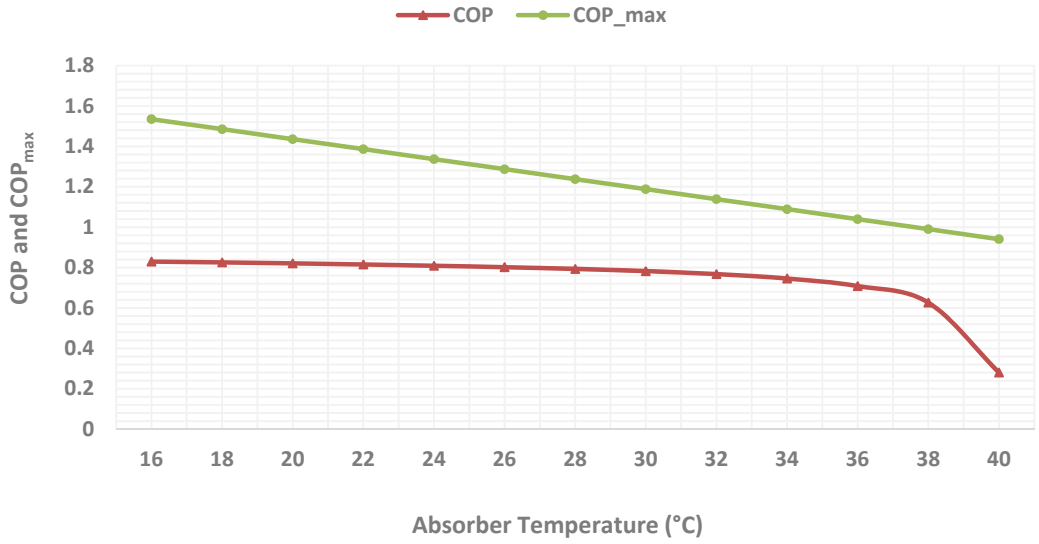

Fig. 5.17 Effect of absorber temperature on COP and COP_{max}

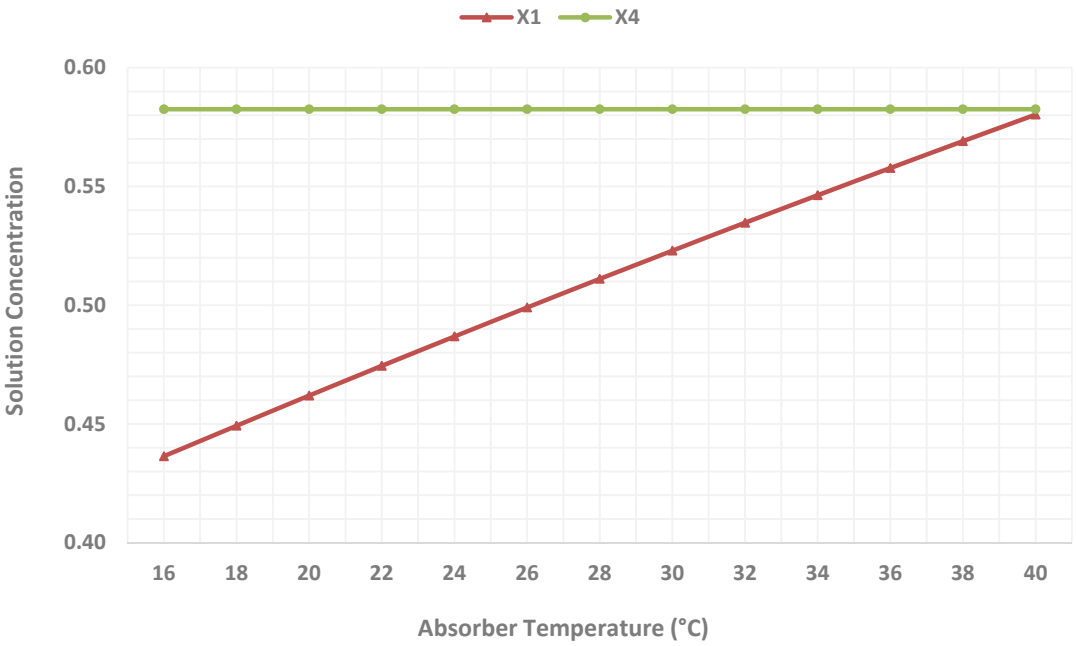

Fig. 5.18 Effect of absorber temperature on weak and strong solution concentration

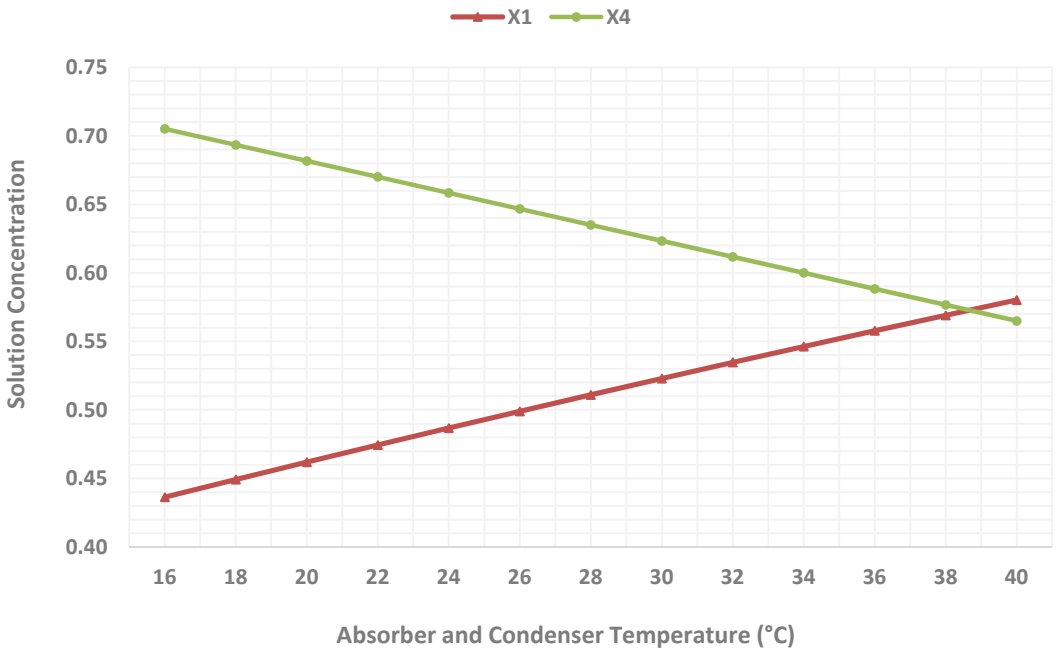

Fig 5.19 Effect of absorber and condenser temperatures on weak and strong solution concentration

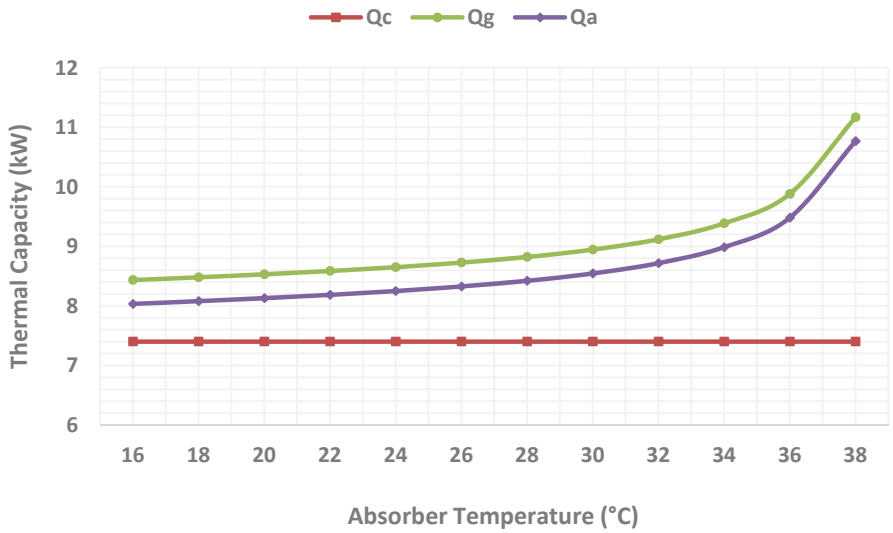

Fig 5.20 Effect of absorber temperature on thermal capacity of other components

5.3.5 Effect of Solution Heat Exchanger Effectiveness Variations on Chiller Performance

This section studies the effect of the solution heat exchanger effectiveness variations on the performance of the absorption chiller. To examine this, the following design conditions were assumed as constant:

Evaporator Capacity, Q_e=7 kW

Evaporator Temperature, T_c=5°C

Generator Temperature, T_g=78°C

Condenser Temperature, T_c=37°C

Absorber Temperature, T_a=36°C

In this analyse the effectiveness of the 0% for the SHX means that the absorption chiller does not use the SHX. Fig. 5.21 shows that the COP of the absorption chiller is increased in a quasi-linear fashion when increasing the effectiveness of the SHX form 0 to 100%. The COP of the chiller will increase from 0.51 to 0.84 when using the SHX with 100% efficiency

compared with the chiller without SHX which means the capability of the 39.3% improvement in COP. The maximum possible COP does not change with the variation of the SHX effectiveness and remains at 1.04.

As known in Fig. 4.1, the SHX is located between absorber and generator to recuperate the thermal energy of the strong solution existing the generator in order to preheat the weak solution leaving the absorber. Increasing the effectiveness of the SHX increases the heat exchange between the weak and strong solutions and therefore, the temperature of the weak solution increases while the temperature of the strong solution decreases as shown in Fig. 5.22. However, when the effectiveness of the SHX is one, the temperature of the strong solution equals the temperature of the weak solution. Increasing the weak solution temperature entering the generator decreases the thermal capacity of the generator and similarly, reduction of the strong solution temperature entering the absorber decreases the heat rejection capacity of the absorber. These outcomes are demonstrated in Fig. 5.23.

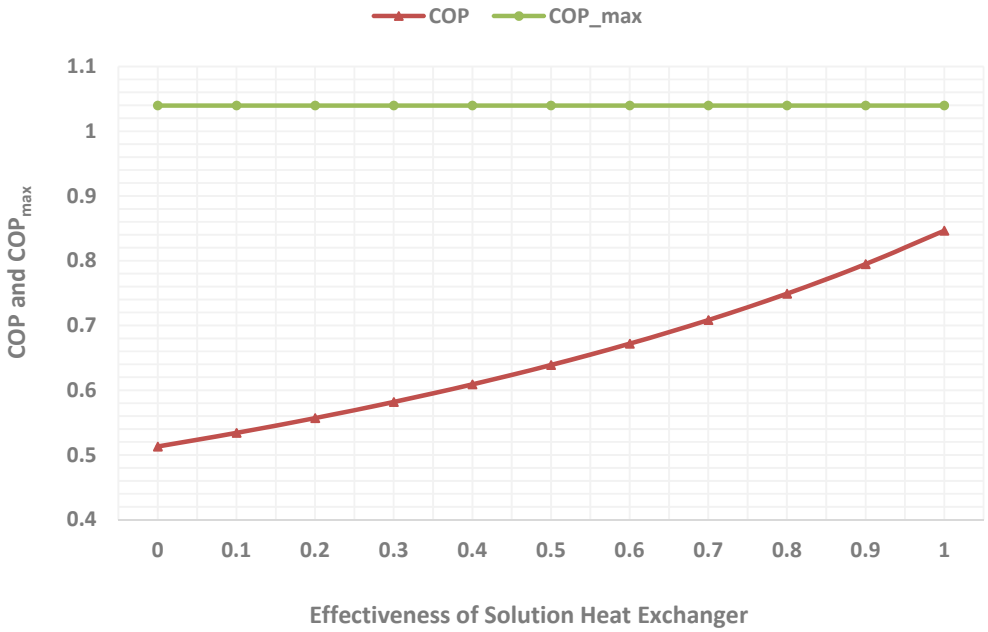

Fig 5.21 Effect of solution heat exchanger effectiveness on COP and COP_{max}

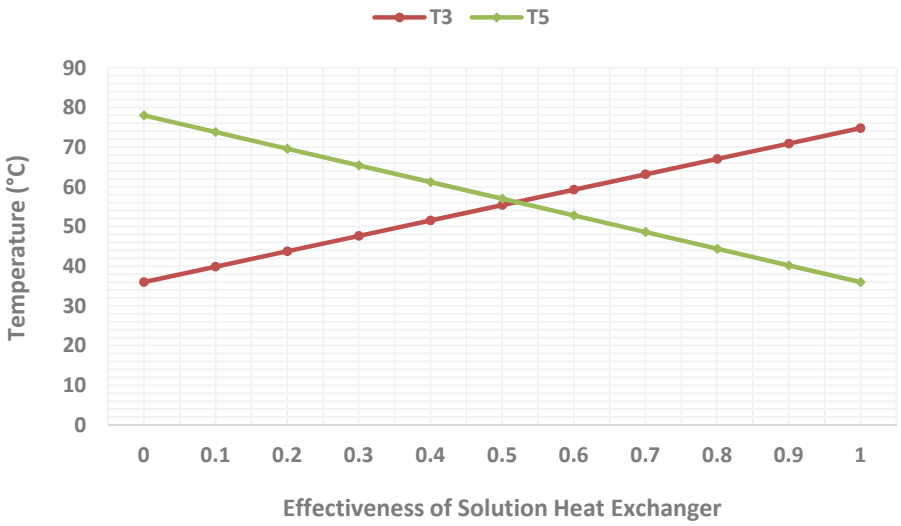

Fig 5.22 Effect of solution heat exchanger effectiveness on solution temperature

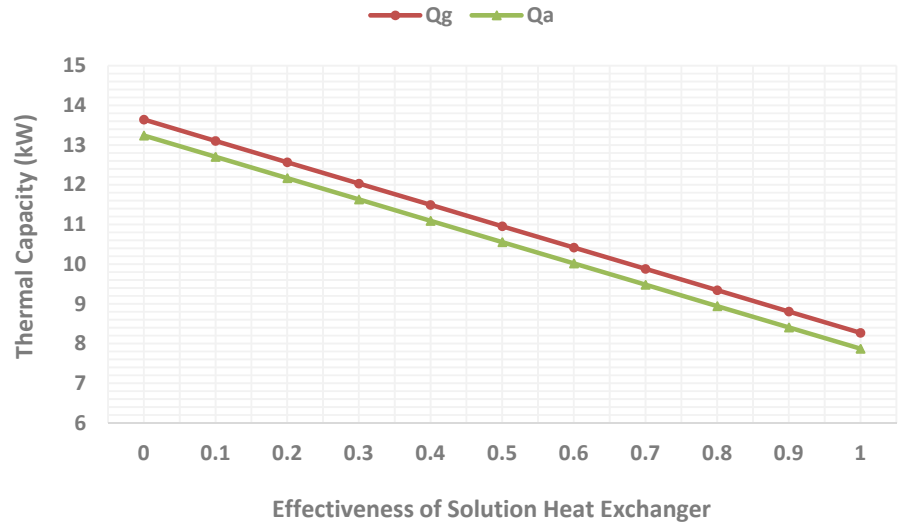

Fig. 5.23 Effect of solution heat exchanger effectiveness on thermal capacity of other components

5.3.6 Effect of Operation Condition Variations on System Efficiency

It is informative to examine the influence of the operating conditions on the second law efficiency of the system. The change in the second law efficiency of the absorption chiller with increasing the the evaporator temperature from 2°C to 15°C is shown in Fig. 5.24. For

this analysis, the rest of parameters are remained constant at their design conditions. It is observed in Fig. 5.24 that the second law efficiency of the system first increases quickly between evaporator temperature of 2°C to 7°C and then sharply decreases. The reason is that with increasing the evaporator temperature from 7°C, the increase in maximum possible COP is faster than that in COP. Similarly, the second law efficiency increases with increasing the generator temperature first and then promptly decreases as shown in Fig. 5.25. This results indicate that in our design conditions, increasing the generator temperature up to 80°C helps to improve the second law efficiency, but keeping the augmentation of the generator temperature will not be advantageous.

Fig. 26 shows the maximum second law efficiency in various evaporator and generator temperature whilst the absorber and condensed temperature are maintained constant at 36°C and 37°C respectively. Results demonstrate that highest second law efficiency occurs at generator temperature of 76°C and evaporator temperature of 7°C. The COP of absorption chiller for this condition is 0.735 while the COP of the absorption chiller in the selected design conditions of this study is 0.708. Therefore, changing the design conditions to the new conditions increases the COP of the chiller by 3.67%.

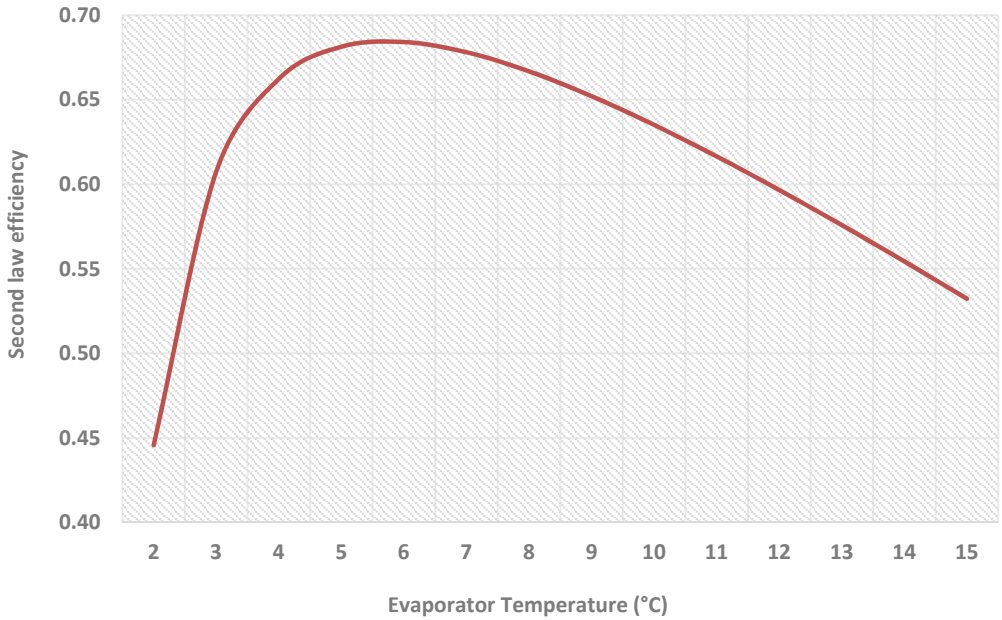

Fig. 5.24 Effect of evaporator temperature on second law efficiency

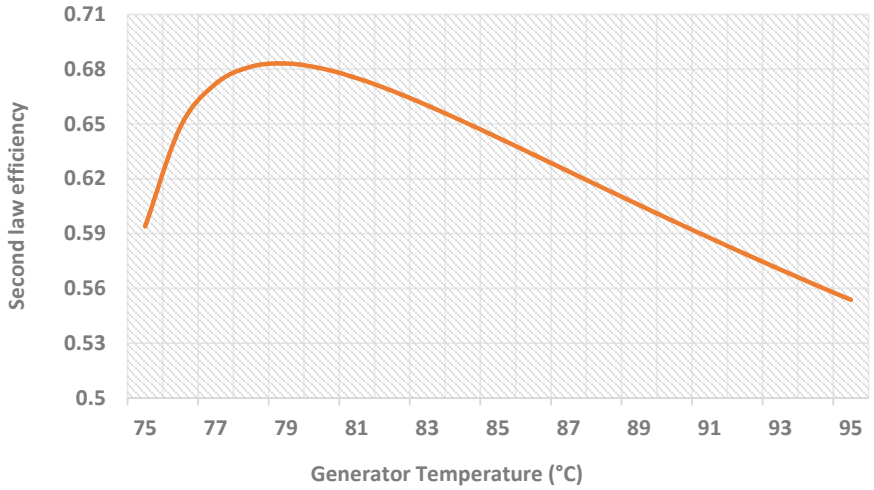

Fig. 5.25 Effect of generator temperature on second law efficiency

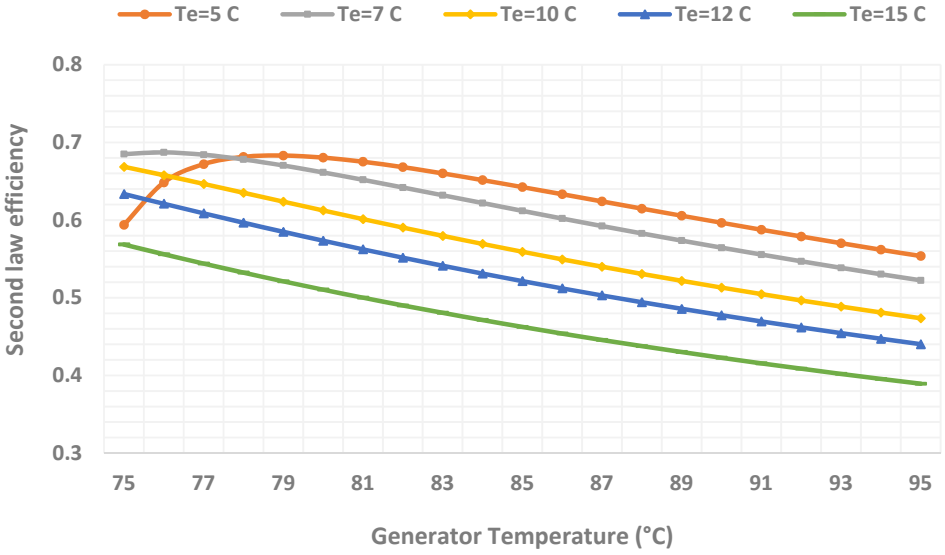

Fig. 5.26 variation of second law efficiency in various evaporator and generator temperature

As mentioned, when the temperature of the condenser and absorber increase, the COP and maximum possible COP decrease, however, results show that the second law efficiency increases in the range of the condenser temperature between 16°C and 36°C and decreases above 36°C due to relatively rapid reduction of COP. In the same way, the second law

efficiency increase with increasing the absorber temperature from 16°C to 34°C and reduces above 34°C. These results are shown in Figs. 5.27 and 5.28 respectively. Fig. 5.29 shows the variation of second law efficiency with both condenser and absorber temperature and indicates that efficiency increases with increasing these both temperatures.

Fig. 5.30 shows the influence of the solution heat exchanger effectiveness on the second law efficiency of the absorption chiller in selected design conditions. The efficiency is about 0.49 when no heat exchanger is used in the system (effectiveness=0) while it increases to 0.81 when using the solution heat exchanger with 100% efficiency which shows about 39.5% improvement. The second law efficiency of the chiller in the selected design conditions with solution heat exchanger effectiveness of 0.7 is 0.68.

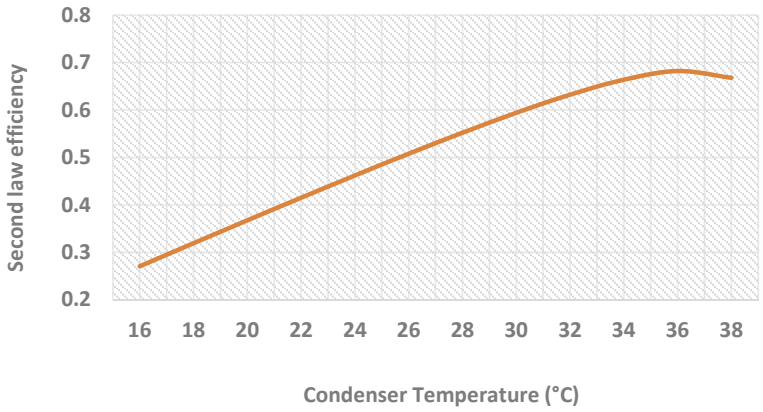

Fig. 5.27 Effect of condenser temperature on second law efficiency

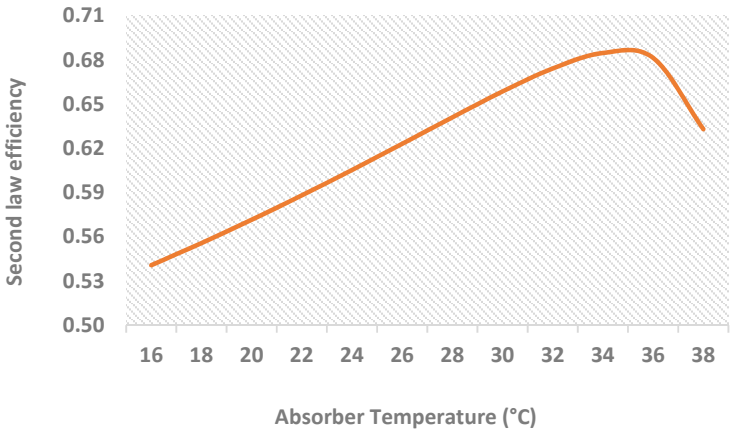

Fig. 5.28 Effect of absorber temperature on second law efficiency

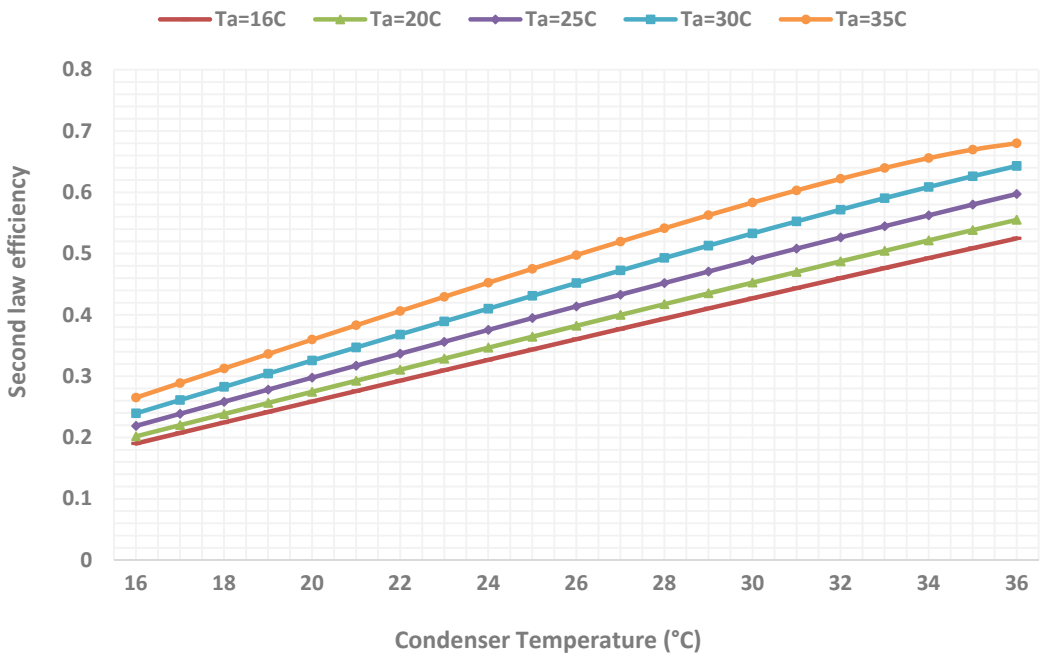

Fig. 5.29 variation of second law efficiency in various condenser and absorber temperature

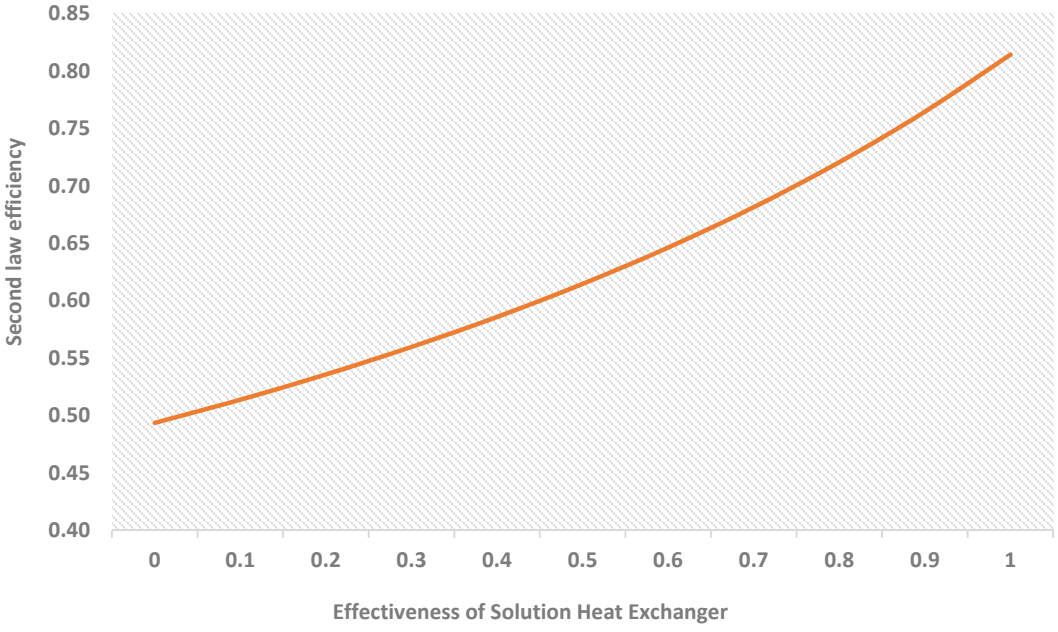

Fig. 5.30 Effect of solution heat exchanger effectiveness on second law efficiency

5.4 Derived Thermodynamic Design Data

Using thermodynamic models presented in chapter 4, the thermodynamic design data for single-effect LiBr-water absorption chiller are derived. In the absorption chiller, the operating temperatures specify the concentration of the weak and strong solution. Therefore, the possible combinations of the operating temperatures, solution concentration, flow rate ratio, COP and Carnot COP can be derived. These data can be used by other authors to examine the various design configuration of the single-effect absorption chiller. These design data have been derived by using the developed computer code, ABSYS. The influence of the operating temperatures on the performance of the single-effect absorption chiller is graphically illustrated. For the LiBr-water solution, the interaction of the operating parameters and the functioning restrictions are determined by the solubility limit of the system. For example, in the absorption chiller, the generator temperature has lower and upper temperature limits at the specified conditions of the other operating temperatures such as evaporator, condenser and absorber temperatures. If the generator temperature is very high, the dissolved solution can be crystallised on the way to the absorber. On the other hand, if the generator temperature is very low, the refrigerant vapour may not be produced. The design data have been derived within these operational limits. Furthermore, the thermodynamic design data for the single-effect absorption chiller depends on the effectiveness of the solution heat exchanger located between the absorber and generator. It means that these design data should be derived for different effectiveness of the solution heat exchanger. The data provided in this section are derived for a single-effect absorption chiller with no solution heat exchanger. In the case that there is the solution heat exchanger in the system, the thermodynamic design data can be derived by using ABSYS which is described in appendix 1. The thermodynamic design data covers the following operating range and are listed in table 4.2 to 4.9:

- Evaporator temperature from 2°C to 15 °C at 2°C intervals.
- Generator temperature from 50°C to 100 °C at 10°C intervals.
- Condenser temperature from 20°C to 40 °C at 10°C intervals.
- Absorber temperature from 20°C to 40 °C at 10°C intervals.

The thermodynamic design data presented in this section provide information on the influence of changes on the COP and show the possible combinations and operational limits of the operating temperatures for the single-effect LiBr-water absorption chiller. Therefore, these data can be used by the process design engineer for the equipment selection and sizing.

Fig. 5.31 shows the variation of the system COP against generator temperature at various evaporator temperatures for fixed condenser and absorber temperature of 20°C. It can be seen that the COP of the chiller is decreased as generator temperature increases and also the COP is higher at higher evaporator temperatures. However, at evaporator temperature of 2°C the COP is increased for generator temperature between 50°C and 60°C and reduced at higher generator temperatures.

The effect of operating temperature on the required minimum generator temperature is shown in Fig. 5.32. Results show that the value of the minimum generator temperature is higher at the higher cooling water temperature and lower evaporator temperature. This can be attributed to the fact that the absorption chiller operates when the strong solution concentration is greater than weak solution concentration to generate refrigerant vapour. In fact, when the difference in concentration between the weak and strong solution is reduced, a higher flow of the absorbent is required to carry the same cooling load. Therefore, in a given absorption chiller, a minimum generator temperature is required for given values of condenser, absorber and evaporator temperature. Fig. 5.32 shows the variation of minimum generator temperature with evaporator temperatures for different condenser and absorber temperatures.

Fig. 5.33 shows the variation of chiller COP against absorber temperature at different evaporator temperatures for the constant condenser and generator temperature at 30°C and 80°C respectively. It can be seen that the COP increases as the absorber temperature decreases and evaporator temperature increases. The effect of condenser temperature on the chiller COP at different evaporative temperature is shown in Fig. 5.34. The generator and absorber temperatures remain constant at 80°C and 30°C respectively. Results show that increasing the condenser temperature decreases COP.

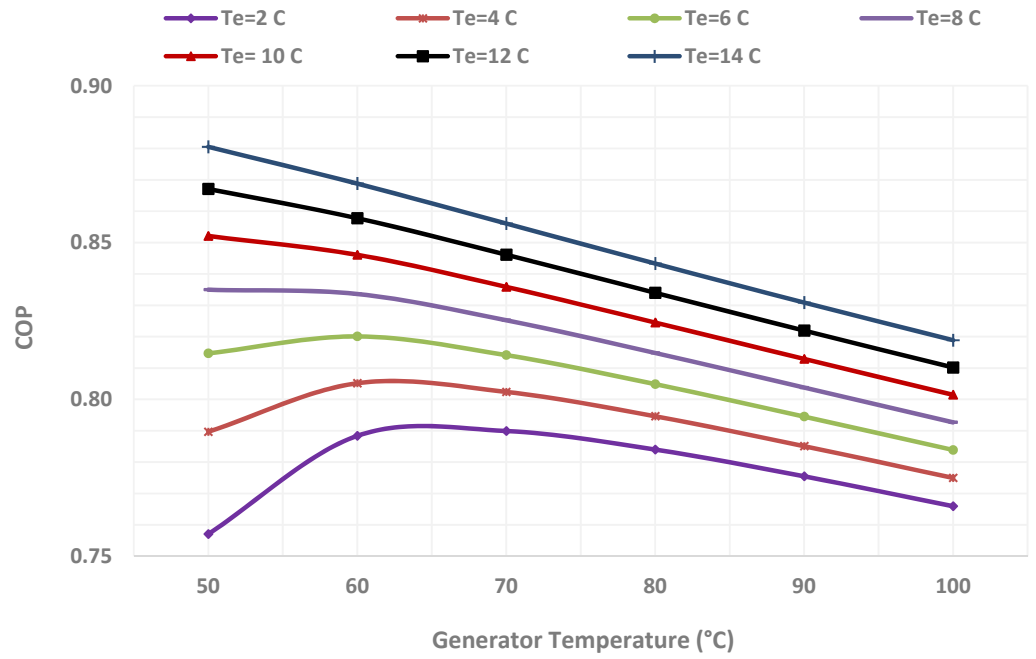

Fig. 5.31 variation of chiller COP against generator temperatures at various evaporator temperatures

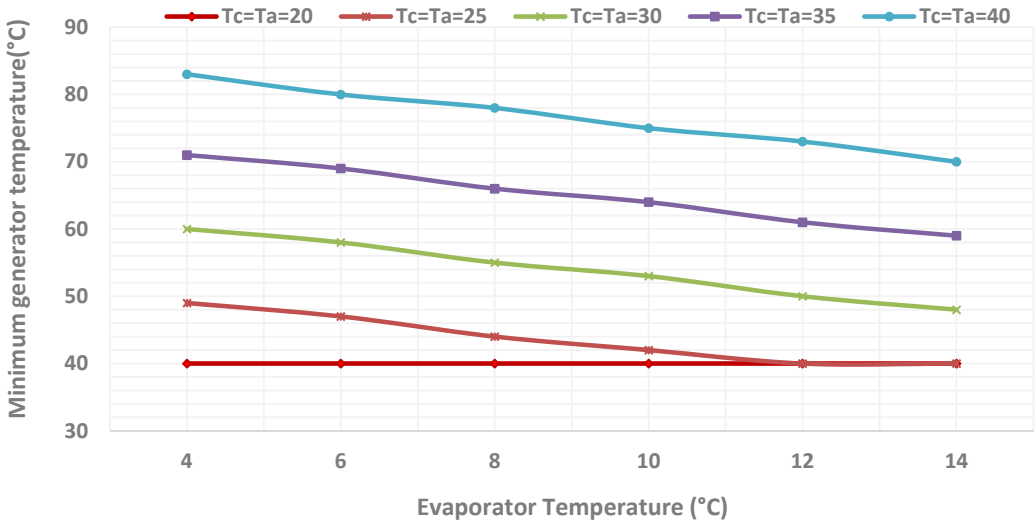

Fig. 5.32 Variation of minimum generator temperature with evaporator temperatures at various condenser and absorber temperatures

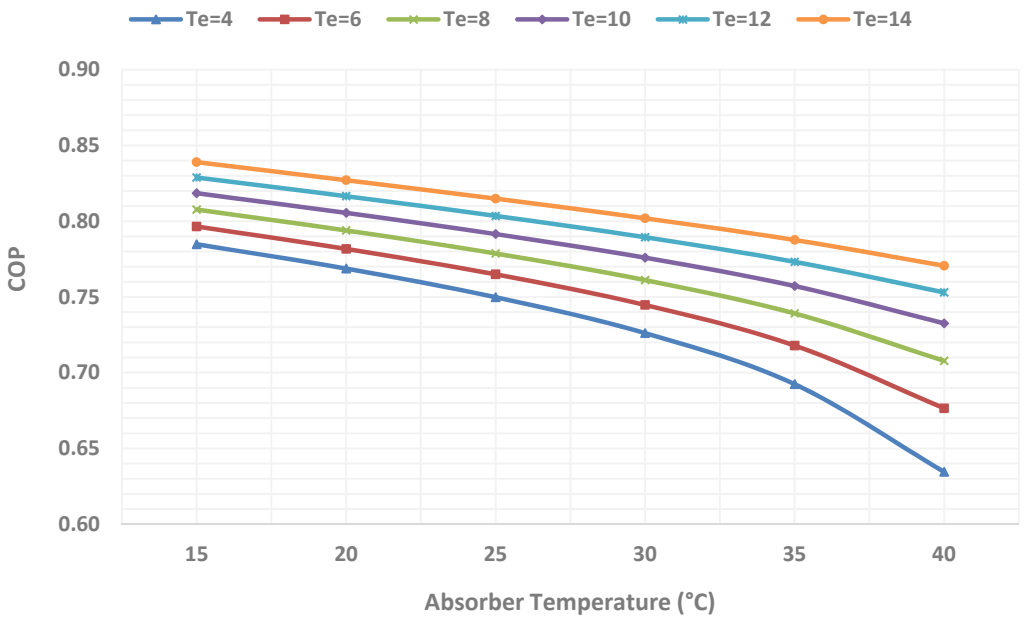

Fig. 5.33 Variation of chiller COP against absorber temperature at different evaporator temperatures

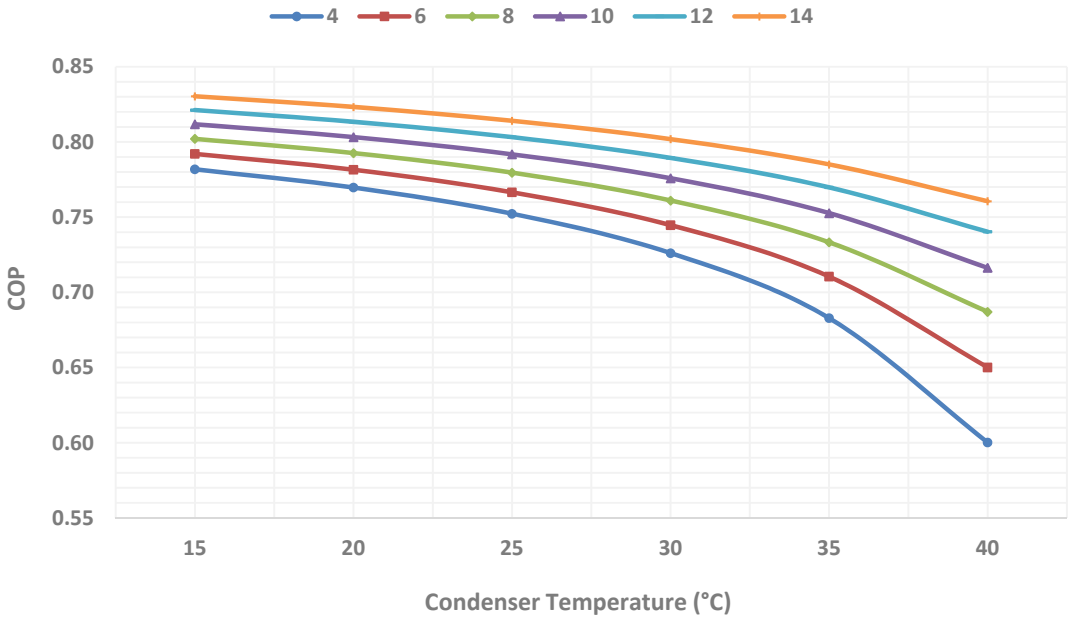

Fig. 5.34 Variation of chiller COP against condenser temperature at different evaporator temperatures

5.4.1 Optimum Design Diagrams

The COP values shown in tables 5.2 to 5.9 are the values that a single-effect LiBr-water absorption chiller can achieve at the specified conditions, however they are not optimum values. In order to obtained detailed optimum operating conditions for single-effect absorption chiller, the computer program, ABSYS, was used. Using this program, different operating conditions in which the absorption chiller reaches its maximum COP were searched. These results are then constructed as optimum design diagrams as shown in Figs 5.35 to 5.43. In these figures, the vertical bars represent the optimum generator temperatures which lead to the maximum COP for given evaporative temperature shown in the horizontal axis. The secondary vertical axis shows the maximum COP for the different evaporator temperatures. If evaporative temperature is specified, from the maps, required generator temperature which results in maximum COP can be found. Taking Fig. 5.39 as an example where $T_a=T_c=30°C$ and for designed evaporator temperature of $T_e=6°C$, from the diagram the required generator temperature to achieve the maximum COP can be found to be 88°C and its relative maximum COP is 0.748. For this conditions, if the generator temperature changes, the cycle COP will be lower than the maximum COP and the conditions are not optimised. These optimum design diagrams are very important in designing the appropriate control system for the absorption chiller for maintaining their optimum operation under various operating conditions.

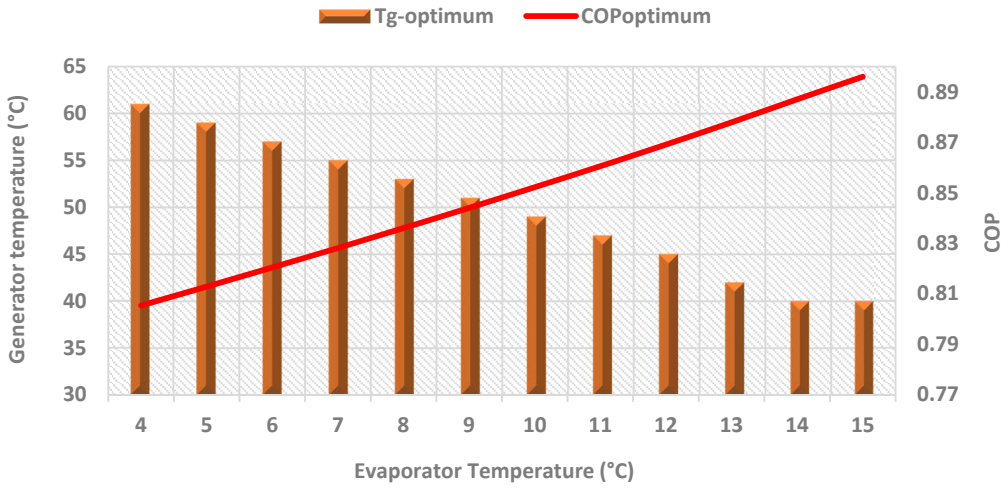

Fig. 5.35 Derived optimum conditions for T_a=20°C and T_c=20°C

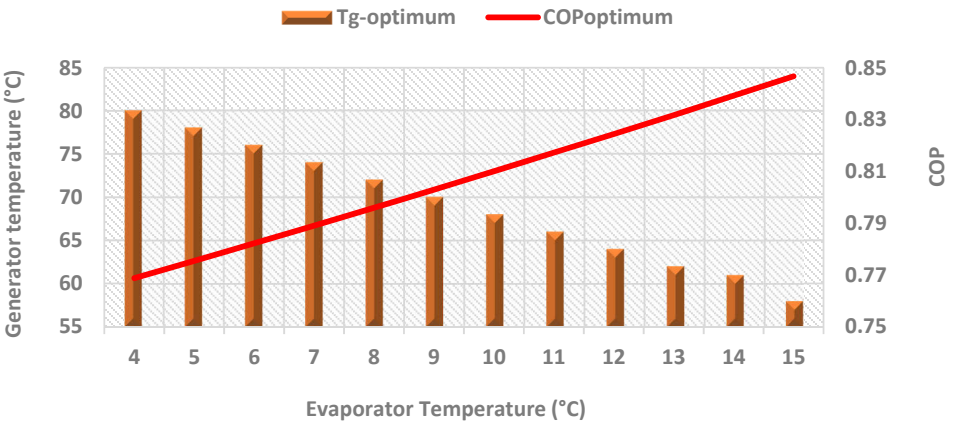

Fig. 5.36 Derived optimum conditions for T_a=20°C and T_c=30°C

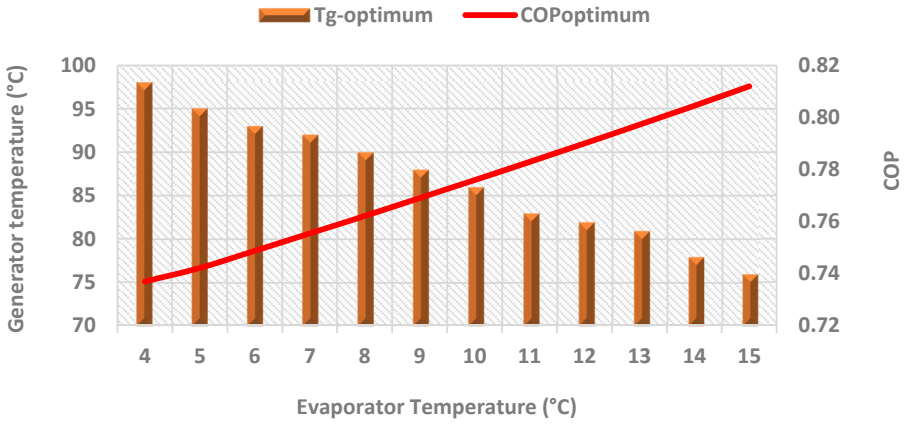

Fig. 5.37 Derived optimum conditions for T_a=20°C and T_c=40°C

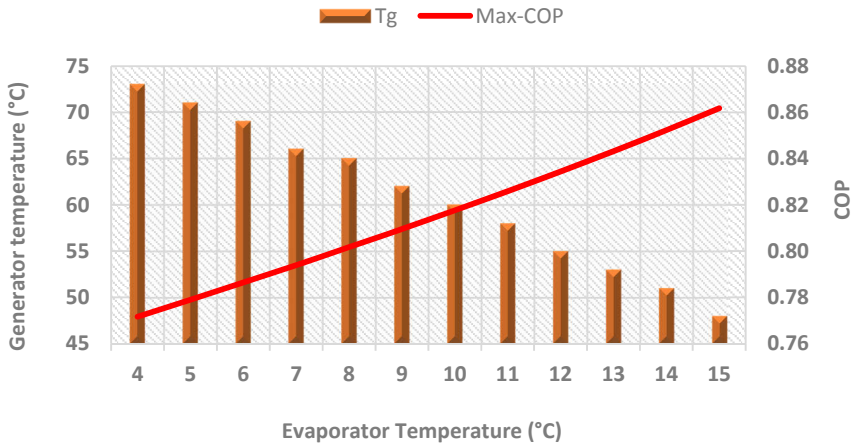

Fig. 5.38 Derived optimum conditions for T_a=30°C and T_c=20°C

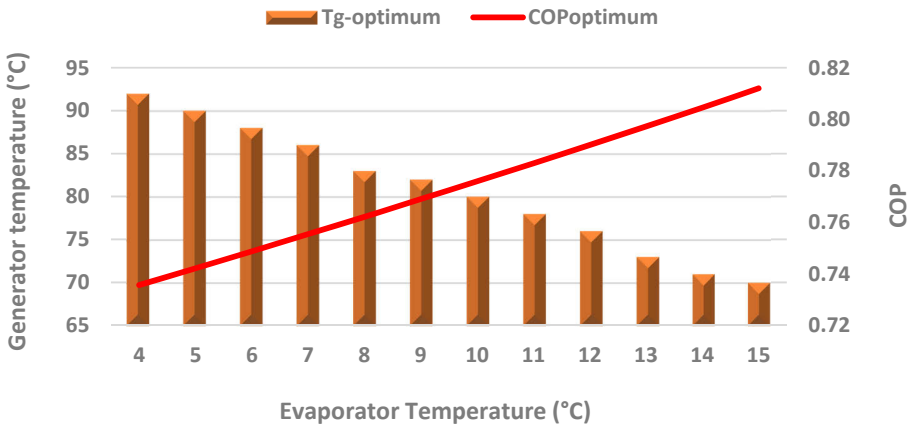

Fig. 5.39 Derived optimum conditions for T_a=30°C and T_c=30°C

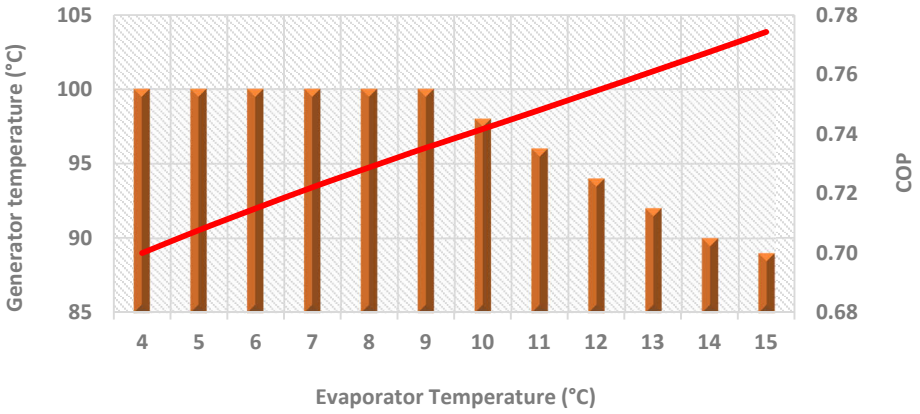

Fig. 5.40 Derived optimum conditions for T_a=30°C and T_c=40°C

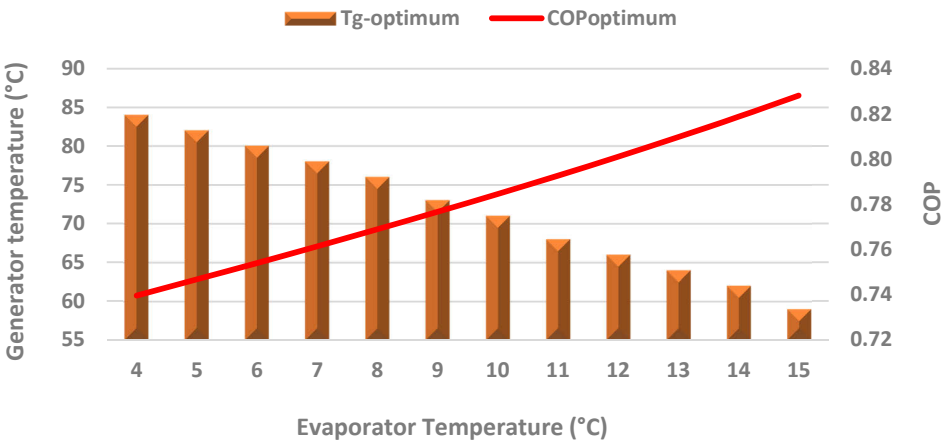

Fig. 5.41 Derived optimum conditions for T_a=40°C and T_c=20°C

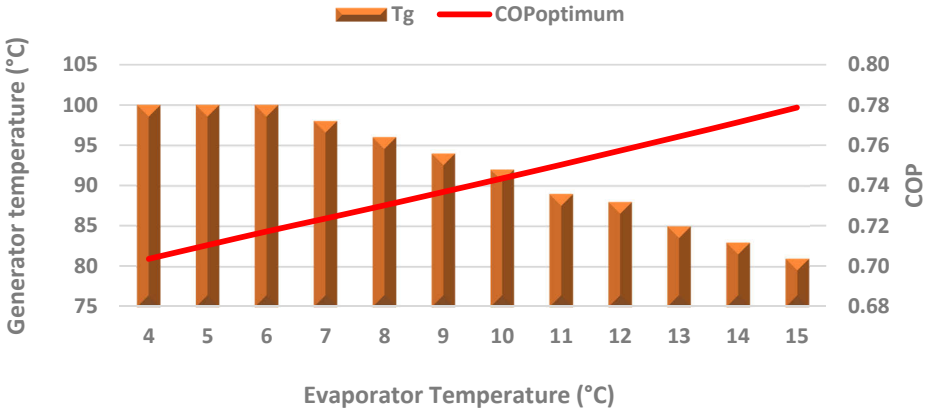

Fig. 5.42 Derived optimum conditions for T_a=40°C and T_c=30°C

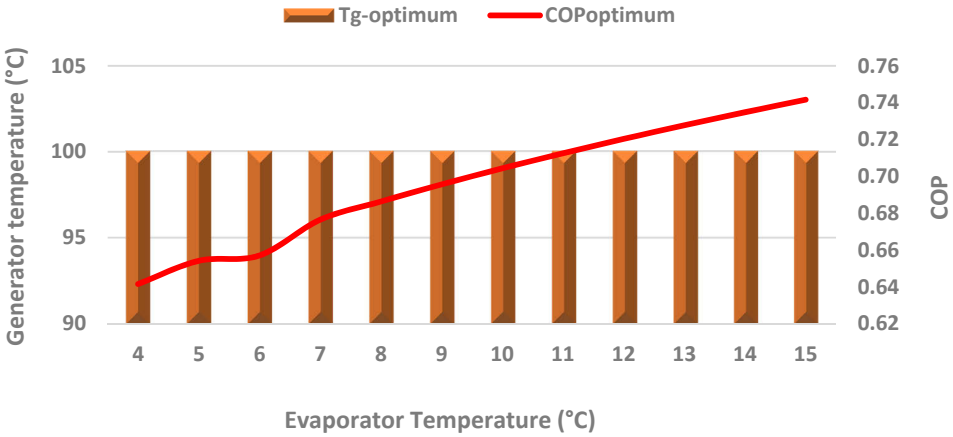

Fig. 5.43 Derived optimum conditions for T_a=40°C and T_c=40°C

Table 5.2 Derived thermodynamic design data for single-effect LiBr-water absorption chiller at T_e=2°C

T_g	T_e	T_a	T_c	X_{ws}	X_{ss}	COP	COP_{max}	CR
50	2	20	20	0.4827	0.5393	0.76	1.42	9.54
60	2	20	20	0.4827	0.5928	0.79	1.84	5.39
70	2	20	20	0.4827	0.6433	0.79	2.23	4.01
80	2	20	20	0.4827	0.6911	0.78	2.60	3.32
90	2	20	20	0.4827	0.7363	0.78	2.95	2.90
100	2	20	20	0.4827	0.7792	0.77	3.28	2.63
60	2	20	30	0.4827	0.5314	0.68	1.18	10.92
70	2	20	30	0.4827	0.5836	0.74	1.43	5.78
80	2	20	30	0.4827	0.6330	0.75	1.67	4.21
90	2	20	30	0.4827	0.6798	0.75	1.89	3.45
100	2	20	30	0.4827	0.7241	0.75	2.11	3.00
70	2	20	40	0.4827	0.5240	0.60	1.06	12.71
80	2	20	40	0.4827	0.5750	0.69	1.23	6.23
90	2	20	40	0.4827	0.6233	0.72	1.40	4.44
100	2	20	40	0.4827	0.6691	0.72	1.55	3.59
60	2	30	20	0.5431	0.5928	0.72	1.38	11.93
70	2	30	20	0.5431	0.6433	0.75	1.78	6.42
80	2	30	20	0.5431	0.6911	0.76	2.16	4.67
90	2	30	20	0.5431	0.7363	0.75	2.53	3.81
100	2	30	20	0.5431	0.7792	0.74	2.87	3.30
70	2	40	20	0.5998	0.6433	0.68	1.34	14.78
80	2	40	20	0.5998	0.6911	0.72	1.73	7.57
90	2	40	20	0.5998	0.7363	0.73	2.10	5.39
100	2	40	20	0.5998	0.7792	0.72	2.46	4.34
70	2	30	30	0.5431	0.5836	0.63	1.15	14.40
80	2	30	30	0.5431	0.6330	0.70	1.39	7.04
90	2	30	30	0.5431	0.6798	0.72	1.62	4.97
100	2	30	30	0.5431	0.7241	0.72	1.84	4.00
80	2	40	30	0.5998	0.6330	0.57	1.11	19.05
90	2	40	30	0.5998	0.6798	0.67	1.35	8.50
100	2	40	30	0.5998	0.7241	0.69	1.58	5.82
80	2	30	40	0.5431	0.5750	0.53	1.03	18.05
90	2	30	40	0.5431	0.6233	0.65	1.20	7.78
100	2	30	40	0.5431	0.6691	0.68	1.36	5.31
90	2	40	40	0.5998	0.6233	0.45	1.00	26.55
100	2	40	40	0.5998	0.6691	0.61	1.16	9.66

Table 5.3 Derived thermodynamic design data for single-effect LiBr-water absorption chiller at T_e=4°C

T_g	T_e	T_a	T_c	X_{ws}	X_{ss}	COP	COP_{max}	CR
50	4	20	20	0.4689	0.5393	0.79	1.61	6.66
60	4	20	20	0.4689	0.5928	0.81	2.08	3.78
70	4	20	20	0.4689	0.6433	0.80	2.52	2.69
80	4	20	20	0.4689	0.6911	0.79	2.94	2.11
90	4	20	20	0.4689	0.7363	0.79	3.34	1.75
100	4	20	20	0.4689	0.7792	0.77	3.71	1.51
50	4	20	30	0.4689	0.4761	0.34	0.99	65.10
60	4	20	30	0.4689	0.5314	0.72	1.28	7.50
70	4	20	30	0.4689	0.5836	0.76	1.55	4.08
80	4	20	30	0.4689	0.6330	0.77	1.81	2.86
90	4	20	30	0.4689	0.6798	0.77	2.05	2.22
100	4	20	30	0.4689	0.7241	0.76	2.29	1.84
70	4	20	40	0.4689	0.5240	0.66	1.12	8.51
80	4	20	40	0.4689	0.5750	0.72	1.31	4.42
90	4	20	40	0.4689	0.6233	0.73	1.48	3.04
100	4	20	40	0.4689	0.6691	0.74	1.65	2.34
50	4	30	20	0.5297	0.5393	0.49	1.07	55.07
60	4	30	20	0.5297	0.5928	0.75	1.56	8.39
70	4	30	20	0.5297	0.6433	0.77	2.02	4.66
80	4	30	20	0.5297	0.6911	0.77	2.45	3.28
90	4	30	20	0.5297	0.7363	0.76	2.86	2.56
100	4	30	20	0.5297	0.7792	0.75	3.25	2.12
60	4	40	20	0.5868	0.5928	0.38	1.04	97.07
70	4	40	20	0.5868	0.6433	0.71	1.51	10.37
80	4	40	20	0.5868	0.6911	0.74	1.96	5.62
90	4	40	20	0.5868	0.7363	0.74	2.38	3.92
100	4	40	20	0.5868	0.7792	0.73	2.79	3.05
70	4	30	30	0.5297	0.5836	0.68	1.24	9.82
80	4	30	30	0.5297	0.6330	0.73	1.51	5.12
90	4	30	30	0.5297	0.6798	0.74	1.76	3.53
100	4	30	30	0.5297	0.7241	0.73	2.00	2.72
80	4	40	30	0.5868	0.6330	0.63	1.21	12.68
90	4	40	30	0.5868	0.6798	0.69	1.47	6.31
100	4	40	30	0.5868	0.7241	0.70	1.71	4.27
80	4	30	40	0.5297	0.5750	0.60	1.09	11.69
90	4	30	40	0.5297	0.6233	0.68	1.27	5.66

100	4	30	40	0.5297	0.6691	0.70	1.44	3.80
90	4	40	40	0.5868	0.6233	0.54	1.06	16.07
100	4	40	40	0.5868	0.6691	0.64	1.24	7.13

Table 5.4 Derived thermodynamic design data for single-effect LiBr-water absorption chiller at T_e=6°C

T_g	T_e	T_a	T_c	X_{ws}	X_{ss}	COP	COP_{max}	CR
50	6	20	20	0.454981	0.539298	0.814691	1.851086	5.396061
60	6	20	20	0.454981	0.592815	0.820075	2.394031	3.30092
70	6	20	20	0.454981	0.64333	0.814119	2.905331	2.415621
80	6	20	20	0.454981	0.691089	0.804868	3.387674	1.927006
90	6	20	20	0.454981	0.73631	0.794514	3.843453	1.617257
100	6	20	20	0.454981	0.779191	0.783868	4.274803	1.403353
50	6	20	30	0.454981	0.476067	0.590132	1.0798	21.57727
60	6	20	30	0.454981	0.531409	0.756973	1.396518	5.953037
70	6	20	30	0.454981	0.583647	0.779883	1.694776	3.536146
80	6	20	30	0.454981	0.633033	0.781684	1.976143	2.555319
90	6	20	30	0.454981	0.679797	0.776889	2.242014	2.023796
100	6	20	30	0.454981	0.72414	0.769471	2.493635	1.69038
60	6	20	40	0.454981	0.470003	0.439123	0.985777	30.28731
70	6	20	40	0.454981	0.523963	0.697734	1.196313	6.595639
80	6	20	40	0.454981	0.574978	0.738964	1.394925	3.791592
90	6	20	40	0.454981	0.623283	0.748778	1.582598	2.703352
100	6	20	40	0.454981	0.669089	0.748559	1.760213	2.125007
50	6	30	20	0.516235	0.539298	0.677771	1.234058	22.38386
60	6	30	20	0.516235	0.592815	0.778315	1.795523	6.741108
70	6	30	20	0.516235	0.64333	0.786299	2.324265	4.061805
80	6	30	20	0.516235	0.691089	0.781452	2.823062	2.952392
90	6	30	20	0.516235	0.73631	0.772877	3.294388	2.345731
100	6	30	20	0.516235	0.779191	0.763014	3.740453	1.963204
60	6	40	20	0.573737	0.592815	0.623399	1.197016	30.07309
70	6	40	20	0.573737	0.64333	0.743399	1.743199	8.244185
80	6	40	20	0.573737	0.691089	0.753922	2.258449	4.889064
90	6	40	20	0.573737	0.73631	0.750205	2.745324	3.529121
100	6	40	40	0.573737	0.669089	0.665692	1.32016	6.017075
60	6	30	30	0.516235	0.531409	0.498939	1.047389	34.02109
70	6	30	30	0.516235	0.583647	0.716071	1.355821	7.657985
80	6	30	30	0.516235	0.633033	0.744724	1.646786	4.419895
90	6	30	30	0.516235	0.679797	0.748629	1.921727	3.15622
100	6	30	30	0.516235	0.72414	0.744961	2.181931	2.48304

70	6	40	30	0.573737	0.583647	0.392273	1.016866	57.89889
80	6	40	30	0.573737	0.633033	0.676482	1.317429	9.675818
90	6	40	30	0.573737	0.679797	0.711064	1.601439	5.409597
100	6	40	30	0.573737	0.72414	0.717072	1.870226	3.814681
70	6	30	40	0.516235	0.523963	0.284074	0.95705	66.80321
80	6	30	40	0.516235	0.574978	0.650056	1.162437	8.788041
90	6	30	40	0.516235	0.623283	0.701622	1.356513	4.82246
100	6	30	40	0.516235	0.669089	0.714912	1.540186	3.377318
80	6	40	40	0.573737	0.574978	0.060907	0.92995	462.3724
90	6	40	40	0.573737	0.623283	0.602659	1.130427	11.57988
100	6	40	40	0.573737	0.669089	0.665692	1.32016	6.017075

Table 5.5 Derived thermodynamic design data for single-effect LiBr-water absorption chiller at T_e=8°C

T_g	T_e	T_a	T_c	X_{ws}	X_{ss}	COP	COP_{max}	CR
50	8	20	20	0.441097	0.539298	0.834961	2.175073	4.491762
60	8	20	20	0.441097	0.592815	0.833608	2.813047	2.907335
70	8	20	20	0.441097	0.64333	0.825238	3.413837	2.181126
80	8	20	20	0.441097	0.691089	0.814807	3.980603	1.764446
90	8	20	20	0.441097	0.73631	0.803774	4.516155	1.494165
100	8	20	20	0.441097	0.779191	0.792693	5.023002	1.304658
50	8	20	30	0.441097	0.476067	0.696279	1.186404	12.61351
60	8	20	30	0.441097	0.531409	0.783119	1.534389	4.884121
70	8	20	30	0.441097	0.583647	0.795627	1.862093	3.094334
80	8	20	30	0.441097	0.633033	0.793904	2.171238	2.298139
90	8	20	30	0.441097	0.679797	0.787445	2.463357	1.847915
100	8	20	30	0.441097	0.72414	0.779092	2.739819	1.558409
60	8	20	40	0.441097	0.470003	0.590733	1.054893	15.25958
70	8	20	40	0.441097	0.523963	0.730291	1.280189	5.323004
80	8	20	40	0.441097	0.574978	0.757105	1.492726	3.294684
90	8	20	40	0.441097	0.623283	0.762193	1.693558	2.421127
100	8	20	40	0.441097	0.669089	0.759791	1.883626	1.934703
50	8	30	20	0.50279	0.539298	0.755311	1.450049	13.77197
60	8	30	20	0.50279	0.592815	0.79974	2.109785	5.584969
70	8	30	20	0.50279	0.64333	0.800124	2.73107	3.577546
80	8	30	20	0.50279	0.691089	0.792593	3.317169	2.670173
90	8	30	20	0.50279	0.73631	0.782705	3.87099	2.153094
100	8	30	20	0.50279	0.779191	0.772082	4.395127	1.819061
60	8	40	20	0.560704	0.592815	0.713747	1.406524	17.46106
70	8	40	20	0.560704	0.64333	0.765868	2.048302	6.786002
80	8	40	20	0.560704	0.691089	0.767959	2.653735	4.30038

90	8	40	20	0.560704	0.73631	0.761318	3.225825	3.192967
100	8	40	20	0.560704	0.779191	0.752051	3.767252	2.566304
60	8	30	30	0.50279	0.531409	0.636553	1.150792	17.56818
70	8	30	30	0.50279	0.583647	0.744729	1.489675	6.21828
80	8	30	30	0.50279	0.633033	0.76114	1.809365	3.860385
90	8	30	30	0.50279	0.679797	0.761037	2.111449	2.840514
100	8	30	30	0.50279	0.72414	0.7555	2.397342	2.271471
70	8	40	30	0.560704	0.583647	0.575009	1.117256	24.43914
80	8	40	30	0.560704	0.633033	0.707781	1.447492	7.752069
90	8	40	30	0.560704	0.679797	0.728112	1.759541	4.708128
100	8	40	30	0.560704	0.72414	0.729632	2.054865	3.430724
70	8	30	40	0.50279	0.523963	0.504191	1.024151	23.74666
80	8	30	40	0.50279	0.574978	0.68714	1.243938	6.964977
90	8	30	40	0.50279	0.623283	0.720964	1.451621	4.172756
100	8	30	40	0.50279	0.669089	0.72874	1.648173	3.023409
80	8	40	40	0.560704	0.574978	0.404748	0.995151	39.28033
90	8	40	40	0.560704	0.623283	0.64501	1.209684	8.95985
100	8	40	40	0.560704	0.669089	0.686288	1.412719	5.173256

Table 5.6 Derived thermodynamic design data for single-effect LiBr-water absorption chiller at T_e=10°C

T_g	T_e	T_a	T_c	X_{ws}	X_{ss}	COP	COP_{max}	CR
50	10	20	20	0.427213	0.539298	0.852107	2.628655	3.811495
60	10	20	20	0.427213	0.592815	0.846091	3.39967	2.579745
70	10	20	20	0.427213	0.64333	0.835877	4.125747	1.976761
80	10	20	20	0.427213	0.691089	0.824498	4.810704	1.618992
90	10	20	20	0.427213	0.73631	0.812904	5.457937	1.382132
100	10	20	20	0.427213	0.779191	0.801457	6.070481	1.213749
50	10	20	30	0.427213	0.476067	0.756934	1.314328	8.744639
60	10	20	30	0.427213	0.531409	0.804656	1.699835	4.100068
70	10	20	30	0.427213	0.583647	0.809916	2.062873	2.730948
80	10	20	30	0.427213	0.633033	0.805472	2.405352	2.075656
90	10	20	30	0.427213	0.679797	0.797663	2.728969	1.691371
100	10	20	30	0.427213	0.72414	0.788529	3.035241	1.43878
60	10	20	40	0.427213	0.470003	0.674086	1.133223	9.98387
70	10	20	40	0.427213	0.523963	0.756559	1.375249	4.415626
80	10	20	40	0.427213	0.574978	0.773339	1.603568	2.891155
90	10	20	40	0.427213	0.623283	0.77477	1.819312	2.178872
100	10	20	40	0.427213	0.669089	0.770587	2.023494	1.766246
50	10	30	20	0.489345	0.539298	0.799747	1.752437	9.795982
60	10	30	20	0.489345	0.592815	0.81763	2.549752	4.729295

70	10	30	20	0.489345	0.64333	0.812796	3.300597	3.177855
80	10	30	20	0.489345	0.691089	0.803211	4.00892	2.425572
90	10	30	20	0.489345	0.73631	0.792262	4.678232	1.981432
100	10	30	20	0.489345	0.779191	0.781003	5.311671	1.68829
60	10	40	20	0.54767	0.592815	0.762726	1.699835	12.1313
70	10	40	20	0.54767	0.64333	0.784371	2.475448	5.725169
80	10	40	20	0.54767	0.691089	0.780737	3.207136	3.818692
90	10	40	20	0.54767	0.73631	0.771864	3.898527	2.903265
100	10	40	20	0.54767	0.779191	0.761444	4.552861	2.365537
60	10	30	30	0.489345	0.531409	0.709067	1.274876	11.63313
70	10	30	30	0.489345	0.583647	0.76789	1.650299	5.189114
80	10	30	30	0.489345	0.633033	0.775903	2.00446	3.405585
90	10	30	30	0.489345	0.679797	0.77272	2.339116	2.569385
100	10	30	30	0.489345	0.72414	0.765663	2.655835	2.084133
70	10	40	30	0.54767	0.583647	0.661951	1.237724	15.22303
80	10	40	30	0.54767	0.633033	0.73255	1.603568	6.41577
90	10	40	30	0.54767	0.679797	0.743289	1.949263	4.145051
100	10	40	30	0.54767	0.72414	0.741386	2.27643	3.103483
70	10	30	40	0.489345	0.523963	0.611634	1.100199	14.13536
80	10	30	40	0.489345	0.574978	0.716314	1.336307	5.714393
90	10	30	40	0.489345	0.623283	0.738065	1.559411	3.653491
100	10	30	40	0.489345	0.669089	0.741609	1.770557	2.722447
80	10	40	40	0.54767	0.574978	0.546483	1.069045	20.05532
90	10	40	40	0.54767	0.623283	0.677379	1.299509	7.243054
100	10	40	40	0.54767	0.669089	0.704255	1.51762	4.510594

Table 5.7 Derived thermodynamic design data for single-effect LiBr-water absorption chiller at T_e=12°C

T_g	T_e	T_a	T_c	X_{ws}	X_{ss}	COP	COP_{max}	CR
50	12	20	20	0.413329	0.539298	0.867087	3.309028	3.281183
60	12	20	20	0.413329	0.592815	0.857765	4.279604	2.302837
70	12	20	20	0.413329	0.64333	0.846129	5.193611	1.797068
80	12	20	20	0.413329	0.691089	0.833988	6.055854	1.488079
90	12	20	20	0.413329	0.73631	0.821931	6.870611	1.279731
100	12	20	20	0.413329	0.779191	0.810178	7.641699	1.129739
50	12	20	30	0.413329	0.476067	0.797327	1.470679	6.588138
60	12	20	30	0.413329	0.531409	0.823031	1.902046	3.500396
70	12	20	30	0.413329	0.583647	0.823085	2.308271	2.426806
80	12	20	30	0.413329	0.633033	0.816515	2.691491	1.881292
90	12	20	30	0.413329	0.679797	0.807604	3.053605	1.551139
100	12	20	30	0.413329	0.72414	0.797816	3.396311	1.329839

60	12	20	40	0.413329	0.470003	0.728008	1.222744	7.293045
70	12	20	40	0.413329	0.523963	0.778554	1.483889	3.735991
80	12	20	40	0.413329	0.574978	0.788109	1.730244	2.556944
90	12	20	40	0.413329	0.623283	0.786667	1.963032	1.968657
100	12	20	40	0.413329	0.669089	0.781022	2.183343	1.616079
50	12	30	20	0.475899	0.539298	0.829747	2.206019	7.506417
60	12	30	20	0.475899	0.592815	0.833112	3.209703	4.070426
70	12	30	20	0.475899	0.64333	0.824585	4.154889	2.842357
80	12	30	20	0.475899	0.691089	0.81341	5.046545	2.211537
90	12	30	20	0.475899	0.73631	0.8016	5.889095	1.827496
100	12	30	20	0.475899	0.779191	0.789809	6.686487	1.569114
50	12	40	20	0.534637	0.539298	0.489069	1.103009	114.6933
60	12	40	20	0.534637	0.592815	0.79478	2.139802	9.189547
70	12	40	20	0.534637	0.64333	0.800218	3.116166	4.918748
80	12	40	20	0.534637	0.691089	0.79256	4.037236	3.41726
90	12	40	20	0.534637	0.73631	0.781958	4.90758	2.651008
100	12	40	20	0.534637	0.779191	0.770597	5.731274	2.18617
50	12	30	30	0.475899	0.476067	0.018567	0.980453	2835.006
60	12	30	30	0.475899	0.531409	0.755179	1.426535	8.573198
70	12	30	30	0.475899	0.583647	0.787364	1.846617	4.416799
80	12	30	30	0.475899	0.633033	0.789407	2.242909	3.028616
90	12	30	30	0.475899	0.679797	0.78382	2.617376	2.334013
100	12	30	30	0.475899	0.72414	0.775519	2.971772	1.917088
70	12	40	30	0.534637	0.583647	0.714333	1.384963	10.90873
80	12	40	30	0.534637	0.633033	0.753049	1.794327	5.433482
90	12	40	30	0.534637	0.679797	0.757059	2.181146	3.683089
100	12	40	30	0.534637	0.72414	0.752497	2.547233	2.821255
70	12	30	40	0.475899	0.523963	0.676751	1.187111	9.901398
80	12	30	40	0.475899	0.574978	0.740272	1.44187	4.803226
90	12	30	40	0.475899	0.623283	0.75347	1.682599	3.228969
100	12	30	40	0.475899	0.669089	0.753708	1.910425	2.463377
80	12	40	40	0.534637	0.574978	0.625618	1.153496	13.25276
90	12	40	40	0.534637	0.623283	0.703387	1.402166	6.031094
100	12	40	40	0.534637	0.669089	0.720264	1.637507	3.976407

Table 5.8 Derived thermodynamic design data for single-effect LiBr-water absorption chiller at T_e=14°C

T_g	T_e	T_a	T_c	X_{ws}	X_{ss}	COP	COP_{max}	CR
50	14	20	20	0.399445	0.539298	0.880514	4.442983	2.856165
60	14	20	20	0.399445	0.592815	0.868805	5.74616	2.065692
70	14	20	20	0.399445	0.64333	0.856068	6.973384	1.637835

80	14	20	20	0.399445	0.691089	0.843317	8.131106	1.369631
90	14	20	20	0.399445	0.73631	0.83088	9.225068	1.18577
100	14	20	20	0.399445	0.779191	0.818872	10.2604	1.051873
50	14	20	30	0.399445	0.476067	0.826958	1.666119	5.213158
60	14	20	30	0.399445	0.531409	0.839148	2.15481	3.026907
70	14	20	30	0.399445	0.583647	0.835377	2.615019	2.168514
80	14	20	30	0.399445	0.633033	0.827131	3.049165	1.710034
90	14	20	30	0.399445	0.679797	0.817318	3.4594	1.424797
100	14	20	30	0.399445	0.72414	0.806983	3.847648	1.230214
50	14	20	40	0.399445	0.412836	0.50235	1.025304	29.82872
60	14	20	40	0.399445	0.470003	0.766585	1.326037	5.661189
70	14	20	40	0.399445	0.523963	0.797518	1.609242	3.207918
80	14	20	40	0.399445	0.574978	0.801735	1.876409	2.275602
90	14	20	40	0.399445	0.623283	0.798012	2.128862	1.784519
100	14	20	40	0.399445	0.669089	0.79116	2.367784	1.481376
50	14	30	20	0.462454	0.539298	0.852183	2.961989	6.018058
60	14	30	20	0.462454	0.592815	0.846886	4.30962	3.547467
70	14	30	20	0.462454	0.64333	0.835689	5.578707	2.556737
80	14	30	20	0.462454	0.691089	0.823271	6.775921	2.022675
90	14	30	20	0.462454	0.73631	0.810759	7.907201	1.688676
100	14	30	20	0.462454	0.779191	0.798524	8.977846	1.460056
50	14	40	20	0.521603	0.539298	0.753759	1.480994	29.47742
60	14	40	20	0.521603	0.592815	0.818281	2.87308	7.324617
70	14	40	20	0.521603	0.64333	0.814207	4.18403	4.285016
80	14	40	20	0.521603	0.691089	0.803647	5.420737	3.07757
90	14	40	20	0.521603	0.73631	0.791689	6.589334	2.429377
100	14	40	20	0.521603	0.779191	0.779557	7.695297	2.024954
50	14	30	30	0.462454	0.476067	0.587777	1.110746	33.97087
60	14	30	30	0.462454	0.531409	0.788008	1.616108	6.706555
70	14	30	30	0.462454	0.583647	0.804254	2.092015	3.815849
80	14	30	30	0.462454	0.633033	0.801933	2.540971	2.711073
90	14	30	30	0.462454	0.679797	0.794448	2.9652	2.127762
100	14	30	30	0.462454	0.72414	0.785123	3.366692	1.767208
60	14	40	30	0.521603	0.531409	0.495924	1.077405	53.19146
70	14	40	30	0.521603	0.583647	0.75039	1.569011	8.407049
80	14	40	30	0.521603	0.633033	0.770609	2.032776	4.680983
90	14	40	30	0.521603	0.679797	0.769748	2.471	3.297249
100	14	40	30	0.521603	0.72414	0.76309	2.885736	2.575351
60	14	30	40	0.462454	0.470003	0.351126	0.994528	61.25793
70	14	30	40	0.462454	0.523963	0.721436	1.287394	7.518447
80	14	30	40	0.462454	0.574978	0.760617	1.563674	4.109807

90	14	30	40	0.462454	0.623283	0.767565	1.824739	2.875426
100	14	30	40	0.462454	0.669089	0.765185	2.071811	2.238021
70	14	40	40	0.521603	0.523963	0.143292	0.965545	221.0306
80	14	40	40	0.521603	0.574978	0.677305	1.250939	9.772405
90	14	40	40	0.521603	0.623283	0.725103	1.520616	5.129835
100	14	40	40	0.521603	0.669089	0.73478	1.775838	3.536633

Table 5.9 Derived thermodynamic design data for single-effect LiBr-water absorption chiller at T_e=15°C

T_g	T_e	T_a	T_c	X_{ws}	X_{ss}	COP	COP_{max}	CR
50	15	20	20	0.392503	0.539298	0.886777	5.350147	2.673805
60	15	20	20	0.392503	0.592815	0.87413	6.919406	1.959448
70	15	20	20	0.392503	0.64333	0.86094	8.397202	1.564829
80	15	20	20	0.392503	0.691089	0.847931	9.791307	1.314538
90	15	20	20	0.392503	0.73631	0.835331	11.10863	1.141636
100	15	20	20	0.392503	0.779191	0.823213	12.35535	1.015037
50	15	20	30	0.392503	0.476067	0.839205	1.783382	4.697006
60	15	20	30	0.392503	0.531409	0.846554	2.306469	2.825657
70	15	20	30	0.392503	0.583647	0.841252	2.799067	2.053439
80	15	20	30	0.392503	0.633033	0.832303	3.263769	1.631819
90	15	20	30	0.392503	0.679797	0.822103	3.702878	1.366206
100	15	20	30	0.392503	0.72414	0.811529	4.118451	1.18353
50	15	20	40	0.392503	0.412836	0.602362	1.070029	19.30343
60	15	20	40	0.392503	0.470003	0.78225	1.383881	5.064519
70	15	20	40	0.392503	0.523963	0.80613	1.67944	2.98571
80	15	20	40	0.392503	0.574978	0.808196	1.958261	2.150986
90	15	20	40	0.392503	0.623283	0.803508	2.221727	1.700759
100	15	20	40	0.392503	0.669089	0.796134	2.471071	1.419096
50	15	30	20	0.455731	0.539298	0.861611	3.566765	5.453479
60	15	30	20	0.455731	0.592815	0.853282	5.189554	3.324457
70	15	30	20	0.455731	0.64333	0.841031	6.717762	2.42928
80	15	30	20	0.455731	0.691089	0.828096	8.159422	1.936336
90	15	30	20	0.455731	0.73631	0.815284	9.521685	1.624255
100	15	30	20	0.455731	0.779191	0.802855	10.81093	1.408927
50	15	40	20	0.515086	0.539298	0.796883	1.783382	21.2742
60	15	40	20	0.515086	0.592815	0.828052	3.459703	6.626684
70	15	40	20	0.515086	0.64333	0.820673	5.038321	4.016456
80	15	40	20	0.515086	0.691089	0.808966	6.527538	2.926591
90	15	40	20	0.515086	0.73631	0.796441	7.934738	2.328354
100	15	40	20	0.515086	0.779191	0.783977	9.266515	1.950313
50	15	30	30	0.455731	0.476067	0.674317	1.188922	22.41014

60	15	30	30	0.455731	0.531409	0.801351	1.729851	6.021962
70	15	30	30	0.455731	0.583647	0.811962	2.239254	3.562749
80	15	30	30	0.455731	0.633033	0.807897	2.719807	2.570362
90	15	30	30	0.455731	0.679797	0.799614	3.173895	2.033919
100	15	30	30	0.455731	0.72414	0.789845	3.603645	1.6979
60	15	40	30	0.515086	0.531409	0.609154	1.153234	31.55601
70	15	40	30	0.515086	0.583647	0.764776	1.67944	7.512892
80	15	40	30	0.515086	0.633033	0.778562	2.175846	4.367099
90	15	40	30	0.515086	0.679797	0.775763	2.644913	3.127228
100	15	40	30	0.515086	0.72414	0.768225	3.088838	2.463897
60	15	30	40	0.455731	0.470003	0.498879	1.037911	31.93188
70	15	30	40	0.455731	0.523963	0.739162	1.343552	6.67915
80	15	30	40	0.455731	0.574978	0.769767	1.631884	3.821736
90	15	30	40	0.455731	0.623283	0.774212	1.904337	2.719933
100	15	30	40	0.455731	0.669089	0.770727	2.162187	2.135994
70	15	40	40	0.515086	0.523963	0.375992	1.007664	58.02712
80	15	40	40	0.515086	0.574978	0.697265	1.305508	8.60027
90	15	40	40	0.515086	0.623283	0.734767	1.586948	4.760631
100	15	40	40	0.515086	0.669089	0.741586	1.853303	3.344661

C h a p t e r 6

COMPONENT MODEL OF THE SINGLE-EFFECT ABSORPTION CHILLER

6.1 Summary

This chapter presents the heat transfer equations to design the different components of the absorption refrigeration system. The heat transfer correlations for laminar and turbulent flow for tube-side and shell-side of all heat exchangers used in the absorption chiller are discussed. Horizontal tube heat exchangers are used for generator, condenser, evaporator and absorber and solution heat exchanger is a plate type heat exchanger. These models are coded in ABSYS program and used to design the system component which is discussed in next chapter.

6.2 Component Model for Absorption Chiller

In a single-pass heat exchanger, the temperature difference ΔT between the hot and the cold fluids varies with distance along the heat exchanger. The heat-transfer rate Q of a given heat exchanger depends on its design and the properties of the two fluid streams. This characteristic can be defined as:

$$Q = AU\Delta T, \tag{6.1}$$

where U is the overall heat-transfer coefficient and shows the ability to transfer heat between the fluid streams, A is the heat-transfer area of the heat exchanger, ΔT_m is the logarithmic mean temperature difference between the two fluid streams over the length of the heat exchanger and is calculated as:

$$\Delta T_m = \frac{\Delta T_2 - \Delta T_1}{\ln\left(\frac{\Delta T_2}{\Delta T_1}\right)}, \tag{6.2}$$

in which ΔT_2 and ΔT_1 are respectively temperature difference between the hot and cold fluid entering the heat exchanger and temperature difference between the hot and cold fluid leaving the heat exchanger. The overall heat transfer coefficient, U based on the outside surface of the tube is defined as [138]:

$$U = \frac{1}{\left(\frac{D_o}{D_i}\right)\left(\frac{1}{\alpha_i}\right) + \left(\frac{D_o}{D_i}\right) f_i + \left(\frac{D_o}{2k_{cu}}\right) \ln\left(\frac{D_o}{D_i}\right) + f_o + \left(\frac{1}{\alpha_o}\right)}, \tag{6.3}$$

where f_i and f_o are the fouling factors at the inside and outside surfaces of the tube respectively, D_o and D_i are the outer and inner diameter of the tube respectively, α_i and α_o are heat transfer coefficient inside and outside the tubes respectively and k_{cu} is the copper thermal conductivity and can be determined using the following equation [138]:

$$k_{cu} = 4.853333 \times 10^{-9} T^4 - 2.916667 \times 10^{-6} T^3 + 6.541667 \times 10^{-4} T^2 - 0.1108333 T + 386, \tag{6.4}$$

The total length of tubes is then:

$$L_{total} = \frac{A_o}{\pi D_o}. \tag{6.5}$$

The number of tube can be calculated as:

$$n = \frac{L_{total}}{L_{tube}}. \tag{6.6}$$

To calculate the overall heat transfer coefficient, the heat transfer coefficients for inside and outside flow α_i and α_0 should be determined first. Next section presents the heat transfer correlations for each heat exchanger of the absorption chiller.

6.2.1 Heat Transfer Correlation Inside Tubes

This section presents heat transfer correlation for laminar and turbulent flow inside the plain circular tubes. The aim is to determine the inside heat transfer coefficient of the absorption

chiller's heat exchangers. Generally, laminar flow is assumed to occur at Reynolds number below 2300. The tubular Reynolds number is defined as:

$$\mathrm{Re} = \frac{\dot{m}_i D_i}{A_i \mu}. \tag{6.7}$$

The Prandtl number is obtained from the physical properties of the fluid and is defined as:

$$\mathrm{Pr} = \frac{C_p \mu}{k}. \tag{6.8}$$

For the fully developed laminar flow, heat transfer coefficient inside the plain round tubes can be determined using the following equation [139]:

$$Nu = \frac{\alpha_i D_i}{k_i} = 4.364, \tag{6.9}$$

in which Nu is the Nusselt number and is based on the tube diameter D_i and α_i is the convective heat transfer coefficient inside the tube. The heat transfer coefficient in this case is not a function of the Reynolds and Prandtl number.

The most commonly used correlation for prediction fully developed turbulent flow heat transfer coefficient inside the plain tubes is known as the Dittus-Boelter equation [140]:

$$Nu = \frac{\alpha_i D_i}{k_i} = 0.023\,\mathrm{Re}^{0.8}\,\mathrm{Pr}^{n}, \tag{6.10}$$

where the exponent on the Prandtl number for cooling a fluid is 0.3 and for heating a fluid is 0.4. This correlation can be used for the following conditions:

$$\begin{aligned} &\mathrm{Re} \geq 10000, \\ &0.7 \leq \mathrm{Pr} \leq 160. \end{aligned} \tag{6.11}$$

6.2.2 Heat Transfer Correlation for Generator Design

In the generator the LiBr/water solution is boiled off using the hot water supply form vacuum solar collectors. Generator of the absorption chiller is usually of the spray type where the falling film of the solution is boiled on the horizontal tubes. In design of the generator, it should be noted that closer temperature approach between hot water and solution in the generator, lead to a higher coefficient of performance for the absorption chiller. In this study, a shell and coil generator of spray type is designed in which hot water flows inside the tubes and solution is distributed over the tubes. To design the generator, the thermodynamic properties of the hot water and LiBr-water solution is determined in their average temperature. The heat transfer coefficient for the hot water flow inside of tubes can be determined based on the following correlations:

For laminar flow in which $Re \leq 2300$:

$$Nu = \frac{\alpha_i D_i}{k_{hw}} = 4.364, \tag{6.12}$$

where k_{hw} is the thermal conductivity of the hot water in its average temperature.

For turbulent flow in which $\mathrm{Re} \geq 10000$ the Dittus-Boelter correlation is used:

$$Nu = \frac{\alpha_i D_i}{k_{hw}} = 0.023(\mathrm{Re})^{0.8}(\mathrm{Pr})^{0.3}. \tag{6.13}$$

The generator provides sensible and latent heat of vaporisation. The outside heat transfer coefficient α_o predicts heat transfer by combined boiling and evaporation of falling liquid films on the horizontal tubes and can be calculated by correlation developed by Lorenz and Yung [141]:

$$\alpha_o = \alpha_d\left(\frac{L_d}{L}\right) + \alpha_c\left(1 - \frac{L_d}{L}\right), \tag{6.14}$$

where h_d is the average heat transfer coefficient in the thermal developing region where the fluid being superheated, h_c is the convective heat transfer coefficient due to evaporation of the liquid films at the vapour-liquid interface and L_d is the thermal developing length. h_d and L_d are given by:

$$\alpha_d = 0.375 C_p \left(\frac{\phi}{L_d} \right), \tag{6.15}$$

$$L_d = \frac{\phi^{(4/3)}}{4\pi \rho_{ss} \lambda_{ss}} \left(\frac{3\mu}{g \rho_{ss}^{\ 2}} \right)^{0.5}, \tag{6.16}$$

α_c for laminar and turbulent flow is determined as:

for laminar flow:

$$\alpha_c = 0.8221 \left(\frac{k_{ss}^{\ 3} g}{\nu_{ss}^{\ 2}} \right)^{1/3} \left(\frac{4\phi}{\mu_{ss}} \right)^{-0.22}, \tag{6.17}$$

for turbulent flow:

$$\alpha_c = 0.0038 \left(\frac{k_{ss}^{\ 3} g}{\nu_{ss}^{\ 2}} \right)^{1/3} \left(\frac{4\phi}{\mu_{ss}} \right)^{-0.4} \left(\frac{\nu_{ss}}{\lambda_{ss}} \right)^{0.65}, \tag{6.18}$$

where ν and λ arerespectivelly the kinematic viscosity and thermal diffusivity and can be determined as:

$$\phi = \frac{\dot{m}_{ss}}{2 L_{tube}}, \tag{6.19}$$

$$\nu_{ss} = \frac{\mu_{ss}}{\rho_{ss}}, \tag{6.20}$$

$$\lambda_{ss} = \frac{k_{ss}}{\rho_{ss} C_{p,ss}}. \tag{6.21}$$

The point of transition from equation (6.17) to (6.18) is:

$$\left(\frac{4\phi}{\mu_{ss}}\right)_{tr} = 5800\left(\frac{\nu_{ss}}{\rho_{ss}\alpha_{ss}}\right)^{-1.06}. \tag{6.22}$$

6.2.3 Heat Transfer Correlation for Condenser Design

A shell and coil condenser is used where cooled water is inside the coil tubes and water vapour is in the shell. In the condenser, condensation occurs on the outside of the tubes where the cooling water supply absorbs the heat of vaporisation from the water vapour. The heat transfer coefficient for the hot water flow on the inside of tubes can be determined based on following correlations:

For laminar flow in which $Re \leq 2300$:

$$Nu = \frac{\alpha_i D_i}{k_{cw}} = 4.364, \tag{6.23}$$

where k_{cw} is the thermal conductivity of the cooled water in its average temperature.

For turbulent flow in which $\mathrm{Re} \geq 10000$, the Dittus-Boelter correlation is used:

$$Nu = \frac{\alpha_i D_i}{k_{cw}} = 0.023(\mathrm{Re})^{0.8}(\mathrm{Pr})^{0.4}. \tag{6.24}$$

Outside heat transfer coefficient for condensation on the outside surface of the horizontal tubes is given by [139]:

$$\alpha_o = 0.725\left[\frac{g\rho_l(\rho_l-\rho_v)h_{fg}k_l^{\ 3}}{\mu_l(T_v-T_{cw})D_o}\right], \tag{6.25}$$

where subscript *l* and *v* indicate liquid and vapour respectively. The thermodynamic properties of the above equation should be obtained at the mean wall surface and vapour saturation temperature.

6.2.4 Heat Transfer Correlation for Evaporator Design

Evaporator is located in the low pressure side of the absorption chiller and its function is to produce the chilled water. A shell and coil evaporator of the falling-film type is considered in our design in which the liquid water refrigerant is evaporated on the outside tubes due to heat exchanging with water supply inside the tubes. As a result, chilled water is produced inside the tubes.

For laminar flow in which $Re \leq 2300$:

$$Nu = \frac{\alpha_i D_i}{k_{chw}} = 4.364, \tag{6.26}$$

where k_{chw} is the thermal conductivity of the chilled water in its average temperature.
For turbulent flow in which $\mathrm{Re} \geq 10000$, the Dittus-Boelter correlation is used:

$$Nu = \frac{\alpha_i D_i}{k_{chw}} = 0.023(\mathrm{Re})^{0.8}(\mathrm{Pr})^{0.3}. \tag{6.27}$$

The outside heat transfer coefficient is calculated by using the followings correlations [141]:

For laminar flow:

$$\alpha_o = 0.8221\left(\frac{k_{ref}^{\ 3}g}{\nu_{ref}^{\ 2}}\right)^{1/3}\left(\frac{4\phi}{\mu_{ref}}\right)^{-0.22}, \tag{6.28}$$

for turbulent flow:

$$\alpha_o = 0.0038\left(\frac{k_{ref}^{\ 3} g}{\nu_{ref}^{\ 2}}\right)^{1/3}\left(\frac{4\phi}{\mu_{ref}}\right)^{-0.4}\left(\frac{\nu_{ref}}{\lambda_{ref}}\right)^{0.65}, \tag{6.29}$$

where ν and λ are respectively the kinematic viscosity and thermal diffusivity which are determined as:

$$\phi = \frac{\dot{m}_{ref}}{2L_{tube}}, \tag{6.30}$$

$$\nu_{ref} = \frac{\mu_{ref}}{\rho_{ref}}, \tag{6.31}$$

$$\lambda_{ref} = \frac{k_{ref}}{\rho_{ref} C_{p,ref}}. \tag{6.32}$$

The point of transition from equation (6.27) to (6.28) is:

$$\left(\frac{4\phi}{\mu_{ref}}\right)_{tr} = 5800\left(\frac{\nu_{ref}}{\rho_{ref}}\right)^{-1.06}. \tag{6.33}$$

6.2.5 Heat Transfer Correlation for Absorber Design

Absorber is located in the low pressure side of the absorption chiller. A shell and coil heat exchanger of the falling film type is considered to be used in which the LiBr-water solution flows over the tubes and cooling water flows inside the tubes. In the absorber, water is absorbed by the low concentration of the solution and circulated back to the generator. Since cooling water is passed through the tubes, it provides the heat of vaporisation for refrigerant vapour.

The inside and outside heat transfer coefficient of the absorber can be calculated as:

For laminar flow in which $Re \le 2300$:

$$Nu = \frac{\alpha_i D_i}{k_{cw}} = 4.364, \tag{6.34}$$

where k_{cw} is the thermal conductivity of the cooled water in its average temperature.
For turbulent flow in which $\mathrm{Re} \ge 10000$ the Dittus-Boelter correlation is used:

$$Nu = \frac{\alpha_i D_i}{k} = 0.023(\mathrm{Re})^{0.8}(\mathrm{Pr})^{0.4}. \tag{6.35}$$

Outside heat transfer coefficient for condensation on the outside surface of the horizontal tubes is given by [142]:

for $\frac{4\phi}{\mu_{ws}} \le 2100$,

$$\alpha_o = 0.5\left[\frac{k_{ws}^2 \rho_{ws}^{4/3} C_{p,ws} g^{2/3}}{\frac{\pi D_o}{2}\mu_{ws}^{1/3}}\right]^{1/3}\left[\frac{\mu_{ws}}{\mu_{wall}}\right]^{1/4}\left[\frac{4\phi}{\mu_{ss}}\right]^{1/9}, \tag{6.36}$$

for $\frac{4\phi}{\mu_{ws}} > 2100$,

$$\alpha_o = 0.01\left[\frac{k_{ws}^3 \rho_{ws}^2 g^{2/3}}{\mu_{ws}^2}\right]^{1/3}\left[\frac{C_{p,ws}\mu_{ss}}{k_{ws}}\right]^{1/3}\left[\frac{4\phi}{\mu_{ws}}\right]^{1/3}, \tag{6.37}$$

in which:

$$\phi = \frac{\dot{m}_{ws}}{2L_{tube}}. \tag{6.38}$$

6.2.6 Heat Transfer Correlation for Solution Heat Exchanger Design

Solution heat exchanger is used to exchange the heat between the hot concentrated solution and cool diluted solution. In fact, solution heat exchanger decreases the required heat energy in the generator to increase the temperature of the weak solution to the boiling point. In this study a plate heat exchanger is considered in which the hot strong solution is in inner space and the cold weak solution is in the outer space. The purpose of solution heat exchanger design is to determine its required dimension. For this purpose, the inside and outside heat transfer coefficients of the heat exchanger should be calculated first.

Since the plate rectangular type heat exchanger is used, the equivalent diameter should be determined and used for calculating the Reynolds number:

$$D_e = \frac{4A_{cross}}{P_w}, \tag{6.39}$$

where A_{cross} and P_w are cross sectional area and wetted area of the heat exchanger respectively.

The inside and outside heat transfer coefficient can calculated as [143]:

for strong solution and laminar flow in which $\mathrm{Re} \le 2300$:

$$Nu = \frac{\alpha_i D_i}{k_{ss}} = 3.66 + \frac{0.0668\left(\frac{D_{equ}}{L}\right) Re_{ss}\, Pr_{ss}}{1 + 0.04\left[\left(\frac{D_{equ}}{L}\right) Re_{ss}\, Pr_{ss}\right]^{2/3}}, \tag{6.40}$$

where k_{ss} is the thermal conductivity of the strong LiBr solution in its average temperature.

For weak solution and laminar flow in which $\mathrm{Re} \le 2300$:

$$Nu = \frac{\alpha_o D_o}{k_{ws}} = 3.66 + \frac{0.0668\left(\frac{D_{equ}}{L}\right) Re_{ws}\, Pr_{ws}}{1 + 0.04\left[\left(\frac{D_{equ}}{L}\right) Re_{ws}\, Pr_{ws}\right]^{2/3}} \tag{6.41}$$

where k_{ws} is the thermal conductivity of the weak LiBr solution in its average temperature.

The overall heat transfer coefficient of the plate type heat exchanger can be determined as:

$$\frac{1}{U} = \frac{1}{\alpha_o} + \frac{t_p}{k_p\left(\frac{A_m}{A_o}\right)} + \frac{1}{\alpha_i\left(\frac{A_i}{A_0}\right)}, \tag{6.42}$$

where k_p and t_p are plate thermal conductivity and plate thickness respectively and A_m is the mean surface area of the inner space.

Chapter 7

MODEL-BASED DESIGN AND EXPERIMENATL RIG OF THE ABSORPTION COOLING SYSTEM

7.1 Summary

In this chapter the design of absorption chiller components are presented. The operation conditions are selected using the results of chapter 5. The design specifications of absorption chiller's heat exchanger are also obtained using the equations presented in chapter 6. Required area of heat transfer and number of tubes in the chiller's heat exchangers are calculated. The influence of the system variables on the heat transfer rate and physical dimension of each heat exchanger is investigated. Finally, experimental set-up of the central cooling plant is described.

7.2 Design of Absorption Chiller's Heat Exchanger

As mentioned earlier, the objective of this work is to design and construct a LiBr-Water absorption cooling system and analyse its performance. In a solar-powered absorption chiller, generator is the most critical heat exchanger distinguishing a solar absorption system from a conventional one. In the solra-powered single-effect absorption chiller, the generator is normally designd for relatively low temperature range like 70°C to 90°C. The generator designed for solar-powered absorption chiller usually uses horizontal tubes for hot water with solution sprayed on their outside surface and desorption taking place in the film. The absorber in the absorption chiller normally comprises a champer fitted with horizontal tubes. The cooling water flows inside these tubes. The refrigerant vapour from the evaporator surrounds the tubes. The absorbent solution is distruibuted over the tubes using spray nozzeles. The detail design for absorption chiller's heat exchangers are presented in this chapter.

7.2.1 Design of Generator

As mentioned a shell and coil heat exchanger of the spray type is considered for generator. In this heat exchanger, hot water flows inside the tubes and solution is distributed over the tubes. The design data are:

Generator capacity Q_g	9.88 kW
Strong solution mass flow rate $\dot{m}_{ss}$	0.0669 kg/s
Strong solution leaving temperature T_4	78°C
Strong solution concentration X_{ss}	0.5825 kg LiBr/kg solution
Weak solution mass flow rate $\dot{m}_{ws}$	0.0699 kg/s
Weak solution leaving temperature T_3	63.5°C
Weak solution concentration X_{ws}	0.5577 kg LiBr/kg solution
Generator temperature T_g	78°C
Hot water entering temperature $T_{hw,g,e}$	85°C
Hot water leaving temperature $T_{hw,g,o}$	81°C

The properties of hot water at its average temperature $\overline{T}_{hw} = \frac{81+85}{2} = 83°C$ are:

$\rho_{hw} = 968.91 \frac{kg}{m^3}$ $\kappa_{hw} = 0.6702 \frac{W}{m°C}$

$C_{p,hw} = 4.19 \frac{kJ}{kg°C}$ $\mu_{hw} = 0.34 \times 10^{-3} \frac{kg}{m.s}$

$\mathrm{Pr}_{hw} = 2.11$

The properties of LiBr-water solution at 78°C and 58.25% are:

$\rho_{ss} = 1231.34 \frac{kg}{m^3}$ $\kappa_{ss} = 0.639 \frac{W}{m°C}$

$C_{p,ss} = 3.803 \frac{kJ}{kg°C}$ $\mu_{ss} = 0.87 \times 10^{-3} \frac{kg}{m.s}$

The heat transfer coefficients inside and outside the tubes should be calculated first and then the overall heat transfer coefficient and tubes arrangement are determined. The hot water mass flow rate inside the tubes can be calculated as:

$$\dot{m}_{hw,g} = \frac{Q_g}{C_{p,hw} \times \left(T_{hw,g,e} - T_{hw,g,o}\right)} = \frac{9.88}{4.19 \times (85-81)} = 0.58\ kg/s. \tag{7.1}$$

Copper tubes with 15 mm nominal diameter and 1.24 mm wall thickness are used. The inside and outside diameters of tube are 13.395 and 15.875 mm respectively.

The Reynolds number can then be obtained as:

$$\mathrm{Re} = \frac{\dot{m}_{hw,g} D_i}{A_i \mu_{hw}} = 165677. \tag{7.2}$$

Therefore the flow inside the tubes is turbulent and Nusselt number is:

$$Nu = \frac{\alpha_i D_i}{k_{hw}} = 0.023(Re)^{0.8}(Pr)^{0.3} \Rightarrow \frac{\alpha_i \times 13.395 \times 10^{-3}}{0.6702} = \\ 0.023 \times (165677)^{0.8} \times (2.11)^{0.3} \Rightarrow \alpha_i = 23254.97 \frac{W}{m^2\,^\circ C}. \tag{7.3}$$

To calculate the outside heat transfer coefficient, the following parameters should be determined first. The tube length is assumed as 1 m. Then:

$$\phi = \frac{\dot{m}_{ss}}{2L_{tube}} = \frac{0.0669}{2 \times 1} = 0.03346, \tag{7.4}$$

$$\nu_{ss} = \frac{\mu_{ss}}{\rho_{ss}} = \frac{0.87 \times 10^{-3}}{1231.34} = 7.0675 \times 10^{-7}, \tag{7.5}$$

$$\lambda_{ss} = \frac{K_{ss}}{\rho_{ss} C_{p,ss}} = \frac{0.639}{1231.34 \times 3.803 \times 10^3} = 1.36 \times 10^{-7} \frac{m^2}{s}, \tag{7.6}$$

$$L_d = \frac{\phi^{4/3}}{4\pi\rho_{ss}\lambda_{ss}}\left(\frac{3\mu_{ss}}{g\rho^2}\right)^{0.5} = \frac{0.03346}{4\times\pi\times1231.34\times1.36\times10^{-7}}\left(\frac{3\times0.87\times10^{-3}}{9.81\times1231.34^2}\right)^{0.5} = 6.77\times10^{-5}\,\frac{m^2}{s}, \tag{7.7}$$

$$\alpha_d = 0.375\times\frac{C_{P,ss}\times\phi}{L_d} = 70471283\frac{W}{m^{\circ}C}. \tag{7.8}$$

The point of transition is:

$$\left(\frac{4\phi}{\mu_{ss}}\right)_{tr} = 5800\left(\frac{\nu_{ss}}{\lambda_{ss}}\right)^{-1.06} = 5800\left(\frac{7.0675\times10^{-7}}{1.36\times10^{-7}}\right)^{-1.06} = 1013.61, \tag{7.9}$$

in this design,

$$\left(\frac{4\phi}{\mu_{ss}}\right) = \frac{4\times0.03346}{0.87\times10^{-3}} = 153.83 \le \left(\frac{4\phi}{\mu_{ss}}\right)_{tr}. \tag{7.10}$$

Therefore, the correlation of the laminar flow is used to calculate the convective heat transfer coefficient due to evaporation of liquid films at the vapour liquid interface:

$$\alpha_c = 0.8221\left(\frac{k_{ss}{}^3 g}{\nu_{ss}{}^2}\right)^{0.33}\left(\frac{4\phi}{\mu_{ss}}\right)^{-0.22} \Rightarrow \alpha_c = 4677.18\,\frac{W}{m^2\,^{\circ}C}, \tag{7.11}$$

the outside heat transfer coefficient can now be determined as:

$$\alpha_o = \alpha_d\left(\frac{L_d}{L}\right) + \alpha_c\left(1-\frac{L_d}{L}\right) = 704712.83\times\left(\frac{6.77\times10^{-5}}{1}\right) + 4677.18\times\left(1-\frac{6.77\times10^{-5}}{1}\right) = 4724.6\,\frac{W}{m^2\,^{\circ}C}. \tag{7.12}$$

The overall heat transfer coefficient, U based on the outside surface of the tube is then:

$$U = \frac{1}{\left(\frac{D_o}{D_i}\right)\left(\frac{1}{\alpha_i}\right)+\left(\frac{D_o}{D_i}\right)f_i+\left(\frac{D_o}{2k_{co}}\right)ln\left(\frac{D_o}{D_i}\right)+f_o+\left(\frac{1}{\alpha_o}\right)} = 1770.68\frac{W}{m^2\,°C}, \tag{7.13}$$

in which the thermal conductivity of copper in 78°C is calculated from equation (6.4) as:

$$k_{cu} = 380.12\frac{W}{m°C}, \tag{7.14}$$

and the following assumption have been made [144]:

Inside fouling factor $f_i = 0.176\times10^{-3}$

outside fouling factor $f_0 = 0.09\times10^{-3}$

The logarithmic mean temperature difference ΔT_m is:

$$\Delta T_m = \frac{\Delta T_2 - \Delta T_1}{\ln\left(\frac{\Delta T_2}{\Delta T_1}\right)} = \frac{\left(T_g - T_{hw,g,o}\right)-\left(T_g - T_{hw,g,e}\right)}{\ln\left(\frac{\left(T_g - T_{hw,g,o}\right)}{\left(T_g - T_{hw,g,e}\right)}\right)} = \frac{(78-81)-(78-85)}{\ln\frac{78-85}{78-81}} = 4.721°C. \tag{7.15}$$

Therefore, the required heat transfer area can be determined as:

$$Q = AU\Delta T_m \Rightarrow A = \frac{Q_g}{(U\times LMTD)_g} = \frac{9880}{1770.68\times4.721} = 1.182\,m^2 \tag{7.16}$$

The total length of tubes is then:

$$L_{total} = \frac{A_o}{\pi D_o} = \frac{1.182}{\pi\times0.015875} = 23.7m. \tag{7.17}$$

The number of tube can be calculated as:

$$n = \frac{L_{total}}{L_{tube}} = \frac{23.7}{1} = 23.7. \tag{7.18}$$

Therefore, 24 tubes will be considered for manufacturing the generator heat exchanger.

The generator is of shell and tube type heat exchanger with horizontal tube bundles. The shell is constructed from copper with 1 m in length, 60 mm external diameter and 1.2 mm thick. The shell is insulated with 15 mm armaflex. 24 copper tubes with 15.87 mm outside diameter and 13.39 mm inside diameter were contained inside the shell as shown in Fig. 7.1. A sight glass is located on the generator to perceive the solution level. In summary, the generator specifications are as:

Material of Coil Tubes:	Copper
Outer Diameter of Tubes:	15.87 mm
Inner Diameter of Tubes:	13.39 mm
Tube Thickness:	1.24 mm
Shell Thickness:	1.2 mm
Tubes Orientation:	Horizontal
Tubes Arrangement:	4 Rows of 6 Tubes
Length of Tubes:	1 m
Number of Tubes:	24
Space between Tubes:	15 mm
Overall Heat Transfer Coefficient:	$1770.68 \frac{W}{m^2 °C}$

7.2.2 Design of Condenser

Condenser is a shell and coil heat exchanger where water vapour is condensing in the shell and cooling water flows inside the coil tubes. The design data for condenser are as:

Condenser capacity Q_g	7.1 kW
Condenser temperature T_c	37°C
Cooled water entering temperature $T_{cw,c,e}$	30°C
Cooled water leaving temperature $T_{cw,c,o}$	32°C

The properties of cooled water at its average temperature $\overline{T}_{hw} = \frac{30+32}{2} = 31°C$ are:

$\rho_{cw} = 996.51 \frac{kg}{m^3}$ $\kappa_{cw} = 0.6153 \frac{W}{m\,°C}$

$C_{p,cw} = 4.17 \frac{kJ}{kg\,°C}$ $\mu_{cw} = 0.778 \times 10^{-3} \frac{kg}{m.s}$

$\mathrm{Pr}_{cw} = 5.28$

The properties of saturated water refrigerant at average temperature $\overline{T}_{hw} = \frac{31+37}{2} = 34°C$ are:

$\rho_{ref} = 995.44 \frac{kg}{m^3}$ $\kappa_{ref} = 0.619 \frac{W}{m\,°C}$

$\rho_{vapour} = 0.0421 \frac{kJ}{kg\,°C}$ $\mu_{ref} = 0.73 \times 10^{-3} \frac{kg}{m.s}$

$\mathrm{Pr} = 4.92$ $h_{fg} = 2420.71 \frac{kJ}{kg}$

The heat transfer coefficients inside and outside the tubes should be calculated first and then the overall heat transfer coefficient and tubes arrangement are determined. The cooling water mass flow rate inside the tubes can be calculated as:

$$\dot{m}_{cw,c} = \frac{Q_c}{C_{p,cw} \times (T_{cw,c,e} - T_{cw,c,o})} = \frac{7.1}{4.17 \times (32-30)} = 0.85\, kg/s \tag{7.19}$$

Copper tubes with 15 mm nominal diameter and 1.24 mm wall thickness are used for construction of the condenser. The inside and outside diameters of tube are 13.395 and 15.875 mm respectively.

The Reynolds number can then be obtained as:

$$\mathrm{Re} = \frac{\dot{m}_{cw,c} D_i}{A_i \mu_{cw}} = 108284.6. \tag{7.20}$$

Therefore the flow inside the tubes is turbulent. The Nusselt number is:

$$Nu = \frac{\alpha_i D_i}{k_{cw}} = 0.023(Re)^{0.8}(Pr)^{0.4} \Rightarrow \frac{\alpha_i \times 13.395 \times 10^{-3}}{0.6153} = 0.023 \times (131588.59)^{0.8} \times (5.28)^{0.4} \Rightarrow \alpha_i = 21907.2 \frac{W}{m^2\,°C}. \quad (7.21)$$

Outside heat transfer coefficient for condensation on the outside surface of a horizontal tube is determined as:

$$\alpha_o = 0.725\left[\frac{g\rho_l(\rho_l - \rho_v)h_{fg}k_l^{\,3}}{\mu_l(T_v - T_{cw})D_o}\right] = 0.725\left[\frac{9.81 \times (995.44 - 0.0421) \times 2420.71 \times 0.619^3}{0.73 \times 10^{-3} \times (34 - 31) \times 0.015875}\right] = 2582.85 \frac{W}{m^2\,°C}. \quad (7.22)$$

The overall heat transfer coefficient, U based on the outside surface of the tube can now be computed as:

$$U = 1345.22 \frac{W}{m^2\,°C}, \quad (7.23)$$

in which same fouling factors used for generator were considered for condenser and the thermal conductivity of copper at 34°C is calculated from equation (6.4) as:

$$k_{cu} = 382.88 \frac{W}{m\,°C}. \quad (7.24)$$

The logarithmic mean temperature difference ΔT_m is:

$$\Delta T_m = \frac{\Delta T_2 - \Delta T_1}{\ln\left(\frac{\Delta T_2}{\Delta T_1}\right)} = \frac{(T_c - T_{cw,c,o}) - (T_c - T_{cw,c,e})}{\ln\left(\frac{(T_c - T_{cw,c,o})}{(T_c - T_{cw,c,e})}\right)} = \frac{(37 - 30) - (37 - 32)}{\ln\frac{37 - 32}{37 - 30}} = 5.944°C, \quad (7.25)$$

therefore, the required heat transfer area can be determined as:

$$Q = AU\Delta T_m \Rightarrow A_c = \frac{Q_c}{(U \times LMTD)_c} = \frac{7100}{1345.22 \times 5.944} = 0.882\, m^2. \quad (7.26)$$

The total length of tubes is then:

$$L_{total} = \frac{A_o}{\pi D_o} = \frac{0.881}{\pi \times 0.015875} = 17.68\, m. \quad (7.27)$$

The length of each tube was assumed as 1 m and thus the number of tube can be calculated as:

$$n = \frac{L_{total}}{L_{tube}} = \frac{17.65}{1} = 17.68, \quad (7.28)$$

therefore, 18 tubes will be considered for manufacturing the condenser heat exchanger. The condenser is of shell and tube type heat exchanger with horizontal tube bundles. The shell is constructed from copper with 1 m in length, 60 mm external diameter and 1.2 mm thick. The shell is insulated with 15 mm armaflex. 18 copper tubes with 15.87 mm outside diameter and 13.39 mm inside diameter were housed inside the shell as shown in Fig. 7.1. There are three rows of six tubes in the condenser. In summary, the condenser specifications are as:

Material of Coil Tubes:	Copper
Outer Diameter of Tubes:	15.87 mm
Inner Diameter of Tubes:	13.39 mm
Tube Thickness:	1.24 mm
Shell Thickness:	1.2 mm
Tubes Orientation:	Horizontal
Tubes Arrangement:	3 Row of 6 tubes
Length of Tubes:	1 m
Number of Tubes:	18
Space between Tubes:	22 mm
Overall Heat Transfer Coefficient:	$1345.22 \frac{W}{m^2 °C}$

7.2.3 Design of Evaporator

Evaporator is a shell and coil heat exchanger where water liquid refrigerant is evaporated outside the tubes and chilled water flows inside the coil tubes. The design data for evaporator, obtained from chapter 5 are as:

Evaporator capacity Q_g	7 kW
Refrigerant flow rate $\dot{m}_{ref}$	0.00297 kg/s
Evaporative temperature T_c	5°C
Chilled water entering temperature $T_{chw,e,e}$	12°C
Chilled water leaving temperature $T_{chw,e,o}$	7°C

The properties of chilled water at its average temperature $\overline{T}_{chw} = \frac{7+12}{2} = 9.5°C$ are:

$\rho_{chw} = 1001.61 \frac{kg}{m^3}$ $\kappa_{chw} = 0.5755 \frac{W}{m°C}$

$C_{p,chw} = 4.19 \frac{kJ}{kg°C}$ $\mu_{chw} = 1.345 \times 10^{-3} \frac{kg}{m.s}$

$\mathrm{Pr}_{chw} = 9.81$

The properties of water refrigerant at evaporative temperature of 5°C are:

$\rho_{ref} = 1002.064 \frac{kg}{m^3}$ $\kappa_{ref} = 0.565 \frac{W}{m°C}$

$\rho_{vapour} = 0.00665 \frac{kJ}{kg°C}$ $\mu_{ref} = 1.537 \times 10^{-3} \frac{kg}{m.s}$

$C_{p,ref} = 4.2 \frac{kJ}{kg°C}$ $\mathrm{Pr}_{ref} = 11.44$

The heat transfer coefficients inside and outside the tubes should be calculated first and then the overall heat transfer coefficient and tubes arrangement are determined. The chilled water mass flow rate inside the tubes can be calculated as:

$$\dot{m}_{chw,e} = \frac{Q_e}{C_{p,chw} \times \left(T_{chw,e,e} - T_{chw,e,o}\right)} = \frac{7}{4.2 \times (12-7)} = 0.334\ kg/s \tag{7.29}$$

Copper tubes with 15 mm nominal diameter and 1.24 mm wall thickness are used for construction of the evaporator. The inside and outside diameters of tube are 13.395 and 15.875 mm respectively.

The Reynolds number can then be obtained as:

$$\mathrm{Re} = \frac{\dot{m}_{chw,e} D_i}{A_i \mu_{chw}} = 23565.81. \tag{7.30}$$

Therefore the flow inside the tubes is turbulent. The Nusselt number is:

$$Nu = \frac{\alpha_i D_i}{k_{chw}} = 0.023(Re)^{0.8}(Pr)^{0.3} \Rightarrow \frac{\alpha_i \times 13.395 \times 10^{-3}}{0.5755} = 0.023 \times (23565.81)^{0.8} \times (9.81)^{0.3} \Rightarrow \alpha_i = 6169.1 \frac{W}{m^2\,^\circ C}. \tag{7.31}$$

To calculate the outside heat transfer coefficient, the following parameters should be determined first. The tube length is assumed as 1 m. Then:

$$\phi = \frac{\dot{m}_{ref}}{2L_{tube}} = \frac{0.00297}{2 \times 1} = 0.001485, \tag{7.32}$$

$$\nu_{ref} = \frac{\mu_{ref}}{\rho_{ref}} = \frac{1.537 \times 10^{-3}}{1002.064} = 1.534 \times 10^{-6}, \tag{7.33}$$

$$\lambda_{ref} = \frac{k_{ref}}{\rho_{ref} C_{p,ref}} = \frac{0.565}{1002.064 \times 4.2 \times 10^3} = 1.342 \times 10^{-7} \frac{m^2}{s}. \quad (7.34)$$

The point of transition is:

$$\left(\frac{4\phi}{\mu_{ref}}\right)_{tr} = 5800\left(\frac{\nu_{ref}}{\lambda_{ref}}\right)^{-1.06} = 5800\left(\frac{1.534 \times 10^{-6}}{1.342 \times 10^{-7}}\right)^{-1.06} = 438.4, \quad (7.35)$$

in this design,

$$\left(\frac{4\phi}{\mu_{ref}}\right) = \frac{4 \times 0.001485}{1.342 \times 10^{-3}} = 4.42 \leq \left(\frac{4\phi}{\mu_{ref}}\right)_{tr}, \quad (7.36)$$

therefore, the correlation of the laminar flow is used to calculate the outside heat transfer coefficient as:

$$\alpha_o = 0.8221\left(\frac{k_{ss}{}^3 g}{\nu_{ss}{}^2}\right)^{0.33}\left(\frac{4\phi}{\mu_{ss}}\right)^{-0.22} \Rightarrow \alpha_o = 5067.02 \frac{W}{m^2 °C}. \quad (7.37)$$

The overall heat transfer coefficient, U based on the outside surface of the tube is then:

$$U = 1446.03 \frac{W}{m^2 °C}, \quad (7.38)$$

in which the thermal conductivity of copper in 5°C is calculated from equation (6.4) as:

$$k_{cu} = 385.46 \frac{W}{m °C}. \quad (7.39)$$

The logarithmic mean temperature difference ΔT_m is:

$$\Delta T_m = \frac{\Delta T_2 - \Delta T_1}{\ln\left(\frac{\Delta T_2}{\Delta T_1}\right)} = \frac{\left(T_e - T_{chw,e,o}\right) - \left(T_e - T_{chw,e,e}\right)}{\ln\left(\frac{\left(T_e - T_{chw,e,o}\right)}{\left(T_e - T_{chw,e,e}\right)}\right)} = \frac{(5-7)-(5-12)}{\ln\frac{5-12}{5-7}} = 3.991°C. \quad (7.40)$$

Therefore, the required heat transfer area can be determined as:

$$Q = AU\Delta T_m \Rightarrow A_e = \frac{Q_e}{(U \times LMTD)_e} = \frac{7000}{1446.03 \times 3.991} = 1.21\,m^2 \tag{7.41}$$

The total length of tubes is then:

$$L_{total} = \frac{A_o}{\pi D_o} = \frac{1.21}{\pi \times 0.015875} = 24.32m \tag{7.42}$$

The number of tube can be calculated as:

$$n = \frac{L_{total}}{L_{tube}} = \frac{24.32}{1} = 24.32 \tag{7.43}$$

Therefore, 24 tubes will be considered for manufacturing the evaporator heat exchanger. The evaporator is of shell and tube type heat exchanger with horizontal tube bundles. The shell is constructed from copper with 1 m in length, 60 mm external diameter and 1.2 mm thick. The shell is insulated with 15 mm armaflex. 24 copper tubes with 15.87 mm outside diameter and 13.39 mm inside diameter were contained inside the shell as shown in Fig. 7.1. In summary, the evaporator specifications are as:

Material of Coil Tubes:	Copper
Outer Diameter of Tubes:	15.87 mm
Inner Diameter of Tubes:	13.39 mm
Tube Thickness:	1.24 mm
Shell Thickness:	1.2 mm
Tubes Orientation:	Horizontal
Tubes Arrangement:	6 Rows of 4 Tubes
Length of Tubes:	1 m
Number of Tubes:	24
Space between Tubes:	15 mm
Overall Heat Transfer Coefficient:	$1446.03\frac{W}{m^2\,°C}$

7.2.4 Design of Absorber

As mentioned a shell and coil of the falling film type is considered for absorber. In this heat exchanger, cooling water flows inside the tubes and solution is flows over the tubes. The design data are:

Absorber capacity Q_a	9.48 kW
Strong solution mass flow rate $\dot{m}_{ss}$	0.0669 kg/s
Strong solution leaving temperature T_4	78°C
Strong solution concentration X_{ss}	0.5825 kg LiBr/kg solution
Weak solution mass flow rate $\dot{m}_{ws}$	0.0699 kg/s
Weak solution leaving temperature T_3	63.5°C
Weak solution concentration X_{ws}	0.5577 kg LiBr/kg solution
Absorber temperature T_a	36°C
Cooled water entering temperature $T_{cw,a.e}$	28°C
Cooled water leaving temperature $T_{cw,a,o}$	30°C

The properties of cooled water at its average temperature $\overline{T}_{cw} = \frac{28+30}{2} = 29°C$ are:

$\rho_{cw} = 997.17 \frac{kg}{m^3}$ $\kappa_{cw} = 0.6122 \frac{W}{m°C}$

$C_{p,cw} = 4.177 \frac{kJ}{kg°C}$ $\mu_{cw} = 0.812 \times 10^{-3} \frac{kg}{m.s}$

$Pr_{cw} = 5.54$

The properties of LiBr-water solution at temperature of 36°C and concentration of 55.77% are as:

$$\rho_{ws} = 1248.25\ \frac{kg}{m^3} \qquad \kappa_{ws} = 0.68\frac{W}{m°C}$$

$$C_{p,ws} = 3.804\frac{kJ}{kg°C} \qquad \mu_{ws} = 6.84\times10^{-3}\ \frac{kg}{m.s}$$

The heat transfer coefficients inside and outside the tubes should be calculated first and then the overall heat transfer coefficient and tubes arrangement are determined. The cooled water mass flow rate inside the tubes can be calculated as:

$$\dot{m}_{cw,a} = \frac{Q_a}{C_{p,cw}\times\left(T_{cw,a,e} - T_{cw,a,o}\right)} = \frac{9.48}{4.177\times(30-28)} = 1.13\ kg/s. \tag{7.44}$$

Copper tubes with 15 mm nominal diameter and 1.24 mm wall thickness are used. The inside and outside diameters of tube are 13.395 and 15.875 mm respectively.

The Reynolds number can then be obtained as:

$$\mathrm{Re} = \frac{\dot{m}_{cw,a}D_i}{A_i\mu_{cw}} = 132793.4. \tag{7.45}$$

Therefore the flow inside the tubes is turbulent and Nusselt number is:

$$Nu = \frac{\alpha_i D_i}{k_{cw}} = 0.023(Re)^{0.8}(Pr)^{0.4} \Rightarrow \frac{\alpha_i\times13.395\times10^{-3}}{0.6122} = \\ 0.023\times(132793.4)^{0.8}\times(5.54)^{0.4} \Rightarrow \alpha_i = 26167.23\frac{W}{m^2\,°C}. \tag{7.46}$$

To calculate the outside heat transfer coefficient, the following parameter should be determined first. The tube length is assumed as 1 m. Then:

$$\phi = \frac{\dot{m}_{ws}}{2L_{tube}} = \frac{0.0699}{2\times1} = 0.035, \tag{7.47}$$

$$\frac{4\phi}{\mu_{ws}} = \frac{4\times 0.035}{6.84\times 10^{-3}} = 20.46 \le 2100, \tag{7.48}$$

therefore, the correlation of the laminar flow is used to calculate the outside heat transfer coefficient as:

$$\alpha_o = 0.5\left[\frac{k_{ws}^2 \rho_{ws}^{4/3} C_{p,ws} g^{2/3}}{\frac{\pi D_o}{2}\mu_{ws}^{1/3}}\right]^{1/3}\left[\frac{\mu_{ws}}{\mu_{wall}}\right]^{1/4}\left[\frac{4\phi}{\mu_{ss}}\right]^{1/9} =$$

$$0.5\times\left[\frac{0.68^2\times 1248.25^{(4/3)}\times 3.804\times 9.81^{(2/3)}}{\frac{\pi\times 0.015875}{2}\times 6.84\times 10^{-3}}\right]^{(1/3)}\times\left[\frac{4\times 0.035}{6.84\times 10^{-3}}\right]^{(1/9)} = 2235.34\frac{W}{m^2\,°C}, \tag{7.49}$$

in which the weak and wall viscosity are assumed to be equal.

The overall heat transfer coefficient, U based on the outside surface of the tube is then:

$$U = 1254.82\frac{W}{m^2\,°C}, \tag{7.50}$$

in which the thermal conductivity of copper in 36°C is calculated from equation (6.4) as:

$$k_{cu} = 382.72\frac{W}{m\,°C}, \tag{7.51}$$

The logarithmic mean temperature difference ΔT_m is:

$$\Delta T_m = \frac{\Delta T_2 - \Delta T_1}{\ln\left(\frac{\Delta T_2}{\Delta T_1}\right)} = \frac{\left(T_a - T_{cw,a,o}\right) - \left(T_a - T_{cw,a,e}\right)}{\ln\left(\frac{\left(T_a - T_{cw,a,o}\right)}{\left(T_a - T_{cw,a,e}\right)}\right)} = \frac{(36-28)-(36-30)}{\ln\frac{36-28}{36-30}} = 6.952°C. \tag{7.52}$$

Therefore, the required heat transfer area can be determined as:

$$Q = AU\Delta T_m \Rightarrow A_a = \frac{Q_a}{(U\times LMTD)_a} = \frac{9480}{1254.82.\times 6.952} = 1.087\,m^2. \tag{7.53}$$

The total length of tubes is then:

$$L_{total} = \frac{A_o}{\pi D_o} = \frac{1.087}{\pi \times 0.015875} = 21.8m. \tag{7.54}$$

The number of tube can be calculated as:

$$n = \frac{L_{total}}{L_{tube}} = \frac{21.73}{1} = 21.8. \tag{7.55}$$

Therefore, 22 tubes is required for manufacturing the absorber heat exchanger. However, to make the absorber and evaporator analogous, 24 tubes are considered for absorber manufacturing.

The absorber is of shell and tube type heat exchanger with horizontal tube bundles. The shell is constructed from copper with 1 m in length, 60 mm external diameter and 1.2 mm thick. The shell is insulated with 15 mm armaflex. 24 copper tubes with 15.87 mm outside diameter and 13.39 mm inside diameter were contained inside the shell as shown in Fig. 7.1. In summary, the absorber specifications are as:

Material of Coil Tubes:	Copper
Outer Diameter of Tubes:	15.87 mm
Inner Diameter of Tubes:	13.39 mm
Tube Thickness:	1.24 mm
Shell Thickness:	1.2 mm
Tubes Orientation:	Horizontal
Tubes Arrangement:	4 Rows of 6 Tubes
Length of Tubes:	1 m
Number of Tubes:	24
Space between Tubes:	22 mm
Overall Heat Transfer Coefficient:	$1254.82 \frac{W}{m^2 °C}$

7.2.5 Design of Solution Heat Exchanger

The solution heat exchange is a plate type heat exchanger. The plates are made by steel in which the hot strong solution flows in inner space and cold weak solution flows in outer space. The purpose of solution heat exchanger design is to determine its required length. The inner and outer spaces are rectangular shells with equal length. The design data for the strong solution in inner space are:

Strong solution mass flow rate $\dot{m}_{ss}$	0.0669 kg/s
Temperature of strong solution entering the solution heat exchanger T_4	78°C
Temperature of strong solution leaving the solution heat exchanger T_5	49.3°C
Strong solution concentration X_{ss}	0.5825 kg LiBr/kg solution

The properties of strong solution at its average temperature $\overline{T}_{ss} = \frac{78 + 49.3}{2} = 63.6°C$ are:

$\rho_{ss} = 1241.14 \frac{kg}{m^3}$ $\kappa_{ss} = 0.6385 \frac{W}{m°C}$

$C_{p,ss} = 3.803 \frac{kJ}{kg°C}$ $\mu_{ss} = 1.491 \times 10^{-3} \frac{kg}{m.s}$

The design data for the weak solution in outer space are:

Weak solution mass flow rate $\dot{m}_{ws}$	0.0699 kg/s
Temperature of weak solution entering the solution heat exchanger T_2	36°C
Temperature of weak solution leaving the heat exchanger T_3	63.5°C
Weak solution concentration X_{ws}	0.5577 kg LiBr/kg solution

The properties of strong solution at its average temperature $\overline{T}_{ws} = \frac{36 + 63.14}{2} = 49.57°C$ are:

$$\rho_{ws} = 1239.4 \frac{kg}{m^3} \qquad \kappa_{ws} = 0.68 \frac{W}{m°C}$$

$$C_{p,ws} = 3.804 \frac{kJ}{kg°C} \qquad \mu_{ws} = 2.923 \times 10^{-3} \frac{kg}{m.s}$$

The heat transfer coefficients inside and outside the tubes should be calculated first and then the overall heat transfer coefficient and tubes arrangement are determined. Since the solution heat exchanger is the rectangular plate type, its equivalent diameter is determined and used for calculation the Reynolds number. The plate type heat exchanger with dimension of 195 mm to 65 mm is selected. The plate thickness is considered as 3 mm and space between inner and outer plates is 10 mm. Therefore, the cross sectional area and wetted area of the heat exchanger are calculated as:

$$A_{cross,i} = 0.195 \times 0.065 = 0.0127 m^2, \tag{7.56}$$

$$P_{w,i} = 2 \times (0.195 + 0.065) = 0.52 m. \tag{7.57}$$

The equivalent diameter and Reynolds number can then be determined as:

$$D_{equ,i} = \frac{4 A_{cross,i}}{P_{w,i}} = \frac{4 \times 0.0127}{0.52} = 0.0977 m, \tag{7.58}$$

$$Re = \frac{\dot{m}_{ss} D_{equ,i}}{A_{cross,i} \mu_{ss}} = \frac{0.0669 \times 0.0977}{0.0127 \times 1.491 \times 10^{-3}} = 345.17. \tag{7.59}$$

Thus, the flow is laminar and the Prandtl and Nusselt number can be calculated as:

$$\mathrm{Pr}_{ss} = \frac{\mu_{ss} C_{p,ss}}{k_{ss}} = 8.88, \tag{7.60}$$

$$Nu = 3.66 + \frac{0.0668\left(\frac{D_{equ,i}}{L}\right) Re_{ss}\, Pr_{ss}}{1 + 0.04\left[\left(\frac{D_{equ,i}}{L}\right) Re_{ss}\, Pr_{ss}\right]^{2/3}}, \tag{7.61}$$

to calculate the *Nu* number the heat exchanger length must be known. The first assumption is *L=0.5m* and then:

$$Nu = 3.69, \tag{7.62}$$

Therefore, the inside heat transfer coefficient is calculated as:

$$Nu = \frac{h_i D_{equ,i}}{k_{ss}} \Rightarrow 3.69 = \frac{h_i \times 0.0977}{0.6385} \Rightarrow \alpha_i = 24.12 \frac{W}{m^2 °C}. \tag{7.63}$$

For weak solution in outer space, the wetted perimeter is the outside perimeter of the inner space. The plate thickness and space between inner and outer plates are 3 mm and 10 mm respectively and thus:

$$A_{cross,o} = (0.211 \times 0.081) - (0.201 \times 0.071) = 0.00282 m^2, \tag{7.64}$$

$$P_{w,o} = 2 \times (0.201 + 0.071) = 0.536 m, \tag{7.65}$$

$$D_{e,o} = \frac{4 A_{cross,o}}{P_{w,o}} = \frac{4 \times 0.00282}{0.536} = 0.021 m, \tag{7.66}$$

$$Re = \frac{\dot{m}_{ws} D_{equ,i}}{A_{cross,i} \mu_{ws}} = \frac{0.0699 \times 0.021}{0.00282 \times 2.923 \times 10^{-3}} = 178.08. \tag{7.67}$$

Therefore, the flow is laminar and Prandtl number, Nusselt number and outside heat transfer coefficient can be determined as:

$$\mathrm{Pr}_{ws} = 16.35, \tag{7.68}$$

$$Nu = 7.44, \tag{7.69}$$

$$Nu = \frac{\alpha_i D_{equ,o}}{k_{ws}} \Rightarrow 7.44 = \frac{h_o \times 0.021}{0.68} \Rightarrow \alpha_o = 240.91 \frac{W}{m^2 °C}. \tag{7.70}$$

The overall heat transfer coefficient of the plate type heat exchanger can be determined as:

$$\frac{1}{U} = \frac{1}{\alpha_o} + \frac{t_p}{k_p\left(\frac{A_m}{A_o}\right)} + \frac{1}{\alpha_i\left(\frac{A_i}{A_0}\right)} =$$
$$\frac{1}{240.91} + \frac{0.003}{69 \times \left(\frac{0.0127 + 0.00282}{0.00282}\right)} + \frac{1}{24.12 \times \left(\frac{0.0127}{0.00282}\right)} \Rightarrow U_{shx} = 74.82 \frac{W}{m^2 °C}, \tag{7.71}$$

where k_p is the plate thermal conductivity and forsteel pale is 69 W/m°C and A_m is the mean surface area of the inner space.

The solution heat exchanger is a counter-flow exchanger and its logarithmic mean temperature difference can be calculated as:

$$LMTD = \frac{\left(T_{ss,i} - T_{ws,o}\right) - \left(T_{ss,o} - T_{ws,i}\right)}{\ln\left(\frac{\left(T_{ss,i} - T_{ws,o}\right)}{\left(T_{ss,o} - T_{ws,i}\right)}\right)} = \frac{\left(T_4 - T_3\right) - \left(T_5 - T_2\right)}{\ln\left(\frac{\left(T_4 - T_3\right)}{\left(T_5 - T_2\right)}\right)}$$
$$= \frac{\left(78 - 63.14\right) - \left(48.6 - 36\right)}{\ln\left(\frac{78 - 63.14}{48.6 - 36}\right)} = \frac{2.26}{0.165} = 13.69°C. \tag{7.72}$$

Therefore, the specification for the solution heat exchanger are:

Material:	Steel
Heat exchanger type:	Counter-flow with parallel plates
Inner rectangular shell dimension:	195 mm × 65 mm × 500 mm
outer rectangular shell dimension:	211 mm × 81 mm × 500 mm
Plate Thickness:	3 mm
Space between plates:	10 mm

Overall Heat Transfer Coefficient: $74.82 \frac{W}{m^2 \, ^\circ C}$

Based on designed data, the single-effect absorption chiller has been manufactured. The arrangement of heat exchangers and their number of tubes are shown in Fig. 7.1.

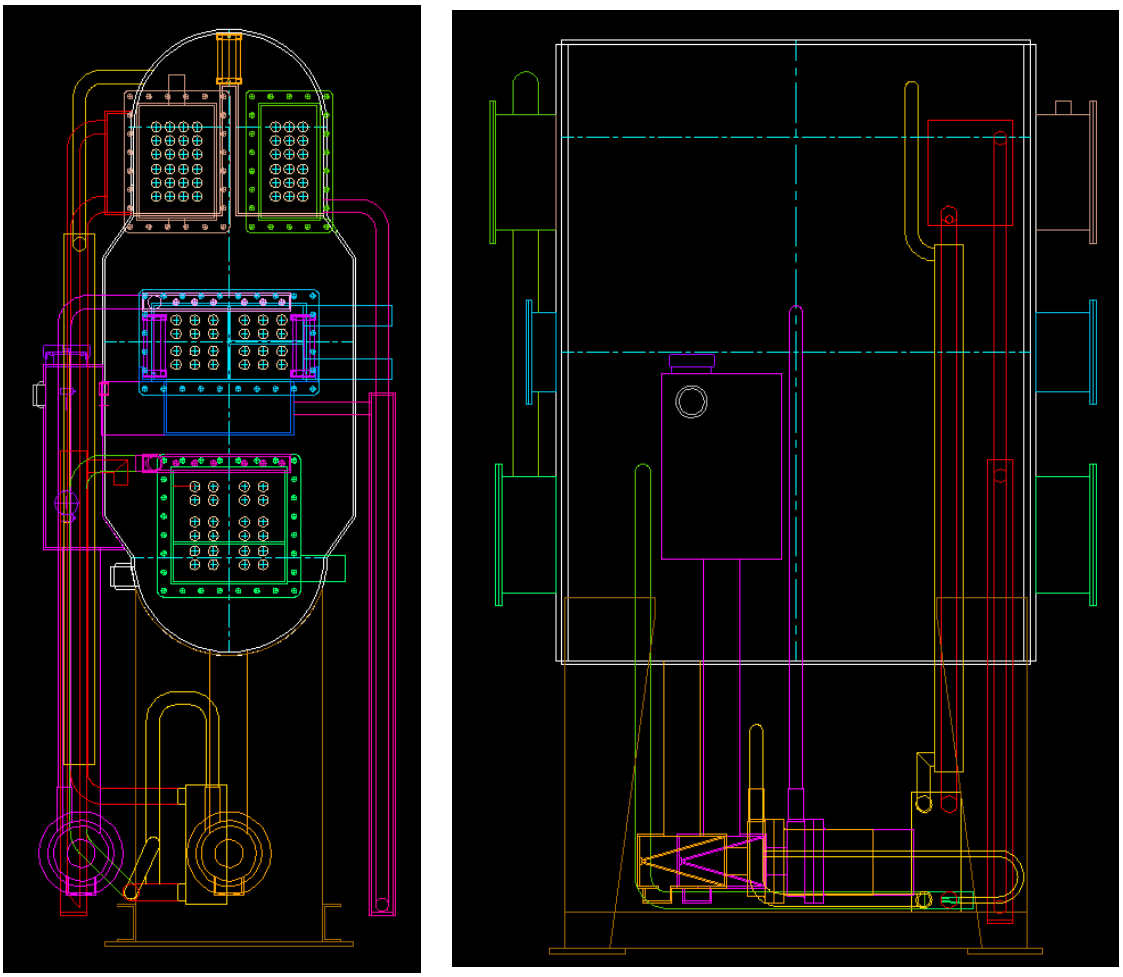

Fig. 7.1 Heat exchanger arrangement for single-effect absorption chiller with 7 kW cooling capacity

7.3 Cycle Performance

The purpose of this section is to investigate the effect of operating conditions on the cycle performance of the developed absorption chiller. The variation of the number of tubes inchiller heat exchangers such as generator, condenser, evaporator and absorber is also plotted against different operating conditions. The initial design of chiller heat exchangers was based on operating conditions presented in this chapter and chapter 5. In fact, a change in any input variable of the absorption chiller operation cycle causes changes in all the other dependent variables. When an input changes, the entire cycle responds to attain a new equilibrium operating condition. By using heat transfer model presented in this chapter in which the absorption chiller is developed and manufactured based on them, the actual behaviour of the chiller can be studied for variation of different inputs.

For this purpose, two program codes were developed and used. ABSYS was used to investigate the effect of operating conditions on the number of tubes for generator, condenser, evaporator and absorber. Another code was developed using EES (Engineering Equation Solver) program which provides numerical solution of the proposed equations. A numerous simulation were carried out by using EES to evaluate the performance of the absorption chiller components. The developed EES code is based on the mass and energy balances, heat transfer equations and thermodynamic properties of water and LiBr-water solution. The thermodynamic properties of water and LiBr-water solution is included in the program library. The developed EES code is presented in Appendix 2. In the followings, sensitivity analyses and simulation results of the individual chiller components are presented. The transient simulation of entire solar-powered absorption cooling plant is modelled and presented in the next chapter.

7.3.1 Generator Performance

To investigate the influence of different operating conditions on the generator number of tubes, the variable which its effect on the number of tubes is subjected to study is varied in a practical range and the rest of variables are kept constant in their designed conditions. For

example, to investigate the effect of generator temperature on the generator number of tubes, other variables are remained constant at their designed conditions as:

Evaporator Capacity, Q_e=7 kW

Effectiveness of Solution Heat Exchanger, ε_{shx}=0.7

Evaporator Temperature, T_e=5°C

Condenser Temperature, T_c=37°C

Absorber Temperature, T_a=36°C

Hot water temperature entering generator, $T_{hw,g,e}$=85°C

Hot water temperature leaving generator, $T_{hw,g,o}$=81°C

To investigate the effect of generator temperature on the system performance, it varies from 75°C to 80°C. It is because the generator temperature should be less than hot water temperature leaving the generator. Besides, the generator temperature for this design should not be less than 75°C to keep the chiller COP in the practical range. Results show that the generator number of tubes increases with increasing the generator temperature as demonstrated in Fig. 7.2. The reason is that increasing generator temperature results in the decreasing of both the generator thermal capacity and the generator logarithmic mean temperature difference. However, the intensity of temperature difference reduction is greater than that of the generator thermal capacity as shown in Fig. 7.3. Also, as expected, the generator overall U-value is increased with increasing the generator temperature as presented in Fig. 7.4. Results show that increasing the generator temperature from 75°C to 80°C increases the generator overall U-value from 1634.18 (kW/(m^2 °C)) to 1830.77(kW/(m^2 °C)).

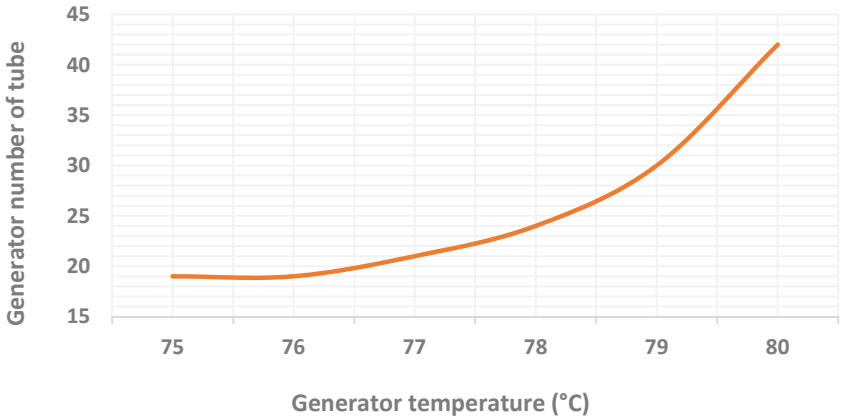

Fig. 7.2 Variation of generator number of tubes eith generator temperature

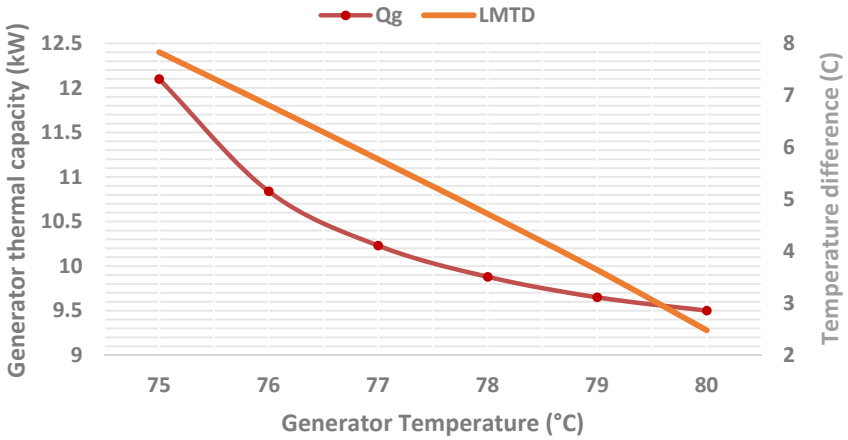

Fig. 7.3 Variation of generator capacity and temperature difference with generator temperature

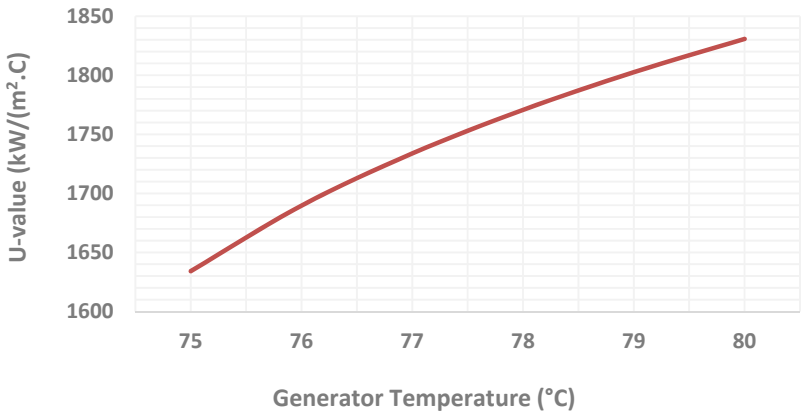

Fig. 7.4 Variation of generator U-value with generator temperature

The variation of the generator number of tubes with evaporator temperature while other operating conditions are remained constant is shown in Fig. 7.5. Since increasing the evaporator temperature reduces both weak and strong solution, the thermal capacity of the absorber and generator is reduced. However, evaporator temperature does not change the generator temperature difference. As a result, increasing the evaporator temperature reduces the number of tubes in the generator. The variation of the generator number of tubes with the solution heat exchanger effectiveness is shown in Fig. 7.6. As discussed in chapter five, increasing the efficiency of the solution heat exchanger reduces the generator capacity and hence decreases the required number of tubes in generator. The influence of the hot water temperature entering the generator on the number of tubes is demonstrated in Fig. 7.7. It can be seen that the increasing the entering hot water temperature results in decreasing the number of tubes in generator. In fact, increasing the entering hot water temperature, increases both the logarithmic temperature difference of the generator and generator thermal capacity while the generator overall U-value is decreased.

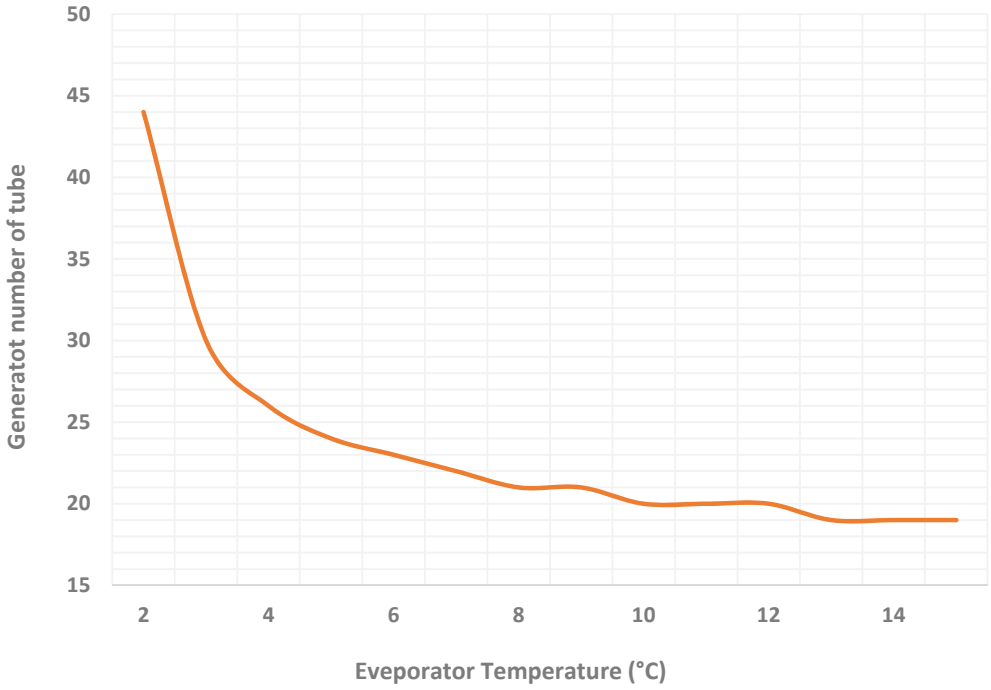

Fig. 7.5 Variation of generator number of tubes with evaporator temperature

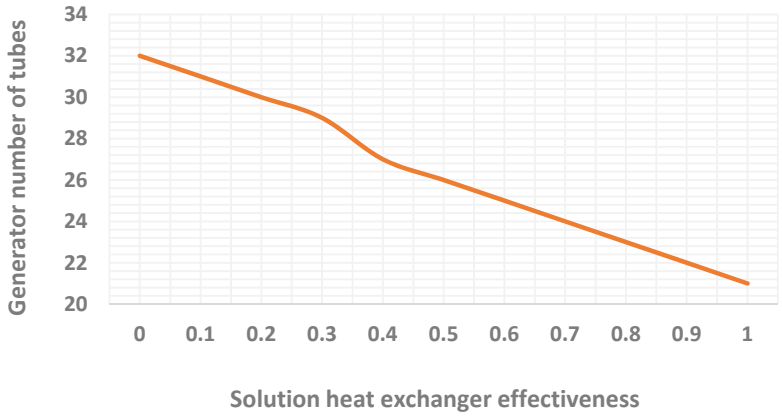

Fig. 7.6 Variation of generator number of tubes with solution heat exchanger effectiveness

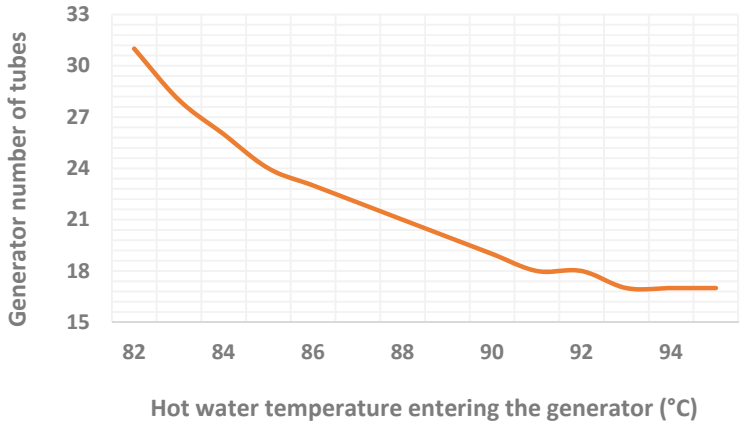

Fig. 7.7 Variation of generator number of tubes with entering hot water temperature

The effect of generator inlet hot water temperature on the absorption chiller cooling capacity and COP while holding all other inputs constant is shown in Fig. 7.8 and 7.9 respectively. The COP raises from a low value of 0.39 to reach a constant value of 0.708. The cooling capacity of the chiller varies from a low value of 0.616 kW up to 9.064 kW as demonstrated in Fig. 7.9. In fact, as the hot water temperature entering the generator increases, the cooling capacity also increases. This then effects the thermal capacity of other heat exchangers as shown in Fig. 7.10. It can be seen that as the heat source temperature increases, the heat transfer in all heat exchangers increases. As shown is Fig. 7.10, when the water temperature entering the generator increases, the generator thermal capacity increases. The reason is that

when hot water temperature at the generator inlet is increased, the solution temperature in the generator increases which means more refrigerant will be generated. This causes an increase in the solution concentration which in turn increases the thermal capacity of the generator.

Moreover, changing the hot water temperature entering the generator changes the internal cycle temperature as a peculiar trend. Results show that increasing the entering hot water temperature increases the solution temperature leaving the generator and reduces the water temperature leaving the evaporator as shown in Fig. 7.11.

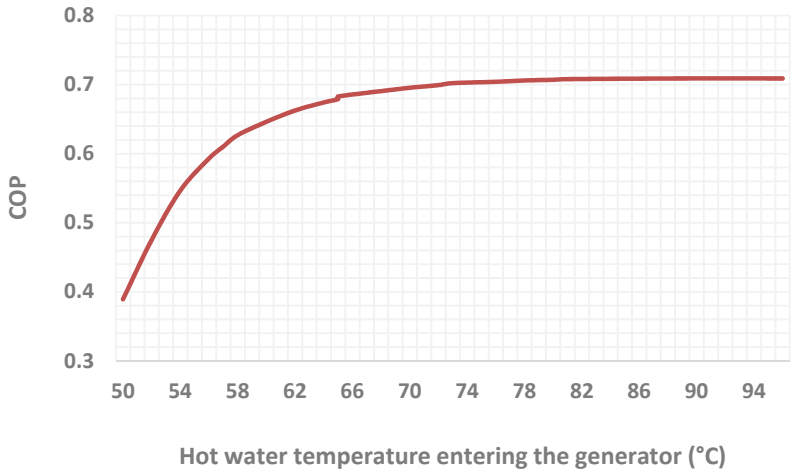

Fig. 7.8 Effect of generator inlet temperature on the chiller COP

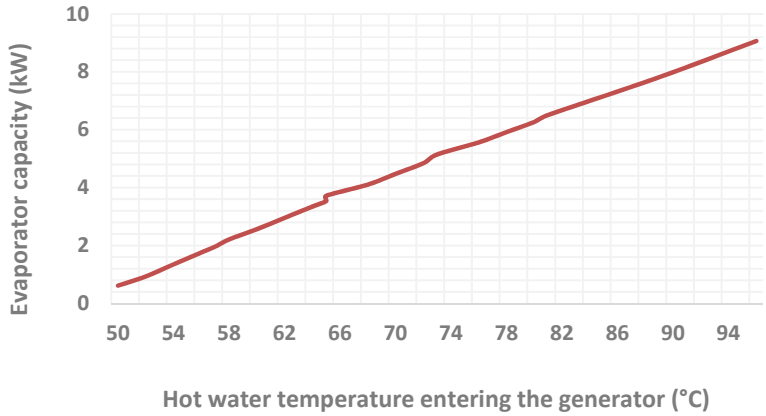

Fig. 7.9 Effect of generator inlet temperature on the chiller cooling capacity

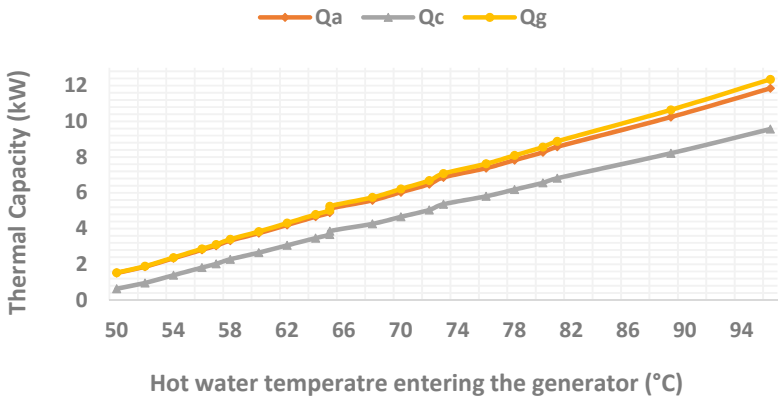

Fig. 7.10 Effect of generator inlet temperature on thermal capacity of other componenets

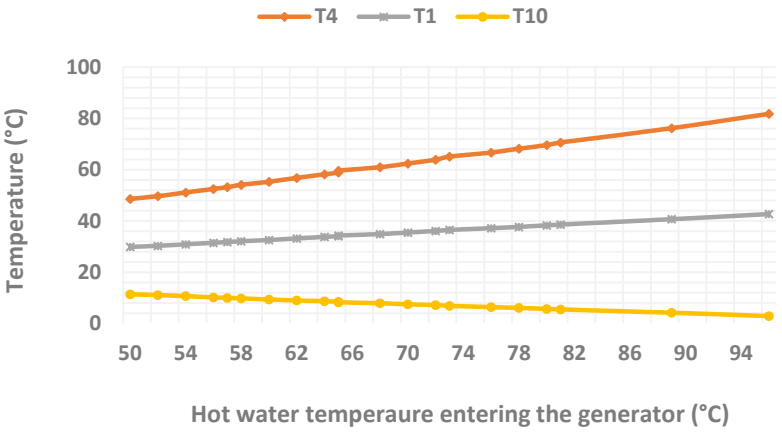

Fig. 7.11 Effect of generator inlet temperature on cycle temperatures

The influence of the generator heat exchanger size on the COP and cooling capacity of the chiller is shown in Fig. 7.12 and 7.13 respectively. Results show that the COP is comparatively insensitive to the changes in $(UA)_g$ except for very small $(UA)_g$ values where the COP decreases as $(UA)_g$ decreases. However, evaporator capacity is more sensitive to $(UA)_g$. In fact, increasing the generator temperature increases overall heat transfer coefficient of the generator which decreases thermal resistance between the hot water inside the tubes and LiBr-water solution outside the tubes. This successively drops the logarithmic mean temperature differences between the hot water and LiBr-water solution and allows the generator to transfer the required heat with less temperature difference. However, the hot water temperature entering the generator should not increase too much due to the

crystallisation of the LiBr. If the solution temperature decreases too low or the solution concentration is too high, crystallisation may occur.

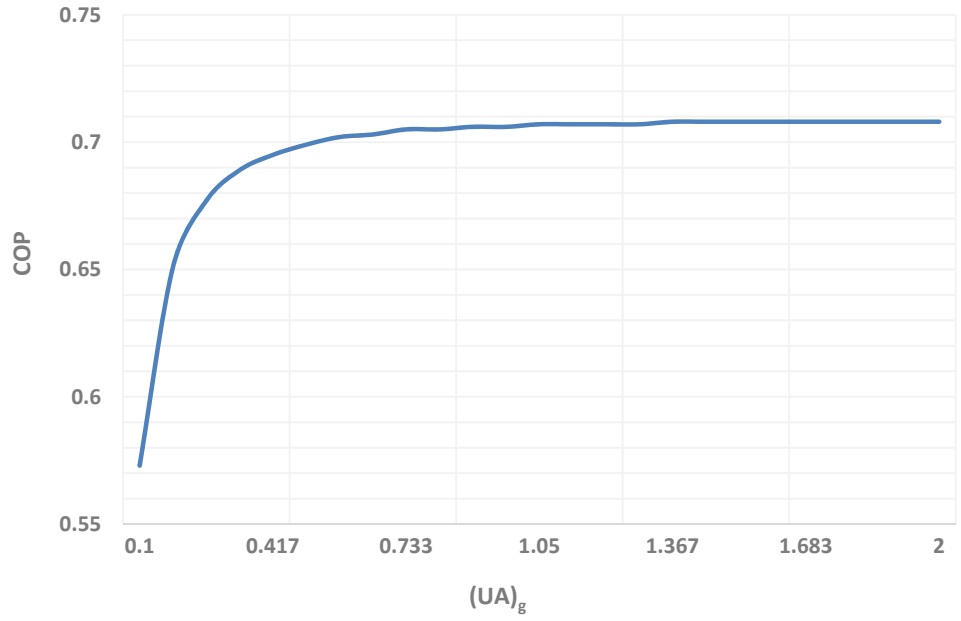

Fig. 7.12 Effect of generator $(UA)_g$ on COP

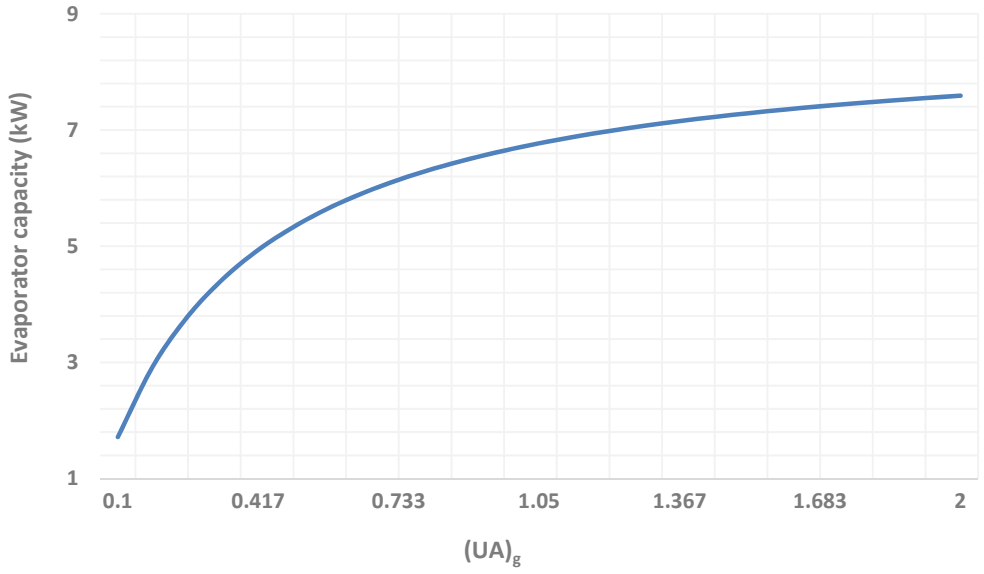

Fig. 7.13 Effect of generator $(UA)_g$ on evaporator capacity

7.3.2 Condenser Performance

The effect of condenser design variables on the condenser number of tubes and operating cycle of the absorption chiller is evaluated in this section. Fig. 7.14 shows the number of tubes in condenser are decreased when condenser temperature is increased. Since for this investigation the cooling water temperature leaving the condenser is remains constant at its designed value (32°C), the condenser temperature is varied from 33°C. In fact, when condenser temperature is increased while the entering cooled-water temperature and condenser area are kept constant, the logarithmic mean temperature difference is increased. Therefore, less heat transfer area is required for heat rejection. Increasing the condenser temperature by 22% increases the number of tubes by 76%. Fig. 7.15 shows the influence of water temperature entering the condenser on the condenser number of tubes. It can be seen that the variation of cooling water inlet temperature does not have significant effect on the number of tubes. Increasing the cooling water temperature at the condenser inlet increases the number of condenser tubes about 26%.

The cooling water flows to the absorber and condenser can be arranged in parallel or series. In our case, the series flow arrangement is designed where the cooled-water leaving cooling tower first passes through the absorber and then condenser to transfer the absorption and condensation heat to the cooling tower. As a result, the absorption temperature is always lower than the condensation temperature. Moreover, the series flow arrangement is preferred as a single water pump will be utilised which can avoid control problem of the water mass flow rate in the partial loads. To evaluate the effect of condenser design variables on the absorption chiller performance, the cooled water entering the condenser is varied from 15°C to 31°C while holding all other inputs constant at their design values. Fig. 7.16 shows the effect of cooling water temperature entering the condenser on the condenser heat rejection capacity. The heat rejection rate is almost insensitive within the cooling water temperature. Increasing the entering water temperature to the condenser by 51.6% increases the condenser capacity by 0.04%.

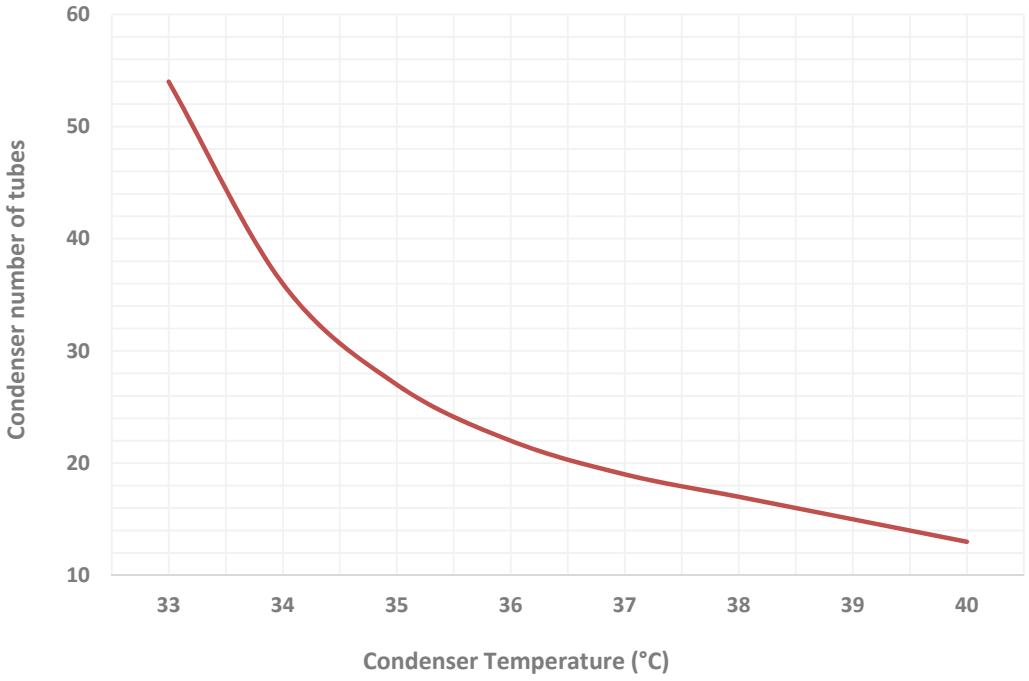

Fig. 7.14 Effect of condenser temperature on condenser number of tubes

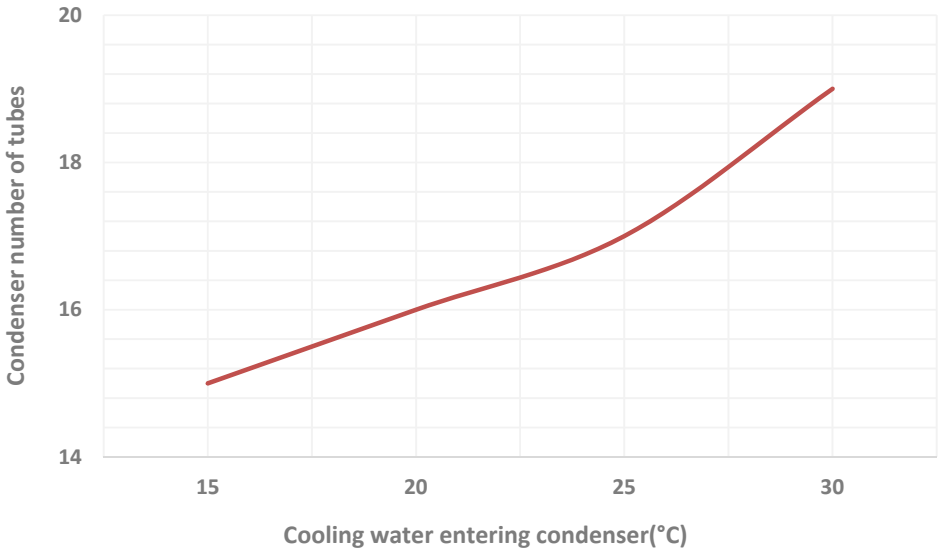

Fig. 7.15 Effect of cooling water temperature entering the condenser on condenser number of tubes

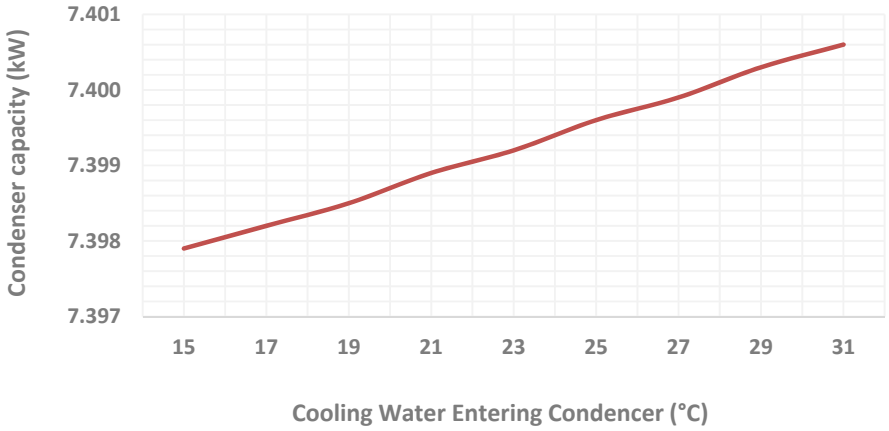

Fig. 7.16 Effect of cooling water temperature entering the condenser on condenser capacity

Results show that when the cooled-water temperature increases, the heat transfer rate in generator and absorber increase as shown is Fig. 7.17. The reason is that when cooled-water temperature at the condenser inlet is increased, the strong solution concentration is reduced while the weak solution concentration remains constant. This causes an increase in both the weak and strong mass flow rate. Therefore, the absorber and generator thermal capacity increase. The effect of condenser inlet cooled-water temperature on the absorption chiller COP is shown in Fig. 7.18. For this investigation, all other system variables remain at their constant designed value. The COP decreases from a high value of 0.81 at 15°C to reach a value of 0.67 at 31°C.

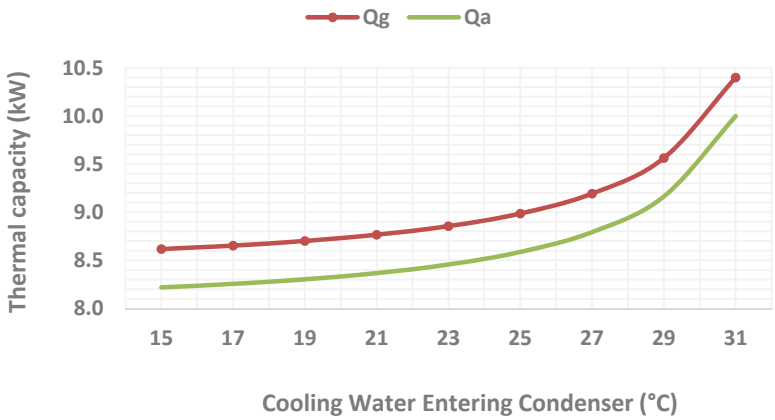

Fig. 7.17 Effect of cooling water temperature entering the condenser on generator and absorber capacity

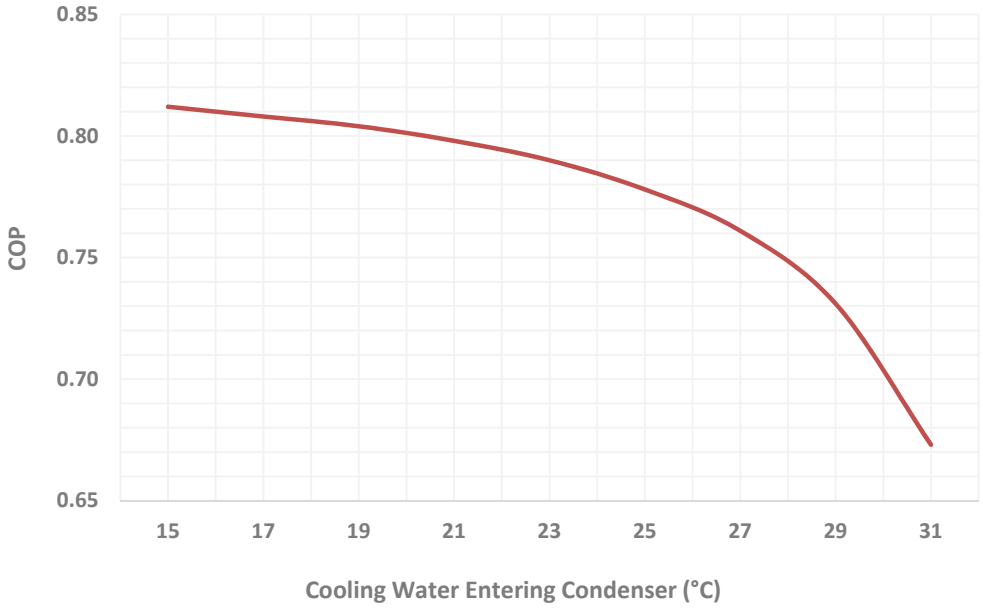

Fig. 7.18 Effect of cooling water temperature entering the condenser on chiller COP

The influence of the condenser heat exchanger size on the COP and cooling capacity of the chiller is shown in Fig. 7.19 and 7.20 respectively. Results show that both the COP and evaporator capacity are sensitive to $(UA)_c$. Increasing the condenser temperature increases the refrigerant flow rate which lead to the higher evaporator cooling capacity which also increases the system COP.

In addition, as shown in Fig. 7.21, increasing the condenser temperature reduces overall heat transfer coefficient of the condenser which increases thermal resistance between the cooled-water inside the tubes and refrigerant outside the tubes. This in turn raises the logarithmic mean temperature differences between the cooled-water and refrigerant water and allows the condenser to transfer the required heat with more temperature difference as shown in Fig. 7.22. However, the cooled-water temperature entering the condenser should not reduce too much due to the crystallisation of the LiBr solution.

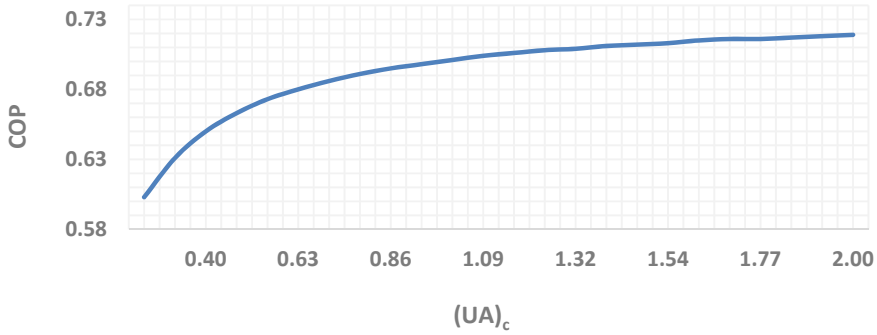

Fig. 7.19 Effect of condenser $(UA)_c$ on chiller COP

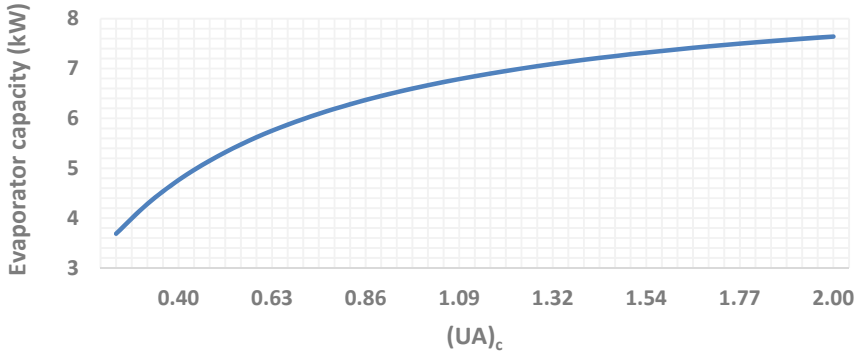

Fig. 7.20 Effect of condenser $(UA)_c$ on evaporator capacity

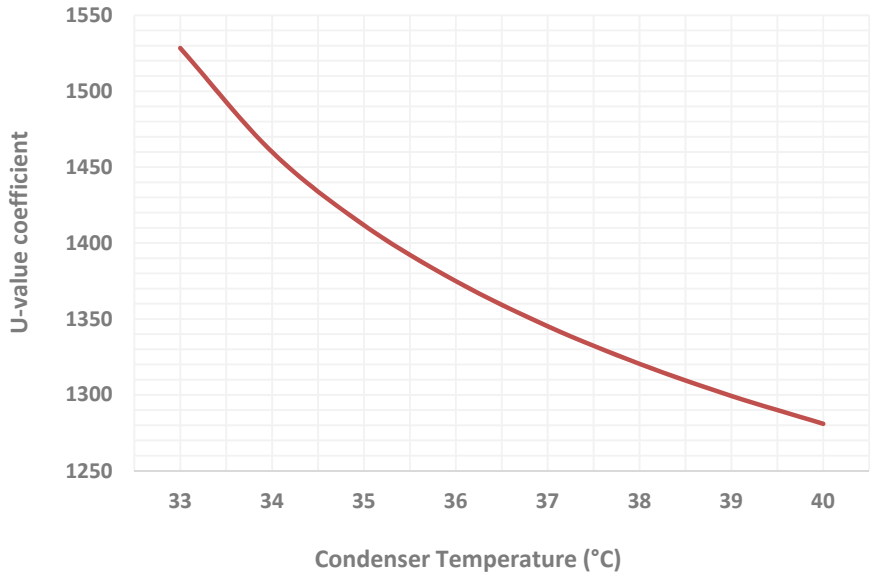

Fig. 7.21 Effect of condenser temperature on condenser overall heat transfer coefficient

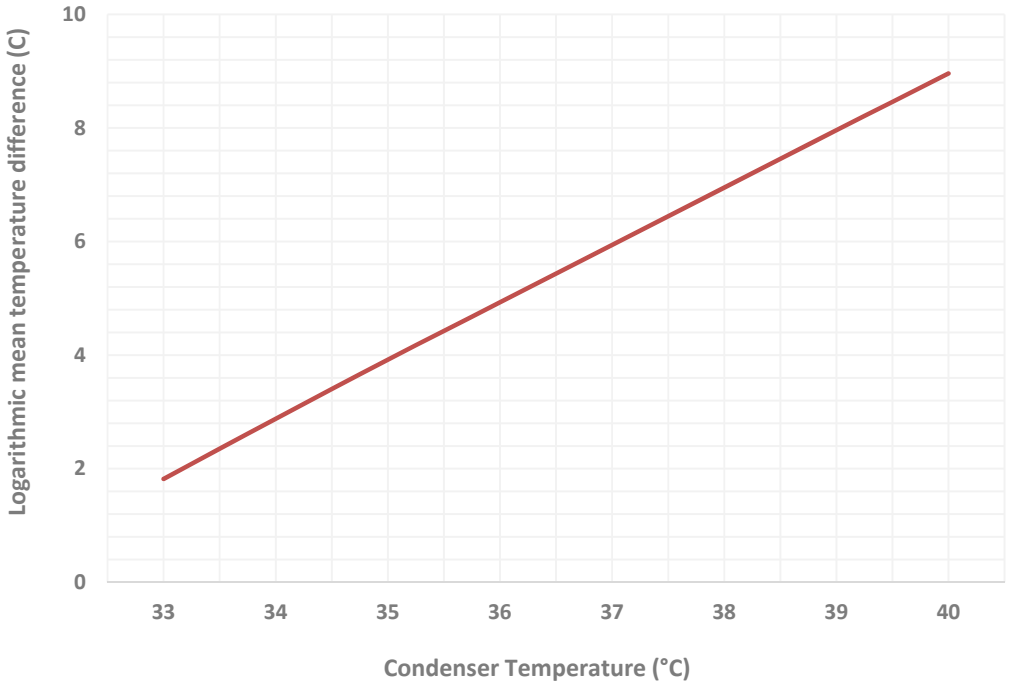

Fig. 7.22 Effect of condenser temperature on condenser logarithmic mean temperature difference

7.3.3 Absorber Performance

The variation of the absorber number of tubes with evaporator temperature while other operating conditions are remained constant is shown in Fig. 7.23. Since increasing the evaporator temperature reduces the weak solution concentration, the thermal capacity of the absorber and generator is reduced. As a result, increasing the evaporator temperature reduces the number of tubes in the absorber as shown in Fig. 7.23. However, evaporator temperatures more than 10°C don't have considerable influence on the absorber number of tubes. Similarly, increasing the absorber temperature the weak solution concentration and thus reduces the required heat transfer area in the absorber. Results show that increasing the absorber temperature from 31°C to 38°C, increases the logarithmic mean temperature difference in the absorber from 1.8°C to 8.1°C. As shown in Fig. 7.24, increasing the absorber temperature from 31°C to 38°C decreases the absorber number of tubes from 84 to 18 tubes.

The number of tubes in absorber are reduced initially with increasing the generator temperature. The reason is that increasing generator temperature increases the strong solution concentration while the weak solution concentration remains constant. Therefore, thermal capacity of absorber reduces and les tubes are required to heat exchange with cooling water entering the tubes. However, results indicate that the generator temperatures more than 79°C have not significant effect on the absorber number of tubes as shown in Fig. 7.25. In addition, results show that for condenser temperatures less than absorber temperature, increasing the condenser temperature does not change the number of tubes in absorber. However, when the condenser temperatures are greater than absorber temperature, increasing the condenser temperature increases the number of tubes in absorber. Since in this design, the absorber temperature is 36°C, increasing the condenser temperature from 20°C to 35°C does not vary the number of tubes. However, increasing the condenser temperature from 36°C to 40°C increase the number of absorber tubes significantly as shown in 7.26. The variation of the absorber number of tubes with the solution heat exchanger effectiveness is shown in Fig. 7.27. As discussed in chapter five, increasing the efficiency of the solution heat exchanger reduces the absorber capacity and hence decreases the required number of tubes in the absorber.

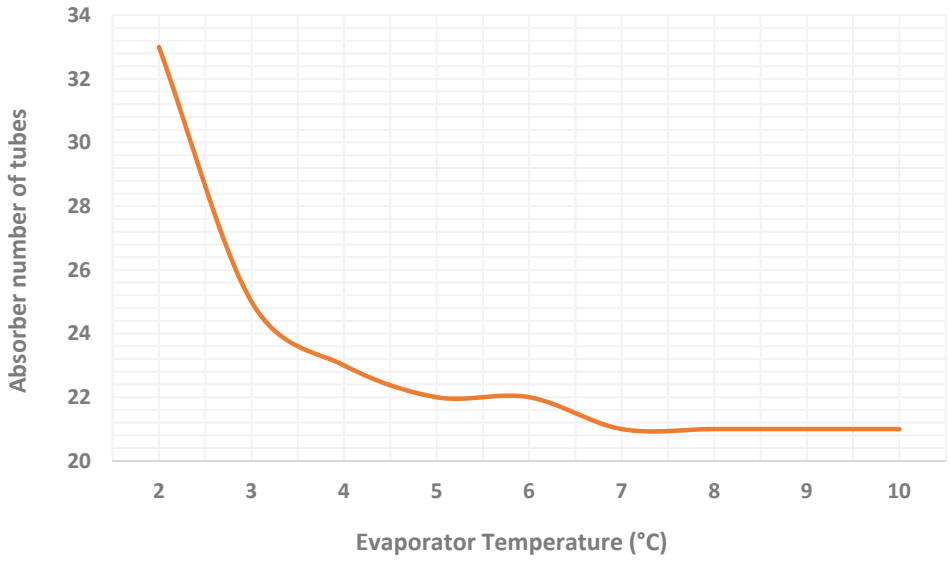

Fig. 7.23 Effect of evaporator temperature on absorber number of tubes

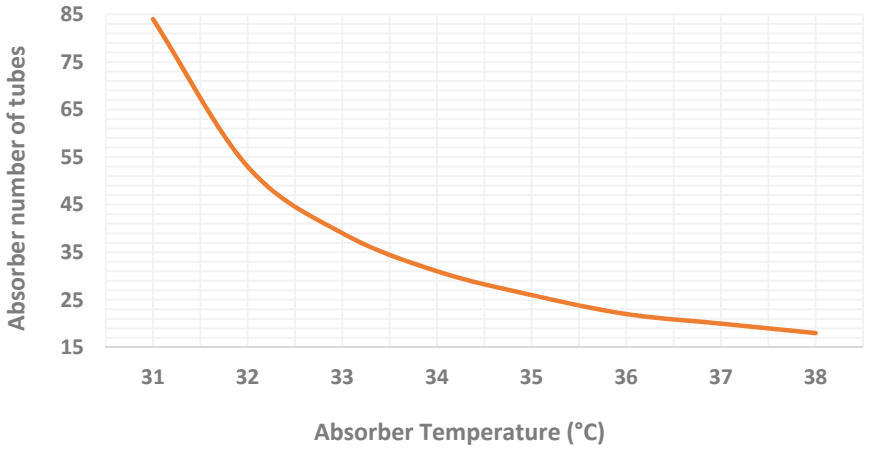

Fig. 7.24 Effect of absorber temperature on absorber number of tubes

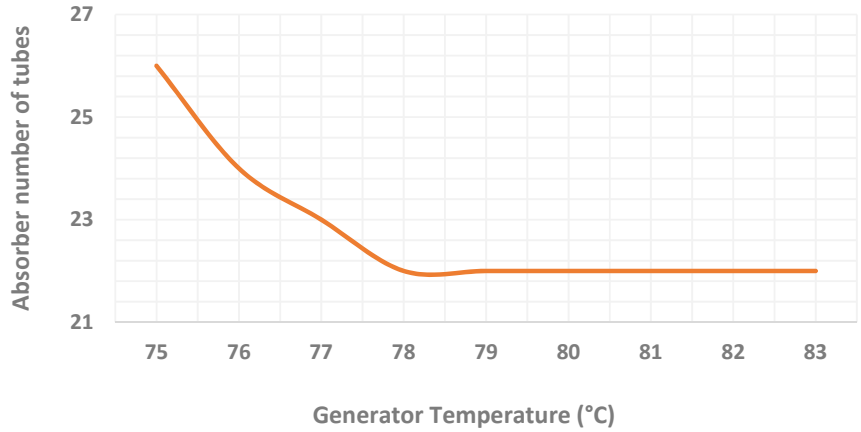

Fig. 7.25 Effect of generator temperature on absorber number of tubes

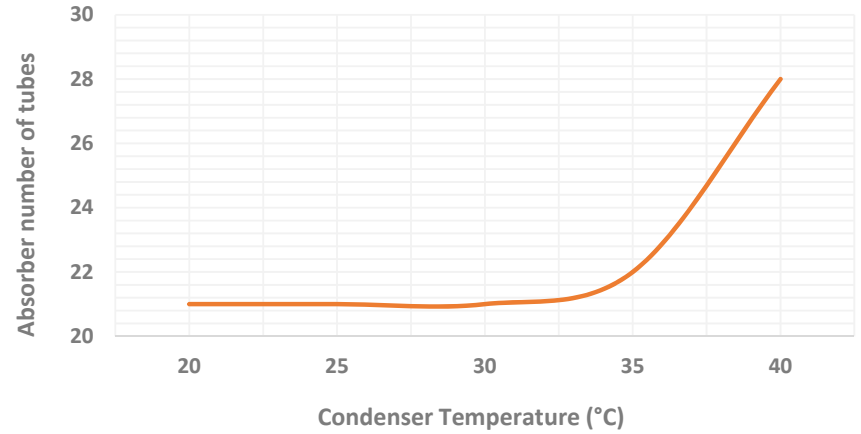

Fig. 7.26 Effect of condenser temperature on absorber number of tubes

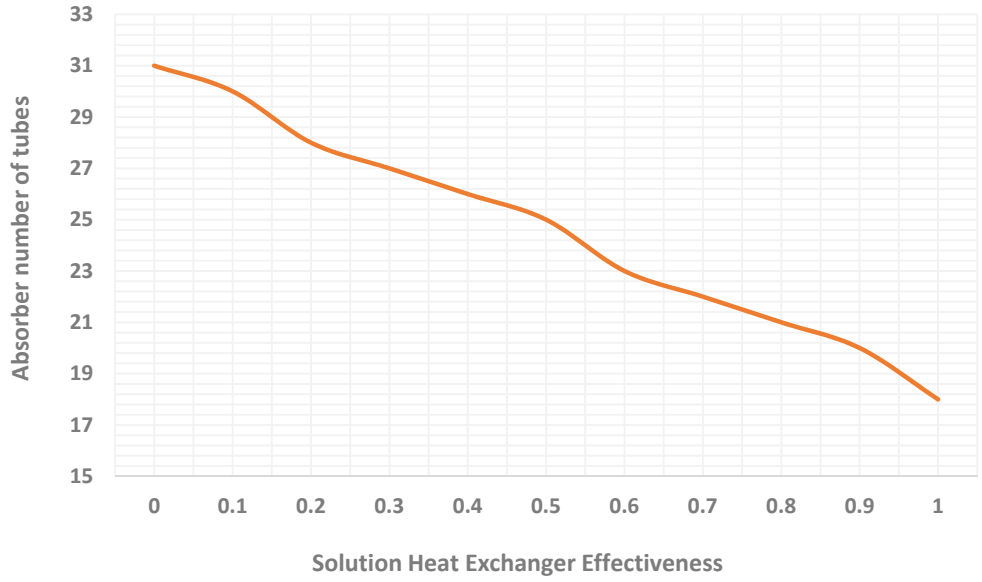

Fig. 7.27 Effect of solution heat exchanger effectiveness on absorber number of tubes

The performance of the absorber has also been evaluated for various input values while keeping the others constant. For this purpose, the cooled water entering the absorber is varied from 15°C to 29°C as possible operating limits in this design. Fig. 7.28 shows the effect of cooling water temperature entering the absorber on the absorber heat rejection capacity. It can be seen that absorber capacity decreases as its entering cooling water temperature is increased. This is because when the temperature of cooled water entering the absorber is increased, less refrigerant is absorbed by the solution which increases the weak solution concentration in the absorber. Therefore, less heat is rejected to the cooling tower. The effect of absorber inlet cooled-water temperature on the absorption chiller COP is shown in Fig. 7.29. For this investigation, all other system variables remain at their constant designed value. The COP decreases from a high value of 0.81 at 15°C to reach a value of 0.69 at 29°C.

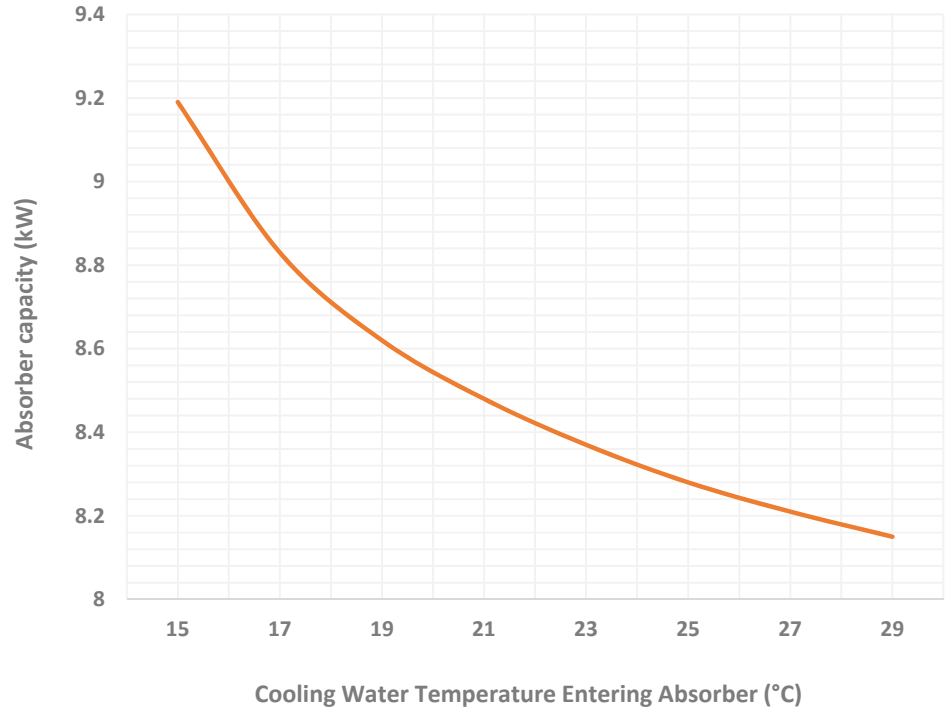

Fig. 7.28 Effect of cooling water temperature entering absorber on absorber capacity

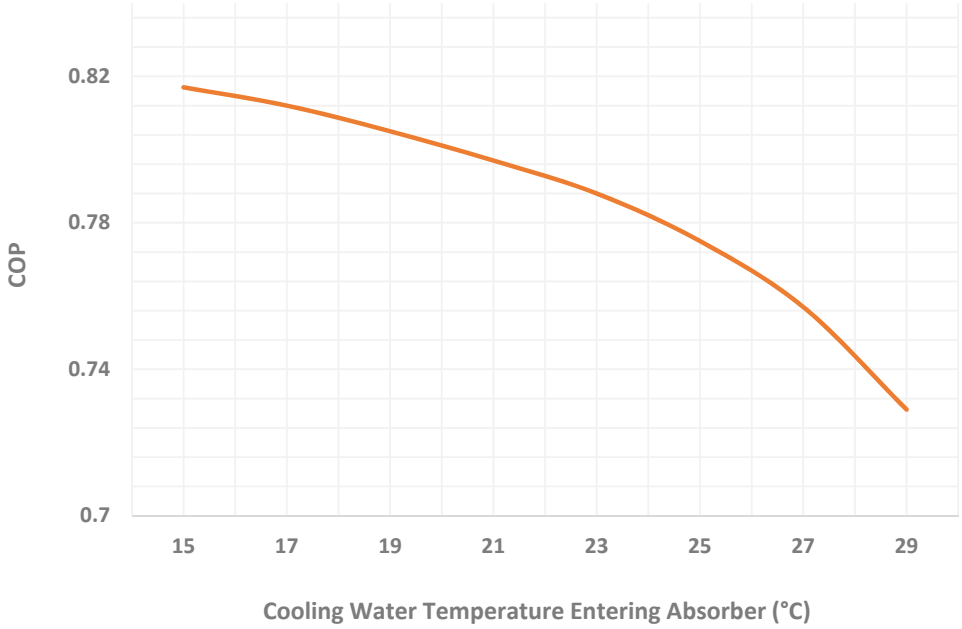

Fig. 7.29 Effect of cooling water temperature entering absorber on chiller COP

7.3.4 Evaporator Performance

The effect of variation of the evaporator temperature and chilled-water temperature entering and leaving the chiller on the chiller performance is investigated in this section. As expected, increasing the evaporator temperature while holding chilled-water temperature leaving the chiller leads to increase the required number of tubes in evaporator. As shown in Fig. 7.30, increasing the evaporator temperature from 2°C to 6°C increases the number of tubes from 14 tubes to 34 tubes. In this analysis, the chilled water temperature leaving and entering the chiller were maintained constant as 7°C and 12°C respectively. The effect of the leaving chilled-water temperature on the evaporator number of tubes is shown in Fig. 7.31. It can be seen that at a constant evaporator temperature of 5°C, increasing the supply chilled-water temperature decreases the number of evaporator tubes. The reason is that increasing the chilled-water temperature leaving the chiller reduces the evaporator thermal capacity which means that less heat transfer area is required for heat exchanging between refrigerant and chilled-water. Similarly, increasing the chilled-water temperature entering the chiller while maintain the leaving chilled-water temperature at its designed value, increases the temperature difference in the evaporator. This means less heat transfer area is required to support the building cooling load. This reduces the number of tubes in the evaporator as shown in Fig. 7.32. Results indicate that the evaporator number of tubes are insensitive to the other operating temperatures such as generator, condenser and absorber temperatures.

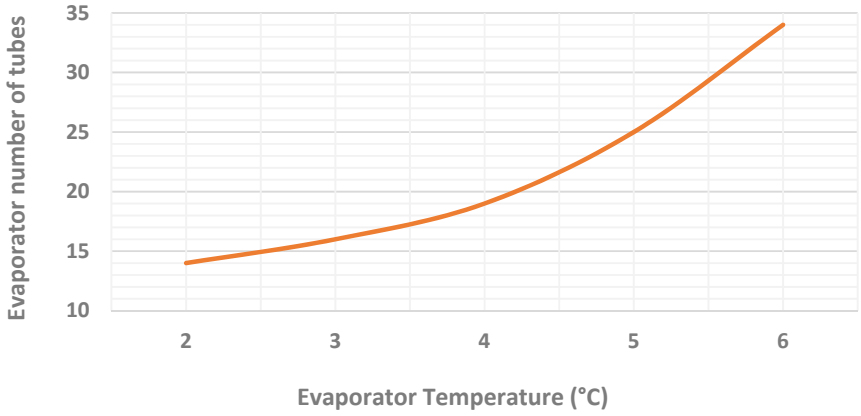

Fig. 7.30 Effect of evaporator temperature on evaporator number of tubes

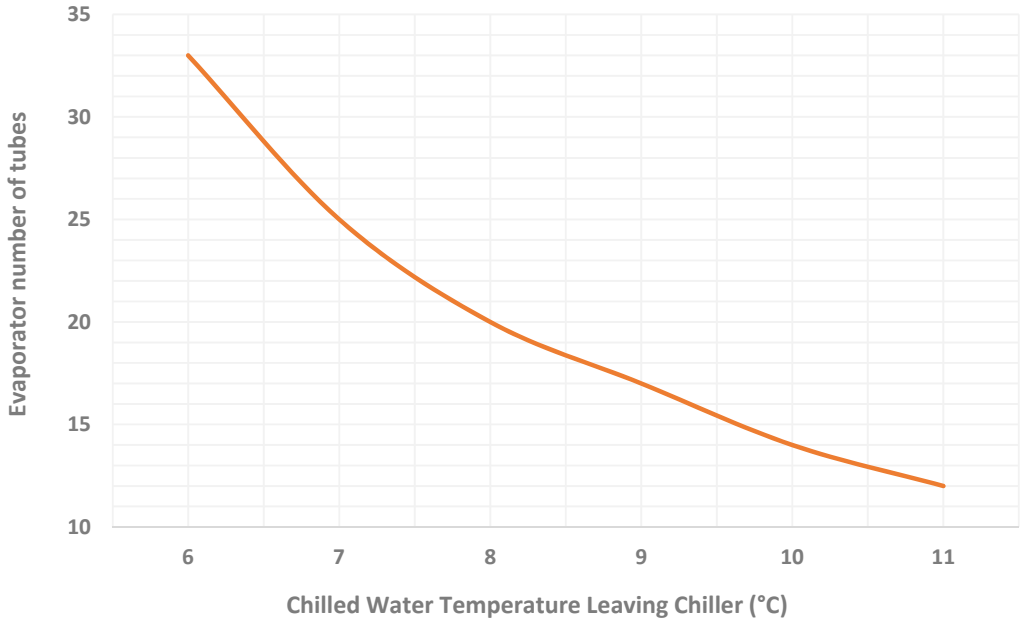

Fig. 7.31 Effect of chilled water temperature leaving chiller on evaporator number of tubes

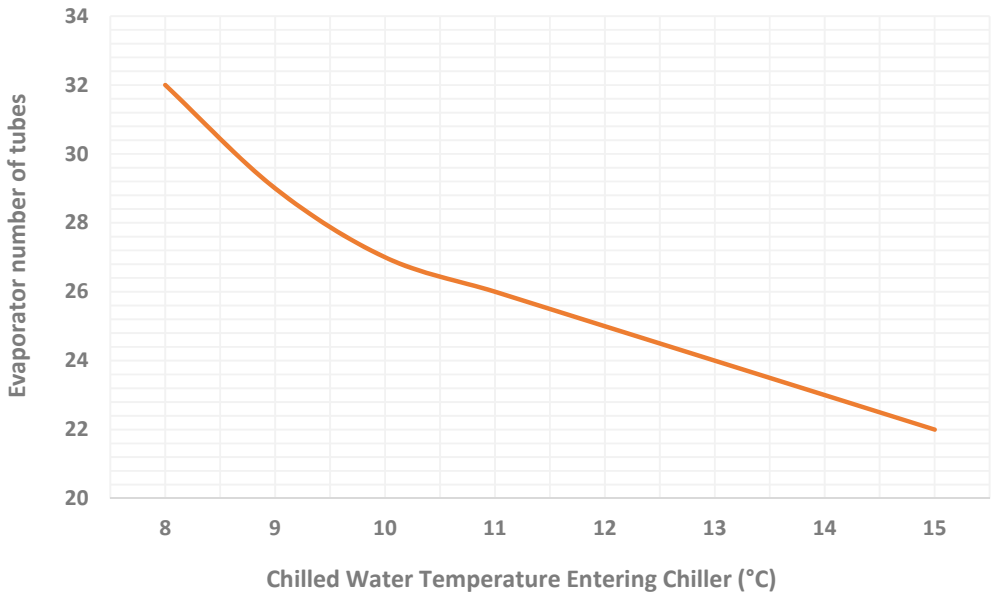

Fig. 7.32 Effect of chilled water temperature entering chiller on evaporator number of tubes

The effect of the inlet chilled-water temperature variations on chiller COP and evaporator capacity is shown in Fig. 7.33 and 7.34 respectively. It can be seen that the chiller COP varies slightly over the range of return chilled-water temperature. Results show that increasing the chilled water temperature entering the chiller from 8°C to 20°C increases the chiller COP by only 10%. In addition, increasing return chilled-water temperature has significant effect on the evaporator cooling capacity. In fact, increasing the chilled-water temperature entering chiller means that building cooling demand is increased and therefore more cooling should be provided by the chiller. To increase the chiller cooling capacity more heat is required by generator which reduces the COP of the chiller. Therefore while increasing the chilled-water temperature entering the chiller significantly increases the evaporator capacity, it has a little effect on the chiller COP. In addition, when both the evaporator and generator capacity increase, the thermal capacity of absorber and condenser increase correspondingly to balance the thermal capacity of the entire system. The effect of chilled-water temperature entering the chiller on the thermal capacity of the generator, absorber and condenser is shown in Fig. 7.35.

The influence of the return chilled-water temperature on the refrigerant temperature leaving the evaporator is demonstrated in Fig. 7.36. Increasing the chilled-water temperature at the inlet of evaporator increases the temperature of the low pressure refrigerant (water) leaving the evaporator. The refrigerant with less temperature then enters the absorber which reduces the solution temperature leaving the absorber. As a result, the solution concentration in the absorber is reduced. However, the cooling system acts till provide new cooling demand required by the building.

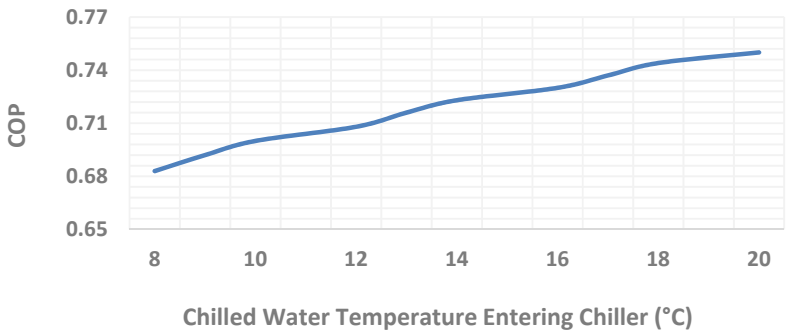

Fig. 7.33 Effect of chilled water temperature entering chiller on chiller COP

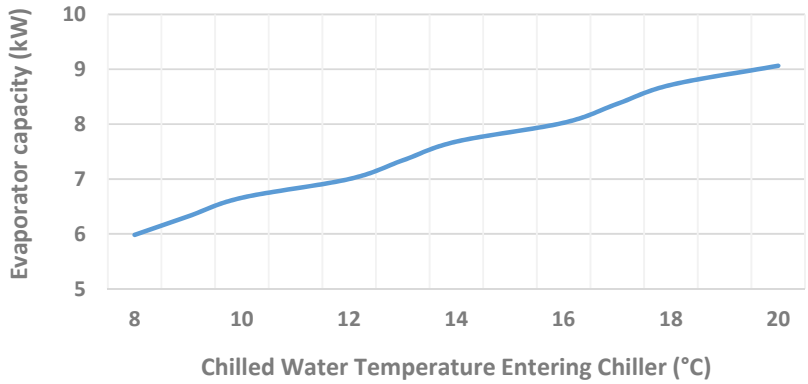

Fig. 7.34 Effect of chilled water temperature entering chiller on evaporator capacity

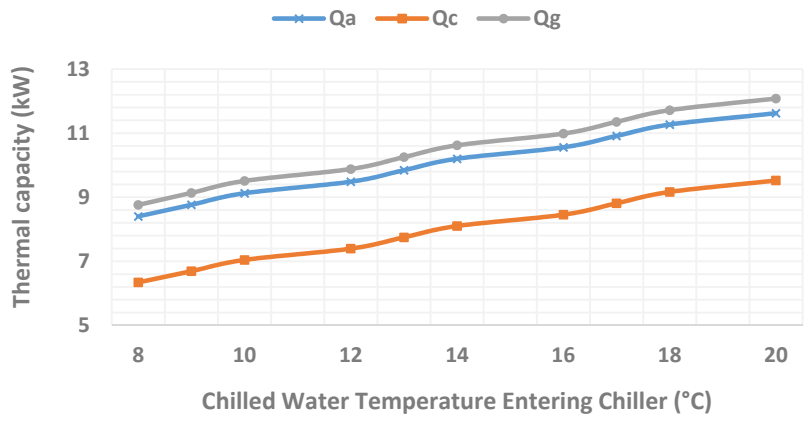

Fig. 7.35 Effect of chilled water temperature entering chiller on thermal capacity of other heat exchangers

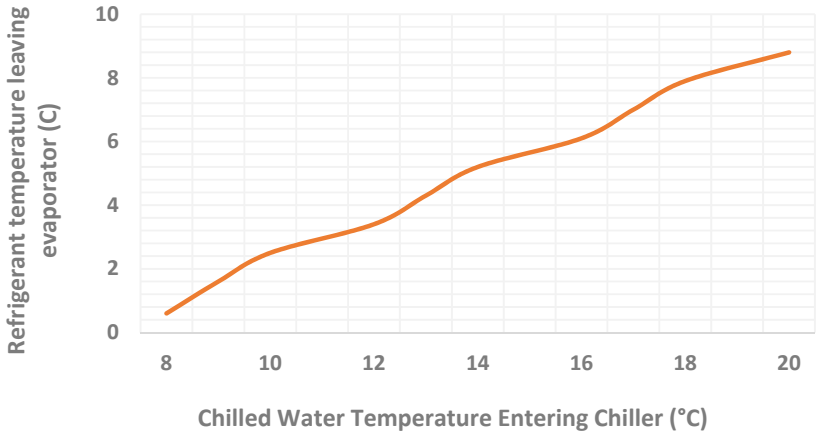

Fig. 7.36 Effect of chilled water temperature entering chiller on refrigerant temperature leaving evaporator

The influence of the evaporator heat exchanger size on the COP and cooling capacity of the chiller is shown in Fig. 7.37 and 7.38 respectively. Results show that both the COP and evaporator capacity are sensitive to $(UA)_e$. Increasing the evaporator $(UA)_e$ value increases the evaporator cooling capacity which also increases the system COP.

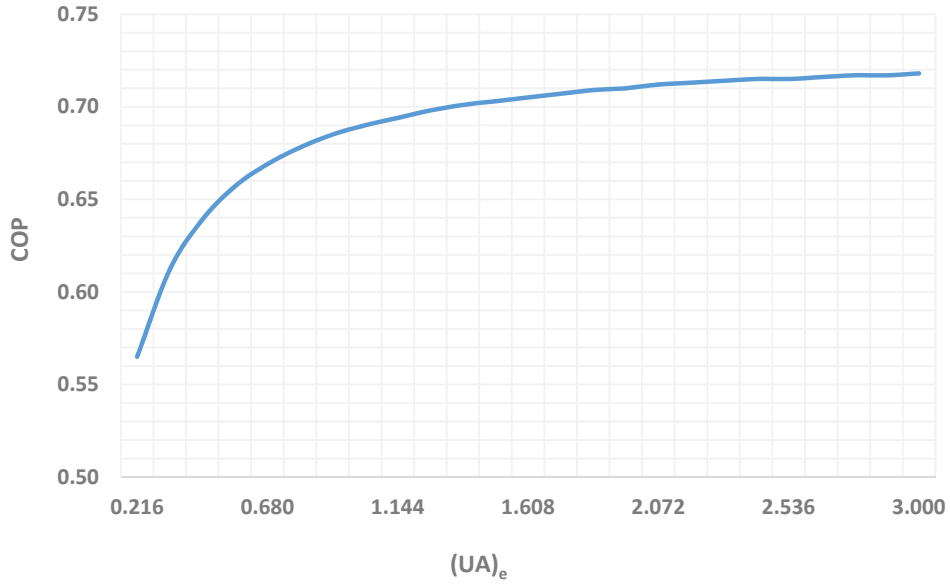

Fig. 7.37 Effect of evaporator $(UA)_e$ on chiller COP

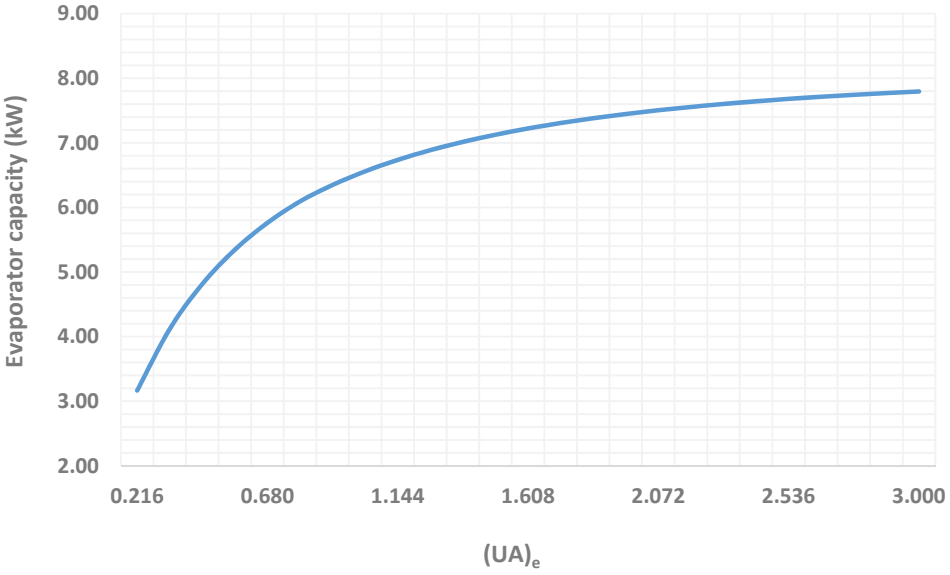

Fig. 7.38 Effect of evaporator $(UA)_e$ on evaporator capacity

7.4 Experimental Rig

Following the thermodynamic design results and component specifications presented in this chapter, the single-effect absorption chiller was constructed. The chiller consists of two sealed vessels which operate near vacuum conditions. Each vessel is composed of two heat exchangers separated by partitions. The counter flow solution heat exchanger is located externally and heats the weak solution from the absorber and cools the strong solution returning from the generator to the absorber. Although, the heat exchangers can be assembled in a single shell, however for simplicity and ease of fabrication they were arranged in two-shell design configuration. For this purpose, the condenser and generator coils were combined inside the same vessel and evaporator and absorber are incorporated in another vessel. The generator-condenser vessel was then placed at the height above the evaporator-absorber vessel.

The cooling load of the lift motor room at university of technology, Sydney (UTS) Building 2 is used as the case study. The gross floor area of the room is 32 square meters with three meters high. The building detail and its thermal load are fully described in chapter 3. The weather data used in the project simulation are based on a typical meteorological year as presented in chapter 3. The central cooling plant installed in the building consists of a water-cooled single-effect absorption chiller, a cross-flow vertical cooling tower, a fan-coil unit, evacuated solar collectors, a chilled-water pump, a hot-water pump and a condenser-water pump. The water absorption chiller with a rated capacity of 7 kW (2 RT) cooling is operating at a designed driving hot water temperature of 85°C, coolant water temperature of 28°C and supply chilled water temperature of 7°C. The rated hot water mass flow rate is 0.58 l/s. the hot water pump with rated 75 kPa total static pressure difference and 50 W energy consumption is located between the solar vacuum collector and absorption chiller's generator. The designed supply and return chilled water temperatures are set respectively at 7°C and 12°C. The chilled water mass flow rate is 0.33 l/s at design conditions. To circulate chilled-water an inline pump with rated 90 kPa head pressure and 65 W power usage is used. The heat rejection is performed by using a cross-flow cooling tower, designed for 1.13 l/s cooled water

flow rate. An inline pump with rated 90 kPa total static pressure difference and 65 W power consumption is used for cooled-water circulation. The cooling tower air flow rate is 6420 m^3/hr and its rated power usage is 420 W. An axial fan (Model: YWF4E-500B) with the rated 1300 rpm motor speed is used for the cooling tower. The fan-coil unit located in the room to be air-conditioned is designed for 378 l/s air flow rate and its rated power consumption is 143 W. The evacuated solar collectors comprise a 31.5 m^2 apparent area for an array of 135 evacuated tubes in nine-collector bays, operating in the range from 75°C to 95°C. The thermal COP of the chiller for this nominal condition is 0.708. The rated total power consumption of the plant is 1.15 kW. An expansion vessel (Model: Aqua system VRV50) with 564 mm height and 356 mm diameter was located in return line between solar vacuum collector and absorption chiller. Table 7.1 shows the specification of the cooling system at designed conditions while table 7.2 shows the specification of the fan-coil unit. Photographs of the experimented absorption chiller, evacuated solar collector, cooling tower and fan-coil unit are shown respectively in Figs. 7.39 (a), (b), (c) and (d). The dimension schematic of the absorption chiller is shown in table 7.3. In addition, the schematic diagram of the system configuration is shown in Fig. 7.40.

Nominal Cooling Capacity at Below Conditions		7	kW
Designed Coefficient of Performance (COP)		0.708	
Thermodynamics Conditions	Chilled Water	Cooling Water	Hot Water
Thermal Capacity	kW	7	16.8	9.8
Flow Rate	l/s	0.33	1.13	0.58
Temperature (Inlet → Outlet)	°C	12→ 7	28 → 32	85 → 81

Table 7.1 Specification of the cooling system at designed conditions

Fan-coil unit specification

No. of fan	2
No. of motor	1
Fan type	Double inlet centrifugal forward-curved fan
Cooling coil tube material	Copper
Cooling coil fin material	Aluminium
Cooling coil number of row	3
Cooling coil number of fin per meter	472
Fan-Coil unit dimension (Length-Wide-Height) (mm)	1634-265-535
Fan-Coil unit weight (kg)	34

Table 7.2 Specification of the fan-coil unit

(a)

(b)

(c)

(d)

Fig. 7.39 Photographs of the experimental rig: (a) single-effect absorption chiller, (b) cross-flow cooling tower, (c) evacuated solar collectors and (d) fan-coil unit

Electric Consumption 220Vx1phx50Hz	Overall Length (L) [m]	Overall Height (H) [m]	Overall Width (W) [m]	Tube Removal (R) [m]	Surrounding Min. Distances (S) [m]	Unit Weight [kg]
400[W]/3[amp]	1.0	1.5	0.9	0.6	0.7	300

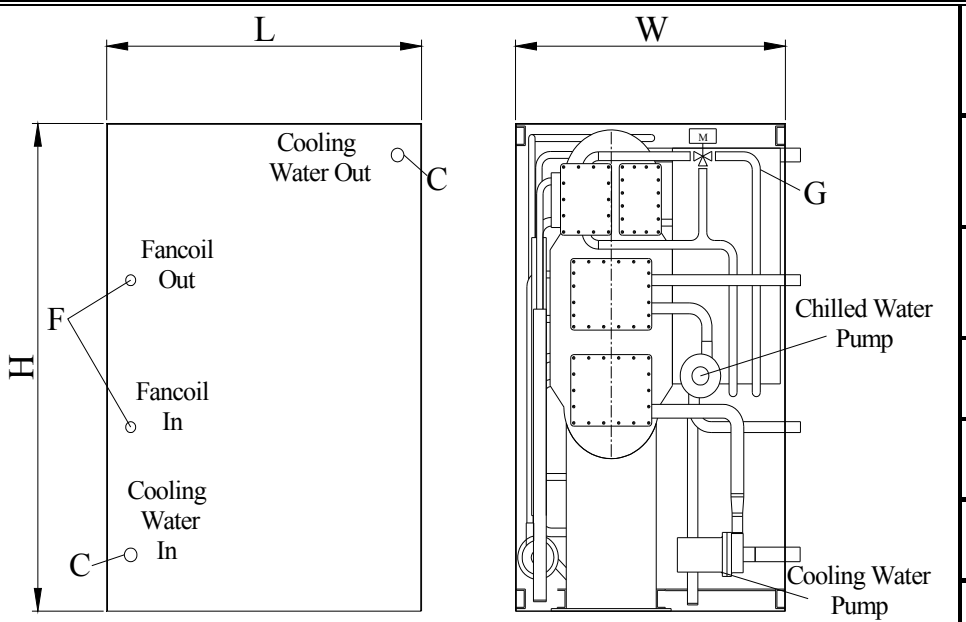

C	40 mm
F	25 mm
G	25 mm
H	1.5 m
L	1.0 m
R	0.6 m
S	0.7 m
W	0.9 m

Table 7.3 Dimension and geometric view of the absorption chiller

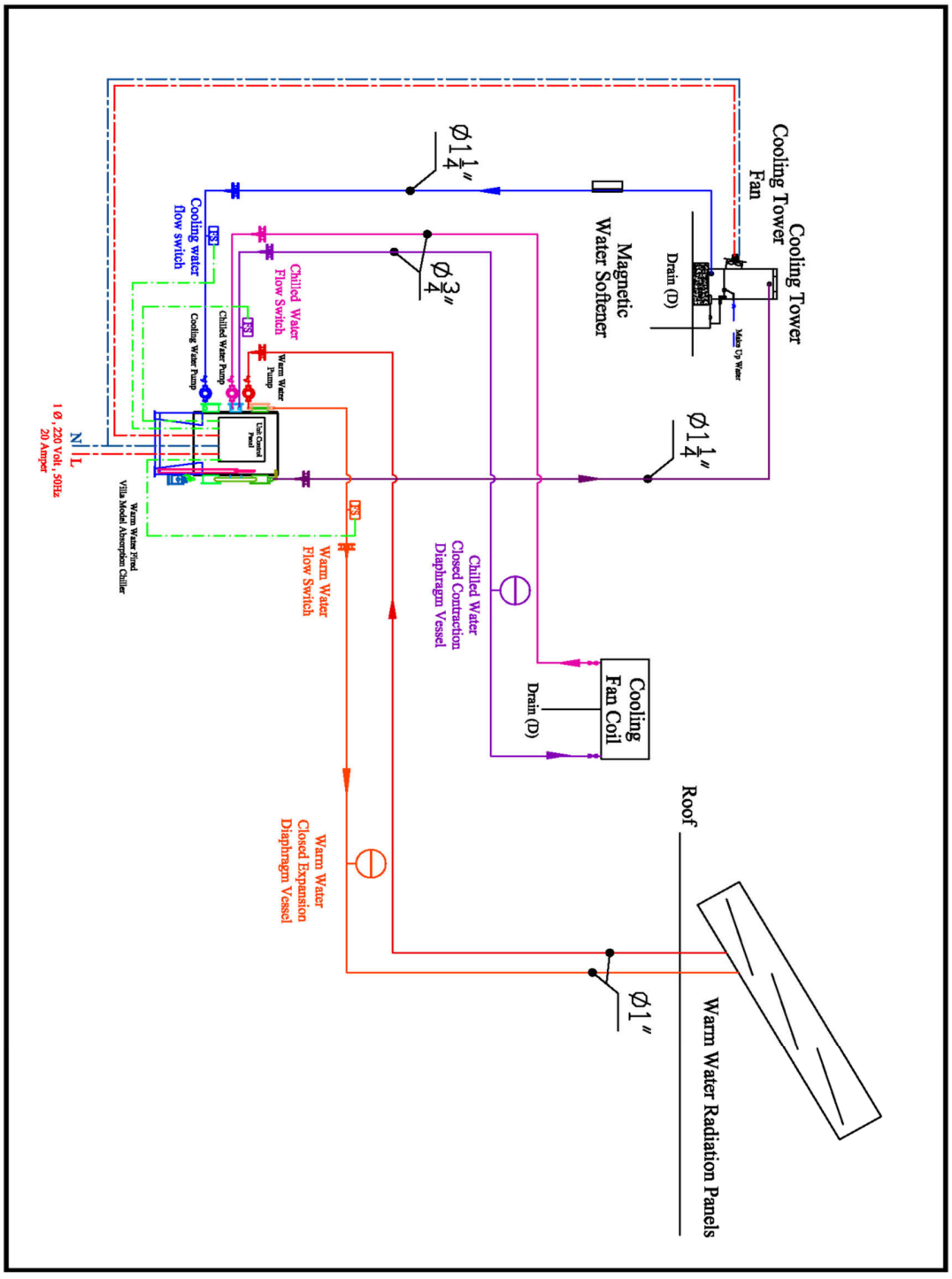

Fig. 7.40 Schematic diagram of the system component configuration

7.4.1 Monitoring Devices

This system has been fully-instrumented to facilitate a number of tests under different operation conditions. High precision sensors/transducers are used for monitoring all operating variables. The following parameters are measured: meteorological parameters (global solar radiation, ambient temperature and ambient relative humidity), indoor temperature and relative humidity, temperature of refrigerant and LiBr-water solution entering and leaving generator, condenser, absorber, evaporator and solution heat exchanger, hot water temperature entering and leaving the generator, chilled water temperature at the evaporator inlet and outlet, cooled-water temperature entering and leaving the cooling tower and total power consumption of the plant. All monitored devices were calibrated by their manufacturers.

7.4.2 Solarimeter Data-Logger

The global radiation is measured by means of a solarimeter of the type CR100-A mounted on a surface parallel to the plane of the collector. The solarimeter is integrated to a computer based-KT250-AO data-logger and its technical data is shown in table 7.4 as:

Measure Range	0-1300 W/m^2
Spectral Response	400-1100 nm
Nominal Sensitivity	100 mv for 1000 W/m^2
Operating Temperature	-30°C to 60°C
Solar Cell Material	Polycristallin silicon
Solar Cell Dimension	30 × 32 mm
Solar Cell Protection	IP 66
Signal	Sends 0-10 V or 4-20 mA analogue signal proportional to the radiated solar power

Table 7.4 Technical data for solarimeter

The photograph of the solarimeter and its connection diagram are shown in Fig. 7.41 and 7.42 respectively.

Fig. 7.41 Global sensor and data logger for solar radiation measurement

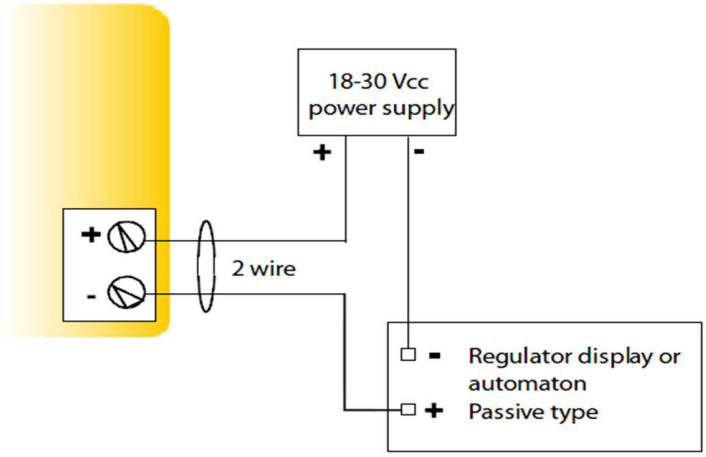

Fig. 7.42 Connection Diagram for Solarimeter

7.4.3 Ambient Temperature and Relative Humidity Sensor

The outdoor temperature and relative humidity are measured by a combined sensor-data-logger device with a calibrated accuracy of ±0.4°C for temperature and ±2% for relative humidity. The measuring range for temperature is between -20°C and +70°C and from 5%

and 95% for humidity. The sensor is integrated with a computer-based KT250-AO data-logger with a memory capacity of 20,000 points. The photograph of this device is shown in Fig. 7.43.

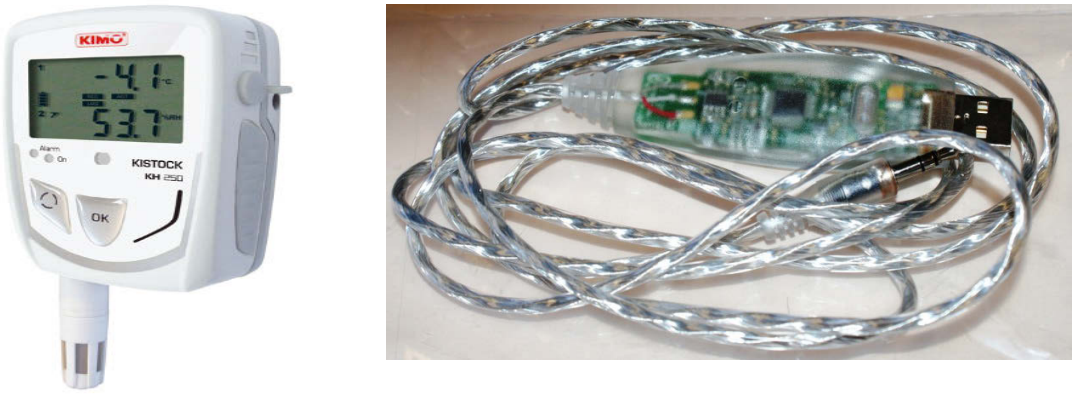

Fig. 7.43 Ambient Temperature and Relative Humidity Sensor

7.4.4 PT100 Temperature Sensor

Platinum resistance thermometers of PT100 type are used with a calibrated accuracy of ±0.5°C for a temperature range from -50°C to +260°C to measure the refrigerant and solution temperature before and after of each component. These sensors are in direct contact with the refrigerant and solution to achieve high accuracy. In addition, PT100 is used to measure the temperature of hot water, chilled water and cooled water entering and leaving the generator, evaporator and cooling tower respectively. The photograph of PT100 used for this experimentation is shown in Fig. 7.44:

Fig. 7.44 Platinum resistance thermometers (PT100)

7.4.5 Power Clamp

The power consumption of the air-conditioner is measured by a digital ac/dc power clamp multimeter of precision ±3.5% which is shown in Fig. 7.45.

Fig. 7.45 MS2205 Power clamp meter

7.4.6 Indoor Temperature/Humidity Meter

The indoor temperature and relative humidity are measured by a temperature/humidity meter of MS6506 model with a calibrated accuracy of ±0.7°C for temperature and ±2.5% for relative humidity. The measuring range for temperature is between -20°C and +60°C and from 0% and 100% for humidity as shown in Fig. 7.46.

7.4.7 Computer-Based DT500 Data-Logger

The aforementioned monitored data were collected and stored in a data acquisition system model DT500. The data-logger has 16 channels which can record up to 1,390,000 data points. The real-time recorded data can then be downloaded in Excel spreadsheets. The photograph of this data-logger is shown in Fig. 7.47.

Fig. 7.46 MS6506 Temperature/Humidity meter

Fig. 7.47 DT500 data-logger

7.5 Working Sequence Algorithm

The operation sequence of the chiller includes all safety and cycling shutdowns and respective reset thresholds. For this purpose, various chiller parameters are monitored by a programmable logic controller (PLC) which is programmed to respond to each of these parameters and shown in Fig. 7.48. Responds from PLC cause chiller shutdown or limit the chiller operation by shutting down a pump or constrain chiller loading.

If the hot water temperature leaving the vacuum solar collector and entering the chiller generator is greater than hot water set-point temperature the control panel check the chilled water temperature and otherwise the control panel will stop the chiller operation until hot water temperature exceed the hot water set-point. The hot water set-point temperature in our study is 70°C. When the hot water temperature entering the chiller generator is greater than 70°C, the chilled water temperature leaving the chiller evaporator is checked by control panel. The leaving chilled water temperature in which chiller can start working is determined by adding 2°C to the leaving chilled water set-point. Correspondingly, when the leaving chilled water temperature falls to 1.5°C below its set-point, the capacity control sequence occurs. The leaving chilled water temperature set-point in this study is 7°C. If all checks are normal, the chilled water pump starts immediately. When then chilled water flow switch closes, the condenser pump is turned on. The chilled water and condenser flow switches are bypassed for 30 seconds each after the corresponding pump is turned on. If the condenser water flow switch does not close within 30 seconds of the condenser pump turn on, a shutdown sequence is accomplished. When the condenser flow switch closes, the hot water 3-way valve is fully opened and the solution pump is turned on. In this stage, refrigerant level in the system is checked by the control panel. The refrigerant pump operation is controlled by float switch. When the refrigerant level float switch closes, the refrigerant pump is turned on based on the start-up delay set-point which is one minute is our design. During this time if refrigerant level reduces below the certain amount, the float switch opens, however, the control panel allows the chiller to run without refrigerant pump for two minutes. If the refrigerant pump is not turned on during this time, the shutdown sequence will occur. If the entering cooling water temperature entering the chiller is between its minimum and

maximum set-points, the control panel adjusts the hot water 3-way valve to regulate the chiller capacity based on the building cooling load. In contrast, if the entering cooling water temperature is less than its minimum set-point or greater than its maximum set-point, the control panel leads the chiller to the shutdown sequence. However, the minimum position of the modulation hot water valve is programmed from 20%. The control panel varies the chiller capacity by pulsing the hot water 3-way valve actuator close and open from 20% to 100%.

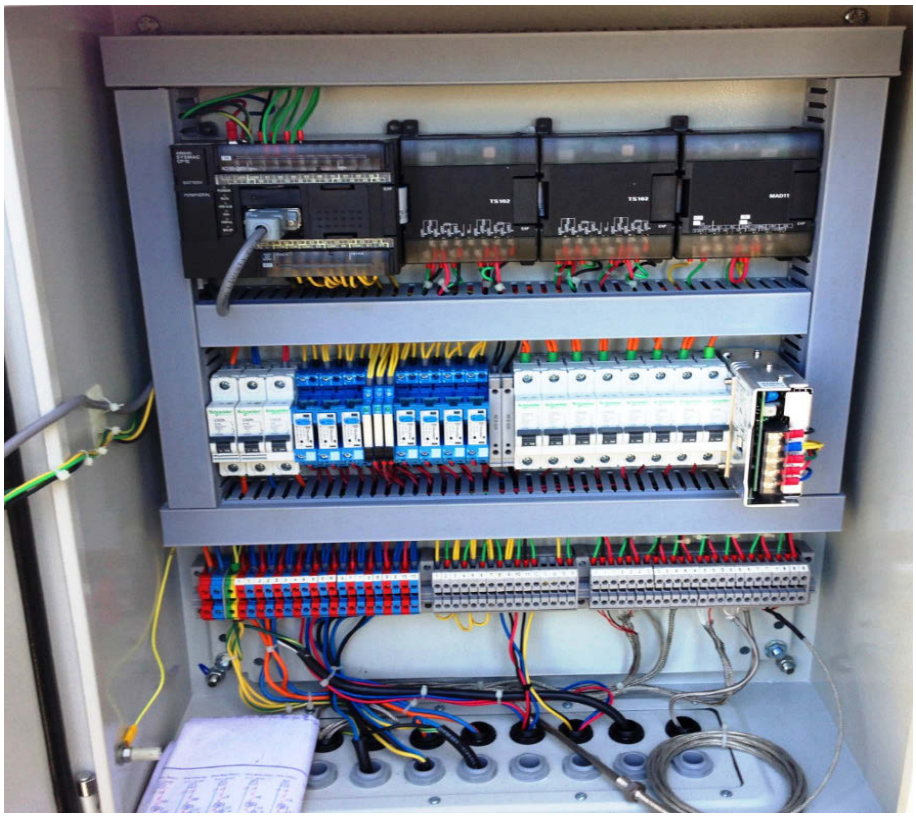

Fig. 7.48 Programmable logic controller of the absorption chiller

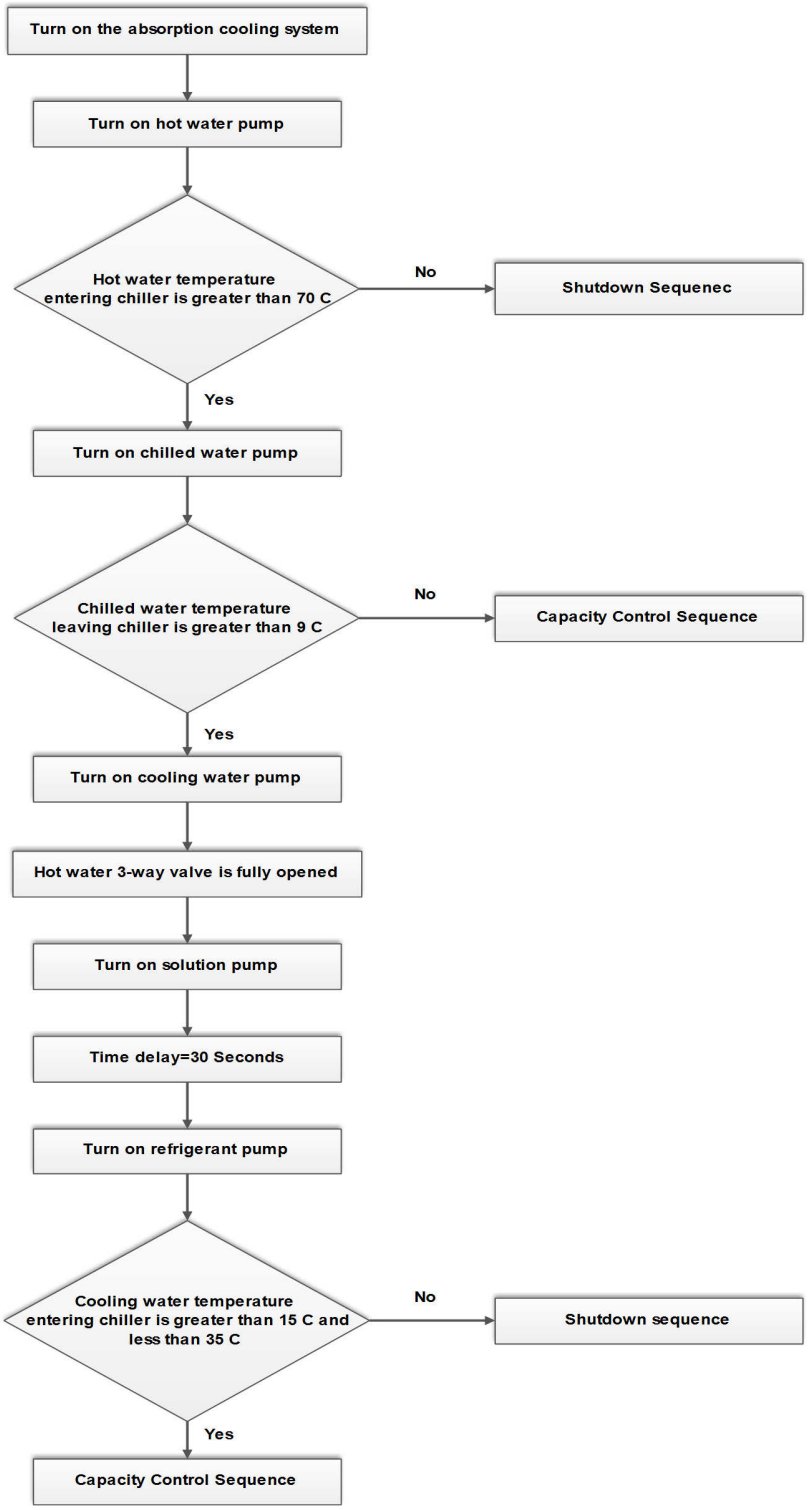

Fig. 7.49 Starting sequence of the absorption chiller

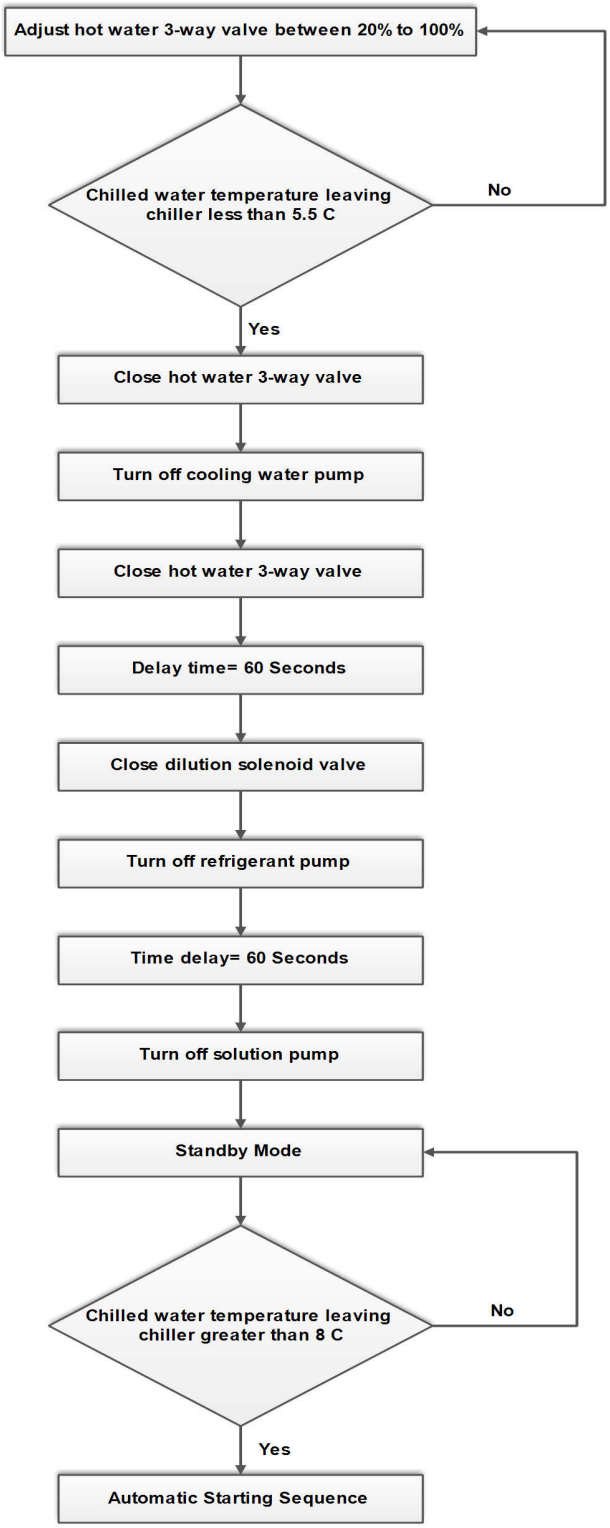

Fig. 7.50 Capacity control sequence of the absorption chiller

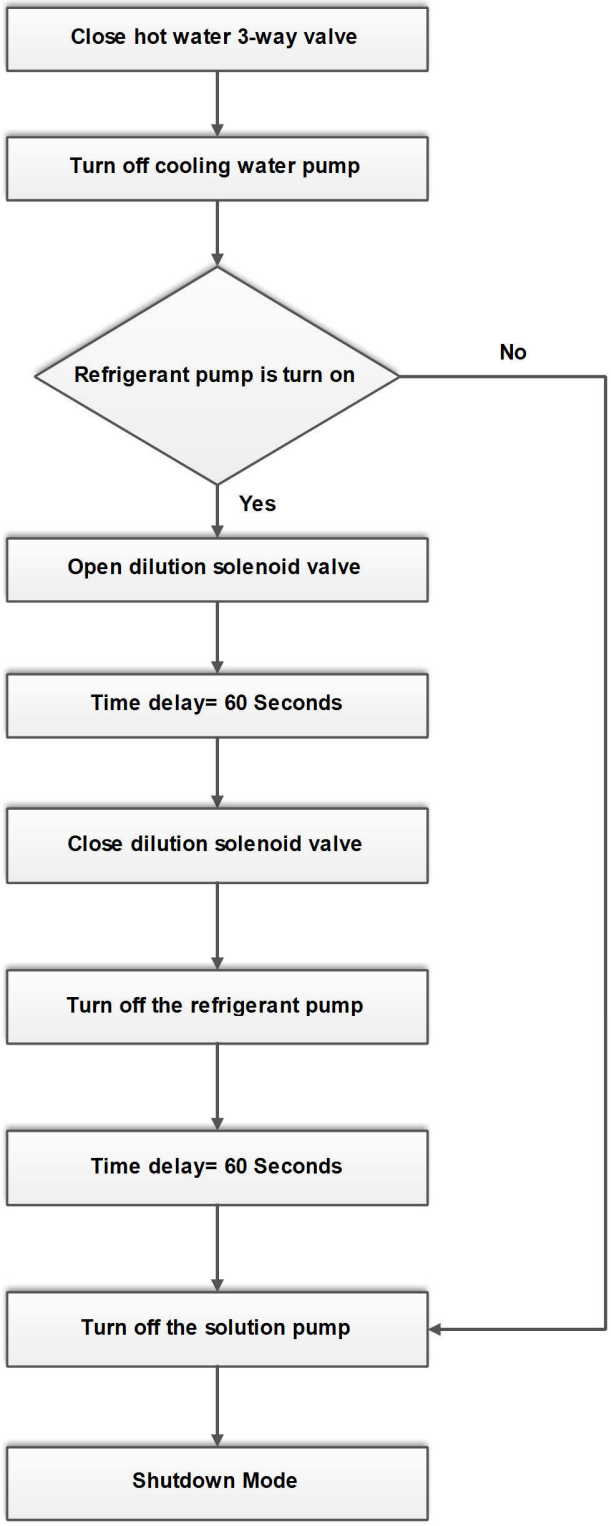

Fig. 7.51 Shutdown sequence of the absorption chiller

Chapter 8

PERFORMANCE EVALUATION OF THE SOLAR ABSORPTION COOLING SYSTEM: SIMULTION-BASED RESULTS

8.1 Summary

The objective of this chapter is to simulate the transient performance of the solar-powered absorption cooling system by using the experimentally monitored data. For this purpose, the developed 7 kW hot water single-effect absorption chiller was manufactured based on aforementioned designed data in chapter 5 and 7. The absorption chiller combined with the vacuum solar collectors, a cross flow cooling tower and a fan-coil unit was then used for experimentation and data collection. The system under investigation was extensively equipped with a number of instrumentation devices for data logging as specified in chapter 7. Mathematical model of system components are developed and implemented in a transient simulation tool, TRNSYS. The predictions from the models exhibit a good coincidence with experimental results, judging by an RE less than 15%. The influence of chilled water, cooling tower water and solar collector hot water temperatures on the system performance is investigated. Our experimental results demonstrate the technical viability of the proposed system in meeting the air-conditioning demand.

8.2 Introduction

The single-effect solar-powered absorption cooling plant was designed, developed and installed in university of technology, Sydney (UTS). A real-world building was served by this system for experimentation and data collection. To incorporate non-linear, time-varying and building-dependent dynamics of the system, a transient simulation software package, TRNSYS, was used to predict the HVAC performance evaluation. The existing central cooling plant was tested under different conditions to obtain the operational parameters of the system components. These field tests have been carried out for two typical summer weeks. A programmable logic controller (PLC)

has been designed to control the working sequence of the absorption chiller as mentioned in chapter 7. On the basis of TRNSYS codes and real test data, a simulation module for the central cooling plant was developed and embedded in the software. This model includes a commercial building, a water-cooled single-effect absorption chiller, an open circuit cross-flow cooling tower, a fan-coil unit, chilled, coolant and hot water pumps. Their dynamic simulation was performed simultaneously. In this system, hot water is fully supplied by vacuum solar collectors without using any other energy sources such as gas or electricity. In other word, the proposed design does not have water storage tank and its associated heat exchanger as an auxiliary heating system. Therefore, the field tests have been carried out from 8 am to 6 pm when the solar radiation was existed. As presented in this chapter, detailed transient simulation results indicate a promising reduction of cooling energy usage for a typical commercial building by using this central cooling system.

The proposed system is, to our knowledge, among the first fully solar-powered vapour-absorption cooling system in Australia, which does not use any backup system and still can operate continuously to serve an air-conditioned room.

8.3 System Modelling

Nonlinearity and complexity inherently existing in the dynamic process of a central cooling plant make it difficult to be represented accurately by using only thermodynamic and heat transfer models. This section presents the mathematical models for the system components by using real-world data experimentally collected. These models then are implemented in the simulation tool TRNSYS-16 to extract the right system dynamics and evaluate its performance, taking the advantage of the versatile software, wherein heat transfer and thermodynamic laws are incorporated for reliable transient analysis.

8.3.1 Single-Effect Absorption Chiller

To model the single-effect absorption chiller and evaluate its performance, normalised experimentally monitored data have been implemented into the TRNSYS. The performance

of the absorption chiller can then be predicted and interpolated within the range of available data but cannot be extrapolated beyond the range. The implemented monitored data into the TRNSYS are including of normalized value of full load fraction as well as energy input fraction for various values of design load, chilled-water temperatures, cooling tower water entering temperatures and entering hot water temperatures. During the absorption chiller is working, the design load fraction in which the chiller must work is determined by calculating of the amount of the energy that must be removed from the chilled-water stream based on building demand as:

$$\dot{Q}_{remove} = \dot{m}_{chw} C_{p,chw} \left(T_{chw,e} - T_{chw,set} \right), \tag{8.1}$$

where $\dot{Q}_{remove}$ is the amount of energy that must be removed from the chilled water stream in order to reach the set-point temperature, $\dot{m}_{chw}$ is the chilled water mass flow rate, $C_{p,chw}$ is the chilled water specific heat and $T_{chw,e}$ and $T_{chw,set}$ are chilled water temperature entering the absorption chiller and chilled water set-point temperature respectively.

The required energy removal by the absorption chiller is then divided by the nominal capacity of the chiller to obtain its design load fraction at which the absorption chiller must operate as:

$$Fr_{Dl} = \frac{\dot{Q}_{remove}}{Cap_{nom}}, \tag{8.2}$$

where Fr_{Dl} is the fraction of design load at which chiller is operating and Cap_{nom} is the nominal cooling capacity of the chiller.

The experimentally monitored data implemented into the TRNSYS such as hot water inlet temperatures, cooling water inlet temperatures, chilled-water set point temperatures and fraction of design load then are called. Using these data, the actual required capacity of the chiller can be determined at any given time using the following equation:

$$Cap_{act} = Fr_{Dl} \times Fr_{nom} \times Cap_{nom}, \tag{8.3}$$

where Fr_{nom} is the fraction of chiller nominal capacity and Cap_{act} is actual cooling capacity of the chiller.

The energy delivered to the absorption chiller by the hot water stream can be calculated as:

$$\dot{Q}_{hw} = \frac{Cap_{nom}}{COP_{nom}} \times Fr_{De}, \tag{8.4}$$

where Fr_{De} is the fraction of the design energy input required by the chiller and COP_{nom} is the chiller nominal coefficient of the performance. The hot water temperature leaving the chiller, $T_{hw,o}$, is then determined by:

$$T_{hw,o} = T_{hw,e} - \frac{\dot{Q}_{hw}}{\dot{m}_{hw} C_{p,hw}}, \tag{8.5}$$

where $T_{hw,e}$ is the hot water temperature entering the chiller, $\dot{Q}_{hw}$ is the energy removed from the hot water stream, $C_{p,hw}$ is the hot water specific heat and $\dot{m}_{hw}$ is the hot water mass flow rate.

Since the capacity of chiller is limited to its nominal capacity, the chilled-water leaving temperature, $T_{chw,o}$ can be calculated as:

$$T_{chw,o} = T_{chw,e} - \frac{Min\left(\dot{Q}_{remove}, Cap_{act}\right)}{\dot{m}_{chw} C_{p,chw}}. \tag{8.6}$$

Using energy balance equation, the energy rejection to the cooling tower water stream may be obtained as:

$$\dot{Q}_{ct} = \dot{Q}_{chw} + \dot{Q}_{hw} + \dot{Q}_{aux}, \tag{8.7}$$

where $\dot{Q}_{ct}$ is the heat rejection capacity of the cooling tower and $\dot{Q}_{aux}$ indicates energy draw of parasitic such as solution pump, fluid stream pump, etc. Finally, the temperature of water leaving the cooling tower can be determined by:

$$T_{ct,o} = T_{ct,e} - \frac{\dot{Q}_{ct}}{\dot{m}_{ct} C_{p,ct}}, \tag{8.8}$$

where $T_{ct,o}$ and $T_{ct,e}$ are the water temperature leaving and entering the cooling tower respectively, $\dot{m}_{ct}$ is the cooling tower water mass flow rate and $C_{p,ct}$ is the cooling tower water specific heat.

The thermal and electric COP of the absorption cooling system is then calculated as:

$$COP = \frac{\dot{Q}_{chw}}{\dot{Q}_{hw}}, \tag{8.9}$$

$$COP = \frac{\dot{Q}_{chw}}{w_{elec}}, \tag{8.10}$$

in which w_{elec} is the total electricity consumption of the absorption cooling system.

8.3.2 Vacuum Solar Collector

The vacuum solar collector uses solar radiation to heat the storage water. The solar collector for this project is a two-layered glass tube and the space in between the tubes is evacuated, creating a vacuum jacket. Therefore, there is a perfect insulation barrier, preventing heat loss due to convection and conduction. The selective coating is deposited onto the outside surface of a glass tubes domed at one end. The evacuated tube solar collector is modelled using a quadratic efficiency curve and a biaxial incidence angle modifier (IAM). The performance of the evacuated solar collector can be given by [145]:

$$\eta_{col} = a_0 - a_1 \frac{T_{w,m} - T_{db}}{I_T} - a_2 \frac{\left(T_{w,m} - T_{db}\right)^2}{I_T}, \tag{8.11}$$

where η_{col} is the collector efficiency, $T_{w,m}$ is the average water temperature in the collector, T_{db} is the ambient dry-bulb temperature, I_T is the total solar radiation intensity absorbed by solar collectors and a_0, a_1 and a_2 are the characteristic parameters of the collector. The value of these parameters for the particular collector used in the developed system are $a_0=0.77$, $a_1=1.5\ W/m^2K$ and $a_2= 0.01\ W/m^2K^2$ which correspond to a commercial model of its manufacture.

Solar collators are normally tested on clear days at normal incidence in which the transmittance-absorptance product (τa) is nearly the normal incidence value for beam radiation $(\tau a)_n$. The intercept efficiency, $F_R(\tau a)_n$, is corrected for non-normal solar incidence by the factor $(\tau a)/(\tau a)_n$. By definition, (τa) is the ratio of the total absorbed radiation to the incident radiation. Therefore, the correction factor for non-normal solar incidence can be expressed as [146]:

$$\frac{(\tau\alpha)}{(\tau\alpha)_n} = \frac{I_{bT}\frac{(\tau a)_b}{(\tau a)_n} + I_d\left(\frac{1+\cos\beta}{2}\right)\frac{(\tau a)_d}{(\tau a)_n} + \rho_{gr} I\left(\frac{1-\cos\beta}{2}\right)\frac{(\tau a)_{gr}}{(\tau a)_n}}{I_T}, \tag{8.12}$$

where I_{bT} is the beam radiation incident on the solar collector, I_d is the diffuse horizontal radiation, I is the total horizontal radiation, ρ_{gr} is the ground reflectance, I_T is the total radiation incident on the solar collector (tilted surface), β is the collector slop above the horizontal plane and subscript n, b, d and gr indicate normal, beam, diffuse and ground respectively.

The temperature of water leaving the vacuum tubes can be determined by solving three differential equations corresponding to the water, absorber plat and transparent glass cover.

The schematic of the vacuum solar collector is shown in Fig. 8.1 while its model parameters are shown in Fig. 8.2. For modelling the solar vacuum tube, the water temperature is assumed as a function of the x. The water is moving in the single line with the velocity of v along x-axis. As a result, a 3-node collector model shown in Fig. 8.3 can be presented by the following differential equation systems:

$$C_{p,gl}\frac{\partial T_g}{\partial t} = \varepsilon_{gl}\sigma\left(T_{sky}^4 - T_{gl}^4\right) + \alpha_{gl-amb}\left(T_{amb} - T_{gl}\right) + \varepsilon_g\sigma\left(T_{pl}^4 - T_{gl}^4\right),$$

$$C_{p,pl}\frac{\partial T_p}{\partial t} = \tau\alpha I_T + \left(T_{sky}^4 - T_{gl}^4\right) + \alpha_{f-pl}\left(T_f - T_{pl}\right) + \varepsilon_{gl}\sigma\left(T_{gl}^4 - T_{pl}^4\right), \tag{8.13}$$

$$C_{p,f}\left(\frac{\partial T_f}{\partial t} + v\frac{\partial T_f}{\partial x}\right) = \alpha_{f-pl}\left(T_{pl} - T_f\right),$$

where C_p is the heat capacity, α is the heat transfer coefficient, T is the temperature, t is time, v is the water velocity and gl, pl, f and amb indicate glass, absorber plate, fluid (pure water in our case), and ambient.

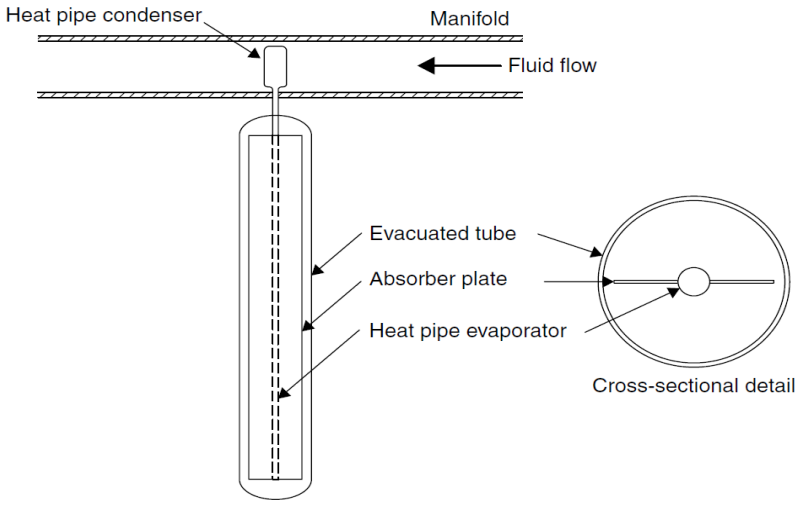

Fig. 8.1 Schematic diagram of a vacuum tube collector (Source [147])

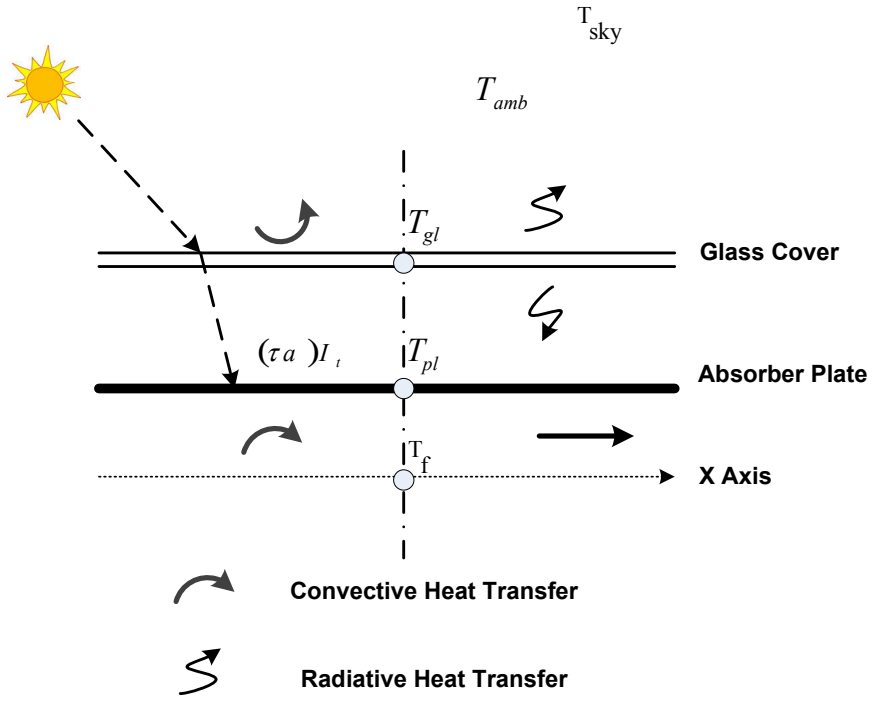

Fig. 8.2 Description of the vacuum tube collector model

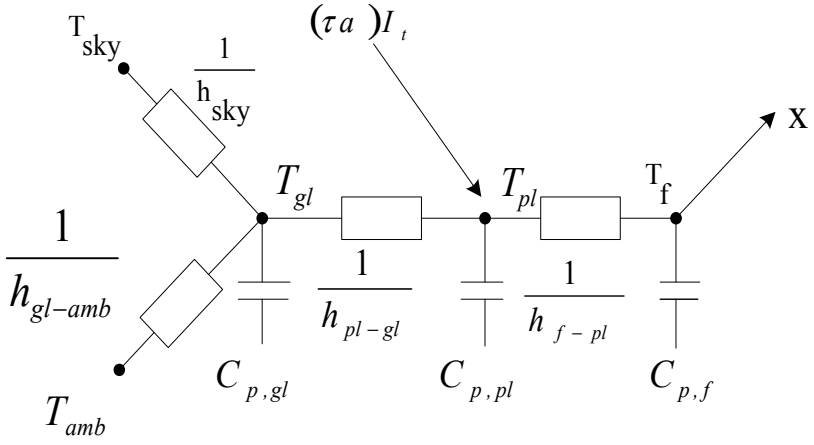

Fig. 8.3 Thermal network for 3-node model

The system given by differential equations (8.13) can be solved numerically. For this purpose, we have assumed that velocity of water along x-axis is constant and therefore the third equation in (8.13) can be re-written as [148]:

$$C_f \frac{dT_f}{dt} = h_{f-pl}\left(T_{pl} - T_f\right). \tag{8.14}$$

by solving this model the temperature of water leaving the vacuum solar collector can be obtained and used to evaluate the performance of the absorption chiller.

In the first equation of (8.13), T_{sky} is the effective sky temperature. To calculate sky temperature, the actual emittance of the clear and the clouded sky must be known. Therefore, the effective sky temperature is the function of the ambient temperature, ambient relative humidity, cloudiness factor of the sky and the air pressure. For this calculation, the sky is considered as an ideal black surface. The sky temperature, T_{sky} can then be obtained by [149]:

$$T_{sky} = T_{amb}\left(e_0 + 0.8\left(1 - \varepsilon_0\right)C_{Cover}\right)^{0.25}, \tag{8.15}$$

in which e_0 is the emittance of the clear sky and can be determined by the dew-point temperature at ambient conditions as:

$$e_0 = 0.711 + 0.005T_{adp} + 7.3\times10^{-5}T_{adp}^2 + 0.013\cos\left[2\pi\frac{time}{24}\right] + 12\times10^{-5}\left(p_{atm} - p_h\right), \tag{8.16}$$

where T_{adp} is the dew-point temperature at ambient conditions and p_{atm} is the atmospheric pressure and can be determined by the following formula:

$$p_{atm} = p_h e^{\frac{\rho_h g h}{p_0}}, \tag{8.17}$$

where P_h is the atmospheric pressure at the height of h, ρ_h is the air density at the height of h, g is the gravitational acceleration and h is the elevation above sea level.

The cloudiness factor, C_{cover} in equation (8.15) can be obtained as:

$$C_{Conver} = \left(1.4286\frac{I_d}{I} - 0.3\right)^{0.5}. \tag{8.18}$$

8.3.3 Solar Radiation Model

Total radiation on the tilted surface is required for system energy simulation. For this purpose, the division of the total horizontal radiation into its beam and diffuse components must be known. However, if only total horizontal radiation is measured, correlations are used to estimate the beam and diffuse radiation on a horizontal surface. The horizontal components are then projected onto the tilted surface.

Following equations estimate the diffuse radiation fraction as a function of the clearness index, solar altitude angle, ambient temperature and relative humidity. The correlations are given as [149]:

$$
\begin{aligned}
&Interval: \quad 0 \le K_T \le 0.3; \quad Constraint: \ \frac{I_d}{I} \le 1.0 \\
&\frac{I_d}{I} = 1.000 - 0.232K_T + 0.0239\,sin(\psi) - 0.000682T_{amb} + 0.0195(RH/100), \\
&Interval: \quad 0.3 \le K_T \le 0.78; \quad Constraint: \ 0.1 \le \frac{I_d}{I} \le 0.97 \\
&\frac{I_d}{I} = 1.329 - 1.716K_T + 0.267\,sin(\psi) - 0.00357T_{amb} + 0.106(RH/100), \\
&Interval: \quad 0.78 \le K_T; \quad Constraint: \ 0.1 \le \frac{I_d}{I} \\
&\frac{I_d}{I} = 0.426 - 0.256K_T + 0.267\,sin(\psi) - 0.00349T_{amb} + 0.0734(RH/100),
\end{aligned}
\tag{8.19}
$$

where K_T is the ratio of the total radiation on the horizontal surface to the extraterrestrial radiation, ψ is the solar altitude angle, T_{amb} is the ambient temperature and RH is the ambient relative humidity.

For the above equation, beam radiation on the horizontal surface is calculated by the difference between the total radiation and the diffuse component as:

$$I_b = I - I_d. \tag{8.20}$$

The sun position in the sky can be specified by knowing the solar zenith and solar azimuth angles. The solar azimuth angle is the angle between the local meridian and the projection of sight line of the sun onto the horizontal plane. Zero solar azimuth angle is facing to equator, west is positive whilst east is negative. The zenith angle is the angle between the vertical and line of sun sight. This is, in other word, 90 minus the angle between the sun and solar altitude angle. These angles can be determined from trigonometric relationship given in ASHRAE [126] as:

$$cos\theta_z = sin\delta sin\varphi + cos\varphi cos\delta cos\omega, \tag{8.21}$$

$$\sin\gamma_s = \frac{\cos\delta \sin\omega}{\sin\theta_z}, \tag{8.22}$$

where θ_z is the solar zenith angle, δ is the solar declination angle, φ is the latitude, ω is the mean hour angle of time step and is negative in morning and zero at noon and γ_s is the solar azimuth angle.

The slope and azimuth angle denote the position of the solar collector surface. For a horizontal axis, the surface slope, β can be presented by:

$$\beta = \tan^{-1}(\tan\theta_z \cos(\gamma_s - \gamma)), \tag{8.23}$$

in which γ is the surface azimuth which is angle between the projection of the normal to the surface into the horizontal plane and the local meridian and is given in terms of the axis as:

$$\begin{aligned} &\gamma = \gamma' + 90^\circ \quad if\ \gamma_s - \gamma' > 0, \\ &\gamma = \gamma' - 90^\circ \quad if\ \gamma_s - \gamma' < 0, \end{aligned} \tag{8.24}$$

where γ' is the azimuth angle of axis which is angle between the projection of the axis line onto the horizontal plane and local meridian.

In general, the total tilted surface radiation is calculated by estimating and adding beam, diffuse and reflected radiation components on the tilted surface. The contribution of the beam radiation on a tilted surface can be estimated by using geometric factor R_b as [149]:

$$R_b = \frac{\cos\theta}{\cos\theta_z}, \tag{8.25}$$

where θ is the angle of incidence of beam radiation on the surface.

Once R_b is found then:

$$I_{bT} = I_b R_b, \tag{8.26}$$

the contribution of the diffuse radiation on the tilted surface is determined by using factor R_d as:

$$R_d = 0.5\cos(1+\cos(\beta)), \tag{8.27}$$

therefore, the diffuse radiation on the tilted surface can be found as:

$$I_{dT} = I_d R_d. \tag{8.28}$$

The contribution of the reflected radiation on the tilted surface can be determined by assuming that the ground acts as an isotropic reflector and defining R_r as the ratio of the reflected radiation on the tilted surface to the total radiation on the horizontal surface as:

$$I_{gT} = IR_r, \tag{8.29}$$

$$R_r = 0.5(1-\cos\beta)\rho_{gr}, \tag{8.30}$$

The total radiation incident on the tilted surface can then be calculated as:

$$I_T = I_{bT} + I_{dT} + I_{gT}. \tag{8.31}$$

8.3.4 Fan-Coil Unit

The purpose of the fan-coil unit is to handle the supply air in buildings. The main parts of a fan-coil unit are the cooling coil and the supply fan. The heat transfer properties of the water cooling coil have a direct influence on the performance of the air-cooled chiller. In the fan-coil unit, water will begin to condensate on the surface of the cooling coil and therefore to determine the heat transfer through the cooling coil, the relative areas associated with wet and dry portions of the coil must be known. The following equations are used to calculate the heat transfer in a partially wet cooling coil [146]:

$$f_{dry} = -\frac{1}{Ntu_{dry}\left(1-\frac{\dot{m}_a C_{pa}}{\dot{m}_w C_{pw}}\right)} \ln\left(\frac{\left(T_{dp}-T_{w,cc,e}\right)+\frac{\dot{m}_a C_{pa}}{\dot{m}_w C_{pw}}\left(T_{a,cc,e}-T_{dp}\right)}{\left(1-\frac{Ntu_{dry}\left(1-\frac{\dot{m}_a C_{pa}}{\dot{m}_w C_{pw}}\right)}{Ntu_o}\right)\left(T_{a,cc,e}-T_{w,cc,o}\right)}\right), \tag{5.32}$$

where f_{dry} is the fraction of the coil surface area that is dry, Ntu is the overall number of transfer units, T_{dp} is the air dew-point temperature, $T_{w,cc,e}$ and $T_{w,cc,o}$ are respectively the water temperature entering and leaving the cooling coil, $T_{a,cc,e}$ is the air temperature entering the cooling coil, C_{pa} is the constant pressure specific heat of the moist air, C_{pw} is the constant pressure specific heat of the liquid water and a and w indicate the air and water respectively. The effectiveness for the wet and dry portions of the cooling coil is as:

$$\varepsilon_{wet,a} = \frac{1-\exp\left(-\left(1-f_{dry}\right)Ntu_{wet}\left(1-\frac{\dot{m}_a C_S}{\dot{m}_w C_{pw}}\right)\right)}{1-\frac{\dot{m}_a C_S}{\dot{m}_w C_{pw}}\exp\left(-\left(1-f_{dry}\right)Ntu_{wet}\left(1-\frac{\dot{m}_a C_S}{\dot{m}_w C_{pw}}\right)\right)}, \tag{5.33}$$

$$\varepsilon_{dry,a} = \frac{1-\exp\left(-f_{dry}\,Ntu_{dry}\left(1-\frac{\dot{m}_a C_S}{\dot{m}_w C_{pw}}\right)\right)}{1-\frac{\dot{m}_a C_S}{\dot{m}_w C_{pw}}\exp\left(-f_{dry}\,Ntu_{dry}\left(1-\frac{\dot{m}_a C_S}{\dot{m}_w C_{pw}}\right)\right)}, \tag{5.34}$$

where $\varepsilon_{wet,a}$ and $\varepsilon_{dry,a}$ are effectiveness for the wet and dry portions of the cooling coil respectively and C_s is average saturation slope of the air enthalpy versus temperature.

The water temperature at the point where condensation begins is:

$$T_{w,x} = \frac{T_{w,cc,e} + \frac{\frac{\dot{m}_a C_S}{\dot{m}_w C_{pw}}\varepsilon_{wet,a}\left(h_{a,cc,e}-h_{s,a,e}\right)}{C_{pa}} - \frac{\dot{m}_a C_S}{\dot{m}_w C_{pw}}\varepsilon_{wet,a}\varepsilon_{dry,a}T_{a,cc,e}}{1-\frac{\dot{m}_a C_S}{\dot{m}_w C_{pw}}\varepsilon_{wet,a}\varepsilon_{dry,a}}, \tag{8.35}$$

where x is the point on the cooling coil where condensation begins, $h_{a,cc,e}$ is the enthalpy of air entering the cooling coil and $h_{s,w,e}$ is the enthalpy of the saturated air entering the cooling coil.

The water temperature leaving the cooling coil can then be calculated by:

$$T_{w,cc,o} = \frac{\dot{m}_a C_S}{\dot{m}_w C_{pw}}\varepsilon_{dry,a}T_{a,cc,e} + \left(1-\frac{\dot{m}_a C_S}{\dot{m}_w C_{pw}}\varepsilon_{dry,a}T_{w,x}\right). \tag{8.36}$$

The air temperature leaving the cooling coil is determined as:

$$T_{a,cc,o} = T_{s,e} + \left(T_{a,x}-T_{s,e}\right)\exp\left(-\left(1-f_{dry}\right)Ntu_o\right), \tag{8.37}$$

where $T_{s,e}$ is the cooling coil surface temperature. Since the dry fraction of the cooling coil is dependent on the water temperature at the cooling coil outlet, an iterative process is required to determine the water temperature leaving the cooling coil.

The air temperature and enthalpy at the point where condensation occurs are:

$$T_{a,x} = T_{a,cc,e} - \varepsilon_{dry,a}\left(T_{a,cc,e} - T_{w,x}\right), \tag{8.38}$$

$$h_{a,x} = h_{a,cc,e} - \varepsilon_{dry,a} C_{pa}\left(T_{a,cc,e} - T_{w,x}\right). \tag{8.39}$$

The total heat transfer across the cooling coil is then:

$$Q_{cc} = \dot{m}_w C_{pw}\left(T_{w,cc,o} - T_{w,cc,e}\right), \tag{8.40}$$

where Q_{cc} is the total heat transfer carried out by cooling coil.

8.3.5 Cooling Tower

In a cooling tower, a warm water stream is in direct contact with ambient air stream and cooled due to sensible heat transfer as a result of temperature difference with the ambient air and mass transfer due to evaporation of the ambient air. In this project we used a cross-flow cooling tower in which ambient air is drawn sideward through the falling water. Water loss from the cooling tower is replaced with make-up water to the sump. The heat rejection of the cooling tower, Q_{ct} can be determined as [146]:

$$Q_{ct} = \varepsilon_{a,ct} \dot{m}_{a,ct}\left(h_{s,a,e} - h_{a,e}\right), \tag{8.41}$$

where $\varepsilon_{a,ct}$ is the air-side heat transfer effectiveness, $\dot{m}_{a,ct}$ is the cooling tower air flow rate, $h_{s,a,e}$ is the saturated air enthalpy at the incoming cooling tower water temperature and $h_{a,e}$ is the enthalpy of the air entering the cooling tower.

We assume that the Lewis number is one and then the air effectiveness can be determined using the relationships for sensible heat exchangers with modified definitions for the number of transfer units and the capacitance rate ratios. Therefore, the air-side heat transfer effectiveness for the cross flow cooling tower can be obtained as:

$$\varepsilon_{a,ct} = \frac{\dot{m}_{a,ct} C_s}{\dot{m}_{w,ct,e} C_{pw}} \left(1 - \exp\left(- \frac{\dot{m}_{w,ct,e} C_{pw}}{\dot{m}_{a,ct} C_s} \left(1 - \exp(-Ntu) \right) \right) \right), \tag{8.42}$$

where $\dot{m}_{w,ct,e}$ is the water flow rate entering the cooling tower, C_{pw} is the constant pressure specific heat of the water, C_s is the specific heat of the saturated air and Ntu is the mass transfer number of transfer units and can be determined as:

$$Ntu = \frac{h_D A_V V_{cell}}{\dot{m}_{a,ct}}, \tag{8.43}$$

$$C_s = \frac{h_{s,a,e} - h_{s,a,o}}{T_{w,ct,e} - T_{w,ct,o}}, \tag{8.44}$$

where h_D is the mass transfer coefficient, A_v is the surface area of water droplets per tower cell exchange volume, V_{cell} is the total cooling tower cell exchange volume, $h_{s,a,e}$ and $h_{s,a,o}$ are saturated air enthalpy at the entering and leaving cooling tower water temperature respectively and $T_{w,ct,e}$ and $T_{w,ct,o}$ are temperature of water entering and leaving the cooling tower respectively.

The following correlations for heat and mass transfer in the cooling tower are used to determine the cooling tower effectiveness [146]:

$$\frac{h_D A_V V_{cell}}{\dot{m}_{a,ct}} = z_0 \left(\frac{\dot{m}_{w,ct}}{\dot{m}_{a,ct}} \right)^m, \tag{8.45}$$

multiplying the both sides of the above equation by $\frac{\dot{m}_{w,ct}}{\dot{m}_{a,ct}}$ gives:

$$Ntu = z_0 \left(\frac{\dot{m}_{w,ct}}{\dot{m}_{a,ct}} \right)^{m+1}, \tag{8.46}$$

where z_0 and m are constant and can be obtained by using the manufacturer technical data.

The outlet temperature of cooling tower water can be determined using the energy balance and is given as following:

$$T_{w,ct,o} = \frac{\dot{m}_{w,e}\, C_{pw}\left(T_{w,ct,e}\right) - Q_{ct}}{\dot{m}_{w,ct,o} C_{pw}}, \tag{8.47}$$

8.4 TRNSYS Development

The mathematical model of the system components is coded into the fully integrated visual interface known as TRNSYS simulation studio using FORTRAN. Under real conditions there are many factors that can influence the HVAC system performance. In this study, all dimensions of the system components are included in the program code. The experimental obtained data were entered through a dedicated visual interface. The simulation information flow diagram for the solar-powered absorption cooling system is shown in Fig. 8.4, where the icon 'building' involved the building information file has been created by PREBID and is compliant with the requirements of the ANSI/ASHRAE Standard 140 [150].This simulation code was then used to calculate the parameters of the main interest such as hot water, cooled-water and chilled-water temperature, supply air temperature, solar radiation intensity, power consumption of the system and system COP. The simulation algorithm is able to interpolate the implemented monitored data. In each iteration of the simulation, the output parameters are calculated and stored in a separate file. The TRNSYS code and relationship between system components are presented in Appendix 3.

8.4.1 Model Validation

Experimental studies usually involve some unpredictable and uncertain factors which occur due to instrumental manufacturing errors, calibration errors and human mistakes. These uncertainties should be treated by using a statistical approach. In this study, the non-dimensional deviation about the mean value was found for each reading from the following equation:

$$\varphi_i = \frac{y_{data,i} - y_{data,m}}{s_x}, \tag{8.48}$$

where $y_{data,i}$ is the measured variables, $y_{data,m}$ is its average value and the standard deviation s_x for a set of N samples is determined by:

$$s_x = \sqrt{\frac{1}{N}\left(\sum_{i=1}^{N}(y_{data,i} - y_{data,m})^2\right)}, \tag{8.49}$$

$$y_{data,m} = \frac{1}{N}\sum_{i=1}^{N} y_{data,i}. \tag{8.50}$$

The value φ_i of each reading was compared with the ratio of the maximum allowable deviation from the mean value and the standard deviation.

For error analysis, the simulated performance of the system is compared with obtained experimental results. The simulation is run with a time interval of 20 minutes, i.e. equal to the monitoring time step in the real test process. This study uses the relative error (RE), the root mean square error (RMSE) and the coefficient of variance (CV) to indicate how well a regression model fits the observations. They are defined as follows:

$$RE = \frac{\sum_{i=1}^{N} \frac{\left|y_{pred,i} - y_{data,i}\right|}{y_{data,i}}}{N} \times 100\%, \tag{8.51}$$

$$RMSE = \sqrt{\frac{1}{N}\left(\sum_{i=1}^{N}(y_{pred,i} - y_{data,i})^2\right)}, \tag{8.52}$$

$$CV = \frac{RMSE}{y_{data,m}} \times 100\%, \tag{8.53}$$

where $y_{pred,i}$ is the predicted variable. For validation of the mathematical model, several field tests were run to cover a wide range of operating conditions.

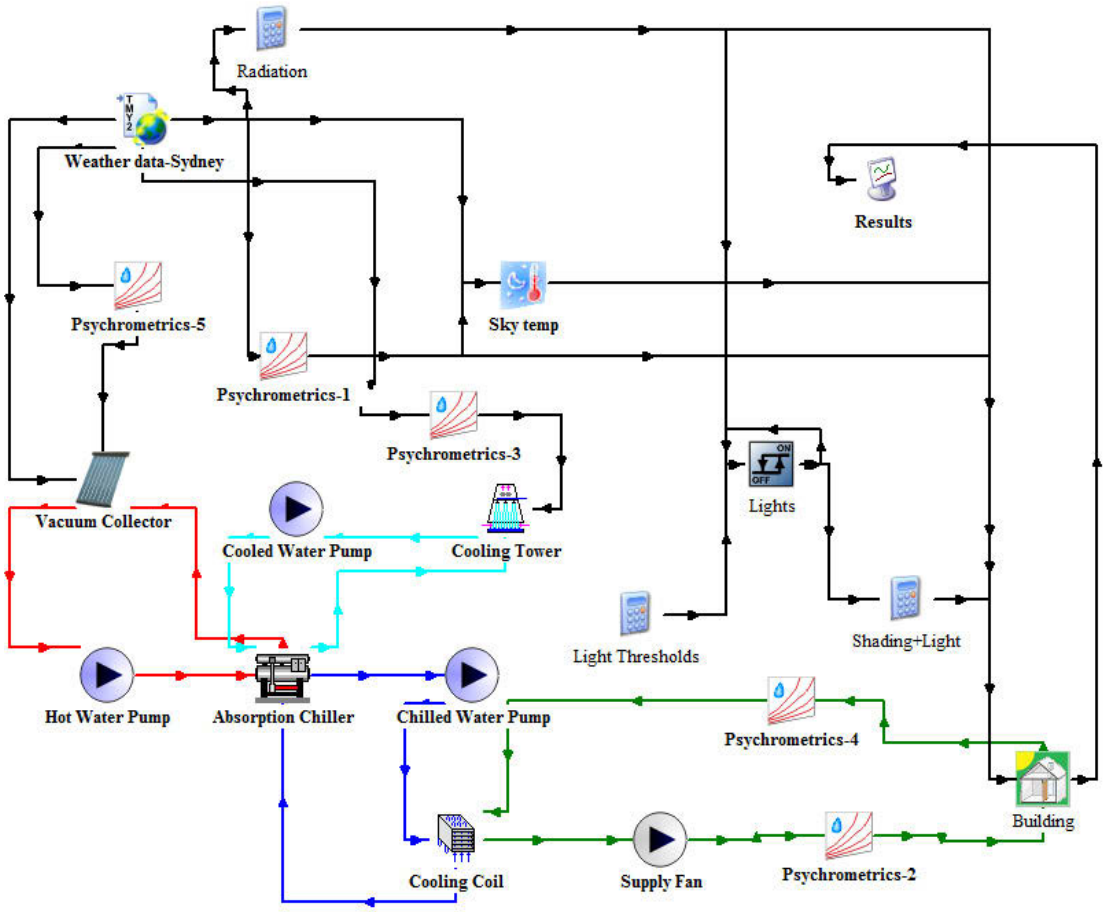

Fig. 8.4 Simulation flow chart in TRNSYS environment

In order to verify appropriateness of the estimated values obtained in the simulation, it is important to validate the accuracy of the models under various operational conditions. To test the accuracy of the cooling plant model, a comparison is conducted between the predicted and actual values of the chilled-water temperature leaving absorption chiller, cooled water temperature leaving the cooling tower and hot water temperature leaving the solar collector over a two weeks period, during which the system was operated continuously from 8 a.m. to 6 p.m. Simulation results of all validations found to be coincident with the experimental

results, as shown in Figs. 8.5, 8.7 and 8.9. In addition, Figs 8.6, 8.8 and 8.10 illustrate the relationship and assess the distributions of the experimentally-monitored and predicted variables. Simulation results of all validations found to be in good agreement with the experimental results. Figure 8.11 compares the predicted and experimental temperature of the water leaving the chiller's evaporator, wherein the deviation between experimental and predicted values falls within 14.43%.

Figure 8.13 shows the plots of predicted and experimental values of the water temperature leaving the cooling tower. It can be seen that the experimental data over predicted the model by 5.6%. Figure 8.15 depicts the comparison of the calculated and measured results for the hot water temperature leaving the vacuum solar collector. The trend of the predicted results is similar to that obtained from experimental data. The calculated results are about 2.43% greater than the measured ones. Therefore, the mathematical models with accuracy being validated by using experimental data are ready to be used for system performance enhancement. The Statistical Characteristics for model validation are shown in the following table:

Parameter	$y_{data,m}$	s_x	RE	RMSE	CV
$T_{chw,o}$	7.28	1.57	14.43%	1.28	20.58%
$T_{ct,o}$	26.18	2.56	5.6%	1.53	5.55%
$T_{hw,o}$	76.41	5.65	2.43%	2.03	2.6%

Table 8.1 Statistical Characteristics

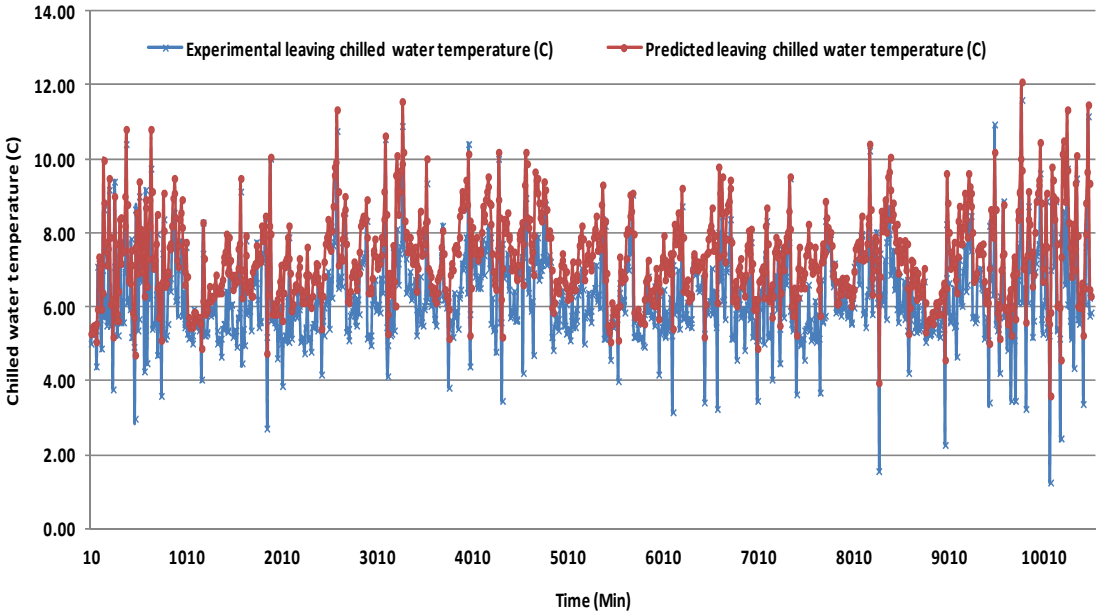

Fig. 8.5 Predicted and experimental chilled water temperature leaving absorption chiller

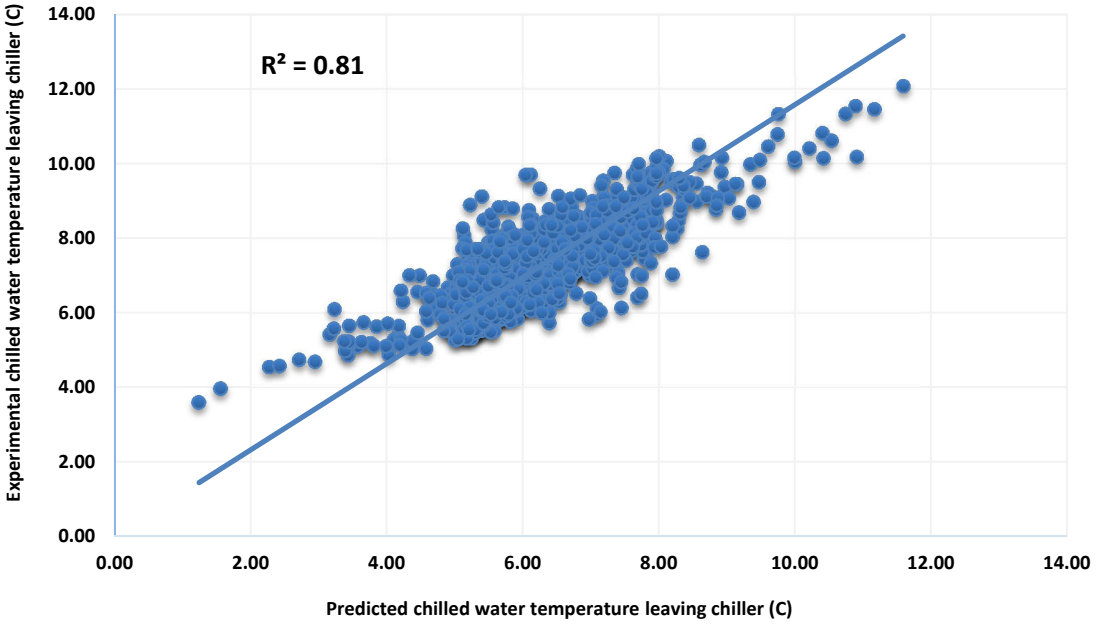

Fig. 8.6 Predicted and experimental chilled water temperature leaving absorption chiller

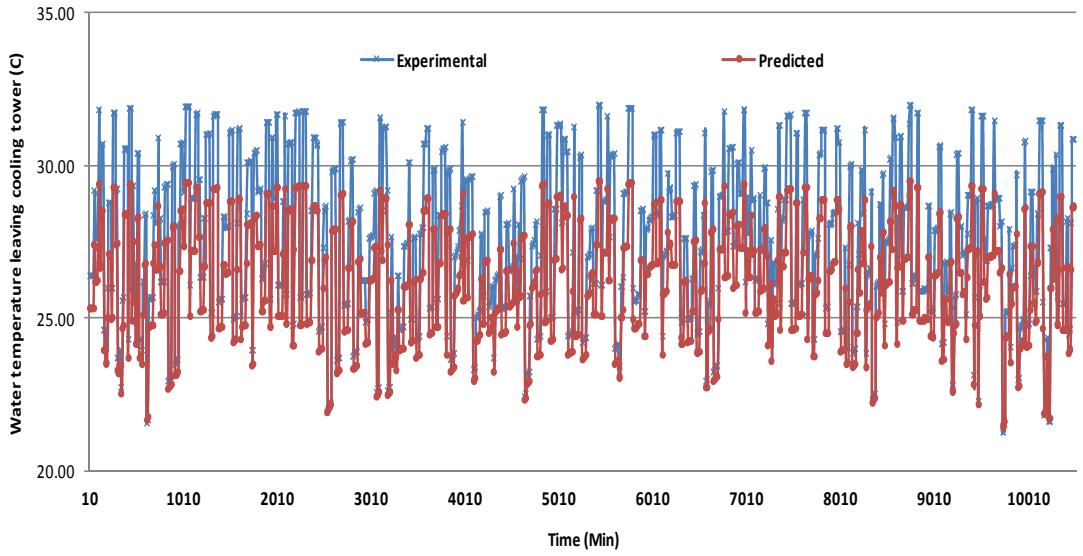

Fig. 8.7 Predicted and experimental water temperature leaving cooling tower

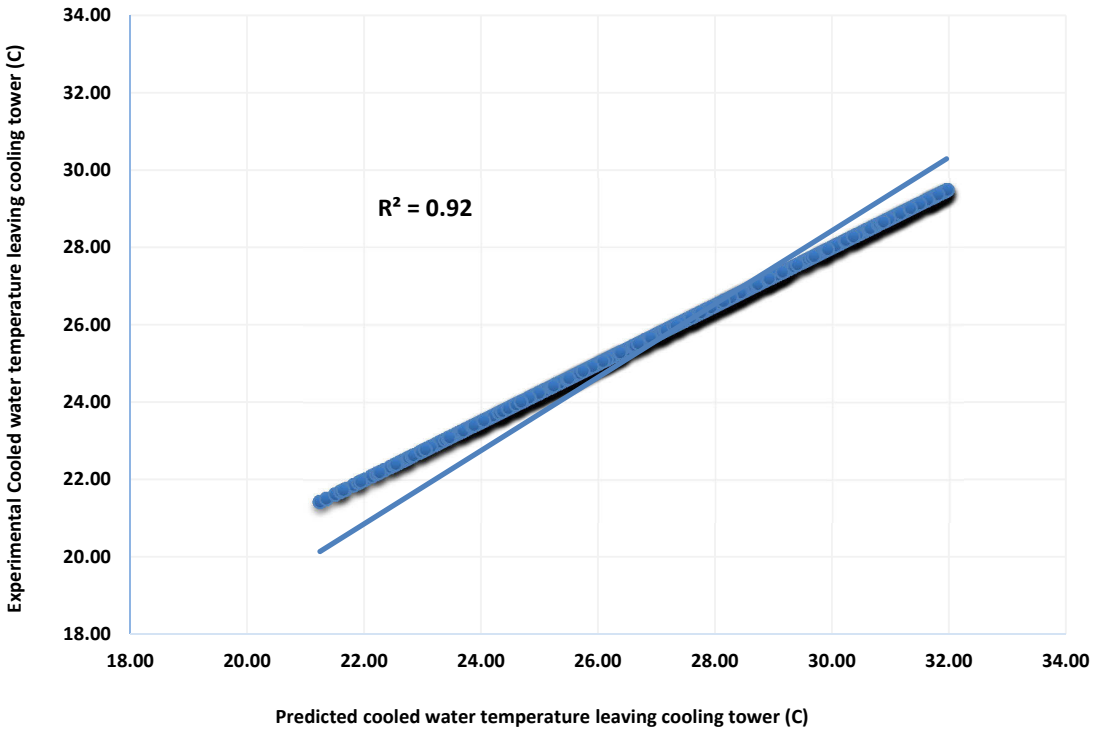

Fig. 8.8 Predicted and experimental water temperature leaving cooling tower

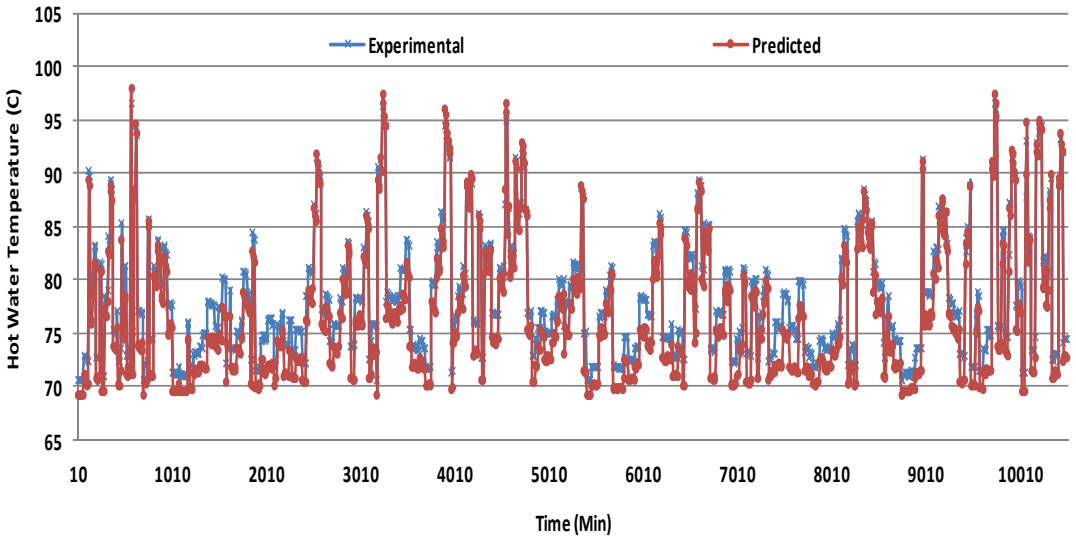

Fig. 8.9 Predicted and experimental hot water temperature entering absorption chiller

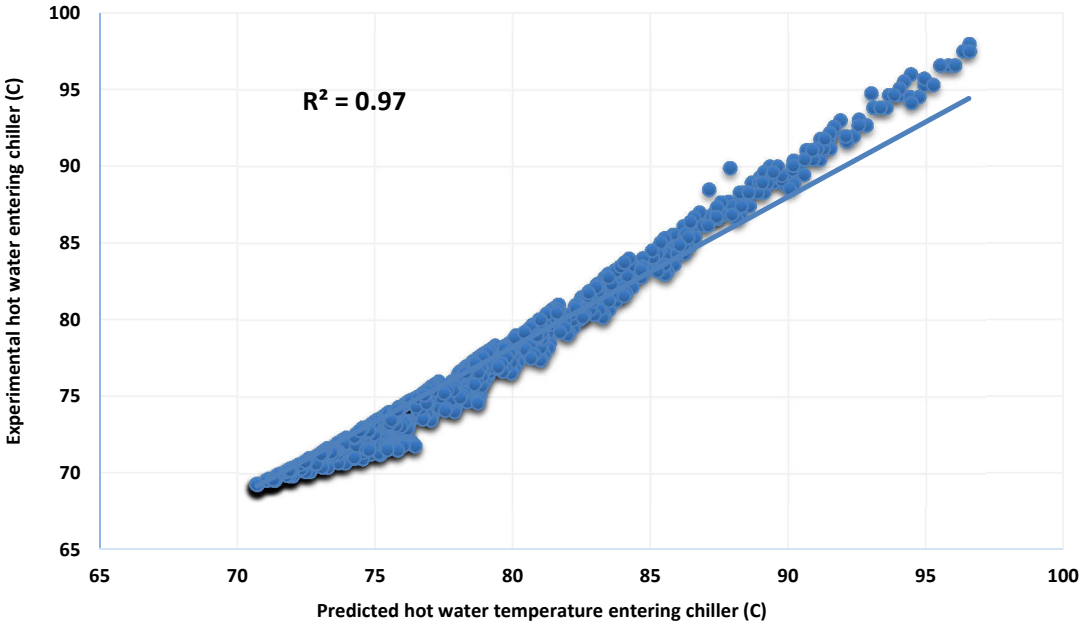

Fig. 8.10 Predicted and experimental hot water temperature entering absorption chiller

8.5 Performance Prediction

Having described the specifications of the cooling plant and developed models, results showing the system performance are presented and discussed in this section. Aforementioned methods are studied and their influences on the system performance are presented. TRNSYS is run to obtain a component-wise energy analysis and performance prediction of the cooling system throughout the summer.

To predict the system performance throughout the summer, the cooling load is calculated by using TRNSYS prior to the simulation process as described in chapter 3. The references for the indoor temperature and relative humidity during the cooling load calculation were set respectively at 23°C and 50%. The peak cooling load is estimated at 6.4 kW in the middle of December. Monitored experimental data for the ambient dry bulb temperature and relative humidity are shown in Fig. 8.11. During testing, the ambient temperature varied between 17.35°C and 33.64°C with an average temperature of 24.42°C. The average monitored ambient relative humidity is 62.25% while its minimum and maximum are 38.5% and 84.5% respectively. The average solar radiation intensity during two typical weeks was measured about 274.1 W/m^2 as shown in Fig. 8.12. The minimum and maximum recorded solar radiation intensity is 10.3 W/m^2 and 1105.26 W/m^2 respectively.

Experimentally collected data for chilled water temperature entering and leaving the chiller evaporator is shown in Fig. 8.13. The minimum, maximum and average chilled-water temperature at the chiller inlet are 5.8°C, 14.9°C and 9.6°C while these temperatures at chiller outlet are 5.3°C, 8.9°C and 6.8°C respectively. Similarly, the average water temperature at inlet and outlet of the cooling tower are measured respectively as 31.1°C and 27.5°C as shown in Fig. 8.14. The water temperature profile at collector inlet and outlet is demonstrated in Fig. 8.15. The average temperatures of the water entering and leaving the vacuum solar collector are measured at 75.45°C and 78.21°C, respectively. The temperature of the water leaving the solar vacuum collector gets increased with an increase in solar intensity. On a sunny day, the water temperature can range from 78°C and 98°C, depending on the solar

radiation intensity and the ambient air dry-bulb temperature. On an overcast day, the water temperature may vary from 70°C to 80°C. However, the minimum and maximum water temperatures leaving the vacuum solar collector were measured as 70.21°C and 98.65°C respectively.

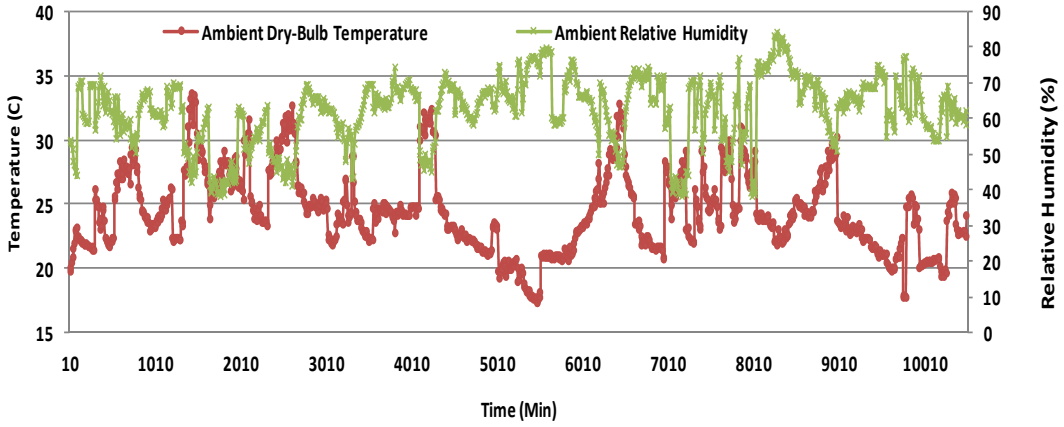

Fig. 8.11 Ambient dry-bulb and relative humidity during the field test

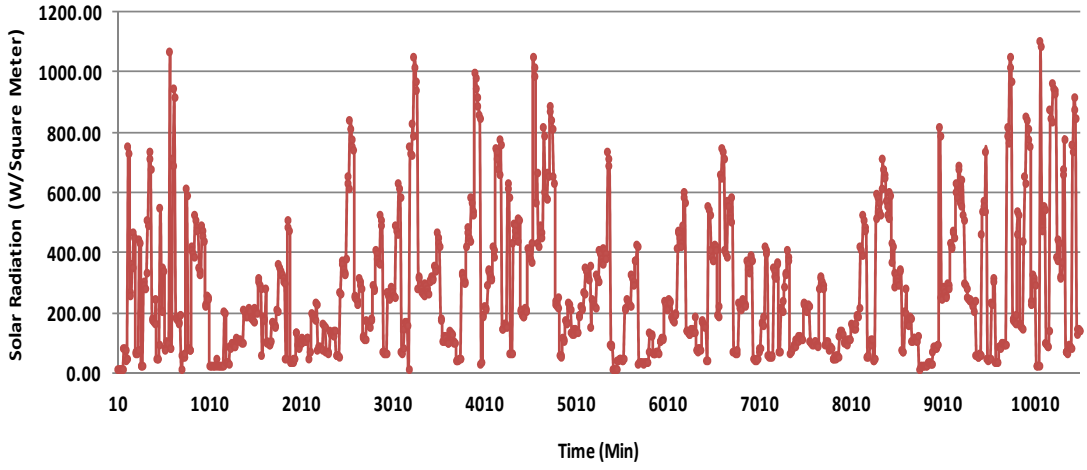

Fig 8.12 Solar radiation intensity during the field test

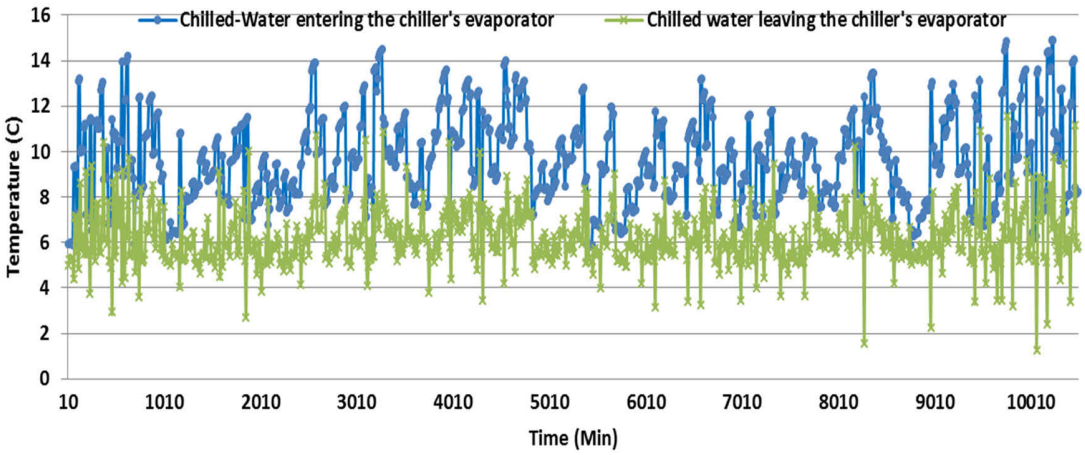

Fig. 8.13 Experimentally monitored data for supply and return chilled-water temperature

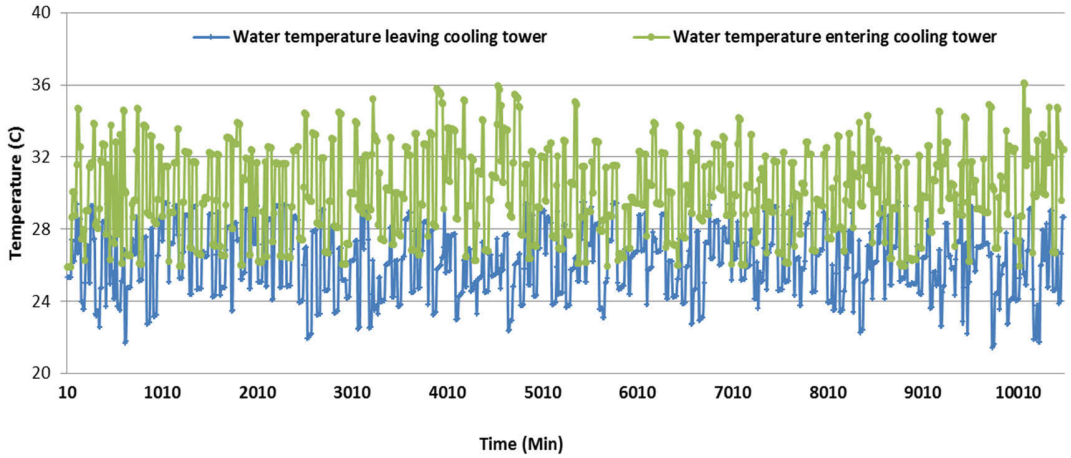

Fig. 8.14 Experimentally monitored data for water temperature entering and leaving cooling tower

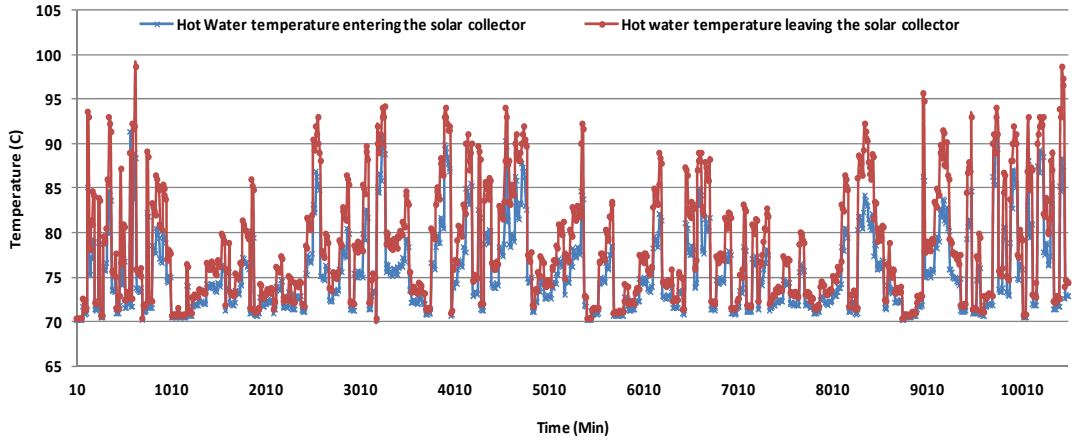

Fig. 8.15 Experimentally monitored data for water temperature entering and leaving solar collector

8.5.1 System Capacity

The solar-powered absorption cooling system must be able to match its capacity with an actual building cooling demand. Because building cooling loads vary with the time of the day, an HVAC system should be designed in tandem with an optimum design scheme that will keep the process variables within their required set-point in order to maintain comfort under any load conditions. The sustainability, energy consumption and life-cycle-cost of an HVAC system depend not only on its performance and operational parameters, but also on the characteristics of the heating and cooling demand and the thermodynamic behaviour of the building. Therefore, the most important factors that contribute to HVAC energy usage reduction in a given building is via properly adjusting and tuning of the heating and cooling demand. In this system, the transient capacity of the chiller can be matched with the building dynamic cooling load via controlling the hot and chilled water flow rate. As shown in Fig. 8.16, the actual capacity of chiller can support the existing cooling demand of the building between 8 am to 6 pm (test period) most of the time. Since this system does not use any backup system, the chiller has been programmed to avoid any damage when its entering hot and cooling water temperatures are not in their practical limits. Therefore, the duty cycling of the absorption chiller follows the sequence implemented on the chiller logic controller.

The chiller was turned off after 6 pm since there was not sufficient sun radiation. Results indicate that the chiller cooling capacity is always greater than actual cooling load of the building. In addition, the difference between the chiller cooling capacity and actual cooling demand of the building is more in the higher solar radiation intensity. In fact, increasing the solar radiation intensity increases both the building cooling load and chiller capacity. However, the influence of the solar radiation on the chiller capacity increment is more than its influence on the building cooling load.

Results also showed that the cooling capacity of the chiller is highly dependent on the water temperature at the condenser outlet as shown in Figs. 8.17 to 8.19, where it can be seen that the cooling capacity of the chiller is increased with a reduction of the condenser's outlet water temperature. As expected, the chilled-water temperature decreases to an increase of the cooling capacity of the chiller. Moreover, it was found that the hot water temperature leaving the solar collector has a significant influence on the chiller performance as increasing the hot water temperature increases the chiller cooling capacity.

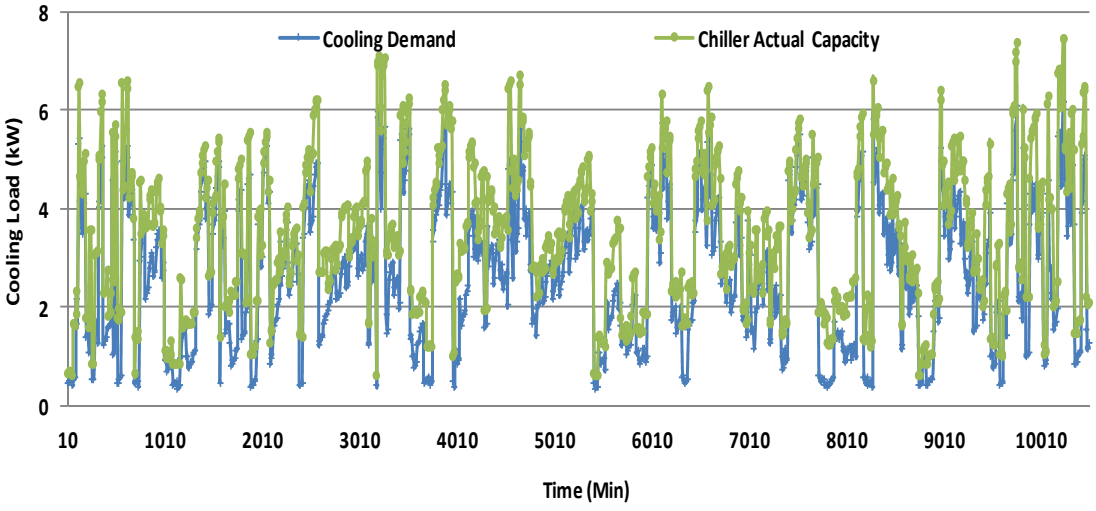

Fig. 8.16 Chiller capacity and building cooling demand comparison

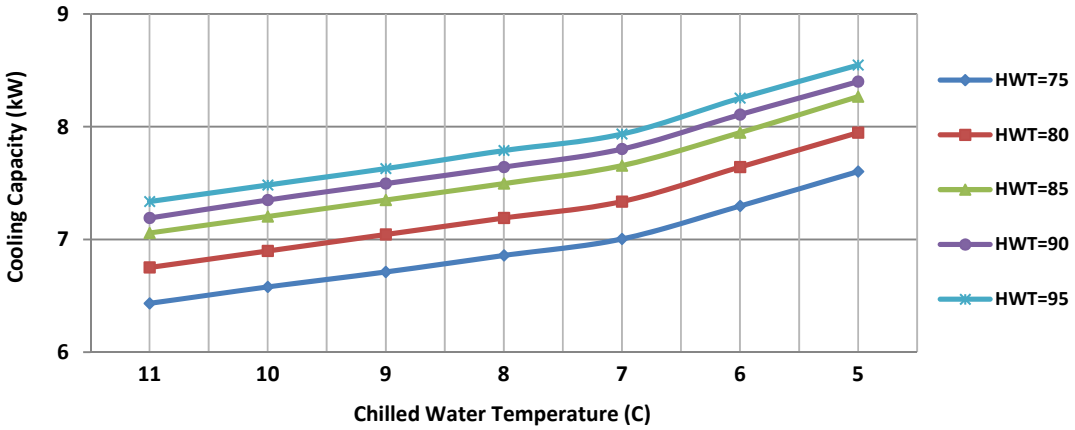

Fig. 8.17 Chiller cooling capacity for condenser water temperature fixed at 26°C

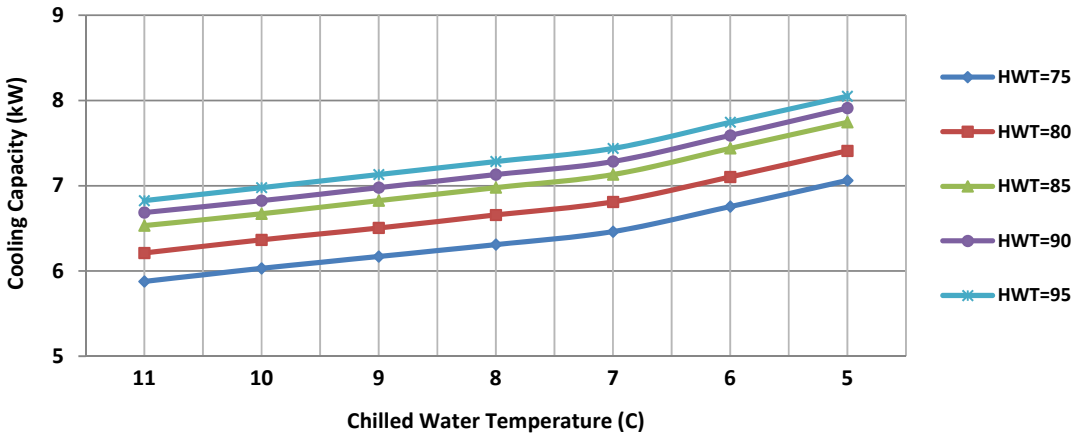

Fig. 8.18 Chiller cooling capacity for condenser water temperature fixed at 29°C

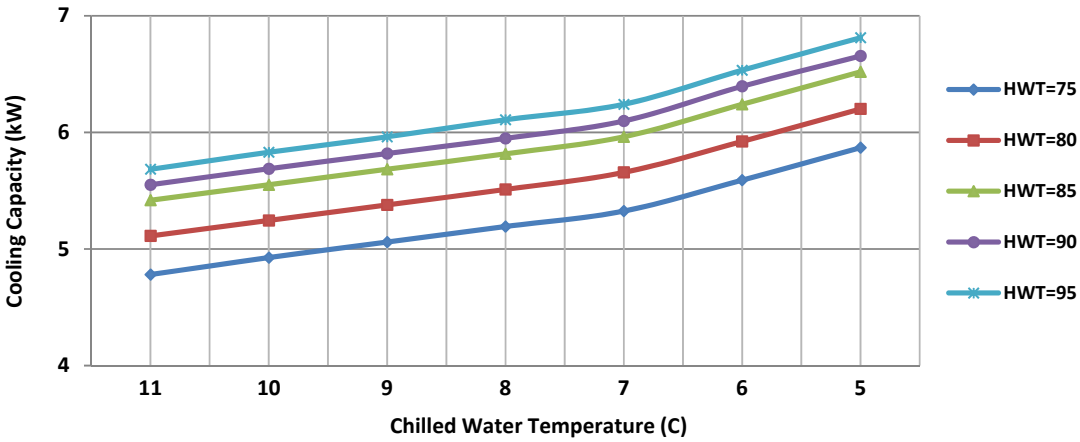

Fig. 8.19 Chiller cooling capacity for condenser water temperature fixed at 32°C

The chiller capacity, solar collector heat gain and cooling tower heat rejection capacity during the field test are shown in Fig. 8.20. The daily chiller cooling output, solar collector heat gain and cooling tower heat rejection capacity for different summer months are obtained from the simulation results and shown in Figs. 8.21 to 8.25.

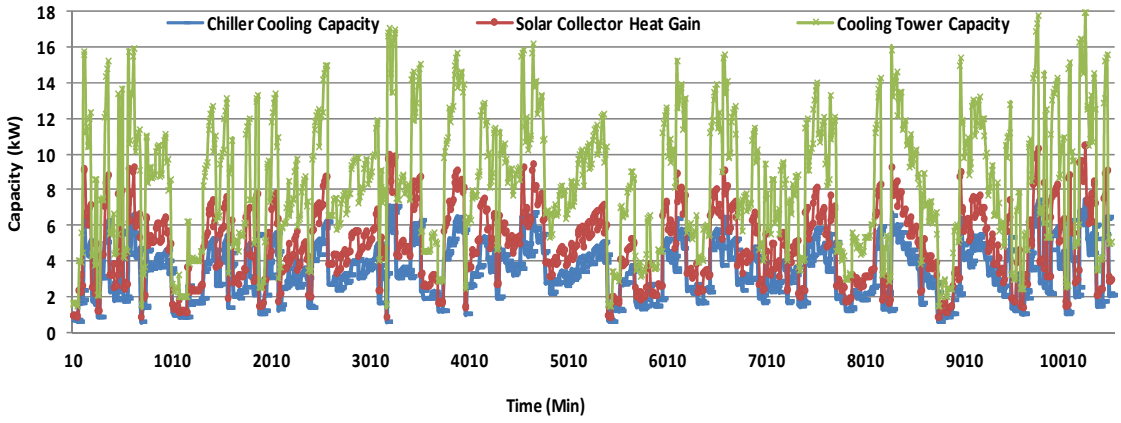

Fig. 8.20 Capacity of cooling plant components

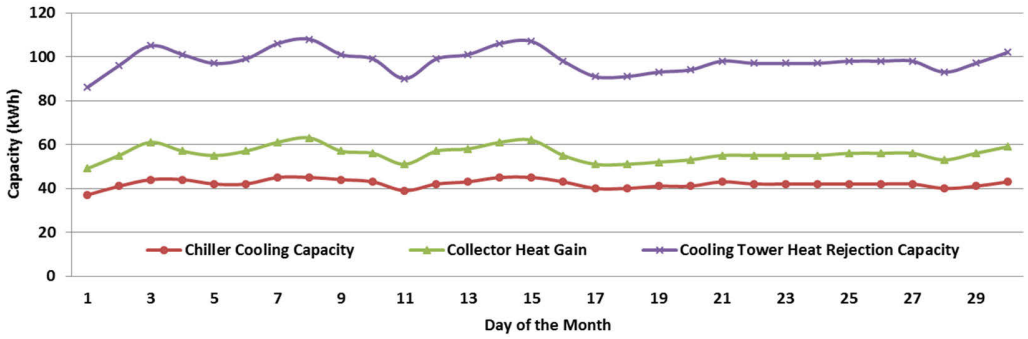

Fig. 8.21 Capacity comparison of cooling plant components for November

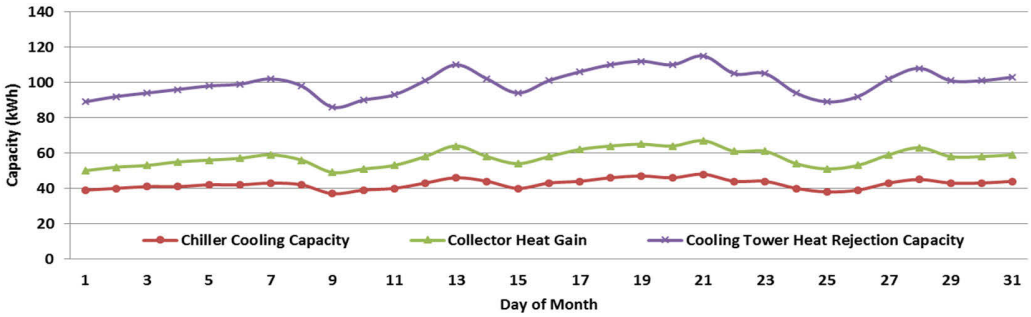

Fig. 8.22 Capacity comparison of cooling plant components for December

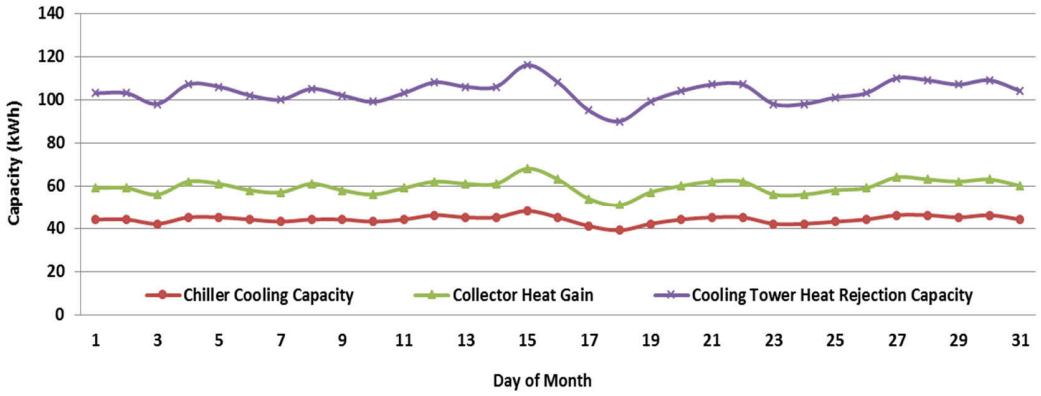

Fig. 8.23 Capacity comparison of cooling plant components for January

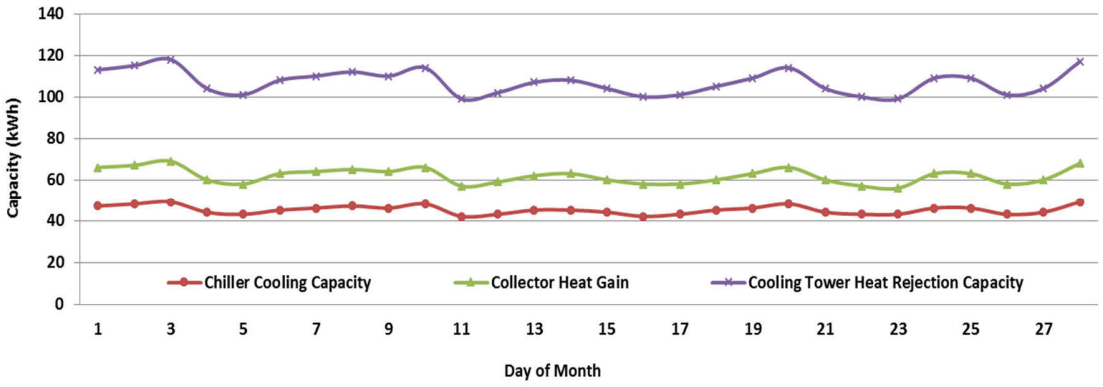

Fig. 8.24 Capacity comparison of cooling plant components for February

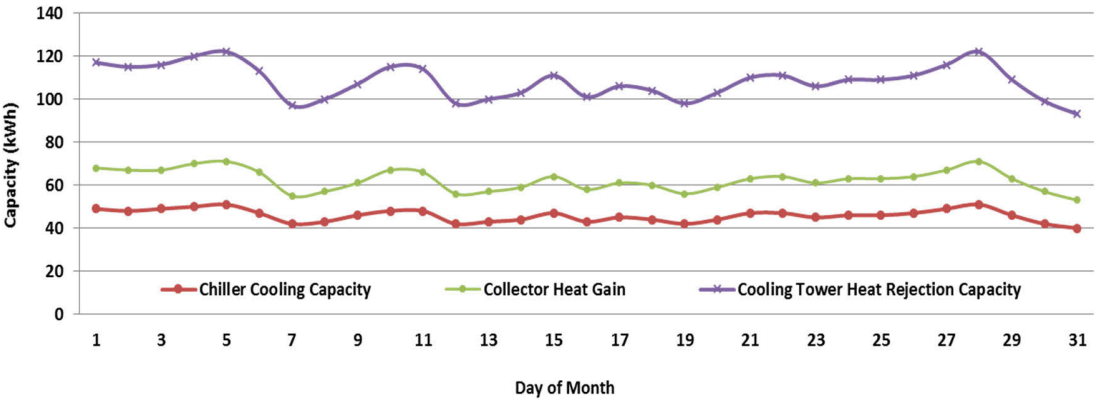

Fig. 8.25 Capacity comparison of cooling plant components for March

The heat gain of the vacuum solar collector in various hot water temperatures leaving the collector and the heat rejection capacity of cooling tower in different water temperatures leaving the cooling tower are shown in Figs. 8.26 and 8.27. As shown in Fig. 8.26, solar collector capacity is increased with increasing of hot water temperature leaving the solar collector. In addition, since increasing the cooling tower capacity means more heat rejection is required, the water temperature leaving the cooling tower is then reduced as shown in Fig. 8.27.

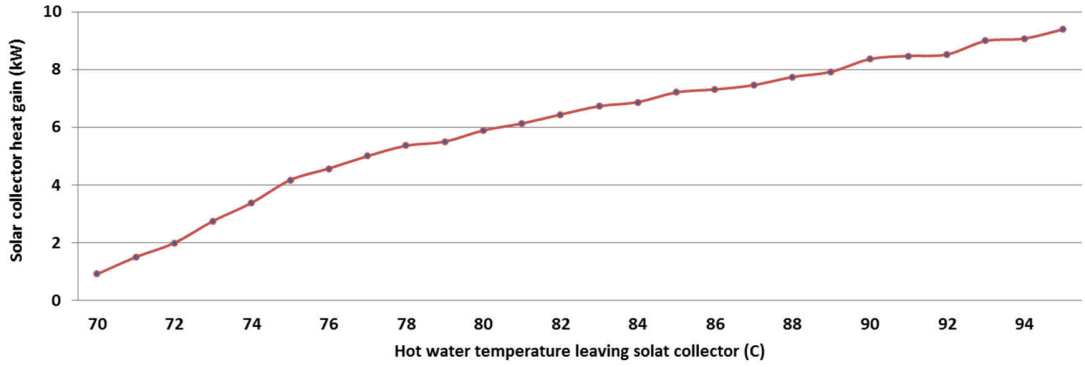

Fig. 8.32 Solar collector capacity versus hot water temperature leaving collector

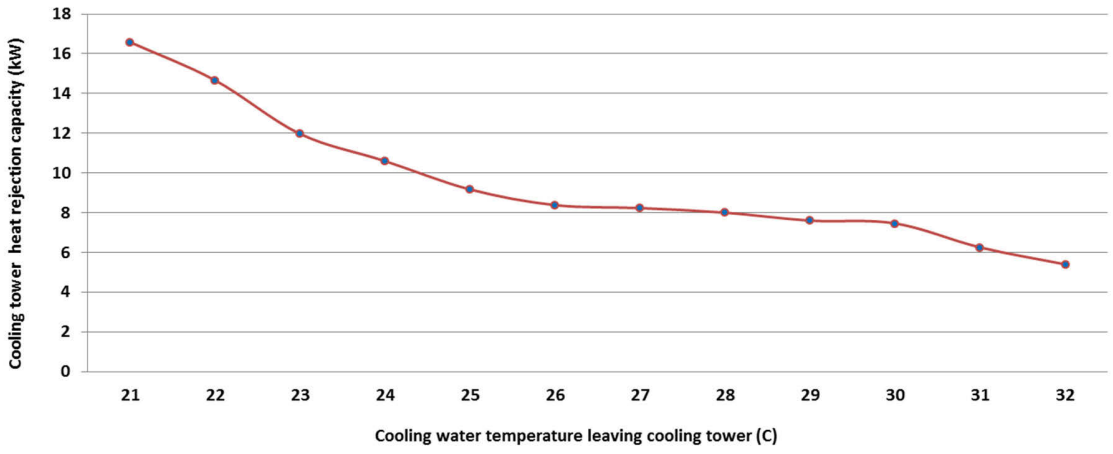

Fig. 8.33 Cooling tower capacity versus water temperature leaving cooling tower

8.5.2 Solar Collector Area

As discussed, the rated cooling demand of the air-conditioned building is about 6.4 kW. Therefore, for the nominal COP of 0.708, the cooling system requires about 9.0395 kW of heating energy. Considering the solar collector efficiency of 40% based on manufacturer data and an average solar radiation intensity of 720 W/m^2 based on solar radiation data for Sydney, a collector area of 31.38 m^2 is required for the 4°C water temperature difference at generator inlet and outlet at the nominal load:

$$Q_{col} = \eta_{col} A_{col} I_t, \qquad (8.57)$$

$$Q_{col} = 0.4 \times A_{col} \times 720 = 9039.5 \Rightarrow Q_{col} = 31.38 m^2,$$

The average solar radiation intensity at the rated building cooling load conditions is shown in Fig. 8.28. However, a solar vacuum collector with 31.5 m^2 area has been used for the system. The solar collector was designed to tilt at an angle of 40° to the horizontal. Solar collectors were divided into nine parallel rows in which each row was composed of fifteen solar collector tubes. Each tube has the length of 1.65 meter and the diameter of 0.045 meter. Therefore, 135 tubes provide the 31.5 m^2 total area which is required to support the nominal cooling demand of the building. The tubes were connected in series to achieve a hot water temperature of 85°C at nominal conditions.

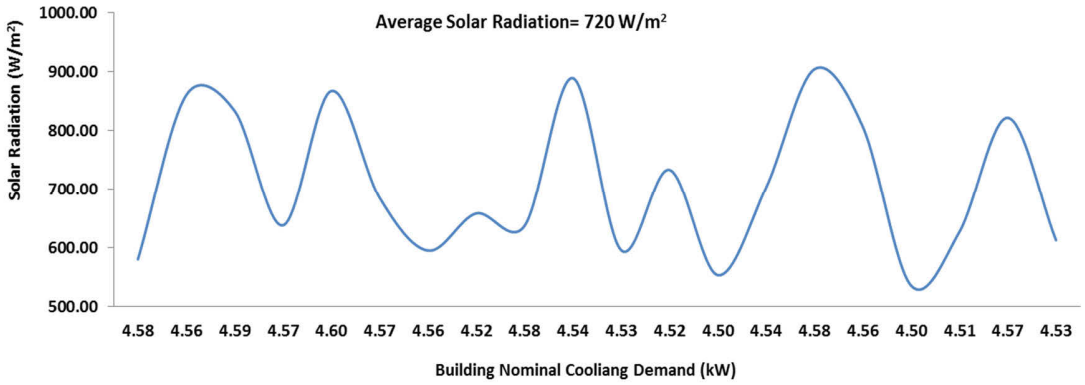

Fig. 8.28 Solar radiation intensity versus building nominal cooling demand

8.5.3 Solar Collector Efficiency

The collector efficiency can be determined using equation 8.11. Figure 8.29 shows the variation of solar collector efficiency with ambient dry-bulb temperature and solar radiation intensity. It can be seen that the solar collector efficiency is increased with increasing both the solar radiation intensity and ambient dry-bulb temperature. Fig. 8.30 shows the variation of solar collector efficiency with the water temperature at the collector outlet at the ambient temperature of 33°C. It can be seen that the efficiency of solar collector decreased with the increase in the outlet water temperature of the solar collector. When the outlet water temperature varied between 70°C to 94°C, the collector efficiency changed from 0.65 to 0.57. The reason is that a higher temperature for the solar collector water leads to a greater temperature difference between the collector and ambient air. This results in the increase in heat loss to the ambient and hence the collector efficiency decreases.

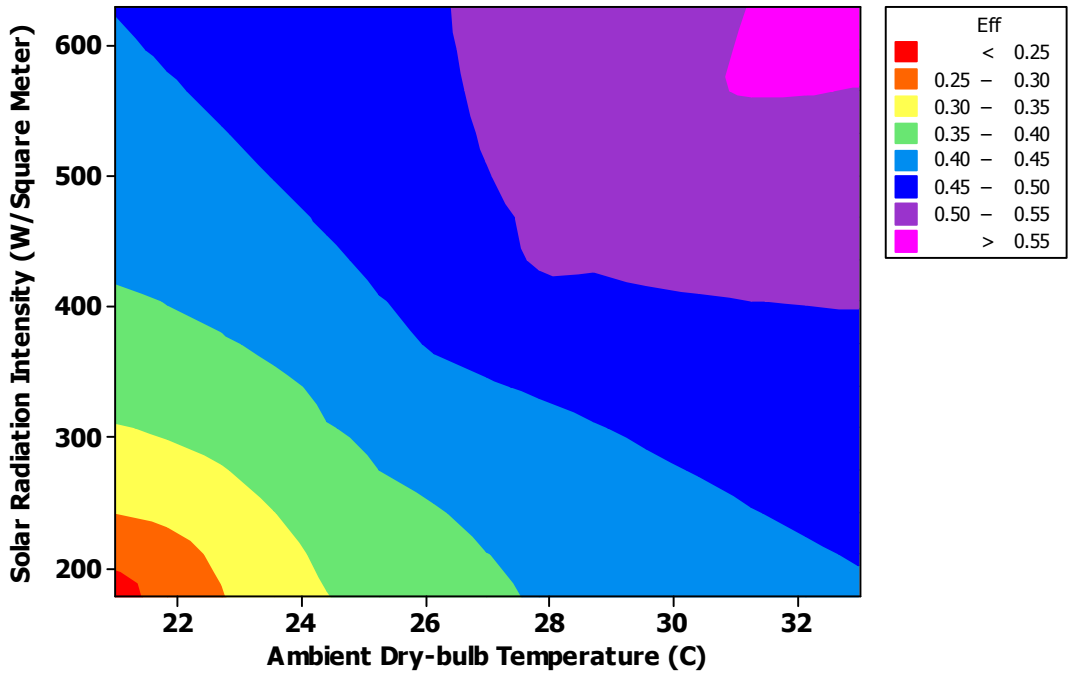

Fig. 8.29 Collector efficiency versus solar radiation intensity and ambient temperature

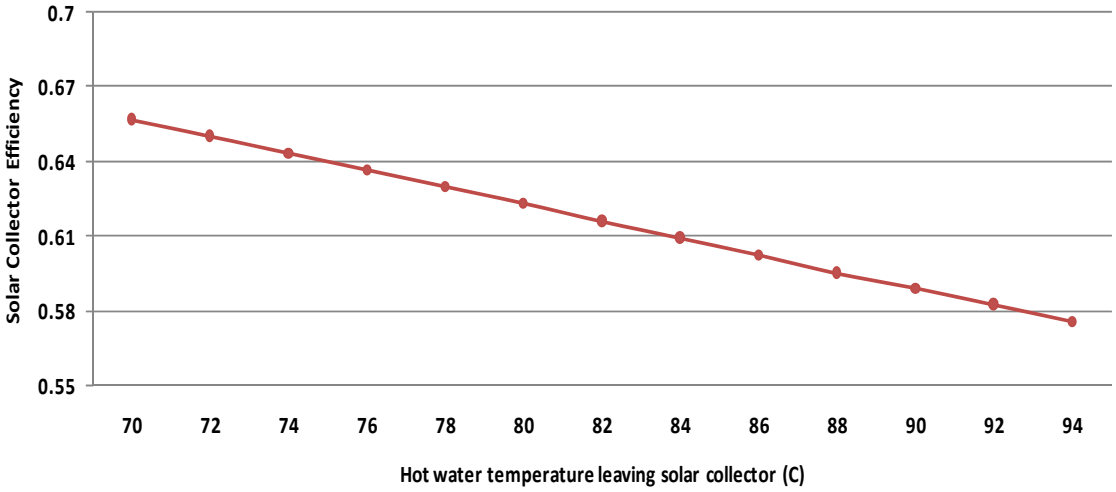

Fig. 8.30 Variation of the solar collector efficiency with the collector outlet temperature

8.5.4 Hot Water Temperature

Fig. 8.31 shows the variation of the hot water temperature leaving the solar collector with the solar radiation intensity when the average ambient temperature is 33°C. As may have been expected, the water temperature leaving the solar collector increases with an increase in the solar radiation intensity. It has also been observed that the solar radiation intensity has a greater impact on the performance of the solar absorption system than the ambient temperature.

8.5.5 Chilled-Water Temperature

Fig. 8.32 shows the variation of the chilled-water temperature leaving the absorption chiller as a function of the solar radiation intensity when the ambient temperature is 33°C. It is observed that the chilled-water temperature leaving the absorption chiller decreases with the increase in the solar radiation intensity. The reason is that the hot water temperature leaving the solar collector increases with an increase in solar radiation intensity which leads to increase of the cooling demand of the building. As a result, the chilled water temperature tends to decrease since the required cooling demand cannot be occurred immediately. Therefore, increasing the solar radiation intensity increases the hot water temperature leaving

the solar collector while reduces the chilled-water temperature leaving absorption chiller is reduced as shown in Figs 8.33 to 8.36.

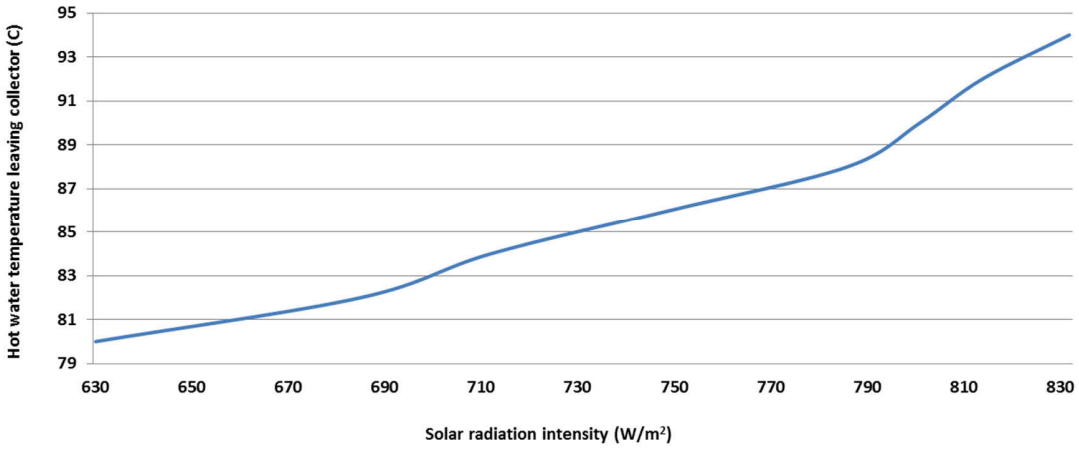

Fig. 8.31 Hot water temperature versus solar radiation intensity

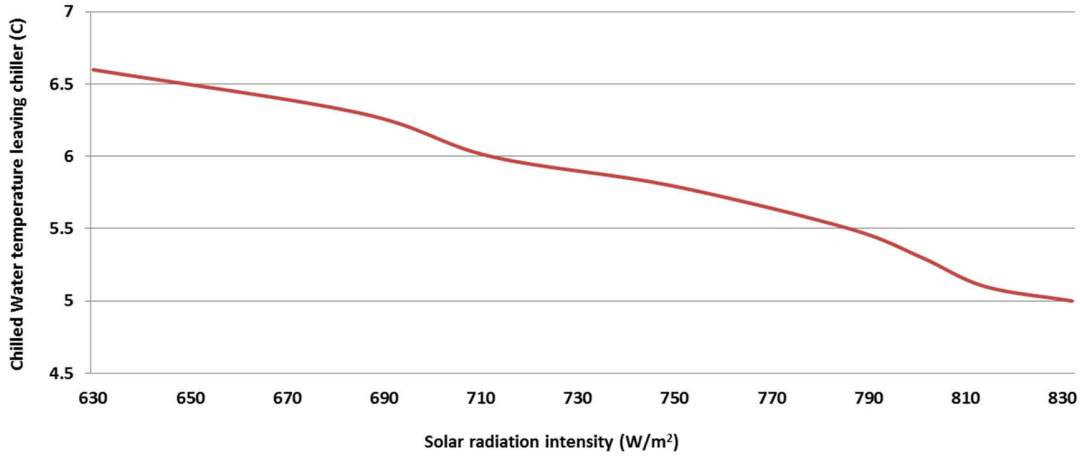

Fig. 8.32 Chilled-water temperature versus solar radiation intensity

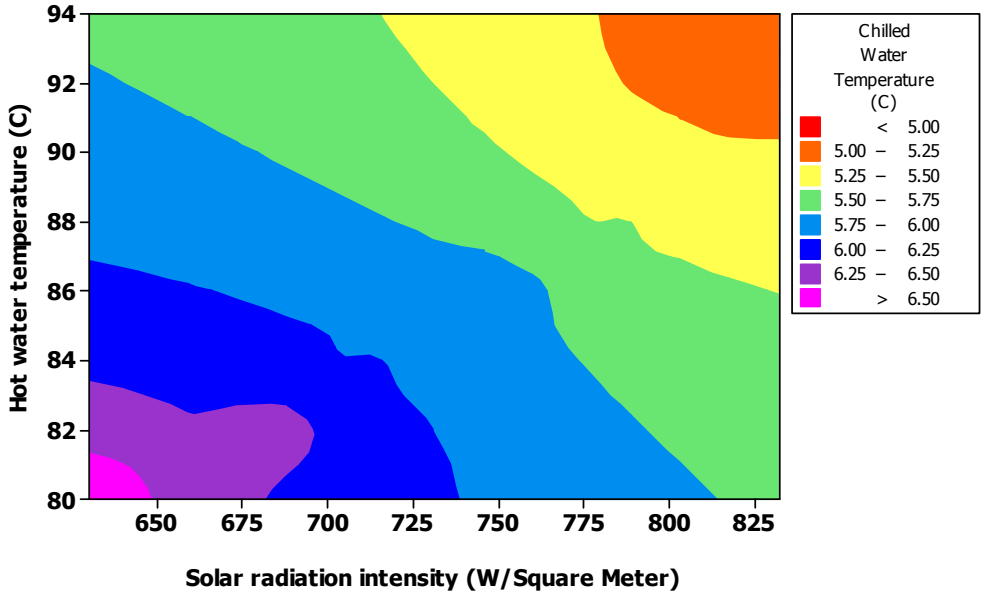

Fig. 8.33 Variation of hot and chilled water temperature with solar radiation intensity at ambient temperature of 33°C

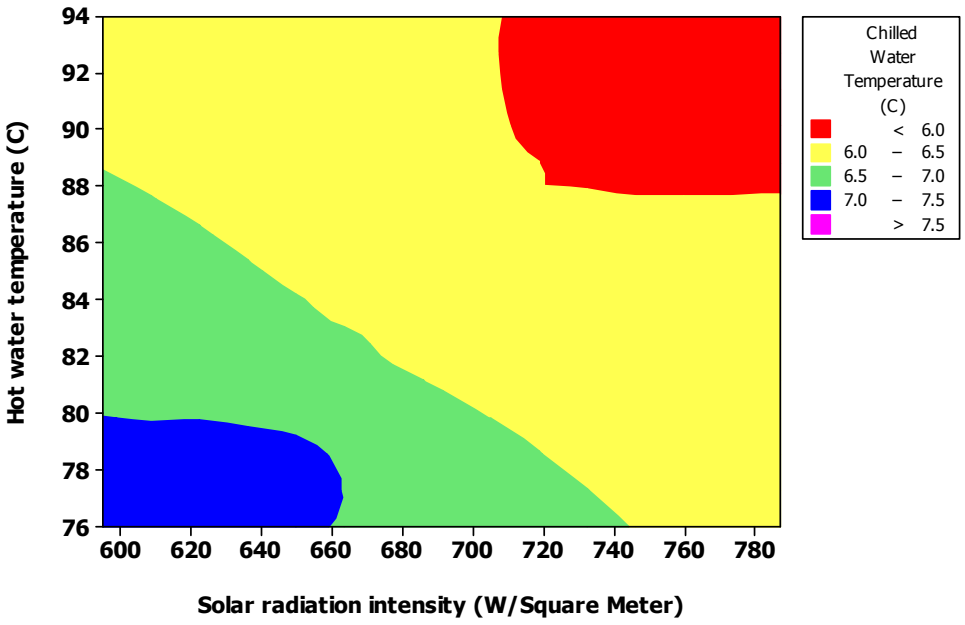

Fig. 8.34 Variation of hot and chilled water temperature with solar radiation intensity at ambient temperature of 30°C

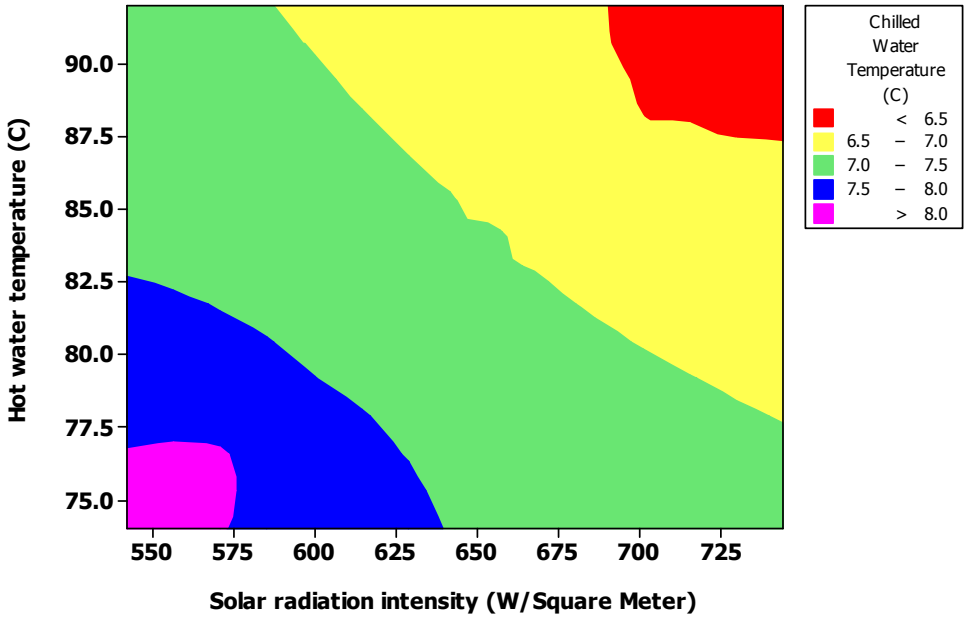

Fig. 8.35 Variation of hot and chilled water temperature with solar radiation intensity at ambient temperature of 27°C

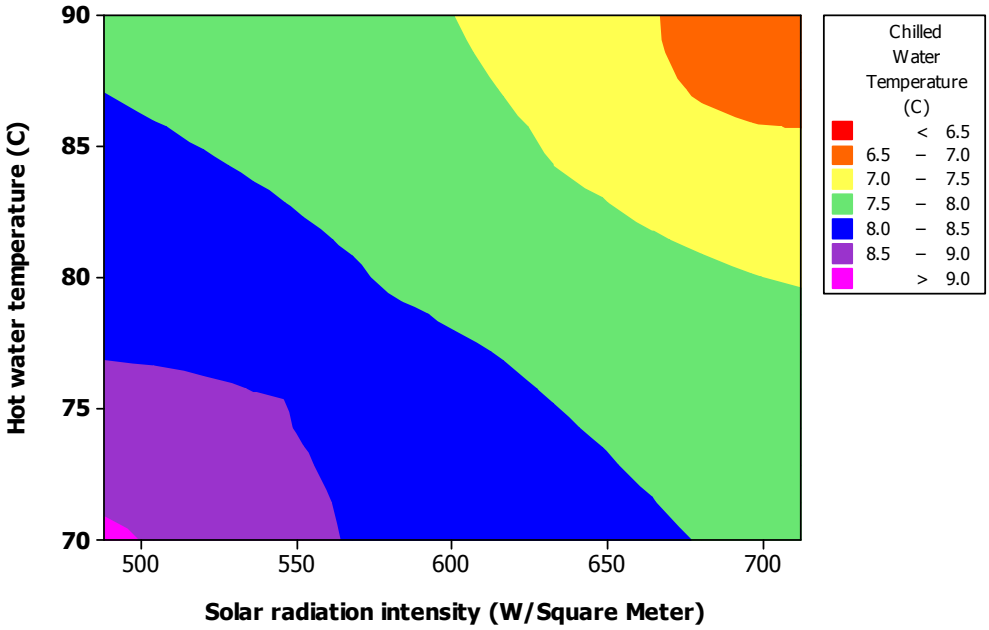

Fig. 8.36 Variation of hot and chilled water temperature with solar radiation intensity at ambient temperature of 23°C

8.5.6 Supply Air Temperature

The supply air temperature is the air temperature leaving the cooling coil of the fan-coil unit to provide the cooling inside the building. Results show that the variation of the supply air temperature with the ambient dry-bulb temperature is contrary to that with the solar radiation intensity. The supply air temperature goes down with an increase in the average solar radiation intensity as shown in Fig. 8.37. The reason is that increasing the solar radiation increases both the building cooling demand and chiller capacity. With more cooling loads inside the building, less supply temperature is required to support indoor temperature. However, the increase in chiller cooling capacity overwhelms the increase in building cooling load led by increasing solar radiation intensity. In addition, the supply air temperature increases with the increment in the ambient temperature as shown in Fig 8.38. This indicates that the increase in cooling load inside the building due to ambient temperature increment overwhelms the increase in chiller cooling capacity. It should be noted that the ambient air temperature normally get higher with increasing the solar radiation intensity. In addition, building cooling demand can increase while solar radiation intensity is decreased due to building internal loads. As a result, a transient behaviour is followed by supply air temperature. The influence of the ambient temperature and solar radiation intensity were considered on the supply air temperature whilst other factors such as building internal loads were remained constant.

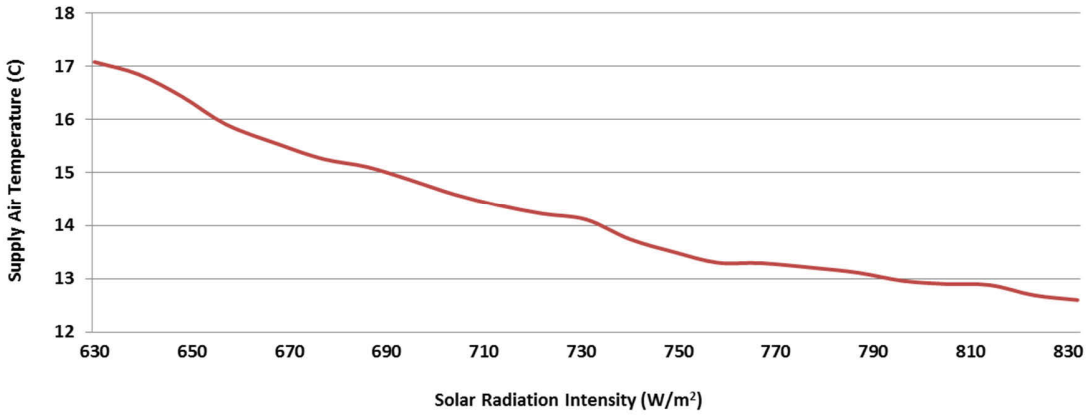

Fig. 8.37 Variation of Supply air temperature versus solar radiation intensity

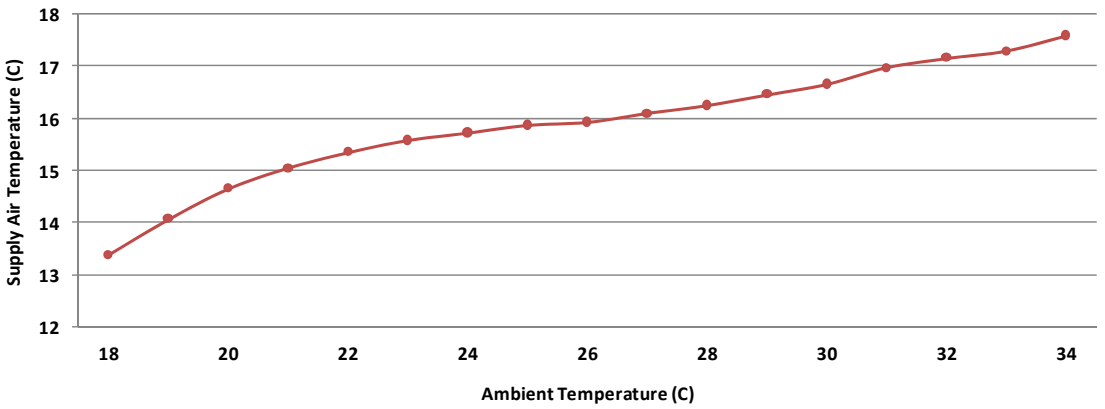

Fig. 8.38 Variation of Supply air temperature versus ambient temperature

Chapter 9

DISCUSSION, CONCLUSION AND FUTURE WORK

9.1 Summary

Producing air conditioning from solar energy remains an attractive prospect. In this context, solar resource availability is a key factor to design the solar cooling technology for a certain location. Currently, using flat plat or evacuated solar collectors, most of the solar cooling systems are mainly based on absorption chillers. Solar absorption air conditioning system is an alternative to cope with the increasing cooling energy demand with sustainability criteria in countries like Australia. In this chapter the main conclusions of this thesis are summarised. In addition, we conclude with recommendations for future research and development to evaluate the performance of absorption chillers.

9.2 Cooling Market in Australia

It has been reported that the residential air conditioning market in Australia is around 800,000 units per year [151]. In 2000, about 35% of all Australian households used air conditioning systems and it has been increased to 70% in 2006 [151]. These air conditioning systems are mostly reversible wall-mounted split units. In addition, it has been estimated that about 800 air-cooled and 200 water-cooled chiller units per year appropriated the commercial cooling market in Australia. This large air conditioning market together with the enormous solar resource is a perfect match for developing solar cooling systems in Australia. However, there are not many solar cooling system installed in Australia. This discrepancy can be explained when considering the economic analysis. For the present situation, the practical development of the solar absorption cooling system is limited because its relatively high capital cost is not competitive with conventional air conditioning systems. However, on the other hand, this system has been accepted as the environmentally-friendly and energy-efficient system.

The literature on national cost-benefit analysis suggests a number of comprehensive sophisticated approaches which are not appropriately tailored to the economic reality of developing countries. It is important that the use of a new system affords electricity savings large enough to pay back initial investments in the system in a suitably short time. In this regard, a newly-developed system that can heat and cool at low cost is very desirable because of the increased financial savings on offer. The main aim of the solar-powered absorption system is to provide maximum cooling performance while minimising electrical power consumption, with a view of slowing the rampant growth of daily peak demand on the electricity grid in summer that is being largely attributed to ever-increasing sales of cheap, traditional air conditioners.

9.2.1 Limitations Associated to Absorption Cooling Systems

With traditional HVAC systems contributing significantly to the building's overall energy consumption, the public's increasing reliance on them as a necessity rather than a luxury is an issue in urgent need of attention. As well as contributing to negative environmental outcomes, HVAC system usage is having a serious impact on electrical infrastructure. Grid failures and blackouts during peak summer periods are becoming increasingly common as electricity companies struggle to keep up with demand. These failures pose additional challenges, not only for the companies themselves but also for the general public. The cost is also quickly becoming unmanageable; ongoing upgrades to existing electricity infrastructure are prohibitively expensive, as well as being an unsustainable long-term solution, and the resulting dramatic increases in wholesale electricity prices are starting to hit consumers in the hip pocket. Therefore, solar HVAC development remains a relatively unconquered engineering landscape when it comes to refining existing system configurations for maximum efficiency. Solar compatible chillers that are currently on the market are aimed squarely at commercial clients. However, the relatively steep upfront costs of installing these systems make them an unattractive option for commercial tenants; because the savings tend to occur over time, building owners may benefit, but there is little incentive for building tenants to invest if the system will deliver only minimal payback during the course of a commercial lease.

As mentioned in this study, solar absorption cooling technology is a process by which refrigeration effect is produced using heat input rather than electrical input. An advantage of absorption cooling system over the vapour compression cooling systems is that a small amount of mechanical work is required in absorption cooling systems. However, the required heat input for absorption cooling systems is many times greater than the work input of the mechanical vapour compression cooling system. Therefore, using the absorption cooling system is economically reasonable if the heat input can be provided sufficiently inexpensive. The COP of the vapour compression cooling system is in the range of 2 to 4 while the COP of the absorption system is limited by thermodynamic considerations. Carnot COP for the solar powered absorption cooling system is typically between 0.5 and 2.5, however the actual are not ideal cycles. As mentioned in chapter two, the practical COP of the single-effect absorption chillers is in the range of 0.5 to 0.7 for ammonia-water systems and 0.6 to 0.8 for the LiBr-water systems. When sufficient heat input in reasonable cost is available, using the solar absorption system is preferable compared with the conventional vapour compression HVAC systems. However, as it was mentioned earlier, Australia has abundant solar energy resources. In addition, solar absorption refrigeration system is an environmentally-friendly system. This study showed that this system is able to provide cooling for a commercial building.

9.3 Conclusion

The main objectives of this work have been to design a new configuration of the absorption cooling system and computational model that allows the performance evaluation of the absorption chiller powered by solar energy. The purpose of developing this model was to optimal design and to size the solar absorption cooling plant. The final objective was to manufacture this system based on the obtained results and investigate its technical feasibility.

In this study, the operation cycle of the single-effect absorption air conditioning system was first described and then using both the first law and second law of thermodynamic, the operation cycle of the absorption chiller was designed. The continuous cycle operates with hot water in generator, chilled water in evaporator and cooled water in the absorber and

condenser. Chiller components such as generator, condenser, evaporator, absorber and solution heat exchanger were designed based on heat transfer correlations. A computer code, ABSYS, was developed to analyse and evaluate the influence of the various operating conditions on the system performance so that the optimum design can be selected. This code can commercially be used for the purpose of single-effect absorption chiller design. The thermodynamic design data for single-effect absorption chiller were derived using ABSYS which can be used for other studies. The results of this analysis were then used to commercialise the absorption chiller. Other parts of the cooling plant such as cooing tower, vacuum solar collector and fan-coil unit were designed and manufactured based on the building cooling load, climatic condition of Sydney city and the outcomes obtained from absorption chiller design. The entire central cooling plant was then configured. The solar vacuum solar collector was directly connected to the chiller's generator without using the hot water storage tank. As the backup system was removed for this design, the performance of cooling plant was highly dependent on the solar radiation intensity. Several field tests were carried out to examine the transient behaviour of the entire cooling plant. A simulation code was then developed using TRNSYS to assess the transient performance of the entire system. Developed models in TRNSYS were verified using the experimentally-monitored data. Results of this analysis showed that the solar-powered absorption air conditioning system can support the building cooling load. However, it was found that system control by simple on-off cycling is not efficient and leads to energy loss. The main conclusions of this study are summarised as follows:

- In operation of a solar absorption cooling system, a change in any input variable, causes changes in all other dependant variables and hence the entire system reacts to reach the new equilibrium operating conditions.

- The most important irreversibility in an actual absorption chiller is due to its heat exchangers and therefore to assess the entire absorption operation cycle, the heat exchanger models should be included in the cycle model. In addition, these models provide more accurate inputs to simulate the entire operating cycle. The influence of these inputs on the system performance is very significant and may lead the designer

to vary the thermodynamic set-points to achieve the optimum design. The developed computer code, ABSYS, uses the heat exchanger models and design set-pints simultaneously to calculate the specification of different heat exchangers. The optimal design can then be selected.

- Results showed that the system COP is increased rapidly with increasing the generator temperature up to a certain point and then level off and reach an asymptotic value. It means that higher generator temperatures will not improve the COP.

- The cooling capacity of the system increases with increasing the hot water temperature entering the generator.

- There is a low generator limitation for the system. It means that for the absorption cycle at the selected operating conditions, if the generator temperature is below its minimum possible temperature, the COP will be very close to zero. Therefor, it is very impractical to operate the absorption chiller at a generator temperature less than its optimum value.

- Results showed that increasing the condenser temperature decreases the system COP. In addition, there is a high limitation set-point for condenser temperature. If the condenser temperature reaches its maximum high temperature limits, the superheated water vapour cannot be cooled down to the liquid phase and the enthalpy difference entering and leaving the evaporator is close to zero which reduce the system COP dramatically.

- The system COP increases when the evaporator temperature increases. In fact, a higher evaporative temperature results in a higher absorbing pressure which enhances the absorption efficiency of the strong solution.

- The COP increases with increasing the solution heat exchanger effectiveness. Also, increasing the solution heat exchanger effectiveness reduces the absorber heat rejection.

- The generator temperature for our proposed design should not be less than 75°C to keep the chiller COP in the practical range. Results show that the generator number of tubes increases with increasing the generator temperature.

- Increasing the efficiency of the solution heat exchanger reduces the generator capacity and hence decreases the required number of tubes in generator.

- The cooled-water temperature entering the condenser should not reduce too much due to the crystallisation of the LiBr solution. In our design it must not be less than 15°C.

- Result indicated that increasing the evaporator temperature reduces the number of tubes in the absorber. In addition, the number of tubes in absorber are reduced initially with increasing the generator temperature. However, results indicated that the generator temperatures more than 79°C have not significant effect on the absorber number of tubes.

- At a constant evaporator temperature of 5°C, increasing the supply chilled-water temperature decreases the number of evaporator tubes. Also, results showed that the evaporator number of tubes are insensitive to the other operating temperatures such as generator, condenser and absorber temperatures.

- Analysis of transient performance of the entire solar cooling plant showed the capability of this system to support the building cooling loads.

9.4 Future Work and Recommendations

At present, a huge potential of the building cooling market is covered by vapour compression based chillers and heat pumps which lead to failures in the electricity supply network which must cover increasingly higher peak load. As mentioned in this study, one solution can be using thermally driven chillers which deliver chilled water. In this case, absorption machines represent the most common solution in the actual installation. However, for this system an emerging research trend must be focused on green automation, which is dedicated to the efficient and sustainable handling of resources and making renewable energies competitive and successful. One essential component for green automation is energy management, whereby the reductions of energy consumption and global carbon-dioxide emissions are of paramount importance [152]. Because building cooling load varies with the time of the day, the solar-powered absorption system should be equipped with an effective controller to reduce the energy consumption by keeping the process variables to their optimal set-point required. This can be the future work to reconfigure the developed system to design and implement an optimal regulator for its closed-loop multivariable control.

The reason is that, solar radiation is a highly time-dependent energy source and it is not necessarily match with the building demand. In other word, although cooling demand of the building and solar radiation intensity take place more or less at the same time of the day, there can be many accessions when the ideal match between sun and absorption chiller does not occur. Examples can be hot days with low radiation intensity, sunny days without cooling demand and morning and late afternoon cooling loads. As a result, there will be a transient effect characterized by continuous ON-OFFs which reduces the system efficiency. Therefore, system cannot follow the building cooling demand and steady cooling cannot be provided. This problem can be addressed by regulating the storage and release of thermal energy according to the building load. Therefore, an appropriate control method should be employed by solar-powered absorption systems to adjust the transient building demand with the stored solar thermal energy. In construction automation, building energy management and the necessity to reduce overall energy consumption are becoming an increasingly important

topic, given highly dynamic environments in association with frequently varying conditions of the building setting and its occupancy. In the control method, the chilled water and hot water mass flow rate should be controlled so that their optimal required temperatures can be provided to support the building transient cooling loads. The recommendations for future work on this system are listed as follows:

- High initial cost: the capital cost of this system is high compared to the conventional vapour compression HVAC systems with equivalent cooling capacity. The important part of this cost is the price of vacuum solar collector. One suggestion can be using of reflectors behind the evacuated solar tubes to enhance their efficiency. This can reduce the number of required solar vacuum tubes.

- As mentioned, the coupling of solar collector and absorption chiller requires a robust control system so that the solar absorption system can operate at its optimal operating conditions. For this purpose, the most important variables to be controlled are hot and chilled water temperatures. The hot water temperature should be controlled as the function of incident solar radiation and ambient temperature. Chilled water temperature should be controlled based on building cooling demand and required comfort conditions inside the building.

- The efficiency of solar collector decreases with the rising of the water temperature while chiller reaches highest efficiency when water temperature is at high temperature. Therefor, the solar collector should be design for an optimum hot water temperature.

- Efficiency of the solar contribution is limited to the day hours. Therefore a backup system together with its storage tank should be designed and implemented if the system wants to work during the night.

REFERENCES

[1] World Energy Council (WEC). Survey of Energy Resources: Promoting the sustainable supply and use of energy for the greatest benefit of all. London: World Energy Council, 2007.

[2] Hassan HZ, Mohamad AA. A review on solar-powered closed physisorption cooling systems. Renewable and Sustainable Energy Reviews 2012; 16: 2516– 2538.

[3] Reberto Best B, Juan M. Aceves H, Jorge M. Islas S, Fabio L. Manzini P, IssacPilatowsky F, RossanoScoccia, Mario Motta. Solar cooling in the food industry in Mexico: A case study. Applied Thermal Engineering 2013; 50: 1447-1452.

[4] United State Environment Protection Agency. EPA green building strategy, 2008. <http://www.epa.gov/greenbuilding/pubs/about.htm>.

[5] Rodrıguez Hidalgo MC, Rodrıguez Aumente P, Izquierdo Millan M, Lecuona Neumann A, Salgado Mangual R. Energy and carbon emission savings in Spanish housing air-conditioning using solar driven absorption system. Applied Thermal Engineering 2008; 28: 1734–1744.

[6] G.A. Florides, S.A. Kalogirou, S.A. Tassou, and L.C. Wrobel, "Modelling, simulation and warming impact assessment of a domestic-size absorption solar cooling system," Applied Thermal Engineering, vol. 22, pp. 1313-1325, 2002.

[7] Raja VB, Shanmugam V. A review and new approach to minimize the cost of solar assisted absorption cooling system. Renewable and Sustainable Energy Reviews 2012; 16: 6725-6731.

[8] Kalkan N, Yonug EA, Celikats A. Solar thermal air conditioning technology reducing the footprint of solar thermal air conditioning. Renewable and Sustainable Energy Review 2012; 16: 6352-6983.

[9]Enteria N, Mizutani K. The role of the thermally activated desiccant cooling technologies in the issue of energy and environment. Renewable and Sustainable Energy Reviews 2011; 15: 2095-2122.

[10] Qi R, Lu L, Yang H. Investigation on air-conditioning load profile and energy consumption of desiccant cooling system for commercial buildings in Hong Kong. Energy and Buildings 2012; 49: 509-518.

[11] Pérez-Lombard J, Ortiz J, Pout C. A review on buildings energy consumption information. Energy and Buildings 2008; 40: 394-398.

[12] DoE., Energy Information Administration, Table US-1. Electricity consumption by end use in U.S. households. U.S. Department of Energy, 2001.

[13] DoE., Energy Information Administration, International Energy Outlook. U.S. Department of Energy 2006.

[14] Yao Y, Chen J. Global optimization of a central air-conditioning system using decomposition–coordination method. Energy and Buildings 2010; 42: 570-583.

[15] Balaras CA, Grossman G, Henning H, Ferreira CAI, Podesser E, Wang L, Wiemken Edo. Solar air conditioning in Eroupe- an overview. Renewable and Sustainable Energy Reviews 2007; 11: 299-314.

[16] Brodribb P, McCann M. A study of the refrigeration and air conditioning industry in Australia. Cold Hard Facts 2, 2013.

[17] Energy Conversation Building Code (ECBC), Bureau of Energy Efficiency, Ministry of Power, Government of India, 2007.

[18] Fong KF, Chow TT, Lee CK, Lin Z, Chan LS. Comparative study of different solar cooling systems for buildings in subtropical city. Solar Energy 2010; 84: 227-244.

[19] Long J, Zhu D. Numerical and experimental study on heat pump water heater with PMC for thermal storage. Energy and Buildings 2008; 40: 666-672.

[20] Spitler JD. Ground-source heat pump research- past, present and future. HVAC&R Research 2005; 11: 165-167.

[21] El-Dessouky H, Ettouney H, Al-Zeefari A. Performance analysis of two-stage evaporative coolers. Chemical Engineering Journal 2004; 102: 255-266.

[22] IEO, International Energy Outlook (IEO), energy information administration. http://www.eia.doe.gov/oiaf/ieo.

[23] Desideri U, Proietti S, Sdringola P. Solar-powered cooling system: Technical and economic analysis on industrial refrigeration and air-conditioning applications. Applied Energy 2009; 86: 1376-1386.

[24] Ma Q, Wang RZ, Dai YJ, Zhai XQ. Performance analysis on a hybrid air conditioning system of a green building. Energy and Buildings 2006; 38: 447-453.

[25] Securing a Clean Energy Future: The Australian Government's Climate Change Plan. Department of Climate Change and Energy Efficiency, Australia, 2012.

[26] Australia's emissions projections: National targets. Australian Government, Department of the Environment. http://www.climatechange.gov.au/climate-change/greenhouse-gas-measurement-and-reporting/australias-emissions-projections/national

[27] Baseline Energy Consumption and Greenhouse Emissions in Commercial Buildings in Australia' (CBBS) - Part 1-Report. Council of Australian Governments (COAG), National Strategy on Energy Efficiency, 2012.

[28] Edwards T. The role of refrigeration and air conditioning in GHG emissions reduction. Australian Refrigeration Association (ARA), 2013.

[29] Edwards T. HVAC&R Co_2e emissions. Australian Refrigeration Association (ARA), 2013.

[30] Australian Energy and Tourism, Department of Resources, Energy and Tourism, Chapter 10, Solar Energy, 2010.

[31] Solar Energy Perspectives. International Energy Agency. Paris, France, 2011.

[32] Technology roadmap: Solar heating and cooling. International Energy Agency. Paris, France, 2012

[33] V. Vakiloroaya, M. Khatibi, Q.P. Ha, and B. Samali, "New Integrated Hybrid Evaporative Cooling System for HVAC Energy Efficiency Improvement," IEEE/SICE International Symposium on System Integration, Kyoto, Japan, pp. 591-596, 2011.

[34] Vakiloroaya V, Zhu JG, and Ha QP. Modelling and Optimization of Direct Expansion Air Conditioning Systems for Commercial Buildings Energy Savings. The 28th International Symposium on Automation and Robotics in Construction, Seoul, Korea, pp. 232-237, 2011.

[35] Hajidavalloo E, Eghtedari H. Performance improvement of air-cooled refrigeration system by using evaporatively cooled air condenser. International Journal of Refrigeration 2010; 33: 982-988.

[36] Youbi-Idrissi M, Macchi-Tejeda H, Fournaison L, Guilpart J. Numerical model of sprayed air cooled condenser coupled to refrigeration system. Energy Conversion and Management 2007; 48: 1943-1951.

[37] Yu FW, Chan KT. Improved energy performance of air-cooled chiller system with mist pre-cooling mist improvement on air-cooled chiller. Applied Thermal Engineering 2011; 31: 537-544.

[38] Vrachopoulos M, Filios AE, Kotsiovelos GT, Kravvaritis ED. Incorporated evaporative condenser. Applied Thermal Engineering 2007; 27: 823-828.

[39] Omer AM. Ground-source heat pumps systems and applications. Renewable and Sustainable Energy Reviews 2008; 12: 344-371.

[40] Zogou O, Stamatelos A. Effect of climate conditions on the performance of heat pump systems for space heating and cooling. Energy Conversion and Management 1998; 39: 609-622.

[41] Hwang Y, Lee JK, Jeong YM, Koo KM, Lee DH, Kim SW, Kim SH. Cooling performance of a vertical ground-coupled heat pump system installed in a school building. Renewable Energy 2009; 34: 578-582.

[42] Yang Y, Zhai XQ. Experience on the application of a ground source heat pump system in an archives building. Energy and Buildings 2011; 43: 3263-3270.

[43] Hackel S, Pertzborn A. Effective design and operation of hybrid ground-source heat pumps: three case studies. Energy and Buildings 2011; 43: 3497-3504.

[44] Hepbasli A, Akdemir O, Hancioglu E. Experimental study of a closed loop vertical ground source heat pump system. Energy Conversion and Management 2003; 44: 527-548.

[45] Agyenim F, Hewitt N. The development of a finned phase change material (PMC) storage system to take advantage of off-peak electricity tariff for improvement cost of heat pump operation. Energy and Buildings 2010; 42: 1552-1560.

[46 Long J, Zhu D. Numerical and experimental study on heat pump water heater with PMC for thermal storage. Energy and Buildings 2008; 40: 666-672.

[47] Spitler JD. Ground-source heat pump research- past, present and future. HVAC&R Research 2005; 11: 165-167.

[48] Lee JY. Current status of ground source heat pumps in Korea. Renewable and Sustainable Energy Reviews 2009; 13: 1560-1568.

[49] Gao Q, Li M, Yu M, Spitler JD, Yan YY. Review of development from GSHP to UTES in China and other countries. Renewable and Sustainable Energy Reviews 2009; 13: 1383-1394.

[50] Yang W, Zhou J, Xu W, Zhang G. Current status of ground-source heat pumps in china. Energy Policy 2010; 38: 323-332.

[51] Pardo N, Montero A, Sala A, Martos J, Urchueguia JF. Efficiency improvement of a ground coupled heat pump system from energy management. Applied Thermal Engineering 2011; 31: 391-398.

[52] Jeon J, Lee S, Hong D, Kim Y. Performance evaluation and modeling of a hybrid cooling system combining a screw chiller with a ground source heat pump in a building. Energy 2010; 35: 2006-2012.

[53] Rahman MM, Rasul MG, Khan MMK. Feasibility of thermal energy storage system in an institutional building in subtropical climates in Australia. Applied Thermal Engineering 2011; 31: 2943-2950.

[54] Yau YH, Rismanchi B. A review on cool thermal storage technologies and operating strategies. Renewable and Sustainable Energy Reviews 2012; 16: 787-797.

[55] Al-Abidi AA, Mat SB, Sopian K, Sulaiman MY, Lim CH, Th A. Review of thermal energy storage for air conditioning systems. Renewable and Sustainable Energy Reviews 2012; 16: 5802-5819.

[56] Ezan MA, Erek A, Dincer I. Energy and exergy analysis of an ice-on-ice thermal energy storage system. Energy 2011; 36: 6375-6386.

[57] Pu J, Liu G, Feng X. Cumulative exergy analysis of ice thermal storage air conditioning system. Applied Energy 2012; 93: 564-569.

[58] Hasnain SM, Alabbadi NM. Need for thermal-storage air-conditioning in Saudi Arabia. Applied Energy 2000; 65: 153-164.

[59] Chaichana C, Charters WWS, Aye L. An ice thermal storage computer model. Applied Thermal Engineering 2001; 21: 1769-1778.

[60] ASHRAE Handbook- HVAC Systems and Equipment. American Society of Heating, Refrigerating and Air-Conditioning Engineers 2008, Atlanta, GA, USA.

[61] Nagano K, Takeda S, Mochida T, Shimakura K, Nakamura T. Study of a floor supply air conditioning system using granular phase change material to augment building mass thermal storage-Heat response in small scale experiments. Energy and Buildings 2006; 38: 436-446.

[62] Stoecker WF, Jones JW. Refrigeration and air conditioning. McGraw-Hill, New York, 1982.

[63] Roulet CA, Heidt FD, Foradini F, Pibiri MC. Real heat recovery with air handling units. Energy and Buildings 2001; 33: 495-502.

[64] Manz H, Huber H. Experimental and numerical study of a duct/heat exchanger unit for building ventilation. Energy and Buildings 2000; 32: 189-196.

[65] Zhang LZ. Progress on heat and moisture recovery with membranes: From fundamentals to engineering applications. Energy Conversion and Management 2012; 63: 173-195.

[66] Zhang LZ, Niu JL. Energy requirements for conditioning fresh air and the long-term savings with a membrane-based energy recovery ventilator in Hong Kong. Energy 2001; 26: 119-135.

[67] Ke Z, Yaming K. Applicability of air-to-air heat recovery ventilators in China. Applied Thermal Engineering 2009; 29: 830-840.

[68] Fernandez-Seara J, Diz R, Uhia FJ, Dopazo A, Ferro JM. Experimental analysis of an air-to-air heat recovery unit for balanced ventilation systems in residential buildings. Energy Conversion and Management 2011; 52: 635-640.

[69] Yeo THC, Tan IAW, Abdullah MO. Development of adsorption air-conditioning technology using modified activated carbon- A review. Renewable and Sustainable Energy Reviews 2012; 16: 3355-3363.

[70] Dieng AO, Wang RZ. Literature review on solar adsorption technologies for ice-making air-conditioning purposes and recent developments in solar technology. Renewable and Sustainable Energy Reviews 2001; 5: 313-342.

[71] Choudhury B, Saha BB, Chatterjee PK, Sarkar JP. An overview of developments in adsorption refrigeration system towards a sustainable way of cooling. Applied Energy 2013; 104: 554-567.

[72] Srivastava NC, Eames IW. A review of adsorbents and adsorbates in solid-vapor adsorption heat pump systems. Applied Thermal Engineering 1998; 18: 707-714.

[73] Zhu R, Han B, Lin M, Yu Y. Experimental investigation on an adsorption system for producing chilled water. International Journal of Refrigeration 1992; 15: 31-34.

[74] Lu ZS, Wang RZ, Xia ZZ, Lu XR, Yang CB, Ma YC, Ma GB. Study of a novel solar adsorption cooling system and a solar absorption cooling system with new CPC collectors. Renewable Energy 2013; 50: 299-306.

[75] Liu X, Li Z, Jiang Y, Lin B. Annual performance of liquid desiccant based independent humidity control HVAC system. Applied Thermal Engineering 2006; 26: 1198-1207.

[76] Abdul-Wahab SA, Abu-Arabi MK, Zurigat YH. Effect of structured packing density on performance of air dehumidifier. Energy Conversion and Management 2004; 45: 2539-2552.

[77] Kessling W, Laevemann E, Kapfhammer C. Energy storage for desiccant cooling systems components development. Solar Energy 1998; 64: 209-221.

[78] Baccali M, Finocchiaro P, Nocke B. Energy and economic assessment of desiccant cooling systems coupled with single glazed air and hybrid PV/thermal solar collectors for applications in hot and humid climate. Solar Energy 2009; 83: 1828-1846.

[79] Li Y, Lu L, Yang H. Energy and economic performance analysis of an open cycle solar desiccant dehumidification air-conditioning system for application in Hong Kong. Solar Energy 2010; 84: 2085-2095.

[80] Baccali M, Finocchiaro P, Nocke B. Energy performance evaluation of a demo solar desiccant cooling system with heat recovery for the regeneration of the adsorption material. Renewable Energy 2012; 44: 40-52.

[81] Feldman D, Barbose G, Margolis W, Darghouth N, Goodrich A .U.S. Department of Energy. Photovoltaic (PV) pricing trends: Historical, Recent, and Near-Term Projection, 2012.

[82] Sen Z. Solar energy in progress and future research trends. Progress in Energy and Consumption Science 2004; 30: 367-416.

[83] Mittelman G, Kribus A, Dayan A. Solar cooling with concentrating photovoltaic/thermal (CPVT) systems. Energy Conversion and Management 2007; 48: 2481-2490.

[84] Vokas G, Christandonis N, Skittides F. Hybrid photovoltaic-thermal systems for domestic heating and cooling-A theoretical approach. Solar Energy 2006; 80: 607-615.

[85] Keliang L, Jie J, Tin-tai C, Gang P, Hanfeng H, Aiguo J, Jichun Y. Performance study of a photovoltaic solar assisted heat pump with variable-frequency compressor- A case study in Tibet. Renewable Energy 2009; 34 2680-2687.

[86] Wolf M. Performance analysis of combined heating and photovoltaic power systems for residences. Energy Conversion and Management 1976; 16: 79-90.

[87] Fu HD, Pei G, Ji J, Long H, Zhang T, Chow TT. Experimental study of a photovoltaic solar-assisted heat pump/ heat –pipe system. Applied Thermal Engineering 2012; 40: 343-350.

[88] Ha QP, Vakiloroaya V. A New Single-Effect Hot-Water Absorption Chiller Air Conditioning Using Solar Energy. Australasian Universities Power Engineering Conference (AUPEC), Hobart, Australia, 2013.

[89] International Energy Agency (IEA). Technology roadmap: Solar photovoltaic energy, 2010.

[90] Hartman N, Glueck C, Schmidt FP. Solar cooling for small office buildings: Comparison of solar thermal and photovoltaic options for two different European climates. Renewable Energy 2011; 36: 1329-1338.

[91] Sukamongkol Y, Chungpaibulpatana S, Limmeechokchai B, Sripadungtham P. Condenser heat recovery with a PV/T air heating collector to regenerate desiccant for reducing energy use of an air conditioning room. Energy and Buildings 2010; 42: 315-325.

[92] Chen X, Omer S, Worall M, Riffat S. Recent developments in ejector refrigeration technologies. Renewable and Sustainable Energy Reviews 2013; 19: 629-651.

[93] Elbel S, Hrnjak P. Ejector Refrigeration: An Overview of Historical and Present Developments with an Emphasis on Air-Conditioning Applications. International Refrigeration and Air Conditioning Conference, Purdue, USA, July 14-17, 2008.

[94] Cardemil JM. Colle S. A general model for evaluation of vapor ejectors performance for application in refrigeration. Energy Conversion and Management 2012; 64: 79-86.

[95] Yapici R. Yetisen. Experimental study on ejector refrigeration system powered by low grade heat. Energy Conversion and Management 2007; 48: 1560-1568.

[96] Allouche Y. Bouden C. Riffat S. A solar-driven ejector refrigeration system for Mediterranean climate: Experience improvement and new results performed. Energy Procedia 2012; 18: 1115-1124.

[97] Vidal H. Colle S. Pereira GDS. Modelling and hourly simulation of a solar ejector cooling system. Applied Thermal Engineering 2006: 26: 663-672.

[98] Huang BJ. Chang JM. Wang CP. Petrenko VA. A 1-D analysis of ejector performance. International Journal of Refrigeration 1999; 22: 354-364.

[99] Chesi A, Ferrara G, Ferrari L, Tarani F. Analysis of a solar assisted vapour compression cooling system. Renewable Energy 2013; 49: 48-52.

[100] Vakiloroaya V, Ha QP, Samali B. Energy-Efficient HVAC Systems: Simulation-Empirical Modelling and Gradient Optimization. Automation in Construction 2013; 31: 176-185.

[101] Vakiloroaya V, Madadnia J, and Samali B. Modeling and performance prediction of an integrated central cooling plant for HVAC energy efficiency improvement. Building Simulation: An International Journal 2013; 6: 127-138.

[102] Vakiloroaya V, Samali B, Pishghadam K. Investigation of Energy-Efficient Strategy for Direct Expansion Air-Cooled Air Conditioning Systems. Applied Thermal Engineering 2014; 66: 84-93.

[103] Al-Rabghi OM, Akyurt MM. A survey of energy efficient strategies for effective air conditioning. Energy Conversion and Management 2004; 45: 1643-1654.

[104] Fasiuddin M, Budaiwi I. HVAC system strategies for energy conversation in commercial buildings in Saudi Arabia. Energy and Buildings 2011; 43: 3457-3466.

[105] Lee SK, Teng MC, Fan KS, Yang KH, Horng RS. Application of an energy management system in combination with FMCS to high energy consuming IT industries of Taiwan. Energy Conversion and Management 2011; 52: 3060-3070.

[106] Plessis GED, Liebenberg L, Mathews EH, Plessis JND. A versatile energy management system for large integrated cooling system. Energy Conversion and Management 2013; 66: 312-325.

[107] Vakiloroaya V. Design optimization of the cooling coil for HVAC energy saving and comfort enhancement. Environment Progress and Sustainable Energy 2012; doi: 10.1002/ep.11729.

[108] Vakiloroaya V, and Madadnia J. Cooling Coil Design Improvement for HVAC Energy Savings and Comfort Enhancement. Sustainability in Energy and Buildings, Springer Berlin Heidelberg, Chapter 85, pp. 965-974, 2013.

[109] Sanaye S, Malekmohammadi HR. Thermal and economical optimization of air conditioning units with vapor compression refrigeration system. Applied Thermal Engineering 2004; 24: 1807-1825.

[110] Henning HM. Solar assisted air conditioning for buildings-an overview. Applied Thermal Engineering 2007; 27: 1734-1749.

[111] Wang RZ, Zhai XQ. Development of solar thermal technologies in China. Energy 2010; 35: 4407-4416.

[112] Li ZF, Sumathy K. Technology development in the solar absorption air-conditioning systems. Renewable and Sustainable Energy Review 2007; 4: 267-293.

[113] ANSI/ARI Standard 560, Absorption water chilling and water heating packages. Air Conditioning and Refrigeration Institute, US, 2000.

[114] ASHRAE Handbook Refrigeration. American Society of Heating, Refrigerating and Air-Conditioning Engineers 2002; Atlanta, GA, USA.

[115] Du S, Wang RZ, Lin P, Xu ZZ, Pan QW, Xu SC, Experimental studies on an air-cooled two-stage NH_3-H_2O solar absorption air-conditioning prototype. Energy 2010; 45: 581-587.

[116] Elsafty A, Al-Daini AJ. Economical comparison between a solar-powered vapour absorption air-conditioning system and a vapour compression system in the Middle East. Renewable Energy 2002; 25: 569-583.

[117] Romero RJ, Rivera W, Best R. Comparison of the theoretical performance of a solar air conditioning system operating with water/lithium bromide and an aqueous ternary hydroxide. Solar Energy Materials and Solar Cells 2000; 63: 387-399.

[118] Xu SM, Huang XD, Du R. An investigation of the solar powered absorption refrigeration system with advanced energy storage technology. Solar Energy 2011; 85: 1794-1804.

[119] Escriva EJS, Sivila EVL, Frances VMS, Air conditioning production by a single effect production cooling machine directly coupled to a solar collector field. Application to Spanish climates. Solar Energy 2011; 85: 2108-2121.

[120] Li ZF, Sumathy K. Simulation of a solar absorption air conditioning system. Energy Conversion and Management 2001; 42: 313-327.

[121] Molero-Villar N, Cejudo-Lopez JM, Domminguez-Munoz F, Carrillo-Andres A. A Comparison of solar absorption system configurations. Solar Energy 2012; 86: 242-252.

[122] Yin YL, Song ZP, Li Y, Wang RZ, Zhai XQ. Experimental investigation of a mini-type solar absorption cooling system under different cooling modes. Energy and Buildings 2012; 47: 131-138.

[123] ASHRAE Handbook Fundamentals. American Society of Heating, Refrigerating and Air-Conditioning Engineers 1972; Atlanta, GA, USA.

[124] ASHRAE Handbook Fundamentals. American Society of Heating, Refrigerating and Air-Conditioning Engineers 1977; Atlanta, GA, USA.

[125] TRNSYS software, A Transient System Simulation Program, version 16. Wisconsis-Madison University, USA, 2006. Available: <http://sell.me.wisc.edu/trnsys/>.

[126] ASHRAE Handbook Fundamentals. American Society of Heating, Refrigerating and Air-Conditioning Engineers 2009; Atlanta, GA, USA.

[127] Florides GA, Kalogirou SA, Tassou SA and Wrobel LC. Design and construction of a LiBr-water absorption machine. Energy Conversion and Management 2003; 44: 2483-2508.

[128] Rogers GFC and Mayhew YR. Thermodynamic and transport properties of fluids: SI units. Blackwell Publisher, 4th edition, UK. 1992.

[129] Lansing FL. Computer modelling of a single-stage lithium bromide/water absorption refrigeration unit. JPL Deep Space Network Progress Report, DSN 42-32, Jet Propulsion Laboratory, Pasadena, California, 1976; 247-257.

[130] Jeter SM, Lenard JLY, Teja AS. Properties of lithium bromide-water solutions at high temperatures and concentration. Part IV: Vapour pressure. ASHRAE Transactions 1992; 98: 167-172.

[131] Rockenfeller U. Laboratory results: Solution=LiBr-H2O, Properties= P-T-X, heat capacity. Rocky Research Inc, Boulder city 1987.

[132] McNeely LA. Thermodynamic properties of aqueous solutions of lithium bromide. ASHRAE Transactions 1979; 85: 413-434.

[133] Wilbur PJ, Mancint TR. A comparison of solar absorption air conditioning systems. Solar Energy 1976; 18: 569-576.

[134] Kaita Y. Thermodynamic properties of lithium bromide-water solutions at high temperatures. International Journal of Refrigeration 2001; 24: 374-390.

[135] Lee RJ, Diguilio RM, Jeter SM, Teja AS. Properties of lithium bromide-water solutions at high temperatures and concentration. Part II: Density and viscosity. ASHRAE Transactions 1990; 96: 709-728.

[136] Abdullagatov IM, Magomedov UB. Measurements of thermal conductivity of aqueous LiCl and LiBr solutions. Phys Chem 1997; 101 (4): 708-711.

[137] AIRAH Technical Handbook, Australian Institute of Refrigeration, Air conditioning and Heating, 4th Editing 2007; Melbourne, VIC, Australia.

[138] Ozisik MN. Heat transfer-a basic approach. McGraw-Hill Book Company 1985.

[139] Lienhard IV JH, Lienhard V JH. A Heat Transfer Text Book. 3th Edition, Phlogiston Press, 2008.

[140] Bejan A, Kraus AD. Heat Transfer Handbook. John Wiley & Sons INC, 2003.

[141] Lorenz JJ, Yung D. A note on combined boiling and evaporation of films on horizontal tubes. Journal of Heat Transfer 1979; 101: 178-180.

[142] Perry RH, Chilton CH. Chemical Engineer's Handbook. 5th Edition, Mc Graw-Hill, Chapter 12, 1973.

[143] Thome JR. Engineering Data Book. Laboratory of Heat and Mass Transfer, Faculty of Engineering Science and Technology, Swiss Federal Institute of Technology Lausanne, Switzerland, 2004.

[144] Stoecker WF, Jones JW. Refrigeration and Air Conditioning. 2nd Edition, Mc Graw-Hill, 1982.

[145] TRNSYS Mathematical Reference. Evacuated tube solar collector. Solar Energy Library, University of Wisconsin, Madison, USA, 2006.

[146] Braun JE. Methodologies for the design and control of chilled water systems. PhD thesis, University of Wisconsin, Madison, USA, 1988.

[147] Kalogirou S. Solar energy engineering: Processes and Systems. Elsevier Inc, USA, 2009.

[148] Praene JP, Garde F, Lucas F. Dynamic modeling and elements of validation of solar evacuated tube collectors. Ninth International IBSPA Conference, Montreal, Canada, 2005.

[149] TRNSYS Mathematical Reference. Solar Radiation Processor. Solar Energy Library, University of Wisconsin, Madison, USA, 2006.

[150] ANSI/ASHRAE Standard 140. Standard Method of Test for the Evaluation of Building Energy Analysis Computer Program. American Society of Heating, Refrigerating and Air-Conditioning, 2007.

[151] Kohlenbach P, Dennis M. Solar cooling in Australia: The future of air conditioning?. ECOLIBRIUM Journal, Australian Institute of Refrigeration, Air Conditioning and Heating, December 2010: 32-38.

[152] Vakiloroaya V, Samali B, Pishghadam K. A comparative Study on the Effect of Different Strategies for Energy Saving of Air-Cooled Vapor Compression Air Conditioning System. Energy and Buildings 2014; 74: 163-172.

APPENDIX 1: ABSYS SOFTWATER DESCRIPTION AND CODE

A steady state computer code, ABsorption SYstem Simulation (ABSYS), has been developed for simulation of the single-effect absorption chiller to predict the performance of the chiller using LiBr-water as the working pair. The model is based on detailed mass and energy balances and heat transfer relationship for the cycle components as described in chapter 4 and 6. The effect of various operating conditions on the performance of the individual chiller components was then investigated using ABSYS as presented in chapters 5 and 7. Thermodynamic properties of the water and LiBr-water solution has been incorporated in the code. The program is a user-friendly windows version which provides the schematic diagram of the designed operation cycle based on the user input data on the computer screen and make it possible to observe the results superimposed on the cycle diagram and plot it. ABSYS has been written under visual basic (VB) programming language and user does not have to do any programming. After entering the input data by user, the coded equations are solved so that mathematically valid results that are not physically valid are eliminated. Using this tool, the operation cycle of the single-effect absorption chiller is first calculated and then based on heat transfer models, the generator, evaporator, condenser, absorber and solution heat exchanger are designed. Results can be used for the real construction of the chiller as it has been carried out in this study. During the calculation, a change in any input variable results in changes in all the other related variables. When an input changes, the entire operation cycle reacts to reach a new equilibrium operating conditions. In this appendix the schematic diagram of each heat exchanger, temperature patterns and ABSYS work space are first shown and then the program code is presented.

Appendix1-1 Generator:

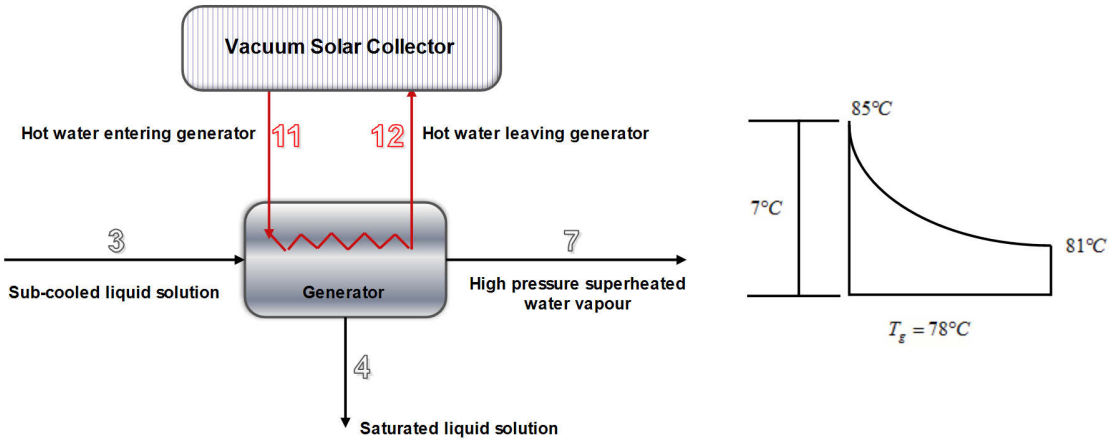

Fig. 1 Left: Schematic diagram of generator, Right: Temperature patterns along generator for this study

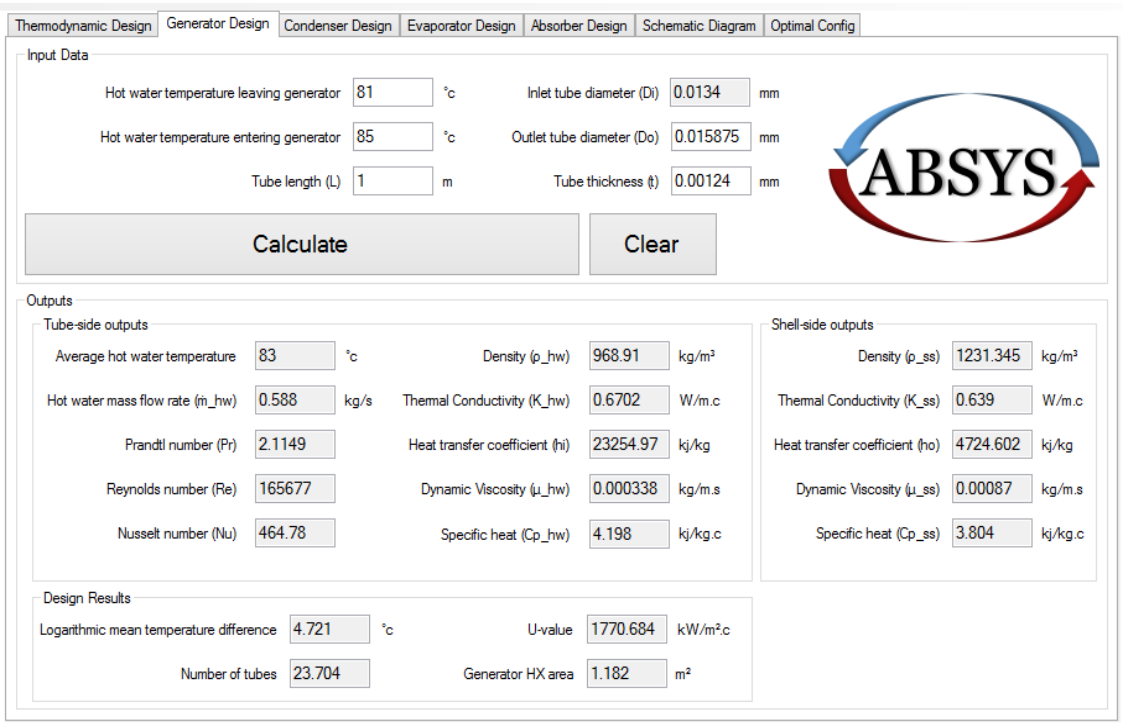

Fig. 2 ABSYS work space and design data for generator

Appendix1-2 Condenser:

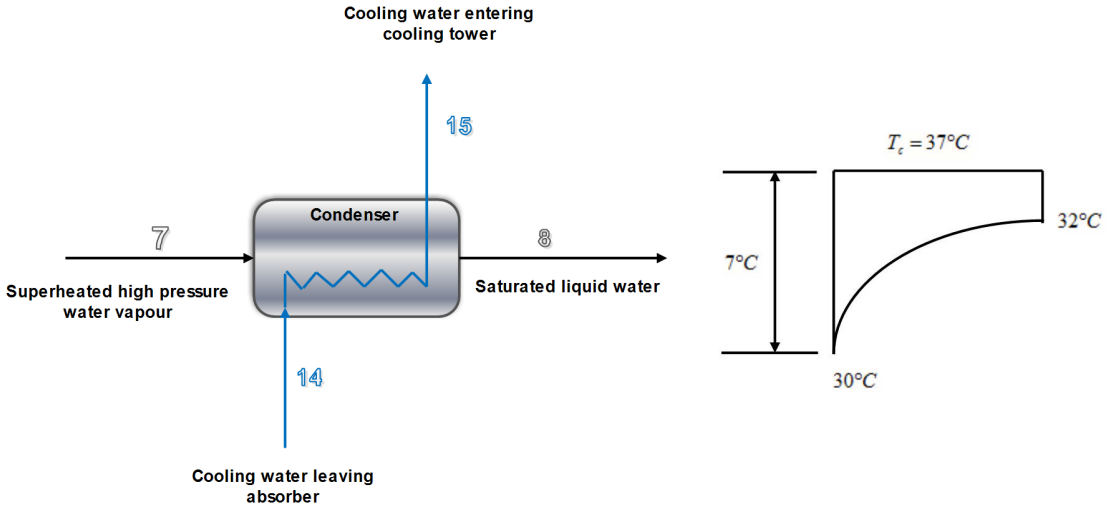

Fig. 3 Left: Schematic diagram of condenser, Right: Temperature patterns along condenser for this study

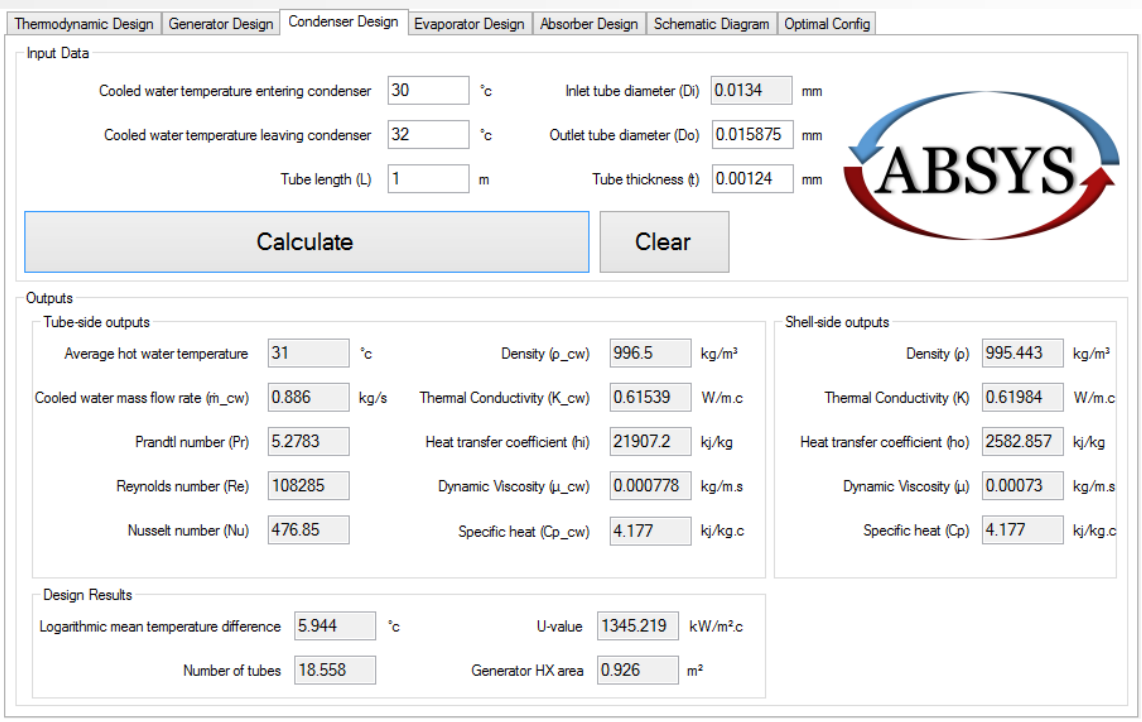

Fig. 4 ABSYS work space and design data for condenser

Appendix1-3 Evaporator:

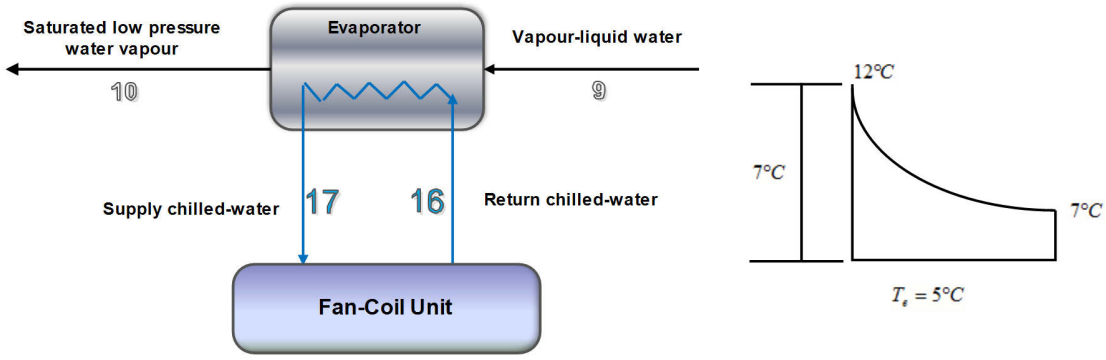

Fig. 5 Left: Schematic diagram of evaporator, Right: Temperature patterns along evaporator for this study

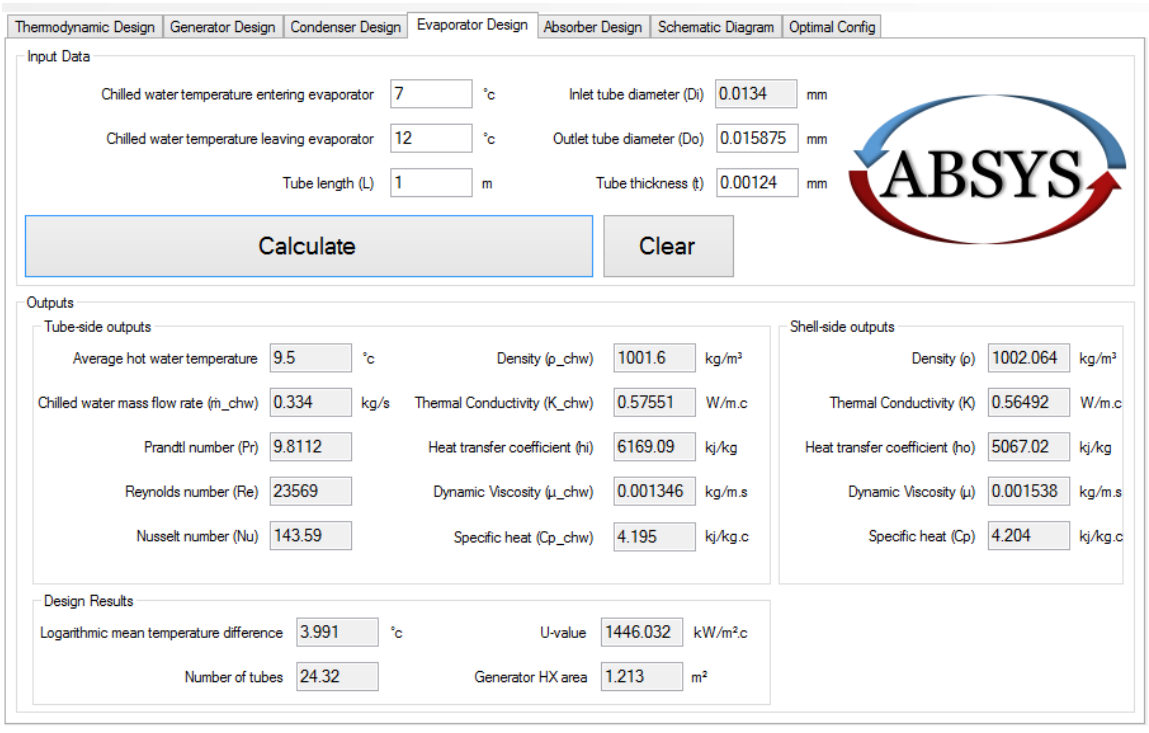

Fig. 6 ABSYS work space and design data for evaporator

Appendix1-4 Absorber:

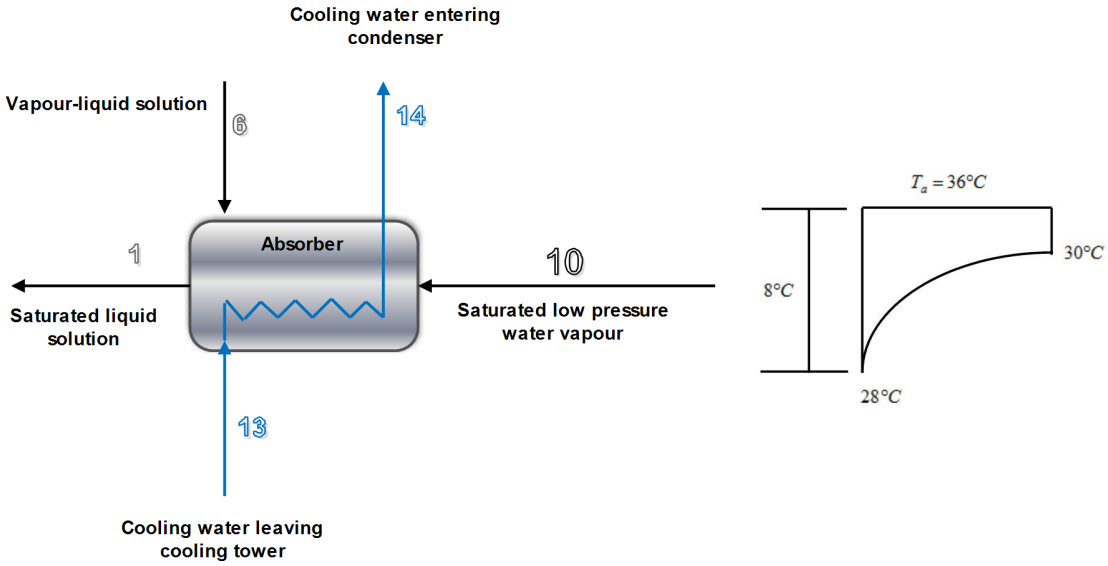

Fig. 7 Left: Schematic diagram of absorber, Right: Temperature patterns along absorber for this study

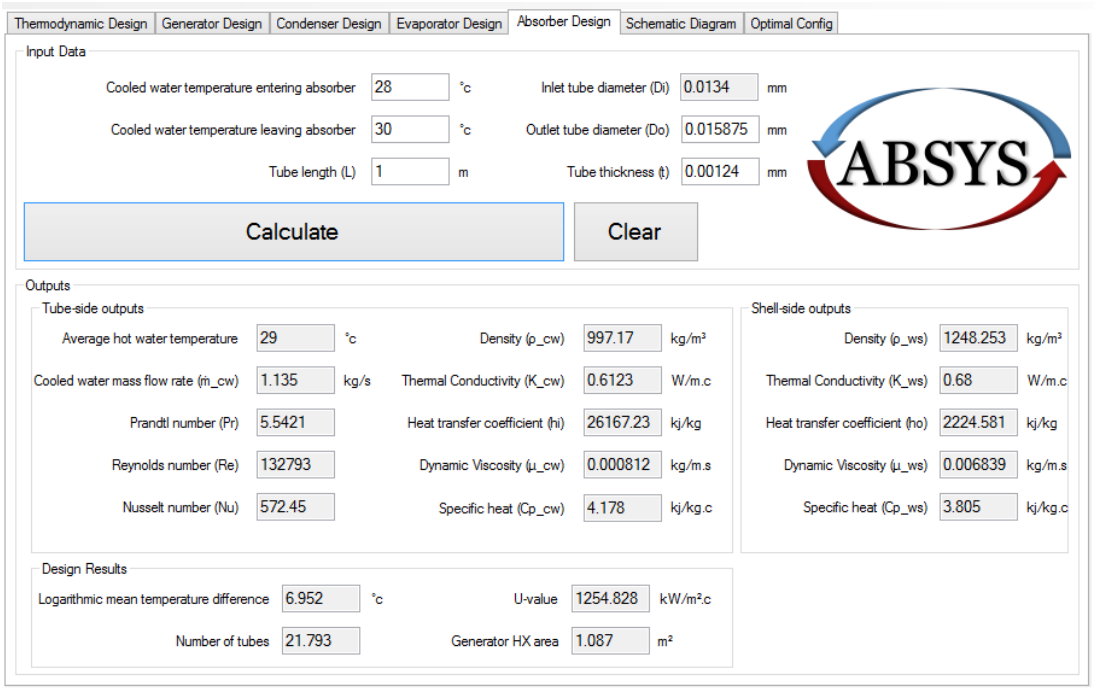

Fig. 8 ABSYS work space and design data for absorber

Appendix1-5 Schematic Diagram in ABSYS:

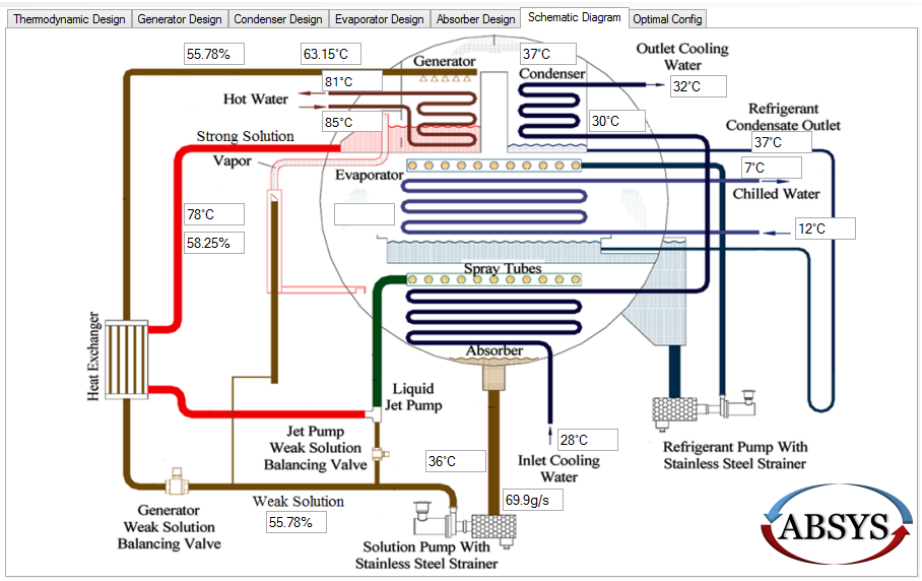

Fig. 9 Schematic diagram of the single-effect absorption cooling system in ABSYS work space

Appendix1-6 Derived Possible Combinations for Absorption Chiller Using ABSYS:

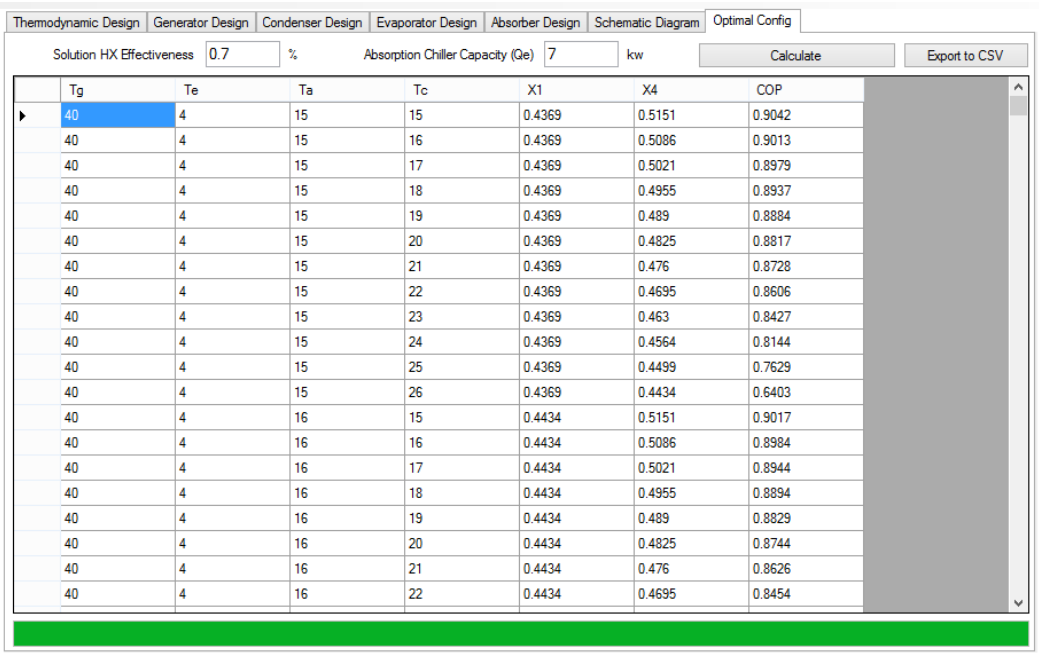

Tg	Te	Ta	Tc	X1	X4	COP
40	4	15	15	0.4369	0.5151	0.9042
40	4	15	16	0.4369	0.5086	0.9013
40	4	15	17	0.4369	0.5021	0.8979
40	4	15	18	0.4369	0.4955	0.8937
40	4	15	19	0.4369	0.489	0.8884
40	4	15	20	0.4369	0.4825	0.8817
40	4	15	21	0.4369	0.476	0.8728
40	4	15	22	0.4369	0.4695	0.8606
40	4	15	23	0.4369	0.463	0.8427
40	4	15	24	0.4369	0.4564	0.8144
40	4	15	25	0.4369	0.4499	0.7629
40	4	15	26	0.4369	0.4434	0.6403
40	4	16	15	0.4434	0.5151	0.9017
40	4	16	16	0.4434	0.5086	0.8984
40	4	16	17	0.4434	0.5021	0.8944
40	4	16	18	0.4434	0.4955	0.8894
40	4	16	19	0.4434	0.489	0.8829
40	4	16	20	0.4434	0.4825	0.8744
40	4	16	21	0.4434	0.476	0.8626
40	4	16	22	0.4434	0.4695	0.8454

Fig. 10 Derived possible combinations in ABSYS work space

Thermodynamic Design Code:

```
Tg_Thermo = txtTg_Thermo.Text
Tc_Thermo = txtTc_Thermo.Text
Te_Thermo = txtTe_Thermo.Text
Ta_Thermo = txtTa_Thermo.Text
Qe_Thermo = txtQe_Thermo.Text
HX_Thermo = txtEFF_HX_Thermo.Text

X1_Thermo = (49.04 + 1.125 * Ta_Thermo - Te_Thermo) / (134.65 + 0.47 * Ta_Thermo)
X4_Thermo = (49.04 + 1.125 * Tg_Thermo - Tc_Thermo) / (134.65 + 0.47 * Tg_Thermo)
h8_Thermo = 4.187 * (Tc_Thermo - 25)
h10_Thermo = 4.187 * (572.8 + 0.417 * Te_Thermo)
m_ref_Thermo = Qe_Thermo / (h10_Thermo - h8_Thermo)
m_ss_Thermo = m_ref_Thermo * (X4_Thermo / (X4_Thermo - X1_Thermo))
m_ws_Thermo = m_ref_Thermo * X1_Thermo / (X4_Thermo - X1_Thermo)
C_x1_Thermo = 4.187 * (1.01 - 1.23 * X1_Thermo + 0.48 * X1_Thermo ^ 2)
C_x4_Thermo = 4.187 * (1.01 - 1.23 * X4_Thermo + 0.48 * X4_Thermo ^ 2)
T3_Thermo = Ta_Thermo + (HX_Thermo * (X1_Thermo / X4_Thermo) * (C_x4_Thermo / C_x1_Thermo) *
(Tg_Thermo - Ta_Thermo))
T5_Thermo = Tg_Thermo - HX_Thermo * (Tg_Thermo - Ta_Thermo)
h1_Thermo = (C_x1_Thermo * Ta_Thermo) + 4.187 * (42.81 - 425.92 * X1_Thermo + 404.67 * X1_Thermo ^ 2)
h5_Thermo = (C_x4_Thermo * T5_Thermo) + 4.187 * (42.81 - 425.92 * X4_Thermo + 404.67 * X4_Thermo ^ 2)
h7_Thermo = 4.187 * (572.8 + 0.46 * Tg_Thermo - 0.043 * Tc_Thermo)
Qc_Thermo = m_ref_Thermo * (h7_Thermo - h8_Thermo)
Qa_Thermo = m_ws_Thermo * h5_Thermo + m_ref_Thermo * h10_Thermo - m_ss_Thermo * h1_Thermo
Qg_Thermo = m_ws_Thermo * h5_Thermo + m_ref_Thermo * h7_Thermo - m_ss_Thermo * h1_Thermo
COP_Thermo = Qe_Thermo / Qg_Thermo
COP_max_Thermo = ((Te_Thermo + 273.15) * (Tg_Thermo - Ta_Thermo)) / ((Tg_Thermo + 273.15) *
(Tc_Thermo - Te_Thermo))
η_Thermo = COP_Thermo / COP_Max_Thermo
Pe_Thermo = 10 ^ (7.8553 - (1555 / (Te_Thermo + 273.15)) - (112414 / (Te_Thermo + 273.15) ^ 2))
Pc_Thermo = 10 ^ (7.8553 - (1555 / (Tc_Thermo + 273.15)) - (112414 / (Tc_Thermo + 273.15) ^ 2))

txtX1_Thermo.Text = Math.Round(X1_Thermo, 4)
txtX4_Thermo.Text = Math.Round(X4_Thermo, 4)

'h8=h9
txtH8_Thermo.Text = Math.Round(h8_Thermo, 2)
txtH9_Thermo.Text = txtH8_Thermo.Text

txtH10_Thermo.Text = Math.Round(h10_Thermo, 2)
txtMref_Thermo.Text = Math.Round(m_ref_Thermo, 5)
txtMss_Thermo.Text = Math.Round(m_ss_Thermo, 5)
txtMws_Thermo.Text = Math.Round(m_ws_Thermo, 5)
txtPe_Thermo.Text = Math.Round(Pe_Thermo, 4)
txtPc_Thermo.Text = Math.Round(Pc_Thermo, 4)
txtT3_Thermo.Text = Math.Round(T3_Thermo, 2)
txtT5_Thermo.Text = Math.Round(T5_Thermo, 2)
txtH1_Thermo.Text = Math.Abs(Math.Round(h1_Thermo, 2))

'h5=h6
txtH5_Thermo.Text = Math.Abs(Math.Round(h5_Thermo, 2))
```

```
txtH6_Thermo.Text = txtH5_Thermo.Text

txtH7_Thermo.Text = Math.Round(h7_Thermo, 2)
txtQc_Thermo.Text = Math.Round(Qc_Thermo, 3)
txtQg_Thermo.Text = Math.Round(Qg_Thermo, 3)
txtQa_Thermo.Text = Math.Round(Qa_Thermo, 3)
txtQe_Output_Thermo.Text = Math.Round(Qe_Thermo, 3)
txtCOP_Thermo.Text = Math.Round(COP_Thermo, 3)
txtCOPmax_Thermo.Text = Math.Round(COP_Max_Thermo, 3)
txtη_Thermo.Text = Math.Round(η_Thermo, 2)

'Schematic Presentation
txtXws_Sch_1.Text = Convert.ToString(Math.Round(X1_Thermo, 4) * 100) & "%"
txtXws_Sch_2.Text = Convert.ToString(Math.Round(X1_Thermo, 4) * 100) & "%"
txtXss_Sch.Text = Convert.ToString(Math.Round(X4_Thermo, 4) * 100) & "%"
txtT3_Sch.Text = Convert.ToString(Math.Round(T3_Thermo, 2)) & "°C"
txtTc_Sch_1.Text = Math.Round(Tc_Thermo, 2) & "°C"
txtTc_Sch_2.Text = Math.Round(Tc_Thermo, 2) & "°C"
txtTa_Sch.Text = Math.Round(Ta_Thermo, 2) & "°C"
txtTg_Sch.Text = Math.Round(Tg_Thermo, 2) & "°C"
txtM_ss_Sch.Text = Math.Round(m_ss_Thermo, 4) * 1000 & "g/s"
```

Generator Design Code:

```
'tube-side calculations
Di_Gen = Do_Gen - 2 * t_Gen
T_aveg_Gen = (T_hw_i_Gen + T_hw_o_Gen) / 2
μ_hw_Gen = 0.000001 * (0.000031538716146 * T_aveg_Gen ^ 4 - 8.91305542819999 * 0.001 *
T_aveg_Gen ^ 3 + 0.9795876934 * T_aveg_Gen * T_aveg_Gen - 55.4567974 * T_aveg_Gen + 1791.74424)
ρ_hw_Gen = 0.000015451 * T_aveg_Gen * T_aveg_Gen * T_aveg_Gen - 0.0059003 * T_aveg_Gen *
T_aveg_Gen - 0.019075 * T_aveg_Gen + 1002.3052
Cp_ts_Gen = ((0.000003216145833 * T_aveg_Gen ^ 4) - (0.000798668982 * T_aveg_Gen ^ 3) +
(0.0780295139 * T_aveg_Gen ^ 2) - (3.0481614 * T_aveg_Gen) + 4217.7377) / 1000
K_hw_Gen = -0.00000000065104167 * T_aveg_Gen ^ 4 + 0.00000018923611 * T_aveg_Gen ^ 3 -
0.00002671875 * T_aveg_Gen * T_aveg_Gen + 0.0027103175 * T_aveg_Gen + 0.5520119
Pr_Gen = (Cp_ts_Gen * μ_hw_Gen / K_hw_Gen) * 1000
m_hw_Gen = Qg_Thermo / (Cp_ts_Gen * (T_hw_o_Gen - T_hw_i_Gen))
Ai_Gen = (3.1415 / 4) * Di_Gen * Di_Gen
Re_Gen = (m_hw_Gen * Di_Gen) / (Ai_Gen * μ_hw_Gen)
Nu_Gen = 0.023 * (Re_Gen ^ 0.8) * (Pr_Gen ^ 0.4)
hi_Gen = Nu_Gen * K_hw_Gen / Di_Gen

'shell-side calculations
K_cooper_Gen = 0.000000004583333 * Tg_Thermo ^ 4 - 0.000002916667 * Tg_Thermo ^ 3 +
0.0006541667 * Tg_Thermo ^ 2 - 0.1108333 * Tg_Thermo + 386
ρ_ss_Gen = 1145.36 + 470.84 * X4_Thermo + 134.79 * X4_Thermo * X4_Thermo - (0.333393 + 0.571749 *
X4_Thermo) * (273.15 + Tg_Thermo)
Cp_ss_Gen = (0.0976 * X4_Thermo * X4_Thermo - 37.512 * X4_Thermo + 3825.4) / 1000
Constant_Gen = m_ws_Thermo / (2 * 1)
Density_Gen = 1145.36 + 470.84 * X4_Thermo + 134.79 * X4_Thermo * X4_Thermo - (0.333393 +
0.571749 * X4_Thermo) * (273.15 + Tg_Thermo)
A1_Gen = -494.122 + 16.3967 * X4_Thermo - 0.14511 * X4_Thermo * X4_Thermo
A2_Gen = 28606.4 - 934.568 * X4_Thermo + 8.52755 * X4_Thermo * X4_Thermo
```

```
A3_Gen = 70.3848 - 2.35014 * X4_Thermo + 0.0207809 * X4_Thermo * X4_Thermo
K1_Gen = -0.3081 * (X4_Thermo / 100) + 0.62979
K2_Gen = -0.3191795 * (X4_Thermo / 100) + 0.65388
D12_Gen = ((K2_Gen - K1_Gen) / 20) * (T5_Thermo + 273.15 - 313)
K_ss_Gen = K1_Gen + D12_Gen
Alfa_Gen = K_ss_Gen / (Density_Gen * 1000 * Cp_ss_Gen)
Term1_Gen = (Constant_Gen ^ (4 / 3)) / (4 * 3.1415 * Density_Gen * Alfa_Gen)
B_Gen = A1_Gen + (A2_Gen / (273.15 + Tg_Thermo) + A3_Gen * Math.Log(273.15 + Tg_Thermo))
μ_ss_Gen = (2.71 ^ B_Gen) / 1000
Term2_Gen = ((3 * μ_ss_Gen) / (9.81 * Density_Gen * Density_Gen)) ^ 0.5
Ld_Gen = Term1_Gen * Term2_Gen
hd_Gen = 375 * Cp_ss_Gen * Constant_Gen / Ld_Gen
DynVisco_Gen = μ_ss_Gen / Density_Gen
hc_Gen = 0.8221 * (((K_ss_Gen * K_ss_Gen * K_ss_Gen * 9.81) / (DynVisco_Gen * DynVisco_Gen)) ^ (1 /
3)) * (4 * Constant_Gen / μ_ss_Gen) ^ -0.22
ho_Gen = hd_Gen * (Ld_Gen / 1) + hc_Gen * (1 - (Ld_Gen / 1))

'design results calculations
U_Gen = 1 / ((Do_Gen / Di_Gen) * (1 / hi_Gen) + (Do_Gen / Di_Gen) * 0.000176 + (1 / (2 *
K_cooper_Gen)) * Do_Gen * Math.Log(Do_Gen / Di_Gen) + 0.00009 + (1 / ho_Gen))
LMTD_Gen = ((Tg_Thermo - T_hw_i_Gen) - (Tg_Thermo - T_hw_o_Gen)) / Math.Log((Tg_Thermo -
T_hw_i_Gen) / (Tg_Thermo - T_hw_o_Gen)) * (-1)
Area_Gen = (Qg_Thermo / (U_Gen * LMTD_Gen)) * 1000
Tubes_Gen = Area_Gen / (3.1415 * Do_Gen * L_Gen)

txtDi_Gen.Text = Math.Round(Di_Gen, 5)

'tube-side data presentation
txtT_aveg_Gen.Text = Math.Round(T_aveg_Gen, 2)
txtμ_hw_Gen.Text = Math.Round(μ_hw_Gen, 6)
txtρ_hw_Gen.Text = Math.Round(ρ_hw_Gen, 2)
txtCp_ts_Gen.Text = Math.Round(Cp_ts_Gen, 3)
txtK_hw_Gen.Text = Math.Round(K_hw_Gen, 4)
txtPr_Gen.Text = Math.Round(Pr_Gen, 4)
txtm_hw_Gen.Text = Math.Round(m_hw_Gen, 3)
txtRe_Gen.Text = Math.Round(Re_Gen, 0)
txtNu_Gen.Text = Math.Round(Nu_Gen, 2)
txthi_Gen.Text = Math.Round(Hi_Gen, 2)

'shell-side data presentation
txtρ_ss_Gen.Text = Math.Round(ρ_ss_Gen, 3)
txtK_ss_Gen.Text = Math.Round(K_ss_Gen, 3)
txtho_Gen.Text = Math.Round(ho_Gen, 3)
txtμ_ss_Gen.Text = Math.Round(μ_ss_Gen, 6)
txtCp_ss_Gen.Text = Math.Round(Cp_ss_Gen, 3)

'design results data presentation
txtU_Gen.Text = Math.Round(U_Gen, 3)
txtLMTD_Gen.Text = Math.Round(LMTD_Gen, 3)
txtArea_Gen.Text = Math.Round(Area_Gen, 3)
txtTubes_Gen.Text = Math.Round(Tubes_Gen, 3)

'Shematic data presentation
txtI_Gen_Sch.Text = T_hw_i_Gen & "°C"
```

```
txtO_Gen_Sch.Text = T_hw_o_Gen & "°C"
```

Condenser Design Code:

```
'tube-side calculations
Di_Con = Do_Con - 2 * t_Con
T_aveg_ts_Con = (T_cw_i_Con + T_cw_o_Con) / 2
μ_cw_Con = 0.000001 * (0.000031538716146 * T_aveg_ts_Con ^ 4 - 8.91305542819999 * 0.001 *
T_aveg_ts_Con ^ 3 + 0.9795876934 * T_aveg_ts_Con * T_aveg_ts_Con - 55.4567974 * T_aveg_ts_Con +
1791.74424)
ρ_cw_Con = 0.000015451 * T_aveg_ts_Con * T_aveg_ts_Con * T_aveg_ts_Con - 0.0059003 *
T_aveg_ts_Con * T_aveg_ts_Con - 0.019075 * T_aveg_ts_Con + 1002.3052
Cp_ts_Con = ((0.000003216145833 * T_aveg_ts_Con ^ 4) - (0.000798668982 * T_aveg_ts_Con ^ 3) +
(0.0780295139 * T_aveg_ts_Con ^ 2) - (3.0481614 * T_aveg_ts_Con) + 4217.7377) / 1000
K_cw_Con = -0.00000000065104167 * T_aveg_ts_Con ^ 4 + 0.00000018923611 * T_aveg_ts_Con ^ 3 -
0.00002671875 * T_aveg_ts_Con * T_aveg_ts_Con + 0.0027103175 * T_aveg_ts_Con + 0.5520119
Pr_ts_Con = (Cp_ts_Con * μ_cw_Con / K_cw_Con) * 1000
m_cw_ts_Con = Qc_Thermo / (Cp_ts_Con * (T_cw_o_Con - T_cw_i_Con))
Ai_Con = (3.1415 / 4) * Di_Con * Di_Con
Re_Con = (m_cw_ts_Con * Di_Con) / (Ai_Con * μ_cw_Con)
Nu_Con = 0.023 * (Re_Con ^ 0.8) * (Pr_ts_Con ^ 0.4)
hi_Con = Nu_Con * K_cw_Con / Di_Con

'shell-side calculations
T_aveg_ss_Con = (Tc_Thermo + T_aveg_ts_Con) / 2
μ_ss_Con = 0.000001 * (0.000031538716146 * T_aveg_ss_Con ^ 4 - 8.91305542819999 * 0.001 *
T_aveg_ss_Con ^ 3 + 0.9795876934 * T_aveg_ss_Con * T_aveg_ss_Con - 55.4567974 * T_aveg_ss_Con +
1791.74424)
ρ_ss_Con = 0.000015451 * T_aveg_ss_Con * T_aveg_ss_Con * T_aveg_ss_Con - 0.0059003 *
T_aveg_ss_Con * T_aveg_ss_Con - 0.019075 * T_aveg_ss_Con + 1002.3052
Cp_ss_Con = ((0.000003216145833 * T_aveg_ss_Con ^ 4) - (0.000798668982 * T_aveg_ss_Con ^ 3) +
(0.0780295139 * T_aveg_ss_Con ^ 2) - (3.0481614 * T_aveg_ss_Con) + 4217.7377) / 1000
K_ss_Con = -0.00000000065104167 * T_aveg_ss_Con ^ 4 + 0.00000018923611 * T_aveg_ss_Con ^ 3 -
0.00002671875 * T_aveg_ss_Con * T_aveg_ss_Con + 0.0027103175 * T_aveg_ss_Con + 0.5520119
Pr_ss_Con = (Cp_ss_Con * μ_ss_Con / K_ss_Con) * 1000
m_cw_ts_Con = Qc_Thermo / (Cp_ss_Con * (T_cw_o_Con - T_cw_i_Con))
VapourDensity_Con = 1 / (0.00001147965 * T_aveg_ss_Con ^ 4 - 0.00297197798 * T_aveg_ss_Con ^ 3 +
0.28077931731 * T_aveg_ss_Con * T_aveg_ss_Con - 11.83083758 * T_aveg_ss_Con + 202.9035477661)
h_fg_Con = -0.00132635 * T_aveg_ss_Con * T_aveg_ss_Con - 2.29983657 * T_aveg_ss_Con + 2500.43063
ho_Con = 0.725 * ((9.81 * ρ_ss_Con * (ρ_ss_Con - VapourDensity_Con) * h_fg_Con * K_ss_Con *
K_ss_Con * K_ss_Con) / (μ_ss_Con * (T_aveg_ss_Con - T_aveg_ts_Con) * Do_Con)) ^ 0.25
K_cooper_Con = 0.000000004583333 * T_aveg_ss_Con ^ 4 - 0.000002916667 * T_aveg_ss_Con ^ 3 +
0.0006541667 * T_aveg_ss_Con ^ 2 - 0.1108333 * T_aveg_ss_Con + 386

'design results calculations
U_Con = 1 / ((Do_Con / Di_Con) * (1 / hi_Con) + (Do_Con / Di_Con) * 0.000176 + (1 / (2 *
K_cooper_Con)) * Do_Con * Math.Log(Do_Con / Di_Con) + 0.00009 + (1 / ho_Con))
LMTD_Con = ((Tc_Thermo - T_cw_i_Con) - (Tc_Thermo - T_cw_o_Con)) / Math.Log((Tc_Thermo -
T_cw_i_Con) / (Tc_Thermo - T_cw_o_Con))
Area_Con = (Qc_Thermo / (U_Con * LMTD_Con)) * 1000
Tubes_Con = Area_Con / (3.1415 * Do_Con * L_Con)

txtDi_Con.Text = Math.Round(Di_Con, 5)
```

```
'tube-side data presentation
txtT_aveg_Con.Text = Math.Round(T_aveg_ts_Con, 2)
txtμ_cw_Con.Text = Math.Round(μ_cw_Con, 6)
txtρ_cw_Con.Text = Math.Round(ρ_cw_Con, 2)
txtCp_ts_Con.Text = Math.Round(Cp_ts_Con, 3)
txtK_cw_Con.Text = Math.Round(K_cw_Con, 5)
txtPr_Con.Text = Math.Round(Pr_ts_Con, 4)
txtM_cw_Con.Text = Math.Round(m_cw_ts_Con, 3)
txtRe_Con.Text = Math.Round(Re_Con, 0)
txtNu_Con.Text = Math.Round(Nu_Con, 2)
txtHi_Con.Text = Math.Round(Hi_Con, 2)

'shell-side data presentation
txtρ_ss_Con.Text = Math.Round(ρ_ss_Con, 3)
txtK_ss_Con.Text = Math.Round(K_ss_Con, 5)
txtHo_Con.Text = Math.Round(ho_Con, 3)
txtμ_ss_Con.Text = Math.Round(μ_ss_Con, 6)
txtCp_ss_Con.Text = Math.Round(Cp_ss_Con, 3)

'design results data presentation
txtU_Con.Text = Math.Round(U_Con, 3)
txtLMTD_Con.Text = Math.Round(LMTD_Con, 3)
txtArea_Con.Text = Math.Round(Area_Con, 3)
txtTubes_Con.Text = Math.Round(Tubes_Con, 3)

'Schematic presentation
txtI_Con_Sch.Text = T_cw_i_Con & "°C"
txtO_Con_Sch.Text = T_cw_o_Con & "°C"
```

Evaporator Design Code:

```
'tube-side calculations
Di_Eva = Do_Eva - 2 * t_Eva
T_aveg_ts_Eva = (T_chw_i_Eva + T_chw_o_Eva) / 2
μ_chw_Eva = 0.000001 * (0.000031538716146 * T_aveg_ts_Eva ^ 4 - 8.91305542819999 * 0.001 *
T_aveg_ts_Eva ^ 3 + 0.9795876934 * T_aveg_ts_Eva * T_aveg_ts_Eva - 55.4567974 * T_aveg_ts_Eva +
1791.74424)
ρ_chw_Eva = 0.000015451 * T_aveg_ts_Eva * T_aveg_ts_Eva * T_aveg_ts_Eva - 0.0059003 *
T_aveg_ts_Eva * T_aveg_ts_Eva - 0.019075 * T_aveg_ts_Eva + 1002.3052
Cp_ts_Eva = ((0.000003216145833 * T_aveg_ts_Eva ^ 4) - (0.000798668982 * T_aveg_ts_Eva ^ 3) +
(0.0780295139 * T_aveg_ts_Eva ^ 2) - (3.0481614 * T_aveg_ts_Eva) + 4217.7377) / 1000
K_chw_Eva = -0.00000000065104167 * T_aveg_ts_Eva ^ 4 + 0.00000018923611 * T_aveg_ts_Eva ^ 3 -
0.00002671875 * T_aveg_ts_Eva * T_aveg_ts_Eva + 0.0027103175 * T_aveg_ts_Eva + 0.5520119
Pr_ts_Eva = (Cp_ts_Eva * μ_chw_Eva / K_chw_Eva) * 1000
m_chw_ts_Eva = Qe_Thermo / (Cp_ts_Eva * (T_chw_o_Eva - T_chw_i_Eva))
Ai_Eva = (3.1415 / 4) * Di_Eva * Di_Eva
Re_Eva = (m_chw_ts_Eva * Di_Eva) / (Ai_Eva * μ_chw_Eva)
Nu_Eva = 0.023 * (Re_Eva ^ 0.8) * (Pr_ts_Eva ^ 0.3)
hi_Eva = Nu_Eva * K_chw_Eva / Di_Eva

'shell-side calculations
Constant_Eva = m_ref_Thermo / (2 * L_Eva)
```

```
μ_ss_Eva = 0.000001 * (0.000031538716146 * Te_Thermo ^ 4 - 8.91305542819999 * 0.001 * Te_Thermo ^
3 + 0.9795876934 * Te_Thermo * Te_Thermo - 55.4567974 * Te_Thermo + 1791.74424)
ρ_ss_Eva = 0.000015451 * Te_Thermo * Te_Thermo * Te_Thermo - 0.0059003 * Te_Thermo * Te_Thermo
- 0.019075 * Te_Thermo + 1002.3052
Cp_ss_Eva = ((0.000003216145833 * Te_Thermo ^ 4) - (0.000798668982 * Te_Thermo ^ 3) +
(0.0780295139 * Te_Thermo ^ 2) - (3.0481614 * Te_Thermo) + 4217.7377) / 1000
K_ss_Eva = -0.00000000065104167 * Te_Thermo ^ 4 + 0.00000018923611 * Te_Thermo ^ 3 -
0.00002671875 * Te_Thermo * Te_Thermo + 0.0027103175 * Te_Thermo + 0.5520119
Pr_ss_Eva = (Cp_ss_Eva * μ_ss_Eva / K_ss_Eva) * 1000
DynViscosity_Eva = μ_ss_Eva / ρ_ss_Eva
ho_Eva = 0.8221 * ((K_ss_Eva * K_ss_Eva * K_ss_Eva * 9.81) / (DynViscosity_Eva * DynViscosity_Eva))
^ 0.33 * (4 * Constant_Eva / μ_ss_Eva) ^ -0.22
K_cooper_Eva = 0.000000004583333 * Te_Thermo ^ 4 - 0.000002916667 * Te_Thermo ^ 3 + 0.0006541667
* Te_Thermo ^ 2 - 0.1108333 * Te_Thermo + 386

'design results calculations
U_Eva = 1 / ((Do_Eva / Di_Eva) * (1 / Hi_Eva) + (Do_Eva / Di_Eva) * 0.000176 + (1 / (2 * K_cooper_Eva))
* Do_Eva * Math.Log(Do_Eva / Di_Eva) + 0.00009 + (1 / ho_Eva))
LMTD_Eva = ((Te_Thermo - T_chw_i_Eva) - (Te_Thermo - T_chw_o_Eva)) / Math.Log((Te_Thermo -
T_chw_i_Eva) / (Te_Thermo - T_chw_o_Eva)) * (-1)
Area_Eva = (Qe_Thermo / (U_Eva * LMTD_Eva)) * 1000
Tubes_Eva = Area_Eva / (3.1415 * Do_Eva * L_Eva)

txtDi_Eva.Text = Math.Round(Di_Eva, 5)

'tube-side data presentation
txtT_aveg_Eva.Text = Math.Round(T_aveg_ts_Eva, 2)
txtμ_chw_Eva.Text = Math.Round(μ_chw_Eva, 6)
txtρ_chw_Eva.Text = Math.Round(ρ_chw_Eva, 2)
txtCp_ts_Eva.Text = Math.Round(Cp_ts_Eva, 3)
txtK_chw_Eva.Text = Math.Round(K_chw_Eva, 5)
txtPr_Eva.Text = Math.Round(Pr_ts_Eva, 4)
txtm_chw_Eva.Text = Math.Round(m_chw_ts_Eva, 3)
txtRe_Eva.Text = Math.Round(Re_Eva, 0)
txtNu_Eva.Text = Math.Round(Nu_Eva, 2)
txtHi_Eva.Text = Math.Round(Hi_Eva, 2)

'shell-side data presentation
txtρ_ss_Eva.Text = Math.Round(ρ_ss_Eva, 3)
txtK_ss_Eva.Text = Math.Round(K_ss_Eva, 5)
txtho_Eva.Text = Math.Round(ho_Eva, 3)
txtμ_ss_Eva.Text = Math.Round(μ_ss_Eva, 6)
txtCp_ss_Eva.Text = Math.Round(Cp_ss_Eva, 3)

'design results data presentation
txtU_Eva.Text = Math.Round(U_Eva, 3)
txtLMTD_Eva.Text = Math.Round(LMTD_Eva, 3)
txtArea_Eva.Text = Math.Round(Area_Eva, 3)
txtTubes_Eva.Text = Math.Round(Tubes_Eva, 3)

'Schematic presentation
txtI_Eva_Sch.Text = T_chw_i_Eva & "°C"
txtO_Eva_Sch.Text = T_chw_o_Eva & "°C"
```

Absorber Design Code:

```
'tube-side calculations
Di_Abs = Do_Abs - 2 * t_Abs
T_aveg_Abs = (T_cw_i_Abs + T_cw_o_Abs) / 2
μ_cw_Abs = 0.000001 * (0.000031538716146 * T_aveg_Abs ^ 4 - 8.91305542819999 * 0.001 *
T_aveg_Abs ^ 3 + 0.9795876934 * T_aveg_Abs * T_aveg_Abs - 55.4567974 * T_aveg_Abs + 1791.74424)
ρ_cw_Abs = 0.000015451 * T_aveg_Abs * T_aveg_Abs * T_aveg_Abs - 0.0059003 * T_aveg_Abs *
T_aveg_Abs - 0.019075 * T_aveg_Abs + 1002.3052
Cp_ts_Abs = ((0.000003216145833 * T_aveg_Abs ^ 4) - (0.000798668982 * T_aveg_Abs ^ 3) +
(0.0780295139 * T_aveg_Abs ^ 2) - (3.0481614 * T_aveg_Abs) + 4217.7377) / 1000
K_cw_Abs = -0.00000000065104167 * T_aveg_Abs ^ 4 + 0.00000018923611 * T_aveg_Abs ^ 3 -
0.00002671875 * T_aveg_Abs * T_aveg_Abs + 0.0027103175 * T_aveg_Abs + 0.5520119
Pr_Abs = (Cp_ts_Abs * μ_cw_Abs / K_cw_Abs) * 1000
m_cw_Abs = Qa_Thermo / (Cp_ts_Abs * (T_cw_o_Abs - T_cw_i_Abs))
Ai_Abs = (3.1415 / 4) * Di_Abs * Di_Abs
Re_Abs = (m_cw_Abs * Di_Abs) / (Ai_Abs * μ_cw_Abs)
Nu_Abs = 0.023 * (Re_Abs ^ 0.8) * (Pr_Abs ^ 0.4)
hi_Abs = Nu_Abs * K_cw_Abs / Di_Abs

'shell-side calculations
K_cooper_Abs = 0.000000004583333 * Ta_Thermo ^ 4 - 0.000002916667 * Ta_Thermo ^ 3 + 0.0006541667
* Ta_Thermo ^ 2 - 0.1108333 * Ta_Thermo + 386
ρ_ss_Abs = 1145.36 + 470.84 * X1_Thermo + 134.79 * X1_Thermo * X1_Thermo - (0.333393 + 0.571749 *
X1_Thermo) * (273.15 + Ta_Thermo)
Cp_ss_Abs = (0.0976 * X1_Thermo * X1_Thermo - 37.512 * X1_Thermo + 3825.4) / 1000
Constant_Abs = m_ws_Thermo / (2 * L_Abs)

A1_Abs = -494.122 + 16.3967 * X1_Thermo - 0.14511 * X1_Thermo * X1_Thermo
A2_Abs = 28606.4 - 934.568 * X1_Thermo + 8.52755 * X1_Thermo * X1_Thermo
A3_Abs = 70.3848 - 2.35014 * X1_Thermo + 0.0207809 * X1_Thermo * X1_Thermo
K1_Abs = -0.3081 * (X1_Thermo / 100) + 0.62979
K2_Abs = -0.3191795 * (X1_Thermo / 100) + 0.65388
D12_Abs = ((K2_Abs - K1_Abs) / 20) * (T3_Thermo + 273.15 - 313)
K_ss_Abs = K2_Abs + D12_Abs
B_Abs = A1_Abs + (A2_Abs / (273.15 + Ta_Thermo) + A3_Abs * Math.Log(273.15 + Ta_Thermo))
μ_ss_Abs = (2.71 ^ B_Abs) / 1000
WallVisco_ss_Abs = μ_ss_Abs
Term1_Abs = ((K_ss_Abs * K_ss_Abs) * (ρ_ss_Abs ^ (4 / 3)) * Cp_ss_Abs * (9.81 * (2 / 3)))
Term2_Abs = (3.1415 * Do_Abs / 2) * (0.001 * μ_ss_Abs ^ (1 / 3))
Term3_Abs = (μ_ss_Abs / WallVisco_ss_Abs) ^ 0.25
Term4_Abs = (4 * Constant_Abs / μ_ss_Abs) ^ (1 / 9)

Term1_Term2_Abs = (Term1_Abs / Term2_Abs) ^ (1 / 3)
ho_Abs = 0.5 * Term1_Term2_Abs * Term3_Abs * Term4_Abs

'design results calculations
U_Abs = 1 / ((Do_Abs / Di_Abs) * (1 / hi_Abs) + (Do_Abs / Di_Abs) * 0.000176 + (1 / (2 * K_cooper_Abs))
* Do_Abs * Math.Log(Do_Abs / Di_Abs) + 0.00009 + (1 / ho_Abs))
LMTD_Abs = ((Ta_Thermo - T_cw_i_Abs) - (Ta_Thermo - T_cw_o_Abs)) / Math.Log((Ta_Thermo -
T_cw_i_Abs) / (Ta_Thermo - T_cw_o_Abs))
Area_Abs = (Qa_Thermo / (U_Abs * LMTD_Abs)) * 1000
Tubes_Abs = Area_Abs / (3.1415 * Do_Abs * L_Abs)
```

```
txtDi_Abs.Text = Math.Round(Di_Abs, 5)

'tube-side data presentation
txtT_aveg_Abs.Text = Math.Round(T_aveg_Abs, 2)
txtμ_cw_Abs.Text = Math.Round(μ_cw_Abs, 6)
txtρ_cw_Abs.Text = Math.Round(ρ_cw_Abs, 2)
txtCp_ts_Abs.Text = Math.Round(Cp_ts_Abs, 3)
txtK_cw_Abs.Text = Math.Round(K_cw_Abs, 4)
txtPr_Abs.Text = Math.Round(Pr_Abs, 4)
txtm_cw_Abs.Text = Math.Round(m_cw_Abs, 3)
txtRe_Abs.Text = Math.Round(Re_Abs, 0)
txtNu_Abs.Text = Math.Round(Nu_Abs, 2)
txtHi_Abs.Text = Math.Round(hi_Abs, 2)

'shell-side data presentation
txtρ_ss_Abs.Text = Math.Round(ρ_ss_Abs, 3)
txtK_ss_Abs.Text = Math.Round(K_ss_Abs, 3)
txtho_Abs.Text = Math.Round(ho_Abs, 3)
txtμ_ss_Abs.Text = Math.Round(μ_ss_Abs, 6)
txtCp_ss_Abs.Text = Math.Round(Cp_ss_Abs, 3)

'design results data presentation
txtU_Abs.Text = Math.Round(U_Abs, 3)
txtLMTD_Abs.Text = Math.Round(LMTD_Abs, 3)
txtArea_Abs.Text = Math.Round(Area_Abs, 3)
txtTubes_Abs.Text = Math.Round(Tubes_Abs, 3)

txtI_Abs_Sch.Text = T_cw_i_Abs & "°C"
```

Code for Derived Possible Combinations

```
Dim HX_Opt, Qe_Opt, X1_Opt, X4_Opt, h8_Opt, h10_Opt, m_ref_Opt, _
   m_ss_Opt, m_ws_Opt, C_x1_Opt, C_x4_Opt, T5_Opt, h1_Opt, h5_Opt, _
   h7_Opt, Qg_Opt, COP_Opt As Double

HX_Opt = txtHX_Eff_OptimalConfig.Text
Qe_Opt = txtQe_OptimalConfig.Text

Dim dt As DataTable
Dim dr As DataRow
Dim dcTg, dcTe, dcTa, dcTc, dcX1, dcX4, dcCOP As DataColumn

dt = New DataTable()
dcTg = New DataColumn("Tg", Type.GetType("System.Int32"))
dcTe = New DataColumn("Te", Type.GetType("System.Int32"))
dcTa = New DataColumn("Ta", Type.GetType("System.Int32"))
dcTc = New DataColumn("Tc", Type.GetType("System.Int32"))

dcX1 = New DataColumn("X1", Type.GetType("System.Double"))
dcX4 = New DataColumn("X4", Type.GetType("System.Double"))
dcCOP = New DataColumn("COP", Type.GetType("System.Double"))
```

```
dt.Columns.Add(dcTg)
dt.Columns.Add(dcTe)
dt.Columns.Add(dcTa)
dt.Columns.Add(dcTc)
dt.Columns.Add(dcX1)
dt.Columns.Add(dcX4)
dt.Columns.Add(dcCOP)

ProgressBar1.Maximum = 61 * 12 * 26 * 26 'Set Max Lenght
ProgressBar1.Step = 1 'Set Step
ProgressBar1.Value = 0 'Set Begin value

dgvCOP.DataSource = Nothing
dgvCOP.Refresh()

For Tg_Opt As Integer = 40 To 100
   For Te_Opt As Integer = 4 To 15
For Ta_Opt As Integer = 15 To 40
   For Tc_Opt As Integer = 15 To 40
dr = dt.NewRow()
X1_Opt = (49.04 + 1.125 * Ta_Opt - Te_Opt) / (134.65 + 0.47 * Ta_Opt)
X4_Opt = (49.04 + 1.125 * Tg_Opt - Tc_Opt) / (134.65 + 0.47 * Tg_Opt)

If X4_Opt > X1_Opt Then
   h8_Opt = 4.187 * (Tc_Opt - 25)
   h10_Opt = 4.187 * (572.8 + 0.417 * Te_Opt)
   m_ref_Opt = Qe_Opt / (h10_Opt - h8_Opt)
   m_ss_Opt = m_ref_Opt * (X4_Opt / (X4_Opt - X1_Opt))
   m_ws_Opt = m_ref_Opt * X1_Opt / (X4_Opt - X1_Opt)
   C_x1_Opt = 4.187 * (1.01 - 1.23 * X1_Opt + 0.48 * X1_Opt ^ 2)
   C_x4_Opt = 4.187 * (1.01 - 1.23 * X4_Opt + 0.48 * X4_Opt ^ 2)
   T5_Opt = Tg_Opt - HX_Opt * (Tg_Opt - Ta_Opt)
   h1_Opt = (C_x1_Opt * Ta_Opt) + 4.187 * (42.81 - 425.92 * X1_Opt + 404.67 * X1_Opt ^ 2)
   h5_Opt = (C_x4_Opt * T5_Opt) + 4.187 * (42.81 - 425.92 * X4_Opt + 404.67 * X4_Opt ^ 2)
   h7_Opt = 4.187 * (572.8 + 0.46 * Tg_Opt - 0.043 * Tc_Opt)
   Qg_Opt = m_ws_Opt * h5_Opt + m_ref_Opt * h7_Opt - m_ss_Opt * h1_Opt
   COP_Opt = Qe_Opt / Qg_Opt

   dr("Tg") = Tg_Opt
   dr("Te") = Te_Opt
   dr("Ta") = Ta_Opt
   dr("Tc") = Tc_Opt
   dr("X1") = Math.Round(X1_Opt, 4)
   dr("X4") = Math.Round(X4_Opt, 4)
   dr("COP") = Math.Round(COP_Opt, 4)
   dt.Rows.Add(dr)
End If
ProgressBar1.Value = ProgressBar1.Value + 1
   Next

dgvCOP.DataSource = dt
```

APPENDIX 2: EES CODE FOR CHAPTER 7

{Single-Effect LiBr-water absorption cycle}

{Input data}

```
Eff_Hx=.70                  {Solution heat exchanger effectiveness, dimensionless}
m[1]=.0699                  {Weak solution mass flow rate, kg/s}
UA_a=1.364                  {UA for absorber, kW/K}
UA_c=1.245                  {UA for condenser, kW/K}
UA_g=2.093                  {UA for generator, kW/K}
UA_e=1.753                  {UA for evaporator, kW/K}
T[13]=28                    {Cooling water temperature entering the absorber, °C}
m[13]=0.88                  {Mass flow rate of cooling water entering the absorber, kg/sec}
T[15]=30                    {Cooling water temperature entering the condenser, °C}
m[15]=1.13                  {Mass flow rate of cooling water entering the condenser, kg/sec}
T[11]=85                    {Hot water temperature entering the generator, °C}
m[11]=0.58                  {Mass flow rate of hot water entering the generator, kg/sec}
T[17]=12                    {Chilled water temperature entering the evaporator, °C}
m[17]=.334                  {Mass flow rate of chilled water entering the evaporator, kg/sec}
Q[8]=0                      {Vapour high pressure}
Q[10]=1.0                   {Vapour high pressure}
x[4]=X_LIBR(T[4],Phigh)     {Strong solution concentration}
X[1]=X_LIBR(T[1],Plow-dp)   {Weak solution concentration}
T[7]=T_LIBR(Phigh,x[3])
```

{Set pressures}

```
dp=0
Phigh=pressure (WATER,T=T[8],x=Q[8])        {Cycle high pressure}
Plow=pressure (WATER,T=T[10],x=Q[10])       {Cycle low pressure}
```

{Solution Heat Exchanger Model}

```
Eff_Hx=(T[4]-T[5])/(T[4]-T[2])              {Solution heat exchanger effectiveness}
Chot=m[4]*(h[4]-h[5])/(T[4]-T[5])
Ccold=m[2]*(h[3]-h[2])/(T[3]-T[2])
Qhx=m[1]*(h[3]-h[2])                        {Energy balance}
Qhx=m[4]*(h[4]-h[5])                        {Energy balance}
Lmtds=((T[4]-T[3])-(T[5]-T[2]))/ln((T[4]-T[3])/(T[5]-T[2]))
UAs=Qhx/Lmtds                               {UA for solution heat exchanger, kW/K}
```

{Generator Model}

```
m[3]=m[4]+m[7]                              {Mass balance equation}
m[3]*x[3]=m[4]*x[4]                         {LiBr balance equation}
Qg=-h[3]*m[3]+h[4]*m[4]+h[7]*m[7]           {Generator thermal capacity, kW}
Qg=m[11]*(h[11]-h[12])                      {Energy balance equation}
```

{Condenser}

```
Qc=m[7]*(h[7]-h[8])                         {Condenser thermal capacity, kW}
Qc=m[15]*(h[16]-h[15])                      {Energy balance}
```

{Refrigerant Valve}
h[9]=h[8] {Energy balance}

{Evaporator}
Qe=m[9]*(h[10]-h[9]) {Evaporator thermal capacity, kW}
Qe=m[17]*(h[17]-h[18]) {Energy balance}

{Absorber}
m[10]*h[10]+h[6]*m[6]-Qa-m[1]*h[1]=0 {Energy balance}
Qa=m[13]*(h[14]-h[13]) {Absorber thermal capacity, kW}

{Solution expansion valve model}
h[6]=h[5] {Energy balance}

{Pump calculation}
h[2]=h[1]+Pwork/m[1] {Energy balance}
Pwork=m[1]*v1*(Phigh-Plow)/1000 {Pump work model - isentropic}

{Heat Exchanger Models for External Water Loops, Compute LMTD}
$LMTD_a$=(T[6]-T[14]-T[1]+T[13])/ln((T[6]-T[14])/(T[1]-T[13]))
$LMTD_c$=(T[8]-T[15]-T[8]+T[16])/ln((T[8]-T[15])/(T[8]-T[16]))
$LMTD_g$=(T[11]-T[4]-T[12]+T[7])/ln((T[11]-T[4])/(T[12]-T[7]))
$LMTD_e$=(T[17]-T[10]-T[18]+T[10])/ln((T[17]-T[10])/(T[18]-T[10]))

{Equate water loop energy balance to UA*LMTD}
Q_a=Lmtda*UA_a
Q_c=Lmtdc*UA_c
Q_g=Lmtdg*UA_g
Q_e=Lmtde*UA_e

{Mass balances equations}
m[2]=m[1]
m[3]=m[2]
m[5]=m[4]
m[6]=m[5]
m[8]=m[7]
m[9]=m[8]
m[10]=m[9]

x[2]=X[1]
x[3]=x[2]
x[5]=x[4]
x[6]=x[5]
x[7]=0
x[8]=x[7]
x[9]=x[8]
x[10]=x[9]

{Compute thermodynamic properties}

```
h[1]=H_LIBR(T[1],X[1],SI)
h[2]=H_LIBR(T[2],x[2],SI)
h[3]=H_LIBR(T[3],x[3],SI)
h[4]=H_LIBR(T[4],x[4],SI)
h[5]=H_LIBR(T[5],x[5],SI)
CALL Q_LIBR(h[6],Plow-dp,x[6],SI:q6b,T6b,Xl6b,hl6b,hv6b)
T[6]=T6b
h[7]=enthalpy(WATER,T=T[7],P=Phigh)
h[8]=enthalpy(WATER,T=T[8],x=0)
T[9]=temperature(WATER,h=h[9],P=Plow)
h[10]=enthalpy(WATER,T=T[10],x=1)
h[11]=enthalpy(WATER,T=T[11],x=0.)
h[12]=enthalpy(WATER,T=T[12],x=0)
h[13]=enthalpy(WATER,T=T[13],x=0)
h[14]=enthalpy(WATER,T=T[14],x=0)
h[15]=enthalpy(WATER,T=T[15],x=0)
h[16]=enthalpy(WATER,T=T[16],x=0)
h[17]=enthalpy(WATER,T=T[17],x=0)
h[18]=enthalpy(WATER,T=T[18],x=0)
v1=V_LIBR(T[1],X[1],SI)
```

{Compute COP}

```
COP=m[9]*(h[10]-h[9])/(m[11]*(h[11]-h[12]))
```

{Set Pressures}

```
P[1]=Plow-dp
P[2]=Phigh
P[3]=Phigh
P[4]=Phigh
P[5]=Phigh
P[6]=Plow-dp
P[7]=Phigh
P[8]=Phigh
P[9]=Plow
P[10]=Plow
```

{Set Vapour Quality}

```
Q[1]=0
Q[4]=0
Q[6]=Q6b*0.01
{Q[9]=quality(STEAM_NBS,h=h[9],P=Plow)}
T6sat=T_LIBR(Plow,X[5],SI)
```

APPENDIX 3: TRNSYS CODE FOR CHAPTER 8

Component-wise mathematical models are coded into the fully integrated visual interface known as TRNSYS simulation studio using FORTRAN. An iterative numerical procedure is implemented to solve the heat transfer equations simultaneously for various components of the system. This appendix presents the relationship between different components of the solar absorption cooling system implemented in TRNSYS. The simulation code is then presented. The TRNSYS work space and simulation flow chart in which the experimental obtained data were entered through a dedicated visual interface are demonstrated in chapter 8.

There are various codes for HVAC system components in TRNSYS library identified as "Type". First, the related types of HVAC equipment have been selected, coded and developed according to the aforementioned developed cooling plant. These types have then been configured to build the whole system. Experimentally collected data can be implemented into each "Type" by using the external files. There are some constant parameters for each "Type" which must be defined based on the design cariteria. In addition, the inputs of each "Type" may be considered as constant or linked with the output of another "Type" dependent on the components. The "Types" used for the aforementioned solar absorption cooling plant are as [125]:

Type 71 (Vacuum Solar Collector): Because the Solar Ratings and Certification Commission (SRCC) defines the efficiency of an evacuated tube collector bank using the same equations as those for a flat plat, the main difference (from a modelling point of view) between an evacuated tube collector and a flat plate collector is in the treatment of incidence angle modifiers (IAMs). Type 71 is therefore based on the Type 1 code with the major difference being that Type 71 reads a text file containing a list of transverse and longitudinal IAMs. This component models the thermal performance of a variety of an evacuated tube collector types using theory. The total collector array may consist of collectors connected in series and in parallel. The thermal performance of the total collector array is determined by the number of modules in series and the characteristics of each module. Corrections are

applied to the slope, intercept, and curvature parameters to account for identical collectors in series, and flow rates other than those at test conditions. The effects of off-normal solar incidence are modelled by the provision of a bi-axial incidence angle modifier data file.

Type 109 (Meteonorm TMY Weather Data): This component serves the main purpose of reading weather data at regular time intervals from a data file, converting it to a desired system of units and processing the solar radiation data to obtain tilted surface radiation and angle of incidence for an arbitrary number of surfaces. In this mode, Type 109 reads a weather data file in the standard TMY2 format. TMY2 files can be generated from many programs, such as Meteonorm. For our work, the weather data for Sydney has been used.

Type 56 (Multi-Zone Building): This component models the thermal behaviour of the building having up to 25 thermal zones. However, our case study is consisting of only one zone. The building description is read by this component from a set of external files having the extensions *.bui, *.bld, and *.trn. The files can be generated based on project information by running the pre-processor program called TRNBuild. This instance of Type56 generates its own set of monthly and hourly summary output files. All data for the case study has been coded and implemented in this type.

Type 33 (Psychrometrics): This component takes as input the dry bulb temperature and relative humidity of moist air and calls the TRNSYS Psychrometrics routine, returning the following corresponding moist air properties: dry bulb temperature, dew point temperature, wet bulb temperature, relative humidity, absolute humidity ratio, and enthalpy.

Type 69 (Effective sky temperature for long-wave radiation exchange): This component determines an effective sky temperature, which is used to calculate the long-wave radiation exchange between an arbitrary external surface and the atmosphere. The effective sky temperature is always lower than the current ambient temperature. The black sky on a clear night for example, is assigned a low effective sky temperature to account for the additional

radiative losses from a surface exposed to the sky. In this instance of Type 69, the cloudiness of the sky is calculated based on user provided dry bulb and dew point temperatures.

Type 107 (Hot Water Single-Effect Absorption Chiller): Type 107 uses the experimentally monitored data lookup approach to model a single-effect hot-water fired absorption chiller. "Hot Water" indicates that the energy supplied to the machine's generator comes from a hot water stream which is provided by vacuum solar collector. The collected data are coded and implemented in the chiller as the external file.

Type 51 (Cooling Tower): In a cooling tower, a warm water stream is in direct contact with an air stream and cooled as a result of sensible heat transfer due to temperature differences with the air and mass transfer resulting from evaporation to the air. The air and water streams are configured in cross flow arrangements in our project. Ambient air is drawn upward through the falling water. The cooling tower contains a fill material which increases the water surface area in contact with the air. The cooling tower is composed of tower cells that are in parallel and share a common sump. Water loss from the tower cells is replaced with make-up water to the sump. This component models the performance of the cross flow cooling tower and sump.

Type 114 (Single Speed Pump): Type114 models a single (constant) speed pump that is able to maintain a constant fluid outlet mass flow rate. The pump's power draw is calculated from pressure rise, overall pump efficiency, motor efficiency and fluid characteristics. Pump starting and stopping characteristics are not modelled. Type 114 sets the downstream flow rate based on its rated flow rate parameter and the current value of its control signal input. This type of pump has been used for chilled-water, cooled-water and hot water loop in the solar-powered absorption air conditioning system.

Type 32 (Cooling Coil): This component models a cooling coil where the air is cooled as it passes across a coil containing the chilled water. This model relies on provided external data files which contain the performance of the coil as a function of the entering air and water

conditions. This cooling coil is a part of fan-coil unit which is installed inside the building to deliver the supply air.

Type 112 (Supply Fan): Type744 models a fan that sets its outlet mass flow rate equal to the specified inlet mass flow rate. This type passes the inlet mass flow rate of air through to its output. Type 112 sets the downstream flow but does not take a control signal. The fan's power draw is calculated based upon a specified polynomial.

The TRNSYS input file code is presented as follows:

TRNSYS Input File Code
Model "Weather data-Sydney" (Type 109)

```
UNIT 109 TYPE 109 Weather data-Sydney
UNIT_NAME Weather data-Sydney
MODEL .\Weather Data Reading and Processing\Standard Format\TMY2\Type109-TMY2.tmf
PARAMETERS 4
2  ! 1 Data Reader Mode
30  ! 2 Logical unit
4  ! 3 Sky model for diffuse radiation
1  ! 4 Tracking mode
INITIAL INPUT VALUES
0.2 90 AA_N 90 AA_N 90 AA_N 90 AA_N
External files:ASSIGN "C:\Program Files\Trnsys16\Weather\Meteonorm\Australia-Oceania\AU-Sydney-Australia
EQUATIONS "Light Thresholds"
Toth_L_on = -3.6*120
Eoth_L_off = -3.6*200
$UNIT_NAME Light Thresholds
$LAYER Controls
$POSITION 461 509
EQUATIONS "Radiation"
EQUATIONS 18
AISZ = [109,10]
AISA = [109,11]
IT_H = Max([109,12],0)
IB_H = Max([109,13],0)
ID_H = [109,14]
AI_H = [109,16]
IT_N = [109,18]
AI_N = [109,19]
IB_N = [109,22] * LT(AI_N,90)
IT_S = [109,24]
```

IB_S = [109,25]
AI_S = [109,28]
IT_E = [109,30]
IB_E = [109,31]
AI_E = [109,34]
IT_W = [109,36]
IB_W = [109,37]
AI_W = [109,40]
$UNIT_NAME Radiation
$LAYER Main
$POSITION 196 93
* Model "Psychrometrics-1" (Type 33)
UNIT 331 TYPE 33 Psychrometrics-1
$UNIT_NAME Psychrometrics-1
$MODEL .\Physical Phenomena\Thermodynamic Properties\Psychrometrics\Dry Bulb and Relative Humidity Known\Type33e.tmf
$POSITION 204 325
$LAYER Main #
PARAMETERS 3
2 ! 1 Psychrometrics mode
1 ! 2 Wet bulb mode
INPUTS
109,1 ! Weather data-Sydney: Ambient temperature ->Dry bulb temp.
109,2 ! Weather data-Sydney: relative humidity ->Percent relative humidity
INITIAL INPUT VALUES
20 50 1
Model "Sky temp" (Type 69)
UNIT 69 TYPE 69 Sky temp
$UNIT_NAME Sky temp
$MODEL .\Physical Phenomena\Sky Temperature\read in cloudiness factor\Type69a.tmf
$POSITION 379 273
$LAYER Main # #
PARAMETERS 2
1 ! 1 mode for cloudiness factor
0 ! 2 height over sea level
INPUTS
331,7 ! Psychrometrics-1:Dry bulb temperature ->Ambient temperature
331,8 ! Psychrometrics-1:Dew point temperature. ->Dew point temperature at ambient conditions
109,13 ! Weather data-Sydney: beam radiation on horizontal ->Beam radiation on the horizontal
109,14 ! Weather data-Sydney: sky diffuse radiation on horizontal ->Diffuse radiation on the horizontal
Model "Lights" (Type 2)
UNIT 200 TYPE 2 Lights
$UNIT_NAME Lights
$MODEL .\Controllers\Differential Controller w_Hysteresis\generic\Solver 0 (Successive Substitution) Control Strategy\Type2d.tmf
$POSITION 562 402
$LAYER Controls #
PARAMETERS 2

5 ! 1 No. of oscillations
40000 ! 2 High limit cut-out
INPUTS 6
IT_H ! Radiation:IT_H ->Lower input value
200,1 ! Lights:Output control function ->Input control function
Toth_L_on ! Light Thresholds:Toth_L_on ->Upper dead band
Eoth_L_off ! Light Thresholds:Eoth_L_off ->Lower dead band
Model "Building" (Type 56)
UNIT 56 TYPE 56 Building
$UNIT_NAME Building
$MODEL .\Loads and Structures\Multi-Zone Building\With Standard Output Files\Type56a.tmf
$POSITION 758 626
$LAYER Main
PARAMETERS 6
31 ! 1 Logical unit for building description file (.bui)
1 ! 2 Star network calculation switch
0.5 ! 3 Weighting factor for operative temperature
32 ! 4 Logical unit for monthly summary
33 ! 5 Logical unit for hourly temperatures
34 ! 6 Logical unit for hourly loads
INPUTS
331,7 ! Psychrometrics-1: Dry bulb temperature -> 1- TAMB (AMBIENT TEMPERATURE)
331,6 ! Psychrometrics-1: Percent relative humidity -> 2- ARELHUM (RELATIVE AMBIENT HUMIDITY)
69,1 ! Sky temp: Fictive sky temperature -> 3- TSKY (FIKTIVE SKY TEMPERATURE)
IT_N ! Radiation:IT_N -> 4- ITNORTH (INCIDENT RADIATION FOR ORIENTATION NORTH)
IT_S ! Radiation:IT_S -> 5- ITSOUTH (INCIDENT RADIATION FOR ORIENTATION SOUTH)
IT_E ! Radiation:IT_E -> 6- ITEAST (INCIDENT RADIATION FOR ORIENTATION EAST)
IT_W ! Radiation:IT_W -> 7- ITWEST (INCIDENT RADIATION FOR ORIENTATION WEST)
IT_H ! Radiation:IT_H -> 8- ITHORIZONT (INCIDENT RADIATION FOR ORIENTATION HORIZONT)
IB_N ! Radiation:IB_N -> 9- IBNORTH (INCIDENT BEAM RADIATION FOR ORIENTATION NORTH)
IB_S ! Radiation:IB_S -> 10- IBSOUTH (INCIDENT BEAM RADIATION FOR ORIENTATION SOUTH)
IB_E ! Radiation:IB_E -> 11- IBEAST (INCIDENT BEAM RADIATION FOR ORIENTATION EAST)
IB_W ! Radiation:IB_W -> 12- IBWEST (INCIDENT BEAM RADIATION FOR ORIENTATION WEST)
IB_H ! Radiation:IB_H -> 13- IBHORIZONT (INCIDENT BEAM RADIATION FOR ORIENTATION HORIZONT)
AI_N ! Radiation:AI_N -> 14- AINORTH (ANGLE OF INCIDENCE FOR ORIENTATION NORTH)
AI_S ! Radiation:AI_S -> 15- AISOUTH (ANGLE OF INCIDENCE FOR ORIENTATION SOUTH)
AI_E ! Radiation:AI_E -> 16- AIEAST (ANGLE OF INCIDENCE FOR ORIENTATION EAST)

AI_W ! Radiation:AI_W -> 17- AIWEST (ANGLE OF INCIDENCE FOR ORIENTATION WEST)
AI_H ! Radiation:AI_H -> 18- AIHORIZONT (ANGLE OF INCIDENCE FOR ORIENTATION HORIZONT)
20,7 ! Psychrometrics-2:Dry bulb temperature -> 20- T_COOL_ON (INPUT)
BRIGHT! Shading+Light:BRIGHT -> 25- BRIGHT (INPUT)
Model "Results" (Type 65)
UNIT 25 TYPE 65 Results
$UNIT_NAME Results
$MODEL .\Output\Online Plotter\Online Plotter without File\Type65d.tmf
$POSITION 641 200
$LAYER Main
Model "Supply Fan" (Type 112)
UNIT 12 TYPE 112 Supply Fan
$UNIT_NAME Supply Fan
$MODEL .\Hydronics\Fans\Single Speed\Relative Humidity Inputs\Type112b.tmf
$POSITION 479 669
$LAYER Main #
$# SINGLE-SPEED FAN
PARAMETERS 5
2 ! 1 Humidity mode
378 (l/s) ! 2 Rated flow rate
143 (W) ! 3 Rated power
0.90 ! 4 Motor efficiency
0.1 ! 5 Motor heat loss fraction
INPUTS
16,1 ! Cooling Coil: Outlet dry bulb temperature ->Inlet air temperature
16,3 ! Cooling Coil: Air flow rate ->Air flow rate
INITIAL INPUT VALUES
20.0 0.008 50. 378 1. 1.0 0.0
Model "Hot Water Pump" (Type 114)
UNIT 13 TYPE 114 Hot Water Pump
$UNIT_NAME Hot Water Pump
$MODEL .\Hydronics\Pumps\Single Speed\Type114.tmf
$POSITION 76 552
$LAYER Main
$# SINGLE-SPEED PUMP
PARAMETERS 4
0.58 (l/s) ! 1 Rated flow rate
4.19 ! 2 Fluid specific heat
50 (W) ! 3 Rated power
0.1 ! 4 Motor heat loss fraction
INPUTS
17,1 ! Vacuum Collector: Outlet temperature ->Inlet fluid temperature
17,2 ! Vacuum Collector: Outlet flow rate ->Inlet fluid flow rate
INITIAL INPUT VALUES
85 0.58 1.0 0.6 0.9
Model "Absorption Chiller" (Type 107)
UNIT 14 TYPE 107 Absorption Chiller

```
$UNIT_NAME Absorption Chiller
$MODEL .\HVAC\Absorption Chiller (Hot-Water Fired, Single Effect)\Type107.tmf
$POSITION 204 552
$LAYER Main #
PARAMETERS
7 (kW) ! 1 Rated capacity
0.708    ! 2 Rated C.O.P.
35       ! 3 Logical unit for S1 data file
5        ! 4 Number of HW temperatures in S1 data file
3        ! 5 Number of CW steps in S1 data file
7        ! 6 Number of CHW set points in S1 data file
11       ! 7 Number of load fractions in S1 data file
4.190    ! 8 HW fluid specific heat
4.190    ! 9 CHW fluid specific heat
4.190    ! 10 CW fluid specific heat
25 (W) ! 11 Auxiliary electrical power
INPUTS 8
16,4    ! Cooling Coil: Outlet water temperature ->Chilled water inlet temperature
16,5    ! Cooling Coil: Water flow rate ->Chilled water flow rate
18,1    ! Cooled Water Pump: Outlet fluid temperature ->Cooling water inlet temperature
18,2    ! Cooled Water Pump: Outlet flow rate ->Cooling water flow rate
13,1    ! Hot Water Pump: Outlet fluid temperature ->Hot water inlet temperature
13,2    ! Hot Water Pump: Outlet flow rate ->Hot water flow rate
INITIAL INPUT VALUES
12 1188 30 7 85 1511 7 1.0
External files
ASSIGN "C:\Program Files\Trnsys16\Examples\Data Files\Type107-HotWater Absorption
Chiller.dat"
```

Model "Cooling Tower" (Type 51)

```
UNIT 15 TYPE 51   Cooling Tower
$UNIT_NAME Cooling Tower
$MODEL .\HVAC\Cooling Towers\User-Supplied Coefficients\TYPE51b.tmf
$POSITION 366 434
$LAYER Water Loop #
PARAMETERS 11
1       ! 1 Calculation mode
2       ! 2 Flow geometry
1       ! 3 Number of tower cells
1.13 (l/s) ! 4 Maximum cell flow rate
42 (W)    ! 5 Fan power at maximum flow
4.0824    ! 6 Minimum cell flow rate
1.0          ! 7 Sump volume
20           ! 8 Initial sump temperature
2.3          ! 9 Mass transfer constant
-0.72        ! 10 Mass transfer exponent
1   ! 11 Print performance results?
INPUTS 6
14,3    ! Absorption Chiller: Cooling water temperature ->Water inlet temperature
14,4    ! Absorption Chiller: Cooling water flow rate ->Inlet water flow rate
```

21,7 ! Psychrometrics-3: Dry bulb temperature ->Dry bulb temperature
21,2 ! Psychrometrics-3: Wet bulb temperature ->Wet bulb temperature
INITIAL INPUT VALUES
35 0.7 40 27 25 0.85
Model "Cooling Coil" (Type 32)
UNIT 16 TYPE 32 Cooling Coil
$UNIT_NAME Cooling Coil
$MODEL .\HVAC\Cooling Coils\Simplified\TYPE32.tmf
$POSITION 330 669
$LAYER Water Loop #
PARAMETERS 4
3 ! 1 Number of rows
1 ! 2 Number of coil circuits
2 (m^2) ! 3 Coil face area
0.012875! 4 Inside tube diameter
INPUTS
22,7 ! Psychrometrics-4: Dry bulb temperature ->Inlet dry-bulb temperature
22,2 ! Psychrometrics-4: Wet bulb temperature ->Inlet wet bulb temperature
19,1 ! Chilled Water Pump: Outlet fluid temperature ->Inlet water temperature
19,2 ! Chilled Water Pump: Outlet flow rate ->Flow rate of water
INITIAL INPUT VALUES
23 20 1800000 7 1188
Model "Vacuum Collector" (Type 71)
UNIT 17 TYPE 71 Vacuum Collector
$UNIT_NAME Vacuum Collector
$MODEL .\Solar Thermal Collectors\Evacuated Tube Collector\Type71.tmf
$POSITION 73 413
$LAYER Main #
PARAMETERS 11
1 ! 1 Number in series
31.8 ! 2 Collector area
4.19 ! 3 Fluid specific heat
1 ! 4 Efficiency mode
3.0 ! 5 Flow rate at test conditions
0.7 ! 6 Intercept efficiency
10 ! 7 Negative of first order efficiency coefficient
0.03 ! 8 Negative of second order efficiency coefficient
36 ! 9 Logical unit of file containing biaxial IAM data
5 ! 10 Number of longitudinal angles for which IAMs are provided
5 ! 11 Number of transverse angles for which IAMs are provided
INPUTS
14,5 ! Absorption Chiller: Hot water outlet temperature ->Inlet temperature
14,6 ! Absorption Chiller: Hot water flow rate ->Inlet flow rate
23,7 ! Psychrometrics-5: Dry bulb temperature ->Ambient temperature
109,18 ! Weather data-Sydney: total radiation on tilted surface-1 ->Incident radiation
109,20 ! Weather data-Sydney: sky diffuse radiation on tilted surface-1 ->Incident diffuse radiation
109,22 ! Weather data-Sydney: angle of incidence for tilted surface -1 ->Solar incidence angle
109,10 ! Weather data-Sydney: solar zenith angle ->Solar zenith angle
109,11 ! Weather data-Sydney: solar azimuth angle ->Solar azimuth angle

109,23 ! Weather data-Sydney: slope of tilted surface-1 ->Collector slope
INITIAL INPUT VALUES
80 1511 40 0 0 0 0.0 0.0 45 180
External files: ASSIGN "C:\Program Files\Trnsys16\Single-Axis IAM's\Iam_1d.dat" 36
Model "Cooled Water Pump" (Type 114)
UNIT 18 TYPE 114 Cooled Water Pump
$UNIT_NAME Cooled Water Pump
$MODEL .\Hydronics\Pumps\Single Speed\Type114.tmf
$POSITION 214 434
$LAYER Main #
$# SINGLE-SPEED PUMP
PARAMETERS 4
1.13 (l/s) ! 1 Rated flow rate
4.19 ! 2 Fluid specific heat
65 (W) ! 3 Rated power
0.1 ! 4 Motor heat loss fraction
INPUTS
15,5 ! Cooling Tower: Cell outlet temperature ->Inlet fluid temperature
15,2 ! Cooling Tower: Sump flow rate ->Inlet fluid flow rate
INITIAL INPUT VALUES
30 2519 1.0 0.6 0.9
Model "Chilled Water Pump" (Type 114)
UNIT 19 TYPE 114 Chilled Water Pump
$UNIT_NAME Chilled Water Pump
$MODEL .\Hydronics\Pumps\Single Speed\Type114.tmf
$POSITION 342 552
$LAYER Main
$# SINGLE-SPEED PUMP
PARAMETERS 4
0.33 (l/s) ! 1 Rated flow rate
4.19 ! 2 Fluid specific heat
65 (W) ! 3 Rated power
0.1 ! 4 Motor heat loss fraction
INPUTS
14,1 ! Absorption Chiller: Chilled water temperature ->Inlet fluid temperature
14,2 ! Absorption Chiller: Chilled water flow rate ->Inlet fluid flow rate
INITIAL INPUT VALUES
20.0 1188 1.0 0.6 0.9
Model "Psychrometrics-2" (Type 33)
UNIT 20 TYPE 33 Psychrometrics-2
$UNIT_NAME Psychrometrics-2
$MODEL .\Physical Phenomena\Thermodynamic Properties\Psychrometrics\Dry Bulb and Relative Humidity Known\Type33e.tmf
$POSITION 616 666
$LAYER Main #
PARAMETERS 3
2 ! 1 Psychrometrics mode
1 ! 2 Wet bulb mode
INPUTS

```
12,1    ! Supply Fan: Outlet air temperature ->Dry bulb temp.
12,3    ! Supply Fan: Outlet air %RH ->Percent relative humidity
INITIAL INPUT VALUES
20 50 1
```

Model "Psychrometrics-3" (Type 33)

```
UNIT 21 TYPE 33   Psychrometrics-3
$UNIT_NAME Psychrometrics-3
$MODEL .\Physical Phenomena\Thermodynamic Properties\Psychrometrics\Dry Bulb and Relative Humidity Known\Type33e.tmf
$POSITION 328 367
$LAYER Main
PARAMETERS 3
2  ! 1 Psychrometrics mode
1  ! 2 Wet bulb mode
INPUTS
109,1    ! Weather data-Sydney: Ambient temperature ->Dry bulb temp.
109,2    ! Weather data-Sydney: relative humidity ->Percent relative humidity
INITIAL INPUT VALUES
20 50 1
Model "Psychrometrics-4" (Type 33)
UNIT 22 TYPE 33   Psychrometrics-4
$UNIT_NAME Psychrometrics-4
$MODEL .\Physical Phenomena\Thermodynamic Properties\Psychrometrics\Dry Bulb and Relative Humidity Known\Type33e.tmf
$POSITION 574 570
$LAYER Main #
PARAMETERS 3
2  ! 1 Psychrometrics mode
1  ! 2 Wet bulb mode
INPUTS 3
56,1    ! Building:    1- (air temperature of zone) TAIR   1 ->Dry bulb temp.
56,3    ! Building:    3- (relative humidity of zone...) RELHUM 1 ->Percent relative humidity
INITIAL INPUT VALUES
20 50 1
```

Model "Psychrometrics-5" (Type 33)

```
UNIT 23 TYPE 33   Psychrometrics-5
$UNIT_NAME Psychrometrics-5
$MODEL .\Physical Phenomena\Thermodynamic Properties\Psychrometrics\Dry Bulb and Relative Humidity Known\Type33e.tmf
$LAYER Main
PARAMETERS 3
2  ! 1 Psychrometrics mode
1  ! 2 Wet bulb mode
INPUTS
109,1    ! Weather data-Sydney: Ambient temperature ->Dry bulb temp.
109,2    ! Weather data-Sydney: relative humidity ->Percent relative humidity
INITIAL INPUT VALUES
20 50 1
END
```

APPENDIX 4: LIST OF PUBLICATIONS, AWARDS AND PATENTS

- **Book Chapter**

- V. Vakiloroaya, J. Madadnia, Cooling Coil Design Improvement for HVAC Energy Savings and Comfort Enhancement, Sustainability in Energy and Buildings, Springer Berlin Heidelberg, Chapter 85, pp. 965-974, 2013.

- **Journal Papers**

- V. Vakiloroaya, B. Samali, S. Cuthbert, K. Pishghadam, D. Eager, Thermo-economic optimisation of condenser coil configuration for HVAC performance enhancement, *Energy and Buildings*, 84 (2014) 1-12. (Impact Factor 2.465, Rank: A*)

- V. Vakiloroaya, B. Samali, K. Pishghadam, A comparative Study on the Effect of Different Strategies for Energy Saving of Air-Cooled Vapour Compression Air Conditioning System, *Energy and Buildings*, 74 (2014) 163-172. (Impact Factor 2.465, Rank: A*)

- V. Vakiloroaya, B. Samali, K. Pishghadam, Investigation of Energy-Efficient Strategy for Direct Expansion Air-Cooled Air Conditioning Systems, *Applied Thermal Engineering,* 66 (2014) 84-93. (Impact Factor 2.624, Rank: A)

- V. Vakiloroaya**,** B. Samali, A. Fakhar and K. Pishghadam, "A Review of Different Startegies for HVAC Energy Savings," *Energy Conversion and Management*, 77 (2014) 738-754. (Impact Factor: 3.59)

- V. Vakiloroaya**,** Q.P. Ha and B. Samali, "Energy-Efficient HVAC Systems: Simulation-Empirical Modelling and Gradient Optimization," *Automation in Construction*, 31 (2013) 176-185. (Impact Factor: 1.822, Rank: A)

- V. Vakiloroaya**,** A. Fakhar, B. Samali and K. Pishghadam, "Design Improvement of Central Cooling Plant for Energy Saving Using Cooling Tower Water," *Journal of Renewable and Sustainable Energy*, vol. 5(6), (2013) 531-536., doi: 10.1063/1.4824978. (Impact Factor: 1.51)

- V. Vakiloroaya, J. Madadnia and B. Samali, "Modelling and performance prediction of an integrated central cooling plant for HVAC energy efficiency improvement", *Building Simulation: An International Journal*, 6 (2013) 127-138, DOI: 10.1007/s12273-013-0104-0. (Impact Factor: 0.631)

- V. Vakiloroaya, B. Samali, A. Fakhar and K. Pishghadam, "Thermo-Economic Optimization of Rooftop Unit's Evaporator Coil for Energy Efficiency and Thermal Comfort", *Building Simulation: An International Journal*, (2013), 7 (2014) 345-359, DOI: 10.1007/s12273-013-0151-6. (Impact Factor: 0.631)

- V. Vakiloroaya, "Design optimization of the cooling coil for HVAC energy saving and comfort enhancement", *Environmental Progress and Sustainable Energy*, 32 (2013) 1209-1216, DOI: 10.1002/ep.11729. (Impact Factor: 1.271)

- **Conference Papers**

- V. Vakiloroaya and Q.P. Ha, "Energy Efficient Air-Cooled Direct Expansion Air Conditioning System with Liquid Pressure Amplification," 31th International Symposium on Automation and Robotics in Construction (ISARC), Sydney, Australian, 2014.

- Q.P. Ha, And V. Vakiloroaya, "A New Single-Effect Hot-Water Absorption Chiller Air Conditioning Using Solar Energy," *Australasian Universities Power Engineering Conference (AUPEC 2013)*, Hobart, Australia.

- J. Madadnia, V. Vakiloroaya, and J. Ison, "Experimental Investigation on Influence of Integrated Heat Pump in Performance of Domestic Water Heaters," *ASME 2012 Summer Heat Transfer Conference*, Puerto-Rico, pp. 151-155, USA, 2012, DOI: 10.1115/HT2012-58197. (ERA Rank: A)

- D. Dehestani, S. Su, H. Nguyen, V. Vakiloroaya, J Wall, and Y Guo, "Intelligent Model Based Fault Detection for Heat Ventilating and Air Conditioning (HVAC) System Based on ANN model and SVM Classifier," *10th International Conference on Healthy Buildings, Brisbane, Australia, 8-12 July*, 2012 (ERA Rank: A)

- J. Ison, V. Vakiloroaya, and J. Madadnia, "Computational Modelling of Integrated Heat Pump and Domestic Water Heater," *ASME 2012 Summer Heat Transfer Conference*, Puerto-Rico, USA, 2012. (ERA Rank: A)

- V. Vakiloroaya, J.G. Zhu, and Q.P. Ha, "Modelling and Optimization of Direct Expansion Air Conditioning Systems for Commercial Buildings Energy Savings," *The 28th International Symposium on Automation and Robotics in Construction*, Seoul, Korea, pp. 232-237, 2011. (ERA Rank: A)

- V. Vakiloroaya, S.W. Su, and Q.P. Ha, "HVAC Integrated Control for Energy Saving and Comfort Enhancement," *The 28th International Symposium on Automation and Robotics in Construction*, Seoul, Korea, pp. 244-249, 2011. (Era Rank: A)

- V. Vakiloroaya, B. Samali, J. Madadnia. And Q.P. Ha, "Component-Wise Optimisation for Commercial Central Cooling Plant," *The 37th International Conference of the IEEE Industrial Electronics (IECON)*, Melbourne, Australia, pp. 2686-2691, 2011. (ERA Rank: A)

- V. Vakiloroaya, M. Khatibi, B. Samali, and Q.P. Ha, "An Optimal Control Strategy for Water-Cooled Direct Expansion System in Real World Application,"

International Conference on Measurement and Control Engineering (ICMEC), Puerto Rico, USA, pp. 31-37, 2011.

- V. Vakiloroaya, M. Khatibi, Q.P. Ha, and B. Samali, "New Integrated Hybrid Evaporative Cooling System for HVAC Energy Efficiency Improvement," *IEEE/SICE International Symposium on System Integration*, Kyoto, Japan, pp. 591-596, 2011.

- J. Madadnia, D. Dehestani, A. Mehta, V. Vakiloroaya and H. Koosha, "Design of a micro-probe for direct measurement of convection heat transfer on a vertical building integrated photovoltaic," *4th International Conference on Mechanical Engineering and Mechanics (ICMEM)*, Suzhou, China, August 10-12, 2011.

- **List of Awards**

- Winner of Excellence in Refrigeration and HVAC Research Award 2013 by Australian Institute of Refrigeration, Air Conditioning and Heating (AIRAH), " Toward Green Buildings: Development of a solar-powered absorption chiller."

- Winner of NASSCOM Australia Innovation Student Awards 2013, "Innovative Design of an Hybrid Energy-Efficient Evaporative Air-Conditioning System."

- Highly-Commended Consensus Green Technology Awards 2013, "Energy and Carbon Saving in Australian Housing Air-Conditioning System Using a Novel Evaporative Cooler."

- Winner of UTS Research Showcase Innovation Awards 2013, "Development of a New Energy-Efficient and Eco-Friendly Solar-Powered Single-Stage Hot Water Absorption Air Conditioning System."

- Winner of UTS Annual Green Hero Awards 2013, “Toward Green Buildings: Development of New Energy-Efficient Solar-Powered Absorption HVAC System.”

- Winner of Australian Top 30 Clean Technology Projects 2013, “A Novel Cost-Effective Chilled-Water Evaporative Cooling System for Greenhouse Gas Emission Reduction.”

- Engineering Excellence Awards, 2013 Finalist, IEAust, “New Design of an Energy-Efficient Solar-Powered Absorption Air-Conditioner for Performance Improvement.”

- TRAILBLAZER 2012 Finalist, UTS, Uniquest, Davies Collision Cave, Fisher Adams Kelly.

- Finalist at Australian Refrigeration and Building Services (ARBS) industry award 2014.

- Winner of Consensus Innovation Award, Australian Technology Association, “IP Hybrid HVAC,” 2014.

1.7 List of Pending Patents

- V. Vakiloroaya, **“**A SYSTEM AND A METHOD FOR AIR CONDITIONING,” Application Number: 2014901596, Reference Number: PO1194AP1.

- V. Vakiloroaya, **“**A SYSTEM AND A METHOD FOR EVAPORATIVE AIR CONDITIONING,” Application Number: 2014901352, Reference Number: PO1176AP1.

APPENDIX 5: PROJECT ACHIVEMENTS

The developed solar-powered single-effect absorption cooling plant has achieved the Green Hero Award by University of Technology, Sydney (UTS) in 2013 and the Excellence Research in Refrigeration Award 2013 by the Australian Institute of Refrigeration, Air Conditioning and Heating (AIRAH). Additionally, this system has been selected as the winner of UTS Innovation Research Showcase 2013 in faculty of engineering and information technology. Recently, we have achieved the highly-commended Australian Consensus Green Technology award 2014.

This project have been supported by the Faculty of Engineering and Information Technology at UTS. Its outcomes have great potential in partnership with relevant industrial sectors. Internationally, the project is well-endorsed at large by the International Association for Automation and Robotics in Construction. Through this project, our group has also fostered collaboration with the research group on Energy, Environmental Management, and Sustainable Infrastructure at the Centre of Excellence for Project Management at the University of Maryland, College Park, United States. As a formal acknowledgement, the work of these projects is supported, in part, by a seeding fund obtained from The New South Wales Government through its Environmental Trust, Grant 2012/RDS/034.